



LUND UNIVERSITY

Homogeneous and Heterogeneous Cluster-Based Catalysts for Asymmetric Reactions

Fawzy, Ahmed

2015

[Link to publication](#)

Citation for published version (APA):

Fawzy, A. (2015). *Homogeneous and Heterogeneous Cluster-Based Catalysts for Asymmetric Reactions*. [Doctoral Thesis (monograph), Chemical Physics]. Department of Chemistry, Lund University.

Total number of authors:

1

General rights

Unless other specific re-use rights are stated the following general rights apply:

Copyright and moral rights for the publications made accessible in the public portal are retained by the authors and/or other copyright owners and it is a condition of accessing publications that users recognise and abide by the legal requirements associated with these rights.

- Users may download and print one copy of any publication from the public portal for the purpose of private study or research.
- You may not further distribute the material or use it for any profit-making activity or commercial gain
- You may freely distribute the URL identifying the publication in the public portal

Read more about Creative commons licenses: <https://creativecommons.org/licenses/>

Take down policy

If you believe that this document breaches copyright please contact us providing details, and we will remove access to the work immediately and investigate your claim.

LUND UNIVERSITY

PO Box 117
221 00 Lund
+46 46-222 00 00

Homogeneous and Heterogeneous Cluster-Based Catalysts for Asymmetric Reactions

AHMED FAWZY ABDEL-MAGIED ABDEL-BAKI

CHEMICAL PHYSICS | DEPARTMENT OF CHEMISTRY | LUND UNIVERSITY



Homogeneous and Heterogeneous Cluster-Based Catalysts for Asymmetric Reactions

Ahmed Fawzy Abdel-Magied Abdel-Baki



LUND
UNIVERSITY

DOCTORAL DISSERTATION

by due permission of the Faculty Natural Science, Lund University, Sweden.

To be defended at Lecture Hall B, Kemicentrum, Lund.

Friday, February 6, 2015 at 09.15.

Faculty opponent

Prof. Paul Raithby, University of Bath

Organization Chemical Physics Department of Chemistry LUND UNIVERSITY PO Box 124, 221 00 Lund, Sweden Author: Ahmed Fawzy Abdel-Magied Abdel-Baki	Document name DOCTORAL DISSERTATION Date of issue: February 06. 2015 Sponsoring organization: European Union	
Title and subtitle Homogeneous and Heterogeneous Cluster-Based Catalysts for Asymmetric Reactions		
Abstract <p>Synthesis and characterization of new transition metal carbonyl clusters has been undertaken, and evaluation of the new clusters to act as catalysts/catalysts precursor in asymmetric reactions has been carried out. The catalytic hydrogenation of tiglic acid under relatively mild conditions, using diastereomeric clusters of the general formula $[(\mu-H)_2Ru_3(\mu_3-S)(CO)_7(\mu-1,2-L)]$ (L= chiral diphosphine of the ferrocene-based Walphos and Josiphos families) as catalysts, reveal different catalytic behaviour in terms of conversion and enantioselectivity. The observed reversal in enantioselectivity when the chirality of the cluster framework is changed strongly supports catalysis by intact Ru_3 clusters. A proposed catalytic cycle generated by CO loss from the parent catalyst has been investigated.</p> <p>The ability of carbonyl clusters based on rhenium, ruthenium and osmium derivatised with chiral phosphines and phosphiranes to catalyse the asymmetric hydrogenation of tiglic acid shows high to excellent conversion rates with low to moderate enantioselectivity. A high conversion rate (up to 99%) and an enantioselectivity of 19% have been achieved with the cluster $[(\mu-H)_4Ru_4(CO)_{11}(ArPH_2)]$ {where $ArP = (R)-(2'-methoxy-[1,1'-binaphthalen]-2-ylphosphine)$} acting as catalyst/catalyst precursor; this is, to the best of our knowledge, the first example of an asymmetric hydrogenation induced by a chiral primary phosphine.</p> <p>A chiral solid catalyst derived from the immobilization of $[H_4Ru_4(CO)_{10}(\mu-1,2-W001)]$ (W001 = chiral diphosphine ligand of the Walphos family) onto functionalized MCM-41 has been shown to exhibit excellent conversion rates (> 99%) and as high enantiomeric excesses ($\approx 80\%$) as that of its homogeneous counterpart. The good catalytic properties are coupled with good recyclability of the mesoporous catalyst.</p>		
Key words: Asymmetric synthesis, hydrogenation, ruthenium, osmium, rhenium, phosphine ligands, chirality.		
Classification system and/or index terms (if any)		
Supplementary bibliographical information	Language: English	
ISSN and key title	ISBN 978-91-7422-386-6	
Recipient's notes	Number of pages 122	Price
	Security classification	

I, the undersigned, being the copyright owner of the abstract of the above-mentioned dissertation, hereby grant to all reference sources permission to publish and disseminate the abstract of the above-mentioned dissertation.

Signature __  __ Date February 06. 2015

Homogeneous and Heterogeneous Cluster-Based Catalysts for Asymmetric Reactions

Ahmed Fawzy Abdel-Magied Abdel-Baki



LUND
UNIVERSITY

Copyright © Ahmed Fawzy Abdel-Magied Abdel-Baki

Department of Chemical Physics
Centre for Analysis and Synthesis
Lund University
P.O. Box 124
SE-221 00 Lund
Sweden
ISBN 978-91-7422-386-6

Printed in Sweden by Media-Tryck, Lund University
Lund 2014



**CLIMATE
COMPENSATED
PAPER**



REPA
A part of FFI (the Packaging and
Newspaper Collection Service)

*Dedicated to
The Soul of my father
My mother
My wife, Radwa
My lovely kids: Yousseif, Joody and Yahia*

List of papers

This thesis is based on the following publications, which are referred to in the text by the roman numerals I-VI.

- I.** *Diastereomeric control of enantioselectivity: evidence for metal cluster catalysis.*

Ahmed. F. Abdel-Magied, A. K. Singh, M. Haukka, M. G. Richmond, E. Nordlander. *Chem. Commun.*, 2014, 50, 7705-7708.

- II.** *Asymmetric hydrogenation of an α -unsaturated carboxylic acid catalyzed by intact chiral transition metal carbonyl clusters – diastereomeric control of enantioselectivity.*

Ahmed F. Abdel-Magied, Y. Theibich, I. Doverbratt, A. K. Singh, A. Rahaman, M. Haukka, M. G. Richmond, E. Nordlander. *Manuscript*.

- III.** *Synthesis, characterization and catalytic activity studies of rhenium carbonyl complexes containing chiral diphosphines of the Josiphos and Walphos families*

Ahmed F. Abdel-Magied, M. S. Patil, A. K. Singh, M. Haukka, M. Monari, E. Nordlander. *J. Clust. Sci.*, 2014, accepted manuscript.

- IV.** *Chiral arylphosphido- and phosphinidene-capped tri- and tetraruthenium/osmium hydride clusters.*

Ahmed. F. Abdel-Magied, M. H. Majeed, A. Ficks; W. Clegg, M. Haukka, M. Monari, A. K. Singh, M. Jarenmark, E. Nordlander, L. J. Higham. *Manuscript*.

- V. *Synthesis and characterization of chiral phosphiranes derivatives of $[(\mu-H)_4Ru_4(CO)_{12}]$ and their application in hydrogenation of an α -unsaturated carboxylic acid.*

Ahmed. F. Abdel-Magied, M. H. Majeed, A. Ficks, W. Clegg, R. M. Ashour, A. Rahaman, M. Haukka, E. Nordlander; L. J. Higham. *Manuscript*.

- VI. *Anchored chiral ruthenium clusters in mesoporous silica: one-pot synthesis of a heterogeneous catalyst for asymmetric hydrogenation reactions.*

Ahmed F. Abdel-Magied, C. Tyrsted, K. Herbst, R. Meijboom R. Wallenberg, M. R. Chierotti, R. Gobetto and E. Nordlander. *Manuscript*.

Papers not included in this thesis:

$[\mu$ -Bis(diphenylphosphanyl- κP)methane]decacarbonyltri- μ -hydrido-trirhenium(I)(3 Re—Re) dichloromethane solvate.

Ahmed. F. Abdel-Magied, A. K. Singh, M. Haukka, E. Nordlander. *Acta Creyst.*, 2011, E67, m1816.

Contribution to papers I-VI:

- I.** I performed all synthesis and catalysis experiments, and wrote major parts of the paper.
- II.** I performed all synthesis and catalysis experiments, and wrote most part of the manuscript.
- III.** I performed all synthesis and catalysis experiments, and wrote major parts of the paper.
- IV.** I performed the majority of the synthetic work, evaluation of the catalytic activity and contributed to the writing of the manuscript.
- V.** I performed the majority of the synthetic work, evaluation of the catalytic activity and wrote most part of the manuscript.
- VI.** I performed all synthesis and catalysis experiments, and wrote most part of the manuscript.

Abbreviations

DIPAMP	(<i>R,R</i>)-(-)-1,2-bis[<i>o</i> -methoxy-phenyl](phenyl)phosphine]ethane
BINAP	[2,2'-bis(diphenylphosphino)-1-1'-binaphtyl]
DIPMAP	Ethane-1,2-diylbis[(2-methoxyphenyl)phenylphosphane]
DIOP	O-Isopropylidene-2,3-dihydroxy-1,4-bis(diphenylphosphino)butane
NMDPP	(+)-Neomenthyldiphenylphosphine
T001	(<i>R_P</i>)-1-[(<i>R</i>)- α -(Dimethylamino)-2-(diphenylphosphino)benzyl]-2-diphenylphosphinoferrocene
W001	(<i>R</i>)-1-[(<i>R_P</i>)-2-[2-(Diphenylphosphino)phenyl]ferrocenyl]ethylbis[3,5-bis-(trifluoromethyl)phenylphosphine]
W002	(<i>R</i>)-1-[(<i>R_P</i>)-2-[2-(Diphenylphosphino)phenyl]ferrocenyl]ethyldiphenylphosphine
W003	(<i>R</i>)-1-[(<i>R_P</i>)-2-[2-(Diphenylphosphino)phenyl]ferrocenyl]ethyldicyclohexylphosphine
W005	(<i>R</i>)-1-[(<i>R_P</i>)-2-[2-[Bis(4-methoxy-3,5-dimethylphenyl)phosphino]phenyl]ferrocenyl]ethylbis[3,5-bis(trifluoromethyl)phenyl]phosphine
W006	(<i>R</i>)-1-[(<i>R_P</i>)-2-[2-(Diphenylphosphino)phenyl]ferrocenyl]ethyldi(3,5-xylyl)phosphine
W008	(<i>R</i>)-1-[(<i>R_P</i>)-2-[2-(Dicyclohexylphosphino)phenyl]ferrocenyl]ethylbis[3,5-bis(trifluoromethyl)phenyl]phosphine
W009	(<i>R</i>)-1-[(<i>R_P</i>)-2-[2-[Di(3,5-xylyl)phosphino]phenyl]ferrocenyl]ethyldi(3,5-xylyl)phosphine
J001	(<i>R</i>)-1-[(<i>S_P</i>)-2-(Diphenylphosphino)ferrocenyl]ethyldicyclohexylphosphine
J002	(<i>R</i>)-1-[(<i>S_P</i>)-2-(Diphenylphosphino)ferrocenyl]ethyldi- <i>tert</i> -butylphosphine

J003	(<i>R</i>)-1-[(<i>S_P</i>)-2-(Dicyclohexylphosphino)ferrocenyl]ethylidicyclohexylphosphine
J005	(<i>R</i>)-1-[(<i>S_P</i>)-2-(Diphenylphosphino)ferrocenyl]ethylid(3,5-xylyl)phosphine
J008	(<i>R</i>)-1-{(<i>S_P</i>)-2-[Bis[3,5-bis(trifluoromethyl)phenyl]phosphino]ferrocenyl}ethylid(3,5-xylyl)phosphine
TMNO	Trimethylamine <i>N</i> -oxide
Et	Ethyl
eq	Equivalent
h	Hour(s)
Ph	Phenyl
NMR	Nuclear magnetic resonance
XRD	X-ray diffraction
IR	Infra red
TLC	Thin layer chromatography
SSHC	Single-site heterogeneous catalysis
Py	Pyridine
ee	Enantiomeric excess

Contents

1.	Introduction.....	1
1.1	Transition metal clusters.....	2
1.2	Ligand substitution reactions on transition carbonyl metal clusters.....	3
1.3	Structural characteristic of transition metal clusters.....	4
1.4	Cluster-based catalysts immobilized on solid supports.....	4
1.4.1	Characterization of heterogeneous catalysts.....	5
1.5	Resolving heterogeneity problems in homogeneous transition metal carbonyl cluster catalysis.....	6
1.6	Applications of transition metal clusters in organic transformations	7
1.7	Enantioselective synthesis.....	7
1.8	Aims and outline of this thesis.....	9
2.	Evidence for intact cluster catalysis.....	10
2.1	Background.....	10
2.2	Synthesis of $[(\mu\text{-H}_2)\text{Ru}_3(\mu_3\text{-S})(\text{CO})_9]$ derivatives.....	11
2.3	Catalytic activity studies and evidence for metal cluster catalysis.....	15
2.4	Computational studies for the hydrogenation of tiglic acid employing cluster 4	16
2.5	Concluding remarks.....	18
3.	Cluster-based catalysts for asymmetric hydrogenation of α-unsaturated carboxylic acid.....	19
3.1	Background.....	19
3.2	Transition metal carbonyl clusters as catalysts for asymmetric hydrogenation.....	20
3.2.1	Synthesis of rhenium-based catalysts.....	21
3.2.2	Synthesis of osmium-based catalysts.....	22
3.2.3	Synthesis of ruthenium-based catalysts.....	23
3.2.4	Characterization.....	24
3.3	Catalytic asymmetric hydrogenation study.....	25
3.4	Concluding remarks.....	28
4.	Cluster-based single-site heterogeneous catalysts for asymmetric hydrogenation reactions.....	29

4.1	Background.....	29
4.2	Synthesis of single-site chiral transition metal cluster immobilized on functionalized MCM-41.....	31
4.3	Catalytic asymmetric hydrogenation of α -unsaturated carboxylic acid substrates.....	32
4.4	Recycling experiments and nature of the active catalyst.....	33
4.5	Concluding remarks.....	33
5.	Concluding remarks and future perspectives.....	35
5.1	Future perspectives on the present work.....	36
	Populärvetenskaplig Sammanfattning.....	37
	Acknowledgement.....	38
	References.....	40

Chapter 1. Introduction

The workhorses of virtually all chemical transformations are catalysts. More than 90% of the final products of industrial chemical reactions are made by catalytic processes. Such products include life-saving pharmaceuticals, transportation fuel, polymers and plastics, agricultural fertilizers and fine chemicals. Catalysts also play an important role in making industrial reactions environmentally benign, preventing pollution by avoiding the formation of unnecessary waste and decreasing the use of hazardous solvents and chemicals. Without catalysts, many important chemical reactions would not be economical, and many would not even be possible.

The Swedish chemist Jöns Jacob Berzelius employed the term “catalyst” for the first time in 1836; he derived the term from the Greek word *kata* (down) and *lyein* (loosen). In 1938, Ostwald defined a catalyst as a substance that increases the rate of a chemical reaction by providing an alternative, more rapid reaction path without itself being substantially consumed during the reaction. The catalyst works by offering a different reaction pathway with lower activation energy than that of the uncatalyzed reaction. A catalytic reaction consists of series of transformations where the catalyst enters in one step and is regenerated in another step.¹

In general, catalysts can be categorized as being either homogeneous or heterogeneous. Subsequently, the term “heterogenized catalyst” has also been introduced. The catalyst can either operate in the same phase as that where the reaction takes place (homogeneous catalysts) or in a different phase (heterogeneous and heterogenized catalysts).² The major advantages/disadvantages of homogeneous vs. heterogeneous catalysts are summarized in Table 1. 1. In general, homogeneous catalysts are intrinsically more active and selective in comparison to heterogeneous catalysts.

Table 1.1. Advantages and disadvantages of homogeneous vs. heterogeneous catalysts.

Property	Homogeneous catalysts	Heterogeneous catalysts
Reaction conditions	Mild reaction conditions	Harsh reaction condition
Catalyst recovery	Difficult and expensive	Easy and cheap
Catalyst separation	Difficult	Easy
Selectivity	High	Low
Active site	Single active site	Multiple active site
Thermal Stability	Poor	Good
Catalyst modification	Relatively easy	Relatively difficult
Characterization	Easy	Difficult
Reaction mechanism	Easier to find out	Difficult to find out

1.1 Transition metal clusters

A metal cluster is a compound that contains two or more metal atoms that are held together by direct and substantial metal-metal bonding.³ By considering the presence and nature of the ligands they contain, transition metal clusters may be classified into three different classes as follows:

- I. Naked clusters: Also known as non-ligand-containing Zintl clusters (Zintl anions). Examples of naked clusters are Ag_6 , Pb_5^{2-} and Sn_5^{2-} .
- II. High-valence clusters: In this type of cluster, metal atoms forming the metal network have positive intermediate oxidation states, commonly +2 and +3. The ligands associated with this class of clusters are normally good π -donors such as halides, especially chlorides and bromides. Examples of this class are $[\text{Mo}_6\text{Cl}_8]^{4+}$,⁴ $[\text{Nb}_4\text{Cl}_{14}]^5$ and $[\text{Re}_6\text{Te}_8(\text{TeBr}_2)_6]\text{Br}_2$.⁶
- III. Low-valence clusters: The metal atoms in this class usually have an oxidation state that is zero or negative and are always coordinated to π -acceptor ligands. Carbon monoxide is the most representative of these ligands but there are numerous examples of clusters containing other π -acceptor ligands such as phosphines, olefins, cyclopentadienes, etc. The potential application of this kind of clusters to homogeneous catalysis has been studied extensively. As mentioned previously, metal carbonyl clusters are the most common and important of this type of organometallic complex. There are three common coordination modes for the carbon monoxide ligand in metal clusters; these coordination modes are illustrated in Figure 1. 1.

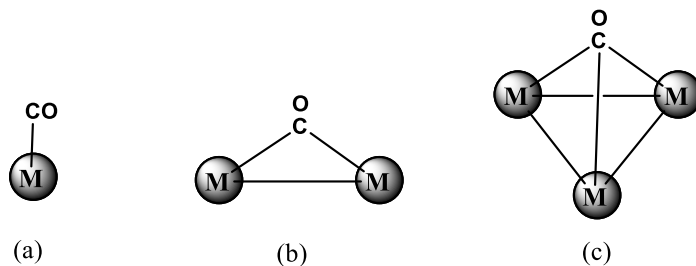


Figure 1.1. Different bonding modes of a CO ligand in metal clusters; (a) terminal, (b) edge-bridging, (c) face-bridging.

In the terminal coordination mode, the CO ligand is bonded to one metal vertex only and the M-C-O bond may be linear or bent. Examples of carbonyl clusters containing only terminally coordinated CO ligands include $[\text{Ru}_3(\text{CO})_{12}]^7$ and $[\text{Os}_3(\text{CO})_{12}]$.⁸ In the edge-bridging coordination mode ($\mu\text{-CO}$), the CO ligand is bonded to two neighbouring atoms, which often indicates the presence of a metal-metal bond. Examples of clusters containing edge-bridging carbonyl ligands are $[\text{Fe}_2(\text{CO})_9]$, $[\text{Fe}_3(\text{CO})_{12}]$, $[\text{Co}_2(\text{CO})_8]$ and $[\text{Co}_4(\text{CO})_{12}]$.^{9, 10} Finally, for the face-bridging coordination mode ($\mu_3\text{-CO}$), the CO ligand is bonded to three metal atoms in a capping mode. An example of a cluster containing face-bridging carbonyl ligands is $[\text{Rh}_6(\text{CO})_{16}]$.¹¹

1.2 Ligand substitution reactions on transition metal carbonyl clusters

Over the last 50 years, much progress has been made in the study of organometallic reaction mechanisms. Investigations show that organometallic clusters undergo different reactions. In general, three classes of reaction pathways may be distinguished in ligand substitution reactions on metal complexes, and they are also applicable to the chemistry of transition metal carbonyl clusters:

- I. Associative mechanism (A). In this type of mechanism, the cluster framework displays an intermediate with a coordination number greater than that of the original cluster due to the association of reactants.
- II. Dissociative mechanism (D). Here, the reaction proceeds via the dissociation of a ligand to form an intermediate in which the coordination number of the carbonyl metal cluster is lower than that of the original compound.
- III. Interchange mechanism (I). When the ligand substitution reaction does not fit neatly into either type (no discernable intermediate), the pathways of these mechanisms are called interchange pathways. The interchange mechanism

can be classified into associative interchange (I_a), where the rate-determining step involves the association of a ligand, and dissociative interchange (I_d , rate-determining step involving the dissociation of a ligand).

1.3 Structural characteristic of transition metal clusters

Many different analytical and spectroscopic techniques can be used for elucidating cluster structures. Among these techniques, the most common and widely used are listed in Table 1.2.

Table 1.2. Different techniques used for cluster characterization.

Technique	Used for
Infrared (IR)	Can be used for determining the coordination mode of the ligands attached to the cluster.
Nuclear magnetic resonance (NMR) spectroscopy	Used to get structural information and dynamic processes in clusters.
Mass spectrometry (MS)	Can provide strong evidence for the empirical formula of a proposed carbonyl cluster.
Single crystal X-ray diffraction (XRD)	Gives information about the transition metal cluster structure, stereochemistry and structural parameters. Although it is a very important technique, it does not always provide unambiguous answers because of disorder problems or poor crystal quality. The identification of hydrides in transition metal clusters is, in general, a tricky task that involves indirect approaches for locating the hydrogen atom position. Unusual distances and angles can reveal the positions of metal-bound hydrogen.

1.4 Cluster-based catalysts immobilized on solid supports

One of the major directions in homogeneous catalysis is to find new pathways for the immobilization of homogeneous catalysts with good catalytic properties on solid supports or liquid supports (biphasic catalysis) so that their separation from the final products is as facile as in heterogeneous catalysis while the high catalytic activity in terms of conversion and enantioselectivities that is found in homogeneous catalysis is maintained. Different strategies and protocols have been developed for tethering molecular catalysts to solid supports. Immobilization of clusters on solid support is a well-developed field, with silica and alumina supports being the most common. The resulting catalytic activities of these cluster-

containing materials have been extensively studied and reviewed.¹² Many of the supported metal carbonyl clusters are anions, often dispersed as ion pairs on metal oxide surfaces. Examples of metal carbonyl clusters supported on/in MgO are $[\text{Ir}_6(\text{CO})_{15}]^{2-}$,¹³ $[\text{HFe}_3(\text{CO})_{11}]^-$,¹⁴ $[\text{H}_3\text{Os}_4(\text{CO})_{12}]^-$,¹⁵ and $[\text{Ru}_6\text{C}(\text{CO})_{16}]^{2-}$.¹⁶ Neutral metal carbonyl clusters such as $[\text{Ir}_4(\text{CO})_{12}]$ and $[\text{Rh}_6(\text{CO})_{16}]$ can also be dispersed on semi-metal oxides that are neither strongly basic nor strongly acidic, e.g. SiO_2 .¹⁷

1.4.1 Characterization of heterogeneous catalysts

Various techniques can be used to characterize solid materials and investigate their surface reactivities. Among these techniques, the most common and widely used are listed in Table 1.3.

Table 1.3. Different techniques used for characterization of heterogeneous catalysts.

Technique	Used for
Infrared (IR)	Confirming the successful immobilization of the cluster by showing carbonyl frequencies in the region $2100\text{-}1500\text{ cm}^{-1}$.
Scanning electron microscopy (SEM)	Used when the diameter of the metal nanoparticles are around 1 nm or below. SEM uses a focused beam of high-energy electrons (30-50 kV) to generate a variety of signals at the surface of solid sample.
High resolution transmission electron microscopy (HRTEM)	Allows a precise image of the solid particles to be formed, showing also the packing of atoms in the interior. Used to recognize the presence of metal nanoparticles with a diameter larger than 1 nm on the solid surface of the catalyst by providing most of necessary fundamental information on morphology and microstructure of the material.
Brunauer-Emmett-Teller (BET) method	Used to calculate the surface area.
Thermogravimetry analysis (TGA)	Used to determine thermal stability of the catalyst.
Solid state nuclear magnetic resonance	Allows the characterization of the chemical and structural environment of atoms in the catalysts (or in species adsorbed).

1.5 Resolving heterogeneity problems in homogeneous transition metal carbonyl cluster catalysis

The use of metal carbonyl clusters as catalysts/catalyst precursors in asymmetric transformations is well studied and investigated.¹⁸⁻²⁰ Determination of the identity of the true catalyst and distinguishing true molecular (homogeneous) catalysis from that effected by soluble metal particles is very important for development of the synthesis of highly selective, stable and active catalysts. This problem becomes more difficult if a soluble colloidal/nanocluster catalyst with a small diameter (~1 nm) is formed. This task has caused considerable discussion (and consternation) in the literature.²¹⁻²³ A list of different strategies that can be used to resolve the title problem are summarized in Table 1.4.

Table 1.4. Tests that can be useful in helping to distinguishing homogeneous from heterogeneous (colloidal) catalysts.

Test	
Hg(0) poisoning test	Hg(0) is well known to poison metal-particles by amalgamating the metal. Addition of Hg(0) in an excess amount to the catalytic reaction mixture and analysis of the final products gives conclusion about the nature of the active catalyst. Suppression of catalysis by Hg(0) is evidence for a heterogeneous catalyst.
Hot filtration test	The catalytic reaction mixture is filtered through a glass frit. The filter with any adhering metal particles is washed and returned to the (rinsed) reaction vessel after adding a new solvent mixture and substrate under the same catalytic condition, and the catalytic activity of the resulting mixture is checked. Any observed catalytic activity is attributed to heterogeneous catalysis.
Dynamic light scattering	Can detect nanoparticles and establish a mean radius for the ensemble.
Transmission electron microscopy (TEM)	Can detect the presence of nanoparticles deposited from catalytic reaction mixtures.

1.6 Applications of transition metal clusters in organic transformations

Transition metal carbonyl compounds are of immense interest because of their structural diversity and potential application in the field of catalysis. The clusters $[\text{Ru}_3(\text{CO})_{12}]$, $[\text{Os}_3(\text{CO})_{12}]$ and $[\text{Ir}_4(\text{CO})_{12}]$ have been shown to catalyze the water gas shift reaction;²⁴ $[\text{Rh}_6(\text{CO})_{16}]$ catalyzes the conversion of carbon monoxide into hydrocarbons;²⁵ $[\text{Co}_2(\text{CO})_8]$ is a precatalyst for the hydroformylation reaction;²⁶ $[\text{Os}_3\text{Ir}(\text{CO})_{13}]$ is a catalyst precursor for the carbonylation of methanol;²⁷ $[\text{Ru}_3(\text{CO})_{12}]$ for the carbonylation of ammonia;²⁸ and the Fischer-Tropsch process for the generation of hydrocarbons from coal is also catalyzed by iron clusters.²⁵ Metal clusters have also been shown to be important as catalyst precursors for the preparation of different heterogeneous catalysts that are useful in asymmetric synthesis.

1.7 Enantioselective synthesis

The ever-increasing demand for chiral chemicals that can be used in industry and academia, make the development of efficient methods to provide such enantiomerically products of great importance. Asymmetric synthesis is the most appealing strategy in terms of economy and environmental aspects. Thousands of chiral ligands and their corresponding transition metal complexes have been synthesized and evaluated in homogeneous as well as heterogeneous catalysis. The ligands coordinated to the metal, if carefully chosen, can tune the reactivity of the metal. Among the various ligands synthesized, phosphine ligands are the most general ligands employed for this purpose.

Asymmetric hydrogenation of prochiral unsaturated compounds such as alkenes, ketones and α -unsaturated carboxylic acids has been intensively studied and is considered to be a very important methodology for the synthesis of chiral compounds. Homogeneous asymmetric hydrogenation is well recognized as one of the most significant development in organotransition metal chemistry. Low valent Ru, Rh, or Ir complexes derivatised with chiral phosphine ligands belongs to the most effective hydrogenation catalyst precursors.²⁹ Calvin used homogeneous hydrogenation for the first time in 1938 when he reports that copper-based catalysts can hydrogenate 1,4-benzoquinone.³⁰ The discovery of Wilkinson's catalyst $[\text{RhCl}(\text{PPh}_3)_3]$ in 1965 was a very important breakthrough in homogeneous catalysis.³¹ In 1968, Horner³² and Knowles³³ independently reported the synthesis of chiral non-racemic rhodium catalysts bearing *P*-chiral monodentate ligands that can be used in hydrogenation reactions with low product enantioselectivity (less than 30%). Knowles³⁴ synthesized DIPAMP (*R,R*)-(-)-1,2-

bis[*o*-methoxy-phenyl](phenyl)phosphine]ethane; a second generation *P*-chiral ligand. Noyori³⁵ developed the next outstanding ligand BINAP [2,2'-bis(diphenylphosphino)-1,1'-binaphtyl] in the 1980s. Interestingly, Ru catalysts containing BINAP are the most active and selective rather than Rh (e.g. [Ru(BINAP)(OAc)₂]). The BINAP ligand can also be used in various catalysis reactions, so it belongs to the group of “privileged ligands”. Burk³⁶ has developed ligands that contain alkylphosphines, such as the DuPhos ligand family, where catalysts based on Rh precursors bearing DuPhos shows excellent results in the asymmetric hydrogenation of olefins. In 1994, Tongi and coworkers developed the Josiphos family of ligands, which was another milestone in the development of bidentate ligands that feature planar chirality in addition to an atom-centered chiral centre.³⁷ During the last few years, hundreds of chiral phosphine ligands have been synthesized and evaluated in asymmetric catalysis reactions. Among all of these ligands, ferrocene-based ligands have been shown to provide more successful results in catalytic hydrogenation reactions. Some of the widely used chiral phosphine ligands used in homogeneous asymmetric hydrogenation synthesis are shown in Figure 1.2.

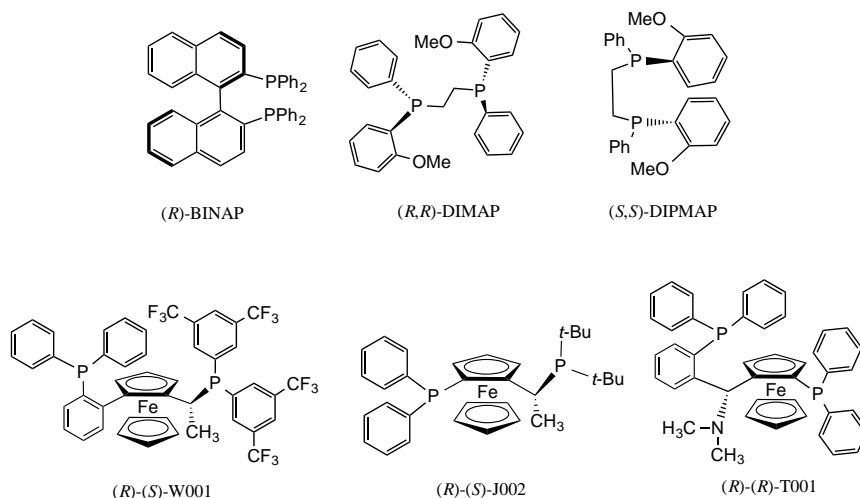


Figure 1.2. Selected efficient phosphine ligands for homogeneous asymmetric hydrogenation synthesis. (W signifies a Walphos ligand,³⁸ J a Josiphos ligand³⁷ and T a Taniaphos ligand³⁹).

1.8 Aims and outline of this thesis

This thesis describes the synthesis, characterization and catalytic activity studies of new ruthenium, rhenium and osmium clusters. There were three general aims of this work:

- I.** To demonstrate catalysis by intact metal clusters in homogeneous hydrogenation reactions.
- II.** To develop more effective cluster-based catalysts for asymmetric hydrogenation reactions.
- III.** To develop new heterogeneous catalysts for asymmetric hydrogenation reactions via heterogenization of homogeneous cluster-based catalysts.

The purpose of this summary is to provide an introduction to the scientific field, and to put the scientific publications and manuscripts (appended at the end of this thesis) into a boarder context. The summary of the work reported in the enclosed papers and manuscripts is as follows.

Papers **I** and **II** report the synthesis and characterization of chiral phosphine derivatives of the sulfido-capped ruthenium carbonyl cluster $[(\mu\text{-H}_2)\text{Ru}_3(\mu_3\text{-S})(\text{CO})_9]$, evaluating their performance as catalysts in asymmetric hydrogenation reaction and demonstrate the nature of the active catalyst.

Papers **III-V** study the use of different chiral phosphine derivatives of various transition metal clusters (Re, Ru and Os) as catalysts/catalyst precursors in asymmetric hydrogenation reactions. Synthesis and characterization of chiral phosphine derivatives of the metal clusters are reported.

Paper **VI** investigates the heterogenization of a homogeneous cluster-based catalyst in mesoporous silica.

Chapter 2. Evidence for intact cluster catalysis (papers I and II)

2.1 Background

There has been much debate about the nature of the active catalyst in reactions involving clusters as catalysts. The importance of knowing the identity of the active catalyst⁴⁰ is that such knowledge forms a basis for the development of more efficient and effective catalysts. Generally speaking, four types of behaviour may occur: (i) the cluster framework remains intact throughout a complete catalytic cycle, (ii) the cluster framework may fragment to mononuclear species, (iii) the cluster framework may agglomerate to form catalytically active nanoparticles, or finally (iv) the cluster framework may be destroyed and rebuilt during the catalytic cycle. Many examples that involve all four possibilities exist and have been published, and in the same reaction more than one catalyst can operate simultaneously.^{23, 40} To investigate whether the cluster catalyst fragments to give mononuclear (active) species, or aggregates to form a heterogeneous catalyst, or remains as an active cluster catalyst, several tests are used to establish whether a reaction is catalyzed by homogeneous or heterogeneous catalytic species. Influential reviews of the field are available from Lewis,⁴¹ Crabtree,²³ Aiken and Finke.^{21, 22, 42} Finke^{21, 22} has suggested a ‘toolkit’ which can provide information about the type of catalysis by running different kinetic measurements, catalyst poisoning and spectroscopic experiments.

After the confirmation of “true” molecular homogeneous catalysis, the next step is to determine the nature of the active catalyst. For clusters, this means to determine whether catalysis is by the intact cluster or by mononuclear species formed by fragmentation of the cluster. Although it is not an easy task, a number of convincing examples of homogeneous cluster catalysis have been reported based on indirect evidence. The heteronuclear catalyst $[\text{H}_4\text{Pt}_3\text{Ru}_6(\text{CO})_{21}]$ catalyzes alkyne transformation without any fragmentation.⁴³ Nombel⁴⁴ has reported that the face-capped trinuclear cluster $[\text{HRu}(\text{CO})_9(\mu_3\text{-}\eta^2\text{-NMePy})]$ is the intact cluster in the hydroformylation of diphenylacetylene to α -phenylcinnamaldehyde.

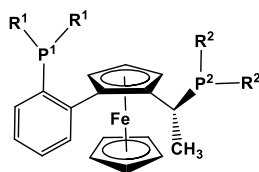
Süss-Fink and coworkers⁴⁵ used an isotope labeling method to suggest that hydroformylation of ethylene catalyzed by the cluster anion $[\text{Ru}_3\text{H}(\text{CO})_{11}]^-$ proceeds via the intermediacy of intact Ru_3 clusters. Nordlander and coworkers¹⁹ have provided indirect evidence for clusters based on $[(\mu\text{-H})_4\text{Ru}_4(\text{CO})_{12}]$ derivatised with chiral bis-phosphine ligands being the intact catalysts in the hydrogenation of tiglic acid. While catalysis by fragmentation products cannot be excluded in the latter case, the parent starting clusters were recovered unaltered after the catalytic reaction and re-evaluation/recycling of the recovered catalyst in the same catalytic reaction shows identical conversion. Finally, direct evidence for cluster-based catalysts has been provided using parahydrogen ($p\text{-H}_2$) NMR methods;⁴⁶ Dyson, Duckett and coworkers^{47, 48} have been able to demonstrate that the clusters $[\text{HRu}_3(\mu\text{-H})(\text{CO})_9(\text{L})_2]$ (where $\text{L} = \text{PMe}_2\text{Ph}$ or PPh_3) are active catalyst intermediates for the hydrogenation of diphenylacetylene.

Norton⁴⁹ has identified a criterion for incontrovertible evidence for cluster-based catalysts, *viz* the observation of asymmetric induction in a catalytic reaction effected only by chirality in the cluster framework, rather than from a chiral ligand. Based on this concept, Vahrenkamp and coworkers⁵⁰ have used chiral tetrahedrane clusters for the silylation of acetophenone, but cluster racemization was observed.

2.2 Synthesis of $[(\mu\text{-H}_2)\text{Ru}_3(\mu_3\text{-S})(\text{CO})_9]$ derivatives

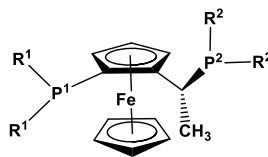
The parent cluster $[(\mu\text{-H})_2(\mu_3\text{-S})\text{Ru}_3(\text{CO})_9]$ **1** was synthesized by heating $[\text{Ru}_3(\text{CO})_{12}]$ in octane at 125 °C while H_2S was bubbled in the solution.⁵¹ This parent cluster **1** was derivatised with chiral diphosphine ligands from the Walphos and Josiphos families (papers I and II) (*cf.* Fig. 2.1). The afore-mentioned ligands are well known in catalytic hydrogenation reactions since they give high enantioselectivities with mononuclear Rh and Ru complexes as well as Ru clusters.^{20, 52-55}

The synthesized clusters of the general formula $[(\mu\text{-H})_2(\mu_3\text{-S})\text{Ru}_3(\text{CO})_7(\mu\text{-L})]$ (L = bulky chiral ferrocene-based diphosphine ligands of the Walphos (**1a-1h**) and Josiphos (**2a-2e**) families) were prepared by using Me_3NO as an oxidative decarbonylation reagent.⁵⁶ All clusters were characterized and identified using ^1H , ^{31}P NMR, IR spectroscopy, mass spectrometry and wherever possible X-ray crystallography. The ^{31}P NMR data confirmed differences in the coordination environments of the diphosphine ligands within each diastereomeric pair. For example, the ^{31}P NMR spectra for the diastereomeric pair $[(\mu\text{-H})_2(\mu_3\text{-S})\text{Ru}_3(\text{CO})_7(\mu\text{-1a})]$ **3** and **4** show different signals: in **3**, the P^1 signal appears as a triplet, indicating coupling to both hydrides, while the signal for P^2 is a doublet. In contrast, the signal for P^1 in **4** appears as a doublet while that of P^2 is a doublet of doublets (*cf.* Fig. 2.2 (a) and (b) for clusters **3** and **4** respectively).



Walphos ligands

- 1a**; $R^1 = \text{Ph}$, $R^2 = 3,5\text{-(CF}_3)_2\text{C}_6\text{H}_3$
S,S-1b; $R^1 = \text{Ph}$, $R^2 = 3,5\text{-(CF}_3)_2\text{C}_6\text{H}_3$
1c; $R^1 = \text{Ph}$, $R^2 = \text{Cy}$
1d; $R^1 = 3,5\text{-(CH}_3)_2\text{-4-(CH}_3\text{O)C}_6\text{H}_2$, $R^2 = 3,5\text{-(CF}_3)_2\text{C}_6\text{H}_3$
1e; $R^1 = \text{Ph}$, $R^2 = 3,5\text{-(CH}_3)_2\text{C}_6\text{H}_3$
1f; $R^1 = \text{Cy}$, $R^2 = 3,5\text{-(CF}_3)_2\text{C}_6\text{H}_3$
1g; $R^1 = 3,5\text{-(CH}_3)_2\text{C}_6\text{H}_3$, $R^2 = 3,5\text{-(CH}_3)_2\text{C}_6\text{H}_3$
1h; $R^1 = \text{Ph}$, $R^2 = \text{Ph}$



Josiphos ligands

- 2a**; $R^1 = 3,5\text{-(CF}_3)_2\text{C}_6\text{H}_3$, $R^2 = \text{Cy}$
2b; $R^1 = \text{Ph}$, $R^2 = \text{Cy}$
2c; $R^1 = \text{Cy}$, $R^2 = \text{Cy}$
2d; $R^1 = \text{Ph}$, $R^2 = 3,5\text{-(CH}_3)_2\text{C}_6\text{H}_3$
2e; $R^1 = 3,5\text{-(CF}_3)_2\text{C}_6\text{H}_3$, $R^2 = 3,5\text{-(CF}_3)_2\text{C}_6\text{H}_3$

Figure 2.1. Structure of Walphos (**1a-1h**) and Josiphos (**2a-2e**) ligands used in this investigation. (*cf.* Papers I and II for more details).

Further investigation on the reversal of the bridging mode of the diphosphine ligands observed for the sulfide-capped clusters **3** and **4** have been done by synthesizing and characterizing the analogous diastereomeric pair based on *S,S*-**1b**, *viz.* **5** (connectivity corresponding to **3**) and **6** (connectivity corresponding to **4**). The identities of the diastereomeric pairs **3** and **4**, **5** and **6** were further confirmed by the determination of their crystal structures (*cf.* Fig. 2.3). (*cf.* Papers I and II for full details).

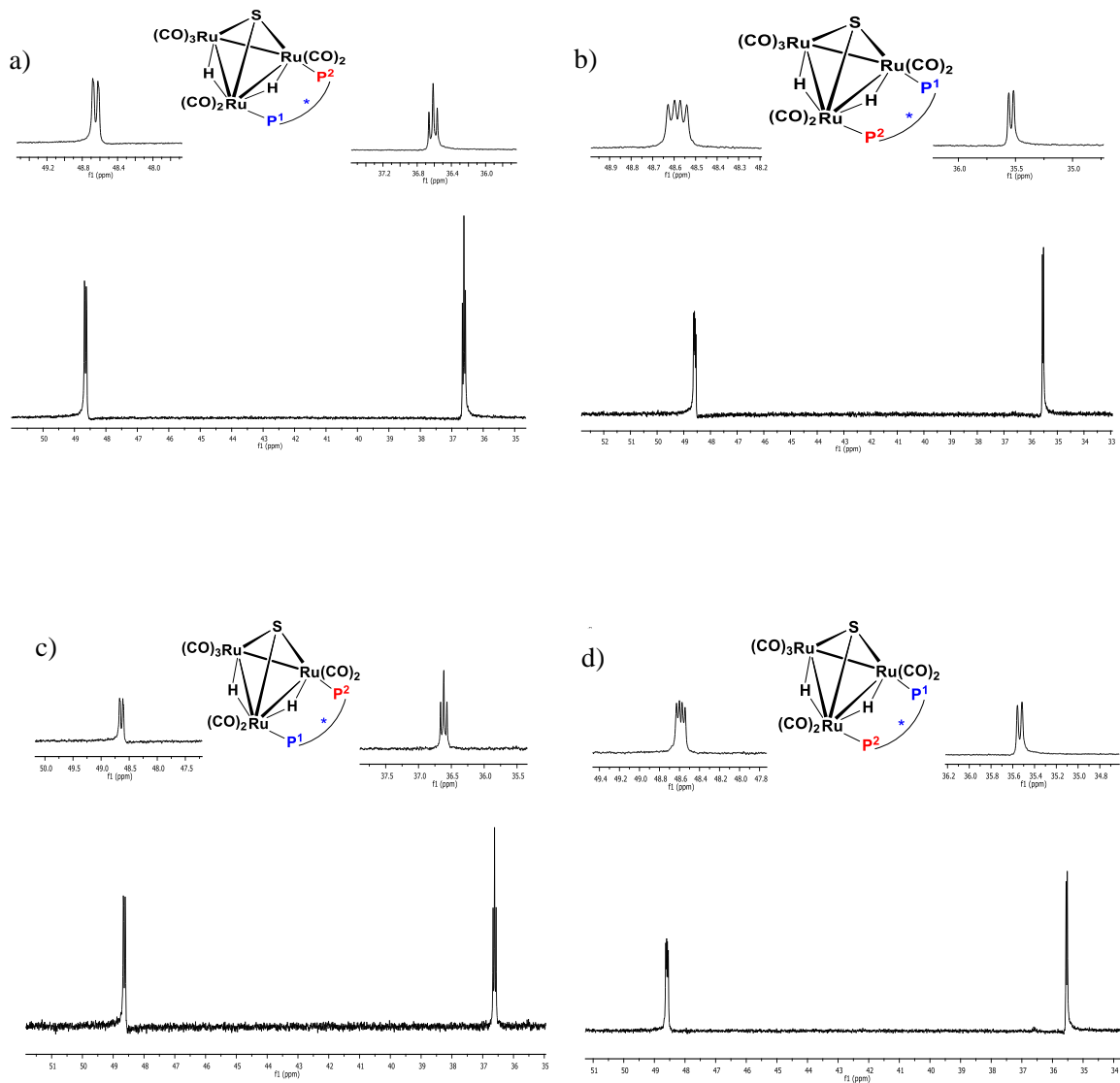


Figure 2.2. ^{31}P NMR data for clusters; a) $[(\mu\text{-H})_2(\mu_3\text{-S})\text{Ru}_3(\text{CO})_7(\mu\text{-1a})]$ **3** and b) **4** and c) $[(\mu\text{-H})_2(\mu_3\text{-S})\text{Ru}_3(\text{CO})_7(\mu\text{-S,S-1b})]$ **5** and d) **6**.

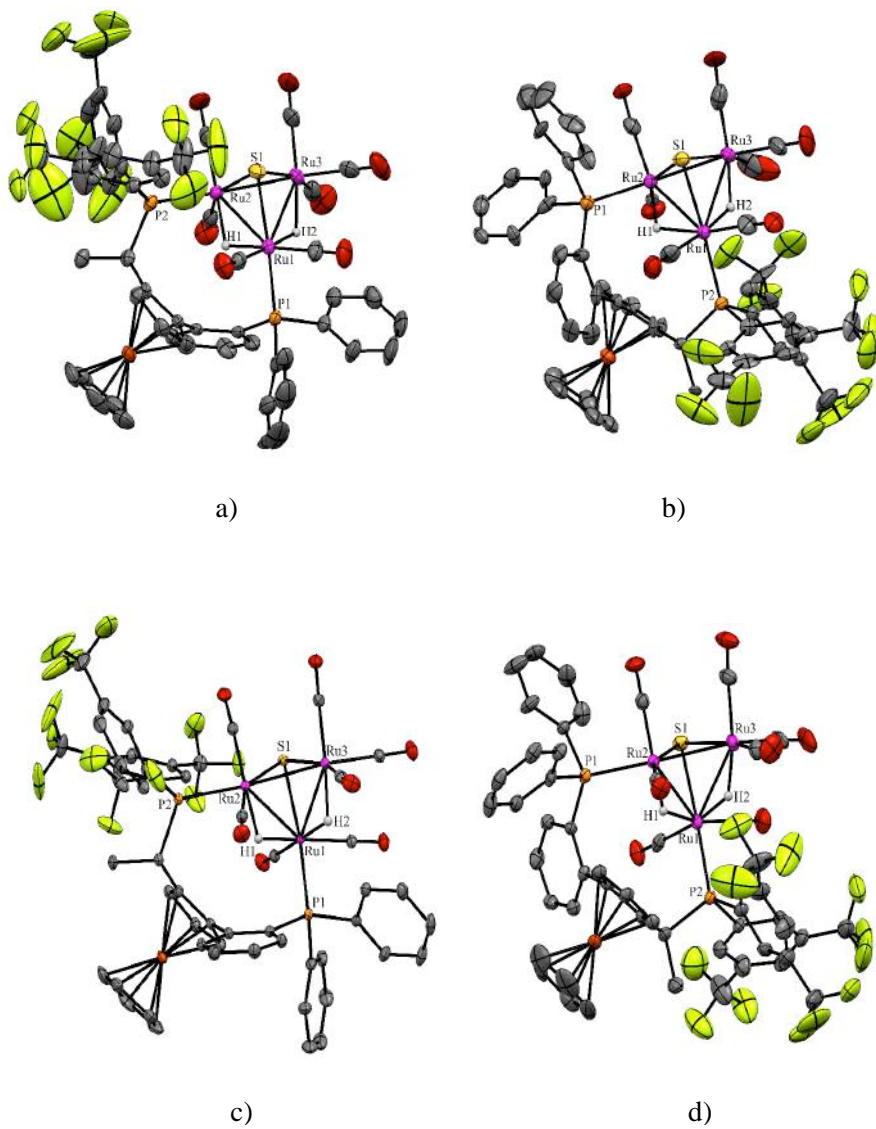
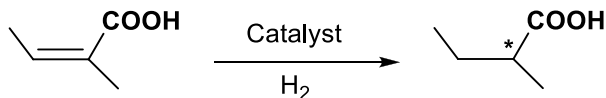


Figure 2.3. The different coordination modes observed for the diastereomeric pairs $[(\mu\text{-H})_2(\mu_3\text{-S})\text{Ru}_3(\text{CO})_7(\mu\text{-1a})]$ **3** and b) **4** and c) $[(\mu\text{-H})_2(\mu_3\text{-S})\text{Ru}_3(\text{CO})_7(\mu\text{-S,S-1b})]$ **5** and d) **6**.

2.3 Catalytic activity studies and evidence for metal cluster catalysis

All the synthesized clusters were tested as catalysts in asymmetric hydrogenation of tiglic acid as shown in scheme 2.1.



Scheme 2.1. General scheme for the catalytic hydrogenation of tiglic acid used in this study.

The catalytic activity results for clusters **3** – **6** are summarized in Table 2.1. The conversion of tiglic acid was assessed by ^1H NMR spectroscopy and the enantioselectivity was investigated according to a published procedure.⁵⁷ All clusters yielded moderate to high conversions; and low conversion rates could be observed for the cluster $[(\mu\text{-H})_2\text{Ru}_3(\mu_3\text{-S})(\text{CO})_7(\mu\text{-1,2-1f})]$ **9**. Only relatively moderate enantiomeric excesses could be observed (9-56 %) and, in case of $[(\mu\text{-H})_2\text{Ru}_3(\mu_3\text{-S})(\text{CO})_7(\mu\text{-1,2-1f})]$ **9** and $[(\mu\text{-H})_2\text{Ru}_3(\mu_3\text{-S})(\text{CO})_7(\mu\text{-1,2-1g})]$ **10**, no enantioselectivity could be detected. We have observed significantly higher enantioselectivities in other cluster-based systems,⁵² but it should be borne in mind that ee's exceeding 40% were unprecedented⁵⁸⁻⁶² in cluster-based asymmetric hydrogenation before we started our studies.

Table 2.1. Summary of catalytic asymmetric hydrogenation activity of clusters **3-6**.

Ligand	Catalyst	Conversion %	ee %	Configuration
1a	3	49	23	<i>R</i>
1a	4	79	56	<i>S</i>
<i>S,S</i> - 1b	5	55	24	<i>S</i>
<i>S,S</i> - 1b	6	64	52	<i>R</i>

Reversal in enantioselectivity for the diastereomeric pairs has been observed, supporting direct evidence for metal cluster catalysis, or closely related triruthenium species. Formation of Noyori-type catalysts of the general formula $[\text{Ru}(\mathbf{1a})(\text{O}_2\text{CR})_2]$ is possible, but cannot explain the reversal in enantioselectivity. On the other hand, cluster decomposition during the catalytic cycle followed by intact cluster regeneration at the end of the catalytic cycle is also possible but formation of both diastereomers will always happen.

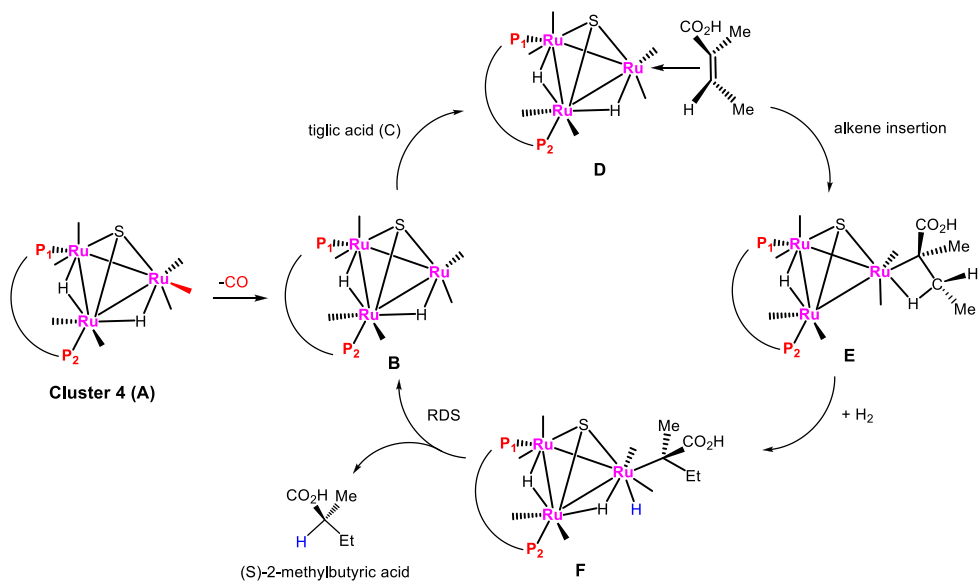
All catalysts were recovered and spectroscopic measurements (IR, $^1\text{H}/^{31}\text{P}$ NMR) and mass spectrometry showed no signs of changes in the clusters after catalytic runs. Catalyst recyclability was tested by recovery of catalyst **3** after catalysis and reuse of the catalyst in exactly the same experiment. Identical conversion rates and enantiomeric excesses were obtained for the two catalytic runs. Another piece of evidence about the nature of the active catalyst was provided by a mercury poisoning test.^{21, 22} As discussed in Chapter 1, $\text{Hg}(0)$ is able to poison metal particle/colloidal catalysts by amalgamating the metal. The suppression of catalysis by $\text{Hg}(0)$ is indirect evidence for cluster decomposition to form colloidal particles. The test was carried out on cluster **3** under typical catalytic hydrogenation reaction conditions. Slightly better results were obtained than in the reactions without $\text{Hg}(0)$ added. Both the conversion and enantioselectivity were increased by 2-3%. The obtained result suggests that the cluster does undergo fragmentation and the formation of colloidal particles occurs during the catalytic reaction, however, the effect of the colloidal particles formed seems very limited for the hydrogenation reaction.

The obtained results indicate that both stereochemistry and bridging modes of the coordinated chiral ligand in these catalytic systems, strongly affects the outcome of hydrogenation in terms of conversion and enantioselectivity and strongly support that the catalytic hydrogenation of tiglic acid proceeds via intact Ru_3 clusters. For the first time, an experiment based on Norton's criterion has been used to demonstrate that intact clusters are most likely the active catalysts. In parallel with the parahydrogen experiments mentioned above, these results constitute the best evidence until now for intact clusters acting as catalysts.

2.4 Computational studies for the hydrogenation of tiglic acid employing cluster **4**

A possible catalytic cycle for the hydrogenation of tiglic acid by cluster **4** is depicted in Scheme 2.2. First, dissociation of a carbonyl ligand to form a coordinatively unsaturated species **B** occurs. This is followed by substrate coordination to afford the alkene-substituted cluster **E**, which reacts with H_2 to furnish the transient trihydride cluster **F**. Reductive elimination to give the hydrogenated product regenerates cluster **B**. The free energy profile for the hydrogenation of tiglic acid catalyzed by cluster **4** is shown in Figure 2.4. Substrate insertion into the proximal bridging hydride occurs *via* transition structure **TSDE**, whose energy is $29.6 \text{ kcal mol}^{-1}$. On the other hand, the alternative alkene insertion route lies $6.6 \text{ kcal mol}^{-1}$ above **TSDE**, where the hydride transfer to the ester-substituted alkene carbon and create (*S*) stereogenic center and the formation of the final product with a net release of $13.2 \text{ kcal mol}^{-1}$. (cf. Supplementary Material for paper I for more details). The obtained computed

results are in agreement with the proposed catalytic hydrogenation cycle of ethane by $[\text{H}_4\text{Ru}_4(\text{CO})_{12}]$.⁶³



Scheme 2.2. Proposed catalytic cycle for the hydrogenation of tiglic acid by cluster 4.

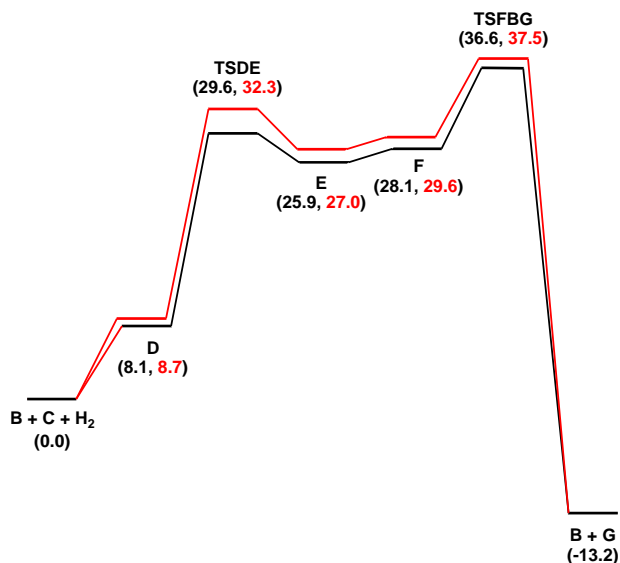


Figure 2.4. Free energy profile for the catalytic hydrogenation of tiglic acid catalyzed by cluster 4. Black and red profiles are for the si- and re-face alkene coordination routes, respectively.

2.5 Concluding remarks

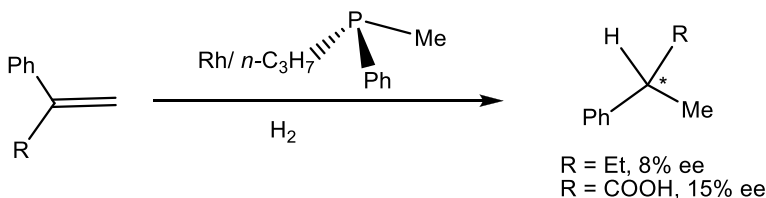
The synthesized diastereomers of the cluster $[(\mu\text{-H})_2\text{Ru}_3(\mu_3\text{-S})(\text{CO})_7(\mu\text{-1,2-P-P}^*)]$ (P-P^* = chiral diphosphine ligands from the Walphos and Josiphos families) have been fully characterized and evaluated as active catalysts in the asymmetric hydrogenation of tiglic acid. The observed reversal in the enantioselectivity is not only reversed with reversal in ligand chirality, but also with reversal in cluster chirality. The obtained results for the catalytic activity, in terms of both conversion and enantioselectivity, strongly support the involvements of intact Ru_3 clusters as the active hydrogenation species.

Chapter 3. Cluster-based catalysts for asymmetric hydrogenation of α -unsaturated carboxylic acid (papers III-V)

3.1 Background

Homogeneous asymmetric hydrogenation of prochiral unsaturated compounds, such as alkenes, ketones, and imines, is one of the most extensively investigated reactions, and is an efficient and straightforward method for the preparation of optically active compounds. The catalytic reaction involves the addition of dihydrogen to the substrate, using a small amount of a chiral transition metal complex/cluster as a catalyst. Asymmetric hydrogenation is frequently used in both academia and industry for the synthesis of chiral amino acids, alcohols and different enantiopure products.

In 1968, Knowles³³ and Horner³² reported independently the first example of a catalytic homogeneous asymmetric hydrogenation reaction by replacing the triphenylphosphine of the well-known Wilkinson's catalyst $[\text{RhCl}(\text{PPh}_3)_3]$ with optically active methylphenyl(*n*-propyl)phosphine and investigating its catalytic activity in the hydrogenation of prochiral alkenes. Although the enantiomeric excesses found were low, catalytic asymmetric hydrogenation was unequivocally shown experimentally to have occurred in the homogeneous system (*cf.* Scheme 3.1).



Scheme 3.1. The first example of homogeneous asymmetric hydrogenation.

Afterwards, other researchers (Horner,³² Kagan,⁶⁴ Morrison⁶⁵ and Bosnich) achieved similar results and contributed by their investigations to opening the doors to a new important field for both academic and industrial research.

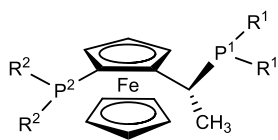
Rhodium-based catalysts for the asymmetric hydrogenation are well studied for the enantioselective reduction of α - and β -dehydroamino acid derivatives and enamides, giving enantiomerically pure products. The development of chiral ruthenium-based catalysts expanded the field of asymmetric hydrogenation significantly. In 1988, Noyori *et al.* made the first breakthrough in this area using a [Ru(II)(BINAP)] dicarboxylate complex.⁶⁶ The complex gave high enantioselectivity in the hydrogenation of carbon-carbon double bonds of different substrates, the asymmetric hydrogenation of which had been difficult to achieve with the rhodium catalysts that had been reported until then.

3.2 Transition metal carbonyl clusters as catalysts for asymmetric hydrogenation

Catalysis by molecular clusters remains a very fascinating area of research. Many transition metal (carbonyl) clusters have been investigated as catalysts in the asymmetric hydrogenation reaction. The cluster $[\text{Rh}_6(\text{CO})_{10}\{(-)\text{DIOP}\}]$ was found to be an effective hydrogenation catalyst for prochiral olefins.¹⁸ Matteoli and coworkers⁵⁸⁻⁶² have demonstrated that catalysts of the type $[(\mu\text{-H})_4\text{Ru}_4(\text{CO})_{10}(\text{L})]$ (where L= BINAP, MOBIPH) and $[(\mu\text{-H})_4\text{Ru}_4(\text{CO})_8\{(-)\text{DIOP}\}_2]$ are effective for the hydrogenation of tiglic acid under harsh conditions. They have also shown that isomerization of prochiral 3-methyl-5-phenylpent-2-ene is possible in the presence of $[(\mu\text{-H})_4\text{Ru}_4(\text{CO})_8\{(-)\text{DIOP}\}_2]$.⁵⁹

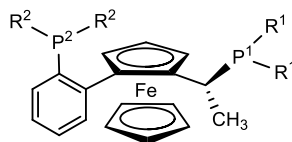
Nordlander and co-workers have shown that $[\text{H}_4\text{Ru}_4(\text{CO})_{10}(\text{W001})]$ (where W001= a chiral diphosphine ligand of the Walphos family) is a superior catalyst for the asymmetric hydrogenation of prochiral α -unsaturated carboxylic acids with excellent conversion rates (99-100%), high product selectivity (99-100%) and good enantioselectivity - up to 92% ee.^{19, 53} They have also shown that the chiral clusters $[\text{H}_4\text{Ru}_4(\text{CO})_{10}(\text{L})]$ (where L= NMDPP, DUPHOS, DIPAMP and DIOP) are able to catalyze the asymmetric hydrogenation of tiglic acid albeit with relatively low selectivity (ee's varying from 0 to 23%).²⁰

In order to find potentially more reactive transition metal clusters, we have studied different transition metal (Re, Os and Ru) carbonyl clusters that are bridged and/or chelated by different chiral mono- and diphosphine/phosphirane ligands. Figure 3.1 shows the different chiral ligands used in this study.



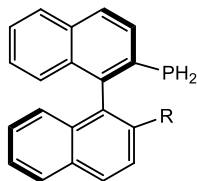
11a; $R^1 = 3,5-(CH_3)_2C_6H_3$, $R^2 = 3,5-(CF_3)_2C_6H_3$

11b; $R^1 = t\text{-Bu}$, $R^2 = O\text{-}C_4H_9$



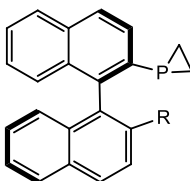
12a; $R^1 = 3,5-(CF_3)_2C_6H_3$, $R^2 = 3,5-(CH_3)_2-4-(OCH_3)C_6H_2$

12b; $R^1 = Cy$, $R^2 = Ph$



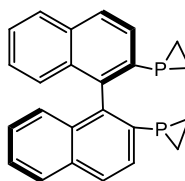
13a; $R = H_2$

13b; $R = OMe$



14a; $R = H$

14b; $R = OMe$



15

Figure 3.1. Different chiral phosphine and phosphirane ligands used in this investigation. Ligands **11a-12b** are discussed in paper III, **13a** and **13b** in paper IV, and **15** in paper V.

3.2.1 Synthesis of rhenium-based catalysts (paper III)

Rhenium carbonyl complexes were synthesized by either (i) thermal substitution on the parent cluster $[Re_3(\mu\text{-}H)_3(CO)_{10}(NCMe)]$ **16** in octane in the presence of the diphosphine (**11a-12b**), or (ii) *in situ* generation of **16** from the reaction of $[Re_2(CO)_8(NCMe)_2]$ **17** in toluene with hydrogen, followed by the addition of the chiral diphosphine ligand (**11a-12b**). A schematic depiction of the structures of the different complexes prepared in this study, describing the different phosphine coordination modes detected, is shown in Figure 3.2.

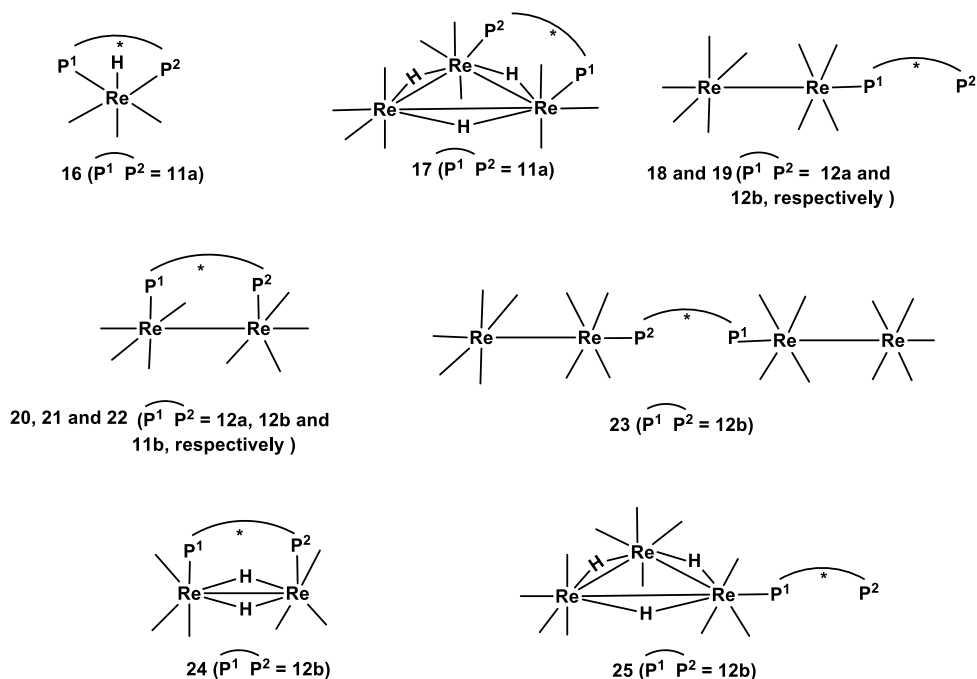
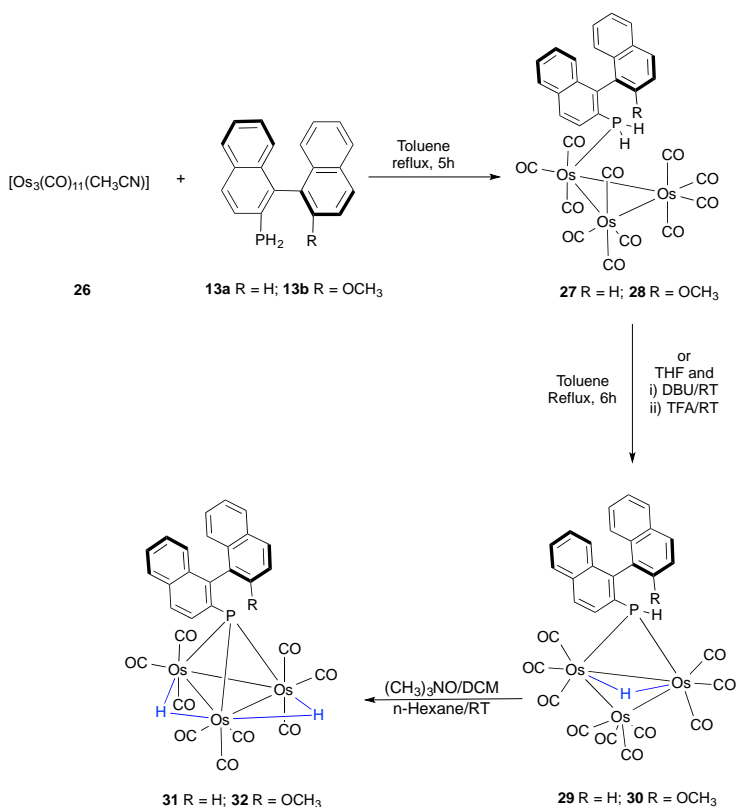


Figure 3.2. Schematic structures of the coordination modes of the diphosphine ligands (11a-12b) in the new rhenium complexes that have been prepared (16-25).

3.2.2 Synthesis of osmium-based catalysts (paper IV)

Osmium clusters containing the chiral primary monophosphine ligands **13a** and **13** were synthesized by reaction between [Os₃(CO)₁₁(NCMe)] **26** and **13a** or **13b** in dichloromethane at room temperature. The formation of one product was observed in each case after *ca.* 2h (Scheme 3.2). After purification, yellow solids were isolated in good yield, and the products were characterized as the clusters **27/28**, with the primary phosphine bound to one of the osmium centres. The phosphide-bridged complexes **29/30** were generated either from sequential deprotonation-protonation reactions or by thermolysis in toluene. Reacting the edge-bridged phosphido clusters **29/30** with 1 eq. of trimethylamine *N*-oxide at room temperature gave the phosphinidene derivatives **31/32** (Scheme 3.2) (*cf.* Paper IV for detailed synthetic procedures).



Scheme 3.2. Synthesis of the osmium clusters **27-32**.

3.2.3 Synthesis of ruthenium-based catalysts (papers IV and V)

Our next objective was to investigate the effect of changing the group eight metal to ruthenium. Reaction of tri- and tetra ruthenium cores with the chiral primary phosphines **13a/13b** and phosphiranes **14a/14b** and **15** gave the phosphine-, phosphido- and phosphinidene-capped clusters **33-49** (*cf.* Papers IV and V for detailed synthetic procedures). Figure 3.3 shows schematic structures for the new ruthenium carbonyl clusters.

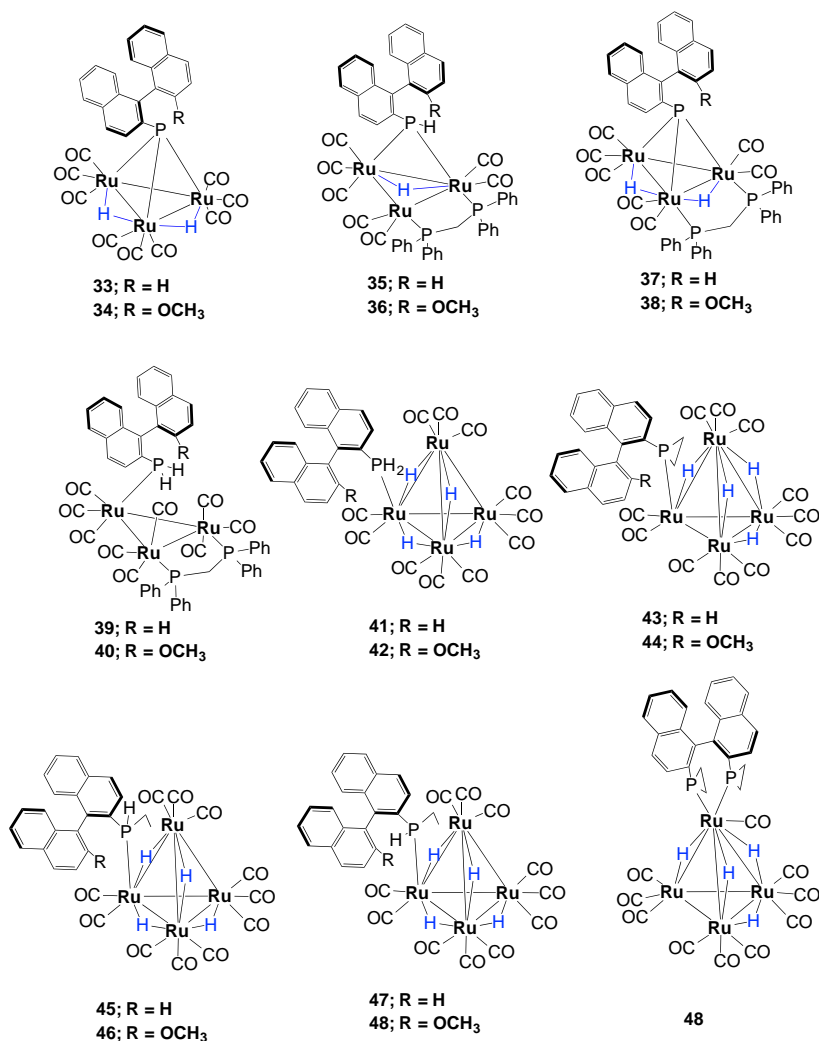


Figure 3.3. Schematic structures of new ruthenium clusters that have been prepared in this study.

3.2.4 Characterization

All clusters were identified via IR, ¹H and ³¹P NMR spectroscopy, mass spectrometry and, wherever possible, X-ray crystallography (*cf.* Papers III, IV and V for detailed discussion). Selected XRD structures are shown in Figure 3.4.

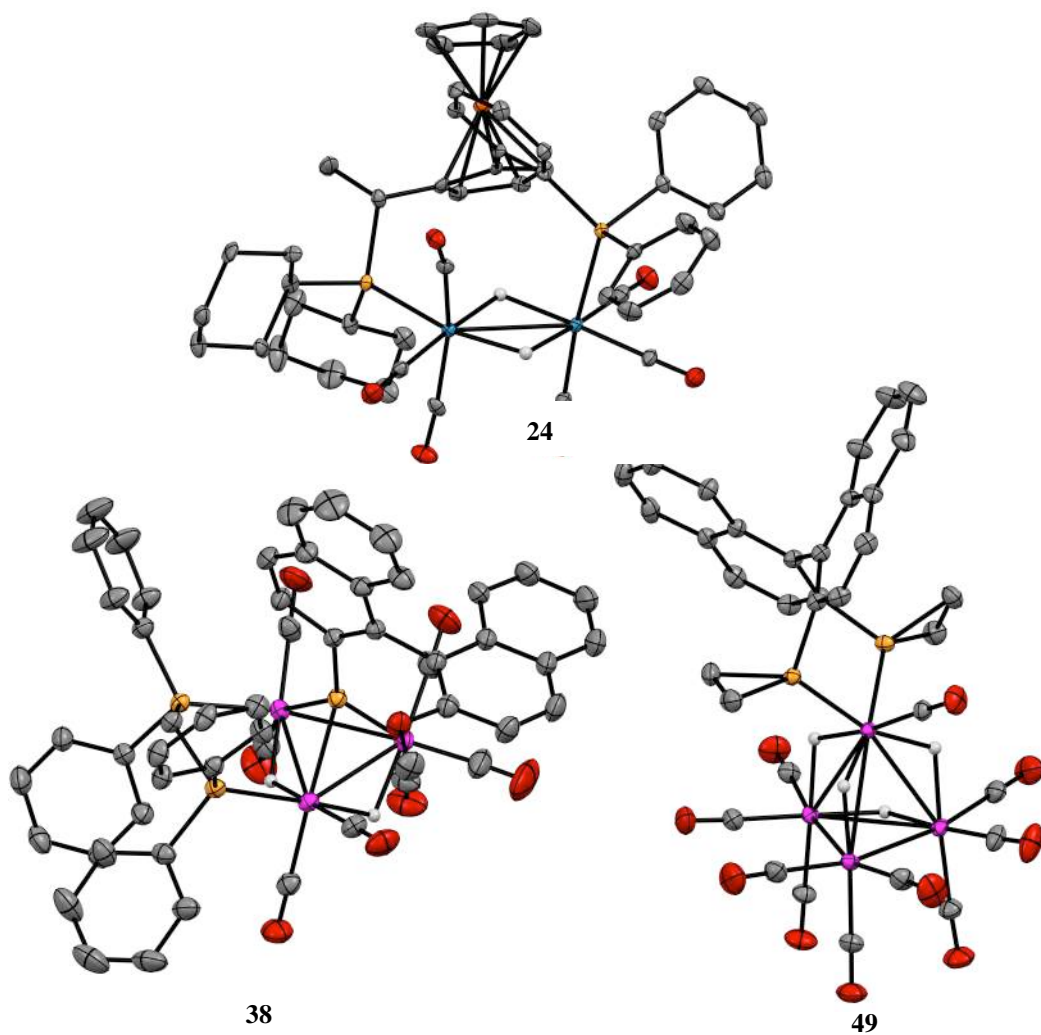


Figure 3.4. Selected XRD structures for clusters $[(\mu\text{-H})_2\text{Re}_2(\text{CO})_6(\mathbf{12b})]$ **24**, $[(\mu\text{-H})_2\text{Ru}_3(\text{CO})_7(\mathbf{13b})]$ **38** and $[(\mu\text{-H})_4\text{Ru}_4(\text{CO})_{10}(\mathbf{15})]$ **49**.

3.3 Catalytic asymmetric hydrogenation study

All clusters were tested as catalysts for asymmetric hydrogenation of tiglic acid. The reaction were carried out under relatively mild conditions that have been

demonstrated to be efficient for hydrogenation of α -unsaturated carboxylic acids using cluster of the general formula $[(\mu\text{-H}_4)\text{Ru}_4(\text{CO})_{10}(\text{P-P}^*)]$ (where P-P*= chiral phosphine ligands).^{19, 20} The results of the catalytic experiments and determined enantiomeric excesses are shown in Table 3.1.

Table 3.1. Summary of catalytic asymmetric hydrogenation activity for selected cluster catalysts/catalysts precursor.

Entry	Catalyst	Conversion %	ee %	Configuration
1	16 /24h	33	8	<i>R</i>
2	16 /48h	38	8	<i>R</i>
3	16 /72h	52	8	<i>R</i>
4	17	33	-	-
5	24	88	57	<i>R</i>
6	25	15	13	<i>R</i>
7	29	0	-	-
8	30	0	-	-
9	31	9	-	-
10	31 /72h	92	-	-
11	32	70	-	-
12	32 /72h	90	-	-
13	33	7	-	-
14	34	18	1	<i>R</i>
15	37	78	-	-
16	38	38	-	-
17	41	77	7	<i>R</i>
18	41 /48h	94	7	<i>R</i>
19	41 /72h	99	7	<i>R</i>
20	42	99	19	<i>R</i>
21	43	51	-	-
22	44	48	-	-
23	45	52	-	-
24	46	49	-	-
25	46 /48h	78	-	-
26	47	55	-	-
27	48	51	-	-
28	48 /48h	80	-	-
29	49	51	-	-

All clusters containing bridging diphosphines from the Josiphos (**11a-11b**) and Walphos (**12a-12b**) families show moderate catalytic activity in terms of conversion and enantioselectivity in the hydrogenation of tiglic acid.

Clusters **16**, **17**, **24** and **25** give (*R*)-2-methylbutyric acid with an enantiomeric excess of 8-57%. While catalysts based on Josiphos ligands (**16** and **17**) gave no, or very low, enantioselectivity, the clusters derivatised with Walphos ligands (**24** and **25**) resulted in good enantioselectivities. This is in agreement with observations for the same catalytic reaction using $[\text{Ru}_4(\mu\text{-H})_4(\text{CO})_{10}(\text{P-P}^*)]$ clusters,¹⁹ where Walphos derivatives consistently gave better enantioselectivities relative to Josiphos derivatives (*cf.* paper III for full details).

The cluster derivatives of the chiral ligands **13a/13b**, **14a/14b** and **15** performed poorly in the catalytic hydrogenation of tiglic acid, with conversion rates ranging from 7 to 99% and a maximum enantiomeric excess (ee) of 19%. In general, the trinuclear osmium clusters **31** and **32** show low reactivity in the catalytic hydrogenation of tiglic acid in comparison with analogous ruthenium clusters. This may be due to the fact that osmium cluster have higher thermal and oxidative stability than their ruthenium analogous, due to the stronger metal-metal bonding in osmium clusters.⁶⁷

The chiral phosphine clusters **41** and **42** were more active in the hydrogenation of tiglic acid than the chiral phosphirane clusters **43-49**. The different substitution in the 2'-position of ligands **13a/b** (H and OMe) leads to a significant difference in the catalytic activity behaviour, so that cluster **32** shows high conversion rate (70%) in comparison with **31** (only 9%) under the same catalytic conditions. Extending the reaction time for both catalysts improves the conversion rate, as expected. The phosphinidene clusters **31** and **32** did not show enantioselectivity, while the tetraruthenium hydride clusters **41** and **42** based on ligands **13a/b** gave low enantioselectivity (enantiomeric excesses varying from 7 to 19%, *cf.* Table 3.1, entries 17 and 20). The analogous clusters **43** and **44** based on ligands **14a/b** showed low conversion rates and no enantioselectivities were observed (*cf.* Table 3.1, entries 21 and 22). The chelated tetraruthenium hydride cluster **49** shows moderate conversion rate with no enantiomeric excesses (*cf.* Table 3.1, entry 21) (*cf.* papers IV and V for full details).

Decomposition of catalyst **49** during the catalysis experiment to give heterogeneous black solid particles was observed. This decomposition is accompanied by the formation of considerable amounts of cyclohexenes and cyclohexane due to hydrogenation of the solvent.²⁰ On the other hand, the phosphinidene clusters **31** and **32** showed high stability under the same catalytic conditions and could be recovered unchanged. After a complete catalytic reaction using cluster **42** (Table 3.1, entry 20), one cluster species was recovered *viz.*, cluster **34**. The difference in the catalytic activity for both clusters (Table 3.1, entries 14 and 20) indicates that cluster **42** stays as an active catalytic species, and possible cluster fragmentation to form **34** occurs at the end of the catalytic cycle.

3.4 Concluding remarks

The catalytic activity of the synthesized rhenium, osmium and ruthenium clusters derivatised with chiral mono/diphosphine and phosphiranes ligands show, in general, good conversion rates but the enantioselectivities are relatively low, albeit good when compared to most other cluster-based catalytic systems for asymmetric reactions.⁵⁸⁻⁶² The rhenium clusters containing diphosphines of the Walphos family gave better enantioselectivities than the related Josiphos-containing clusters, in keeping with observations made for other cluster-based systems;⁵² this highlights the importance of the specific chiral diphosphine ligand for the catalytic performance. The osmium clusters show poor conversion rates and no enantioselectivities. The tetraruthenium hydride cluster shows high conversion rates but low enantioselectivity. Clearly, the choice of (transition) metal, nuclearity, chiral ligand and ancillary ligands all have an effect on the catalytic properties of metal clusters, and optimum catalytic performance may only be obtained after careful optimization of these parameters as well as catalytic reaction conditions.

Chapter 4. Cluster-based single-site heterogeneous catalysts for asymmetric hydrogenation reactions (paper VI)

4.1 Background

Homogeneous asymmetric synthesis is probably one of the most important developments in chemistry that has taken place during the last decades.^{68, 69} Thousands of different chiral ligands and their corresponding transition metal complexes have been synthesized, characterized and evaluated as catalysts in different asymmetric transformations. However, despite the large amount of work devoted to this area of research, until now only a few examples of homogeneous asymmetric catalysis have been developed in the chemical industry. The limited industrial applications are due to the problems of separation and recycling of the relatively expensive chiral catalysts from the reaction mixtures at the end of the catalytic processes. On the other hand, heterogeneous catalysts are, as a rule, not capable of providing good results in asymmetric synthesis. In 1996, during his research on the feasibility of effecting enantioselective hydrogenation of prochiral reactants, Bruner stated that *“the limited success of heterogeneous catalysts in enantioselective reactions is due to the fact that on the surface of a heterogeneous catalyst there are many different catalytically active centers. Each of these centers has its own selectivity and the total selectivity is usually low”*.⁷⁰

Thus, a novel class of catalysts is needed to fill the gap between homogeneous and heterogeneous catalysis, which may combine the advantages of both of them. For this reason, many scientists have focused on the preparation of single site heterogeneous catalysts. For this purpose, different protocols for immobilizing homogeneous chiral catalysts in/on heterogeneous solids have been pursued. J.M. Thomas and coworkers have realized that open-structure solids can, with relatively few modification steps, be used to design new heterogeneous catalysts that can simulate the behaviour of homogeneous and enzymatic catalysts.⁷¹ These investigators have carried out a considerable number of investigations on Single Site Heterogeneous Catalysts, SSHC, and Thomas has defined SSHC as spatially isolated homogeneous catalysts on an inorganic solid surface.^{72, 73}

In general, four distinct methods are available for the heterogenization of homogeneous chiral catalysts on a solid support: (i) by formation of a covalent bond with the chiral catalyst; (ii) by adsorption or ion-pair formation; (iii) by entrapment (*i.e.* building up support cages such as zeolites or a polymer network around a preformed catalytic metal complex); and (iv) by encapsulation (*i.e.* opposite to entrapment, building up the complex inside of a preformed support). Generally, covalent bonds between the chiral catalyst and the solid support is the most often employed method of heterogenization of an enantioselective homogeneous catalyst, as the resultant catalyst will be very stable to leaching. However, the chiral catalyst and/or support must be functionalized in such a way that it is able to effect immobilization. After immobilization, the support materials need to be chemically and thermally stable during the catalytic reaction cycle. Moreover, the active sites in the support structure should be well dispersed and easily accessible. Basically, this requires the support to have a reasonably high surface area ($>100 \text{ m}^2\text{g}^{-1}$) and suitable pore size ($>20 \text{ \AA}$) in order to allow easy diffusion of the reactant to the active sites.⁷⁴ Generally, inorganic supports such as silica, zeolite, alumina, clay, ZnO, *etc.* meet these requirements. There are two distinct classes of chiral catalysts heterogenized on inorganic supports, (i) chirally modified supported metal catalysts, and (ii) immobilized homogeneous chiral catalysts. The former class of heterogeneous chiral catalyst is the most important type.

Greater light has been shed on the immobilization of metal clusters on inorganic solid supports, especially silica, in such a way that the catalyst selectivity is enhanced. Silica was chosen as a support material in view of its numerous practical advantages, (i) it does not swell on exposure to solvent or reactant, (ii) it is highly stable under high temperature and pressure, (iii) it is highly stable during the repeated recycling of the catalyst and the final separation of the products, and (iv) it is easy to prepare (compared with, for example, encapsulation or entrapment within zeolites). The silica material MCM-41 is one of the members of this extensive family of mesoporous sieves and is probably the most commonly used silica material for immobilization of homogeneous catalysts. It is often proposed as a model mesoporous adsorbent. The MCM-41 mesopore consists of an array of uniform hexagonal channels of tuneable size, with diameters ranging from 2 to 10 nm. The larger pore materials typically have surface areas above $700 \text{ m}^2\text{g}^{-1}$. The homogeneity of the pores, the good thermal stability of the material and its high surface area are reasons that make it an attractive molecular sieve for different catalytic applications.⁷⁵

Thomas, Johnson and coworkers have anchored bimetallic nanoparticles (Ru_6Pd_6 , Ru_6Sn , $\text{Ru}_{10}\text{Pt}_2$, Ru_5Pt , $\text{Ru}_{12}\text{Cu}_4$, and $\text{Ru}_{12}\text{Ag}_4$) within MCM-41 and investigated their catalytic activities in selective hydrogenation of different substrates at low temperatures (333-373 K). The catalysts show high efficiency, especially in the

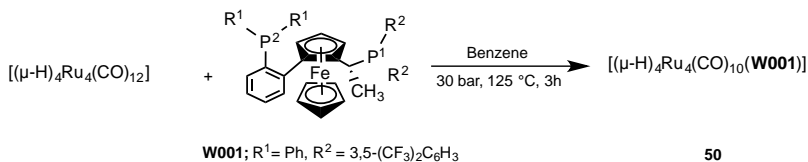
selective hydrogenation of polyenes (such as 1,5,9-cyclododecatriene and 2,5-norbornadiene).⁷⁶ Johnson and coworkers have used a non-covalent immobilization approach for tethering four constrained chiral Rh catalysts and investigating their ability to act as catalysts in the asymmetric hydrogenation of methyl benzoylformate to the corresponding methyl mandelate.⁷⁷ They also showed that immobilization of a chiral catalyst is possible, via anchoring of the diphosphine ligand dppf {1,1-bis(diphenylphosphino)ferrocene} to the inner wall of MCM-41 and coordination of this ligand to Pd^{II}. The catalyst was shown to exhibit superior performance in the allylic amination of cinnamyl acetate, the performance being far good to that of its homogeneous counterpart.⁷⁸ Similarly, Bianchini and coworkers have anchored optically active Rh(I)-chiral diphosphine complexes in porous silica via hydrogen bonding and have evaluated their catalytic activities in the asymmetric hydrogenation of olefins.⁷⁹

Different transition metal carbonyl clusters (*e.g.* [Ru₆C(CO)₁₆Cu₂Cl]²⁻, [Ru₅PtC(CO)₁₂]²⁻ and [Ru₁₂C₂(CO)₃₂Cu₄Cl₂]²⁻) have been deposited onto MCM-41 without any change in the characteristic carbonyl stretching frequencies, implying that they remain intact.⁴⁰ The anionic tetraruthenium carbonyl cluster [Ru₄(μ-H)₃(CO)₁₂]⁻ has been ion-paired with (3-chloropropyl)-trimethoxysilyl-cinchonidium chemically bonded to MCM-41 and the resultant material has shown good conversion (≤75%) and observable enantioselectivities (≤30%) in the asymmetric hydrogenation of methyl pyruvate.⁸⁰

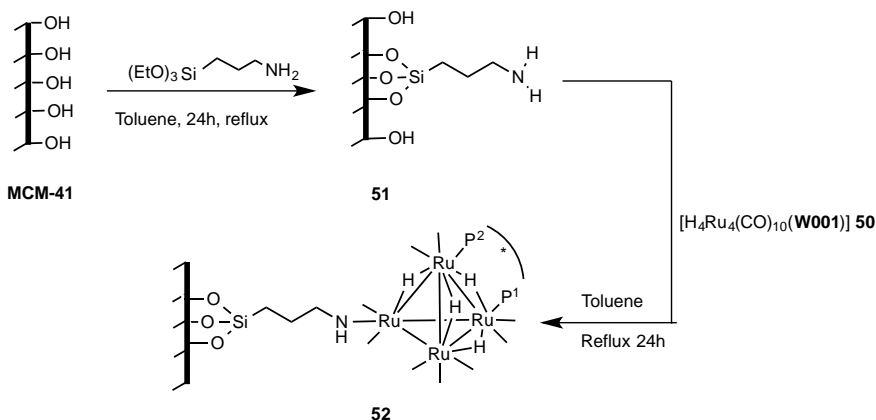
4.2 Synthesis of single-site chiral transition metal cluster immobilized on functionalized MCM-41

In previous studies, it has been shown that homogeneous catalytic systems based on [(μ-H)₄Ru₄(CO)₁₀(μ-1,2-W001)] **50** are very effective for asymmetric hydrogenation reactions of α-unsaturated carboxylic acids.^{19, 53} Considering the methods of heterogenization of molecular transition metal catalysts discussed above, we decided to tether the pre-formed, well-characterized chiral cluster **50** within functionalised MCM-41. The approach to the preparation of the catalytic system is shown in Scheme 4.1. The mesoporous framework was first treated with (3-aminopropyl)triethoxysilane to form the functionalized silica material **51**. Treatment of the activated MCM-41 **51** with an excess of the chiral cluster [(μ-H)₄Ru₄(CO)₁₀(μ-1,2-W001)] **50** gave the chiral single site solid catalyst **52** (*cf.* paper VI for full details).

1. Cluster Preparation



2. Cluster immobilization strategy



Scheme 4.1. Synthesis and immobilization of the chiral $[(\mu\text{-H})_4\text{Ru}_4(\text{CO})_{10}(\mu\text{-1,2-W001})]$ **50** onto functionalized silica **51** yielding the solid catalyst **52**.

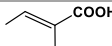
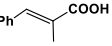
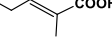
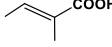
The solid catalyst **52** was fully characterised by a range of techniques, including ICP-MS, FT-IR, low angle X-ray powder diffraction, ^{31}P and ^1H CP-MAS solid state NMR, TEM, SEM and BET (*cf.* paper VI for full details).

4.3 Catalytic asymmetric hydrogenation of α -unsaturated carboxylic acid substrates

The chiral transition metal carbonyl cluster $[(\mu\text{-H})_4\text{Ru}_4(\text{CO})_{10}(\mu\text{-1,2-W001})]$ **50** and the new solid catalyst **52** were evaluated in the asymmetric hydrogenation of benchmark α -unsaturated carboxylic acid substrates, as their hydrogenated products are very important in the pharmaceutical industry.⁸¹ Tiglic acid, α -methylcinnamic acid and *trans*-2-methyl-pentenoic acid were chosen in this investigation since they have been used in earlier assessments,¹⁹ and well-established protocols for the evaluation of enantiomeric excess exist.⁵⁷

Preliminary results of the studies are listed in Table 4.1. In the hydrogenation of tiglic acid, the homogeneous catalyst $[(\mu\text{-H})_4\text{Ru}_4(\text{CO})_{10}(\mu\text{-1,2-W001})]$ **50** shows excellent catalytic conversion ($\approx 100\%$) with high enantiomeric excess, approaching 82%. Under the same catalytic conditions, similar catalytic behaviour for the solid catalyst **52** could be observed, i.e. excellent conversion rate with high enantiomeric excess and mass balance. The catalytic efficiency of $[(\mu\text{-H})_4\text{Ru}_4(\text{CO})_{10}(\mu\text{-1,2-W001})]$ **50** and the solid catalyst **51** was further investigated for the hydrogenation of α -methylcinnamic acid and *trans*-2-methyl-pentenoic acid. The collective results indicate that both catalysts **50** and **52** are able to hydrogenate α -unsaturated carboxylic acid substrates with full conversion ($\approx 100\%$) coupled with high enantioselectivity (up to 75% ee in the case of α -methylcinnamic acid and 68% ee for *trans*-2-methyl-pentenoic acid).

Table 4.1. Asymmetric hydrogenation of tiglic acid, α -methylcinnamic acid and *trans*-2-methyl-pentenoic acid catalyzed by $[(\mu\text{-H})_4\text{Ru}_4(\text{CO})_{10}(\mu\text{-1,2-W001})]$ **50** (in homogeneous phase) and solid catalyst **52** (in heterogeneous phase).

Substrate	Catalyst	Mass balance %	Conversion %	ee %	Configuration
	50	> 70	100	82	<i>S</i>
	52	> 90	100	80	<i>S</i>
	50	> 70	100	75	<i>S</i>
	52	> 90	100	74	<i>S</i>
	50	> 70	100	68	<i>S</i>
	52	> 90	100	66	<i>S</i>
	52+Hg	> 90	99	78	<i>S</i>

4.4 Recycling experiments and nature of the active catalyst

The major advantage of using a heterogenized catalyst is the ease with which the solid catalyst may be recovered as a stable species from the reaction mixture and reused. To investigate catalyst recycling, the solid catalyst **52** was recovered after the catalytic hydrogenation of tiglic acid and reused for three runs under the same catalytic hydrogenation conditions, with fresh tiglic acid as a substrate. Identical catalytic performance was observed in all cases.

Furthermore, the nature of the catalyst was confirmed by a hot filtration test²² and a mercury poisoning test. The obtained results demonstrated that the conversion and enantioselectivity are due to the solid catalyst, i.e. **52**. It is important, however, to draw attention to the fact that mercury is not able to form a stable amalgam with all metals.²³

4.5 Concluding remarks

It has been demonstrated that anchoring of a chiral ruthenium cluster onto functionalized MCM-41 is a valid strategy for the preparation of a viable heterogenized catalyst. The resultant single-site heterogeneous catalyst was observed to be highly active, selective, and recyclable for use in the asymmetric hydrogenation of α -unsaturated carboxylic acid substrates. The generality of this catalyst immobilization method should open a new window for the design of many highly active and enantioselective cluster-based single-site heterogeneous catalysts.

Chapter 5. Concluding remarks and future perspectives

In summary, this thesis presents the synthesis and characterization of new transition metal carbonyl cluster systems intended for, (i) providing direct evidence for intact cluster catalysis (papers I and II), (ii) investigation into their viability to act as catalysts/catalyst precursors in asymmetric reactions (papers III- V) and (iii) preparation of highly active and enantioselective cluster-based single-site heterogeneous asymmetric catalysts (paper VI).

(i) Diastereomeric clusters of the general formula $[(\mu\text{-H})_2\text{Ru}_3(\mu_3\text{-S})(\text{CO})_7(\mu\text{-1,2-L})]$ (L= chiral diphosphine ligand), containing chiral cluster frameworks, have been prepared and characterized. The reactivities of these cluster diastereomers towards the catalytic hydrogenation of tiglic acid under relatively mild conditions reveal different catalytic behaviour in terms of conversion and enantioselectivity. The reversal in enantioselectivity of the hydrogenation reaction when the chirality of the cluster framework is changed, while the chirality of the ligand remains intact, strongly implicates the involvement of intact Ru_3 clusters as the active hydrogenation catalysts. The conversion rates are relatively good but the enantioselectivities are low, albeit good when compared to most other cluster-based catalytic systems for asymmetric reactions. Computational modeling for the proposed catalytic cycle have been performed and they have provided information on a possible mechanism for hydrogenation of tiglic acid by $[(\mu\text{-H})_2\text{Ru}_3(\mu_3\text{-S})(\text{CO})_7(\mu\text{-1,2-L})]$ clusters (papers I and II).

(ii) Transition metal carbonyl clusters based on rhenium (paper III), ruthenium and osmium (papers IV and V) have been tested as catalysts/catalyst precursors for asymmetric hydrogenation of the prochiral substrate tiglic acid. The reactivity of rhenium clusters derivatised with diphosphine ligands of the Walphos and Josiphos families (ferrocene-based chiral ligands) have been studied. The rhenium clusters showed good conversion rates but the enantioselectivities are relatively low. The rhenium clusters containing diphosphines of the Walphos family gave better enantioselectivities than the related Josiphos-containing clusters, in keeping with observations made for other cluster-based systems.

The ability of tri- and tetraruthenium and triosmium cores derivatised with chiral primary phosphines and phosphiranes to catalyse the asymmetric hydrogenation of

tiglic acid was then examined. Relatively high to excellent catalytic conversions were observed, while low (or no) enantioselectivity was generated by the majority of the clusters. The cluster $[(\mu\text{-H})_4\text{Ru}_4(\text{CO})_{11}(\text{ArPH}_2)]$ {where $\text{ArP} = (R)\text{-}(2'\text{-methoxy-[1,1'-binaphthalen]-2-ylphosphine)}$ } was capable of achieving a conversion of 99% and an enantioselectivity of 19%, which is, to the best of our knowledge, the first example of an asymmetric hydrogenation induced by a chiral primary phosphine. The results obtained in this part of the thesis highlight the importance of the specific chiral ligands for the catalytic performance/chiral induction.

(iii) The chiral catalyst $[\text{H}_4\text{Ru}_4(\text{CO})_{10}(\mu\text{-1,2-W001})]$ (W001= the Walphos ligand $(R)\text{-}1\text{-}\{(R_P)\text{-}2\text{-}[2\text{-}(\text{diphenylphosphino})\text{phenyl}]\text{ferrocenyl}\}\text{ethylbis-}[3,5\text{-bis}(\text{trifluoromethyl})\text{phenyl}]\text{phosphine}$) has been immobilized on functionalized MCM-41. The reactivity of the solid catalyst in the hydrogenation of α -unsaturated carboxylic acids has been investigated. Excellent conversion rates (> 99%) high enantiomeric excesses ($\approx 80\%$), and excellent recyclability was obtained.

5.1 Future perspective of the present work

The work presented in Chapters 2 and 3 has introduced direct evidence for intact cluster catalysis in trying to answer the well-known question regarding cluster-based catalysts – is the catalysis due to the intact cluster, or due to catalysts generated by fragmentation of the cluster to form mononuclear species or, alternatively, colloidal metal aggregates? Furthermore, the different abilities of the synthesized clusters to act as catalysts for asymmetric hydrogenation reactions serve to emphasize the influence of the nature of the phosphine ligand on catalytic performance.

Development of efficient high-performance recyclable heterogeneous catalysts for asymmetric reactions that may be utilized in an industrial setting remains a challenging task. The studies summarized in Chapter 4 suggest a new strategy to accelerate the arrival of reliable, robust heterogeneous asymmetric catalysts. The excellent catalytic activity of ruthenium cluster-functionalized MCM-41 in the asymmetric hydrogenation of α -unsaturated carboxylic acids suggests that such single site heterogeneous catalysts can be employed for hydrogenation of many other substrates of interest. So far as the use of this approach to constrained chiral catalysis is concerned, we demonstrate that highly enantioselective hydrogenation of α -unsaturated carboxylic acids that yields products of considerable commercial significance, has been achieved. This opens the field to further studies on the immobilization of chiral clusters to generate mesoporous materials that warrant thorough investigation as catalysts for asymmetric reactions.

Populärvetenskaplig Sammanfattning

Kemisk industri, inklusive petrokemisk industri, är en av de största av alla världens industrier. Mer än 60% av de produkter som framställs och 90% av de processer som används inom kemisk industri är baserade på katalys. Det är tydligt att katalytiska processer utgör en mycket viktig del av ett antal av de största industrierna och att stora ekonomiska vinningar därför kan göras genom förbättring av sådana processer. Allmänhetens ökade uppmärksamhet på negativa miljöeffekter av kemikalier och industriella utsläpp utgör dessutom en drivkraft för utveckling av miljöekonomiska och återvinningsbara katalysatorer.

För närvarande kan man se många spännande utmaningar för utveckling av nya katalysatorer och för att förbättra befintliga katalysatorer. Så, vad är katalysatorer, dessa fantastiska substanser som möjliggör utveckling av bättre kemiska produkter och på så vis har en stark effekt på hälsa, ekonomi och livskvalitet? En katalysator är en substans som underlättar kemiska reaktioner genom att möjliggöra en annorlunda, mindre energikrävande reaktionsväg än den för den icke-katalyserade reaktionen, utan att själv förbrukas under reaktionen.

Denna avhandling behandlar syntes av ett antal flerkärniga metallkomplex med metall-metallbindningar, såsom metallkluster, innehållande rhenium, osmium eller rutenium, samt utvärdering av deras förmåga att användas som katalysatorer för hydreringsreaktioner (reduktion av ett kolväte med hjälp av väte), i synnerhet reaktioner som ger optiskt aktiva molekyler. De erhållna produkterna kan fungera som viktiga byggstenar för andra kemiska produkter, till exempel inom läkemedelsindustrin. De erhållna resultaten i denna avhandling kan bidra till utveckling och design av nya aktiva, miljöekonomiska och återvinningsbara katalysatorer för användning i industriell produktion av kemikalier.

Acknowledgement

First and foremost, I would like to praise and thank ALLAH, the almighty, who has granted countless blessing, patience and knowledge, so that I have been able to accomplish this work.

This thesis arose out of four years of research that have been done since I joined the Nordlander group. From my first day, I have worked with a great number of people, whose contributions in various ways to the research and the making of this thesis deserve special mention. It is a pleasure to convey my gratitude to them all in my humble acknowledgment.

Ebbe Nordlander, there are no words in my vocabulary that can describe my gratitude to you. Thank you for your supervision, advice, and guidance from the early stage of this research as well as giving me extraordinary experiences throughout the work, for all the discussions covering small and large things in life. I am indebted to you more than you know.

I like to thank my co-supervisor *Ivan Scheblykin*, *Ola Wendt* and *Villy Sundström* for your kind assistance and attention whenever it was needed.

Part of my studies was carried out at other institutions. I would like to thank *Selwyn Mapolie* (Stellenbosch University, South Africa) for letting me stay in his group and for his hospitality and I also wish to thank *Alan Hutton* (University of Cape Town, South Africa) for his time and hospitality.

I would also like to take the opportunity to thank all my scientific co-workers in addition to those mentioned above; *Matti Haukka* and *Magda Monari* for your vital help with X-ray crystallography, *Michael G. Richmond* for your computational work, *Lee Higham* for the primary phosphine and phosphiranes ligands, as well as football discussions, *Roberto Gobetto* for solid state NMR and *Göran Carlström* for invaluable help with NMR spectroscopy whenever it was needed.

I would like to thank all the present and past members of the *Nordlander* group, in particular *Mainak*, *Ahibur*, *Erik*, *Biswanath*, *Reena*, *Kamlesh*, *Satish*, *Martin*, *Arup*, *Lotta*, *Manjula*, *Amber* and *Kamal* for providing an excellent working atmosphere in our shared lab and office. Special thanks goes to *Amrendra*, *Maitham* and *Yusuf* for their nice contributions to my project, for the scientific time I have spent with you and for your friendship, mutual advice and help of any kind. For the same reasons my thanks also extend to the vast majority of co-workers in the division of Chemical Physics in general.

There are a number of people in the Chemical Physics Department that I would like to thank for providing different types of services that strongly facilitated my research project: *Arkady* (thank you for the great table tennis games), *Tönu* and *Donatas*.

I convey special acknowledgment to *Thomas* and *Maria* for their indispensable help dealing with travel funds, administration and bureaucratic matters during my stay.

I was extraordinarily fortunate in having *Prof. Mohsen M. Ali* as my professor in the Nuclear Material Authority, Cairo, Egypt. I could never have embarked and started all of this without his help.

It is a pleasure to express my gratitude wholeheartedly to my Egyptian friends here in Sweden: *M. Abdellah* (good luck with your upcoming defense), *H. El-taliawy*, *S. Alghool*, *T. Silem*, *A. Shokry*, *W. Awad*, *W. Mobarak*, *M. Fikry*, *A. Mousa*, *M. Saied*, *M. Hagars*, *M. Reda*, etc.

I would like to thank all the people I have met at Smörlyckan and Victoria for sharing with me their immeasurable passion as football.

I am dedicating this thesis to the soul of my father *Fawzy* who laid the fundament to my learning character, showing me the joy of intellectual pursuit ever since I was a child. My mother, *Nabila*, is the one who sincerely raised me with her caring and prayers. Many thanks to my father-in-law *Mohamed*, and my mother-in-law *Azaa* for their help and support. Thank you to my brothers Mohamed, Osama and my sisters Samah and Basama for their support, understanding and encouragement in whatever choices I have made in life and for always believing in me.

Words fail me to express my appreciation to my dear wife, *Radwa* whose dedication, love and persistent confidence in me has taken the load off my shoulders. I could literally not have done it without all your support. I wish you all the best in your PhD studies. Yousseif, Joody and Yahia, I wish you all a prosperous future ahead, a lifetime of love, knowledge, achievement, and happiness.

The financial support from the Erasmus Mundus (FFEEBB program) is gratefully acknowledged.

Finally, I would like to thank everybody who was important to the successful realization of this thesis, as well as expressing my apology if I somehow forgot to express my gratitude to anyone that made this work possible. All may not be written, but nothing is forgotten.

References

1. J. F. Hartwig, *Organotransition metal chemistry : from bonding to catalysis*, University Science Books, Sausalito, Calif., 2010.
2. F. Cavani and F. Trifiró, *Catal. Today*, 1997, 34, 269-279.
3. D. M. P. Mingos and D. J. Wales, *Introduction to cluster chemistry*, 1990.
4. O. A. Adamenko, G. V. Lukova, N. D. Golubeva, V. A. Smirnov, G. N. Boiko, A. D. Pomogailo and I. E. Uflyand, *Dokl. Phys. Chem.*, 2001, 381, 275-278.
5. A. Simon, H. Georg Schnering, H. Wöhrle and H. Schäfer, *Z. Anorg. Allg. Chem.*, 1965, 339, 155-170.
6. Y. V. Mironov, M. A. Pell and J. A. Ibers, *Inorg. Chem.*, 1996, 35, 2709-2710.
7. M. R. Churchill, F. J. Hollander and J. P. Hutchinson, *Inorg. Chem.*, 1977, 16, 2655-2659.
8. E. R. Corey and L. F. Dahl, *Inorg. Chem.*, 1962, 1, 521-526.
9. J. A. Gladysz, *Angew. Chem. Int. Ed. Eng.*, 1990, 29, 438-438.
10. P. L. Pauson, J. P. Stambuli, T.-C. Chou and B.-C. Hong, in *Encyclopedia of Reagents for Organic Synthesis*, John Wiley & Sons, Ltd, 2001.
11. E. R. Corey, L. F. Dahl and W. Beck, *J. Am. Chem. Soc.*, 1963, 85, 1202-1203.
12. G. Schmid, in *Metal Clusters in Chemistry*, Wiley-VCH Verlag GmbH, 2008, ch4, pp. 1325-1341.
13. S. Kawi and B. C. Gates, *Inorg. Chem.*, 1992, 31, 2939-2947.
14. F. Hugues, J. M. Bassett, Y. B. Taarit, A. Choplin, M. Primet, D. Rojas and A. K. Smith, *J. Am. Chem. Soc.*, 1982, 104, 7020-7024.
15. H. H. Lamb, A. S. Fung, P. A. Tooley, J. Puga, T. R. Krause, M. J. Kelley and B. C. Gates, *J. Am. Chem. Soc.*, 1989, 111, 8367-8373.
16. R. Pierantozzi, E. G. Valagene, A. F. Nordquist and P. N. Dyer, *J. Mol. Catal.*, 1983, 21, 189-202.
17. D. Roberto, R. Psaro and R. Ugo, *Organometallics*, 1993, 12, 2292-2296.
18. R. Mutin, W. Abboud, J. M. Basset and D. Sinou, *Polyhedron*, 1983, 2, 539-541.
19. V. Moberg, R. Duquesne, S. Contaldi, O. Rohrs, J. Nachtigall, L. Damoense, A. T. Hutton, M. Green, M. Monari, D. Santelia, M. Haukka and E. Nordlander, *Chem. Eur. J.*, 2012, 18, 12458-12478.
20. V. Moberg, P. Homanen, S. Selva, R. Persson, M. Haukka, T. A. Pakkanen, M. Monari and E. Nordlander, *Dalton Trans.*, 2006, 279-288.
21. Y. Lin and R. G. Finke, *Inorg. Chem.*, 1994, 33, 4891-4910.
22. J. A. Widegren and R. G. Finke, *J. Mol. Catal.*, 2003, 198, 317-341.
23. R. H. Crabtree, *Chem. Rev.*, 2011, 112, 1536-1554.
24. B. R. James, in *Advances in Organometallic Chemistry*, eds. F. G. A. Stone and W. Robert, Academic Press, 1979, vol. Volume 17, pp. 319-405.

25. C. Masters, in *Advances in Organometallic Chemistry*, eds. F. G. A. Stone and W. Robert, Academic Press, 1979, vol. Volume 17, pp. 61-103.
26. F. Ungváry, *Coordin. Chem. Rev.*, 2001, 213, 1-50.
27. G. Süss-Fink, S. Haak, V. Ferrand and H. Stoeckli-Evans, *J. Mol. Catal.*, 1999, 143, 163-170.
28. D. C. D. Butler and D. J. Cole-Hamilton, *Inorg. Chem. Commun.*, 1999, 2, 305-307.
29. H. Brunner and W. Zettlmeier, *Handbook of enantioselective catalysis with transition metal compounds*, VCH, 1993.
30. M. Calvin and M. Polanyi, *Trans. Faraday Soc.*, 1938, 34, 1181-1191.
31. D. Evans, J. A. Osborn, F. H. Jardine and G. Wilkinson, *Nature*, 1965, 208, 1203-1204.
32. L. Horner, H. Siegel and H. Büthe, *Angew. Chem. Int. Ed. Eng*, 1968, 7, 942-942.
33. W. S. Knowles and M. J. Sabacky, *Chem. Commun.*, 1968, 1445-1446.
34. W. S. Knowles, M. J. Sabacky, B. D. Vineyard and D. J. Weinkauff, *J. Am. Chem. Soc.*, 1975, 97, 2567-2568.
35. A. Miyashita, A. Yasuda, H. Takaya, K. Toriumi, T. Ito, T. Souchi and R. Noyori, *J. Am. Chem. Soc.*, 1980, 102, 7932-7934.
36. M. J. Burk, *J. Am. Chem. Soc.*, 1991, 113, 8518-8519.
37. H.-U. Blaser, W. Brieden, B. Pugin, F. Spindler, M. Studer and A. Togni, *Top. Catal.*, 2002, 19, 3-16.
38. Y. Wang, T. Sturm, M. Steurer, V. B. Arion, K. Mereiter, F. Spindler and W. Weissensteiner, *Organometallics*, 2008, 27, 1119-1127.
39. K. Tappe and P. Knochel, *Tetrahedron*, 2004, 15, 91-102.
40. P. J. Dyson, *Coordin. Chem. Rev.*, 2004, 248, 2443-2458.
41. L. N. Lewis, *Chem. Rev.*, 1993, 93, 2693-2730.
42. J. D. Aiken III and R. G. Finke, *J. Mol. Catal.*, 1999, 145, 1-44.
43. R. D. Adams and T. S. Barnard, *Organometallics*, 1998, 17, 2567-2573.
44. P. Nombel, N. Lugan, B. Donnadiou and G. Lavigne, *Organometallics*, 1998, 18, 187-196.
45. G. Süss-Fink and G. Herrmann, *J. Chem. Soc., Chem. Commun.*, 1985, 735-737.
46. S. B. Duckett and R. E. Mewis, *Acc. Chem. Res.*, 2012, 45, 1247-1257.
47. D. Blazina, S. B. Duckett, P. J. Dyson and J. A. B. Lohman, *Angew. Chem. Int. Ed.*, 2001, 40, 3874-3877.
48. D. Blazina, S. B. Duckett, P. J. Dyson and J. A. B. Lohman, *Chem. Eur. J.*, 2003, 9, 1045-1061.
49. J. Norton, in *Fundamental Research in Homogeneous Catalysis*, eds. M. Tsutsui and R. Ugo, Springer US, ch. 4, pp. 99-114.
50. C. U. Pittman, M. G. Richmond, M. M. Absi-Halabi, H. Beurich, F. Richter and H. Vahrenkamp, *Angew. Chem.*, 1982, 94, 805-806.
51. R. D. Adams and D. A. Katahira, *Organometallics*, 1982, 1, 53-59.
52. V. Moberg, R. Duquesne, S. Contaldi, O. Röhrs, J. Nachtigall, L. Damoense, A. T. Hutton, M. Green, M. Monari, D. Santelia, M. Haukka and E. Nordlander, *Chem. Eur. J.*, 2012, 18, 12458-12478.
53. V. Moberg, M. Haukka, I. O. Koshevoy, R. Ortiz and E. Nordlander, *Organometallics*, 2007, 26, 4090-4093.

54. J.-R. Kong, M.-Y. Ngai and M. J. Krische, *J. Am. Chem. Soc.*, 2005, 128, 718-719.
55. K. Tanaka, Y. Hagiwara and K. Noguchi, *Angew. Chem. Int. Ed.*, 2005, 44, 7260-7263.
56. A. F. Abdel-Magied, A. K. Singh, M. Haukka, M. G. Richmond and E. Nordlander, *Chem. Commun.*, 2014, 50, 7705-7708.
57. E. Tyrrell, M. W. H. Tsang, G. A. Skinner and J. Fawcett, *Tetrahedron*, 1996, 52, 9841-9852.
58. U. Matteoli, V. Beghetto and A. Scrivanti, *J. Mol. Catal.*, 1996, 109, 45-50.
59. U. Matteoli, M. Bianchi, P. Frediani, G. Menchi, C. Botteghi and M. Marchetti, *J. Organomet. Chem.*, 1984, 263, 243-246.
60. U. Matteoli, G. Menchi, P. Frediani, M. Bianchi and F. Piacenti, *J. Organomet. Chem.*, 1985, 285, 281-292.
61. C. Botteghi, S. Gladiali, M. Bianchi, U. Matteoli, P. Frediani, P. G. Vergamini and E. Benedetti, *J. Organomet. Chem.*, 1977, 140, 221-228.
62. M. Bianchi, U. Matteoli, G. Menchi, P. Frediani, F. Piacenti and C. Botteghi, *J. Organomet. Chem.*, 1980, 195, 337-346.
63. Y. Doi, K. Koshizuka and T. Keii, *Inorg. Chem.*, 1982, 21, 2732-2736.
64. T. P. Dang and H. B. Kagan, *Journal of the Chemical Society D: Chem. Commun.*, 1971, DOI: 10.1039/C29710000481, 481-481.
65. J. D. Morrison, R. E. Burnett, A. M. Aguiar, C. J. Morrow and C. Phillips, *J. Am. Chem. Soc.*, 1971, 93, 1301-1303.
66. T. Ohta, H. Takaya and R. Noyori, *Inorg. Chem.*, 1988, 27, 566-569.
67. J. G. de Vries and C. J. Elsevier, *The handbook of homogeneous hydrogenation*, Wiley-VCH, 2007.
68. R. Noyori, *Johm Wiley and sons, London.*, 1993.
69. G. Q. Lin, Y. M. Li and A. S. C. Chan, *Principles and Applications of Asymmetric Synthesis*, Wiley, 2003.
70. H. Brunner, in *Applied Homogeneous Catalysis with organometallic compounds*, eds. B. Cornils and W. A. Hermann, Wiley-VCH, Weinheim, 1996, vol. 1, p. 206.
71. J. M. Thomas, *Angew. Chem. Int. Ed. Eng.*, 1988, 27, 1673-1691.
72. J. Thomas and R. Raja, *Top. Catal.*, 2006, 40, 3-17.
73. J. M. Thomas and R. Raja, *Acc. Chem. Res.*, 2008, 41, 708-720.
74. A. Baiker, *Current Opinion in Solid State and Materials Science*, 1998, 3, 86-93.
75. J. S. Beck, J. C. Vartuli, W. J. Roth, M. E. Leonowicz, C. T. Kresge, K. D. Schmitt, C. T. W. Chu, D. H. Olson and E. W. Sheppard, *J. Am. Chem. Soc.*, 1992, 114, 10834-10843.
76. J. M. Thomas, B. F. G. Johnson, R. Raja, G. Sankar and P. A. Midgley, *Acc. Chem. Res.*, 2002, 36, 20-30.
77. R. Raja, J. M. Thomas, M. D. Jones, B. F. G. Johnson and D. E. W. Vaughan, *J. Am. Chem. Soc.*, 2003, 125, 14982-14983.
78. B. F. G. Johnson, S. A. Raynor, D. S. Shephard, T. Mashmeyer, T. Mashmeyer, J. Meurig Thomas, G. Sankar, S. Bromley, R. Oldroyd, L. Gladden and M. D. Mantle, *Chem. Commun.*, 1999, 1167-1168.
79. C. Bianchini, P. Barbaro, V. Dal Santo, R. Gobetto, A. Meli, W. Oberhauser, R. Psaro and F. Vizza, *Adv. Synth. Catal.*, 2001, 343, 41-45.

80. A. Indra, S. Basu, D. G. Kulkarni, C. S. Gopinath, S. Bhaduri and G. K. Lahiri, *Appl. Catal.*, 2008, 344, 124-130.
81. M. Breuer, K. Ditrich, T. Habicher, B. Hauer, M. Keßeler, R. Stürmer and T. Zelinski, *Angew. Chem. Int. Ed.*, 2004, 43, 788-824.

Diastereomeric control of enantioselectivity: evidence for metal cluster catalysis†

Cite this: *Chem. Commun.*, 2014, 50, 7705

Received 28th March 2014,
Accepted 21st May 2014

DOI: 10.1039/c4cc02319f

www.rsc.org/chemcomm

Ahmed F. Abdel-Magied,^a Amrendra K. Singh,^{*a} Matti Haukka,^b
Michael G. Richmond^c and Ebbe Nordlander^{*a}

Enantioselective hydrogenation of tiglic acid effected by diastereomers of the general formula $[(\mu-H)_2Ru_3(\mu_3-S)(CO)_7(\mu-P-P^*)]$ ($P-P^*$ = chiral Walphos diphosphine ligand) strongly supports catalysis by intact Ru_3 clusters. A catalytic mechanism involving Ru_3 clusters has been established by DFT calculations.

A number of homogeneous catalytic systems that are based on dimetallic complexes and/or clusters have been developed. In several of these systems, the polynuclear complexes have been implicated as the active catalysts, or direct precursors to polynuclear catalysts.¹ It is however difficult to clearly identify clusters as homogeneous catalysts.² Duckett, Dyson and coworkers³ have demonstrated that the clusters $[H_2Ru_3(CO)_{10}(L)_2]$ (L = phosphine) function as homogeneous catalysts for the hydrogenation of alkynes (diphenylacetylene), although a competing catalytic pathway involving fragmentation to form the mononuclear species $[Ru(H)_2(CO)_2(L)(alkyne)]$ as active catalysts is also observed. Norton⁴ has defined an irrefutable criterion that identifies a cluster species as an active catalyst, viz. the observation of asymmetric induction in a reaction that is catalysed by a cluster that is chiral by virtue of the cluster framework only (*i.e.* excluding chiral ligands). This concept has been probed in the silylation of acetophenone using chiral tetrahedrane clusters, but cluster racemization was found to occur faster than productive catalysis.⁵ The generation of a chiral cluster framework through the coordination of a suitable chiral ligand allows the above criterion to be modified such that if

asymmetric induction in a catalytic system is observed, and if the enantioselectivity of the catalytic reaction is reversed by using another diastereomer of the cluster, where the chirality of the ligand remains the same but the chirality of the cluster framework has been changed, then this would constitute *prima facie* evidence for cluster-promoted asymmetric induction. Here we wish to present such a catalytic system that is based on two diastereomeric cluster complexes, where an unprecedented reversal of the enantioselectivity of a catalytic asymmetric reaction occurs upon reversal of the chirality of the cluster framework.

In previous studies, we have obtained excellent conversion and good enantioselectivity in asymmetric hydrogenation of α -unsaturated carboxylic acids, effected by catalytic systems based on $[(\mu-H)_4Ru_4(CO)_{10}(L)]$ clusters (L = bulky chiral ferrocene-based diphosphine).⁶ In continuation of this research, we have focused our attention on triruthenium hydrido clusters containing triply bridging chalcogenide ligands that may function as “clamps” to maintain an intact cluster framework. The trinuclear clusters $[(\mu-H)_2Ru_3(\mu_3-E)(CO)_{9-2x}(dppm)_x]$ (E = O, x = 2; E = S, x = 1,2) have been shown to be efficient precursors for catalytic olefin hydrogenation reactions.^{7,8} Reaction of $[(\mu-H)_2Ru_3(\mu_3-S)(CO)_9]$ with the Walphos diphosphine *R,R*-1 in the presence of Me_3NO results in the formation of clusters 2 and 3 with the common empirical formula $[(\mu-H)_2Ru_3(\mu_3-S)(CO)_7(\mu-1)]$ (Scheme 1). The bridging of adjacent metals by the heterobidentate ligand leads to an intrinsically chiral metallic framework unless there is complete planarity,⁹ and the coordination of the enantiomerically pure diphosphine ligand 1 thus yields a mixture of diastereomers 2 and 3 due to different connectivities of the heterobidentate ligand (*cf.* Scheme 1). Clusters 2 and 3 could be isolated and were characterized by comparing their IR and $^1H/^{31}P$ NMR spectral data with those of $[(\mu-H)_2Ru_3(\mu_3-S)(CO)_7(dppm)]^7$ (*cf.* ESI†). The ^{31}P NMR data confirmed the difference in the bridging mode of the diphosphine ligand in 2 and 3. For 2, the P^1 signal (*cf.* Scheme 1) appears as a triplet, indicating coupling to both hydrides, while the signal for P^2 is a doublet. In contrast, the signal for P^1 in 3 appears as a doublet while that of P^2 is a doublet of doublets. The identities of the two diastereomers were further confirmed by the determination of their crystal structures (Fig. 1 and 2).

^a Inorganic Chemistry Research Group, Chemical Physics, Center for Chemistry and Chemical Engineering, Lund University, Box 124, Lund, SE-221 00, Sweden.
E-mail: Ebbe.Nordlander@chemphys.lu.se; Fax: +46 46 222 4439

^b Department of Chemistry, University of Jyväskylä, Box 35, FI-40014 Jyväskylä, Finland

^c Department of Chemistry, University of North Texas, Denton, TX 76203, USA

† Electronic supplementary information (ESI) available: Experimental details, crystallographic details, FTIR and NMR spectra. Complete ref. 14, computational details, and atomic coordinates of optimized ground-state and transition-state structures. CCDC 993899 (2) and 993900 (3). For ESI and crystallographic data in CIF or other electronic format see DOI: 10.1039/c4cc02319f

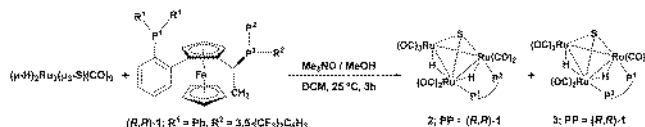
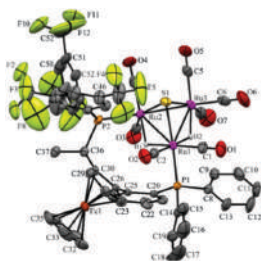
Scheme 1 The synthesis of clusters **2** and **3**.

Fig. 1 Molecular structure of $[(\mu\text{-H})_2\text{Ru}_3(\mu_3\text{-S})(\text{CO})_7(\mu\text{-1})]$ **2** with thermal ellipsoids drawn at the 50% probability level. C–H hydrogen atoms have been omitted for clarity. Selected bond distances [Å] and angles [°]: Ru1–Ru2 2.8951(7), Ru1–Ru3 2.9023(6), Ru2–Ru3 2.7536(6), Ru1–P1 2.359(2), Ru2–P2 2.333(1), Ru1–S1 2.368(2), Ru2–S1 2.375(2), Ru3–S1 2.346(2), Ru1–H1 1.75(5), Ru1–H2 1.69(5), Ru2–H2 1.76(4), Ru3–H1 1.76(5).

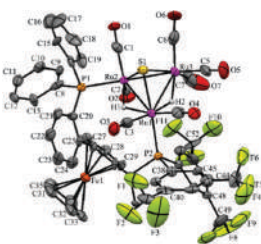


Fig. 2 Molecular structure of $[(\mu\text{-H})_2\text{Ru}_3(\mu_3\text{-S})(\text{CO})_7(\mu\text{-1})]$ **3** with thermal ellipsoids drawn at the 50% probability level. C–H hydrogen atoms have been omitted for clarity. Selected bond distances [Å] and angles [°]: Ru1–Ru2 2.915(2), Ru1–Ru3 2.894(2), Ru2–Ru3 2.746(2), Ru1–P2 2.335(4), Ru2–P1 2.348(5), Ru1–S1 2.361(5), Ru2–S1 2.358(5), Ru3–S1 2.351(5), Ru1–H1 1.53, Ru1–H2 1.57, Ru2–H2 1.90, Ru3–H1 1.67 (riding on Ru atoms).

The catalytic activities of **2** and **3** were examined in asymmetric hydrogenation of tiglic acid.^{6,10} Spectroscopic measurements (IR, $^1\text{H}/^{31}\text{P}$ NMR, cf. ESI†) and mass spectrometry showed no signs of changes in the clusters after catalytic runs. The catalysis results are summarized in Table 1. The enantioselectivities are low in comparison to mononuclear catalysts, but relatively high by the standards of cluster-based systems. This reflects an inherent weakness in the chiral induction effected by clusters – the substrate is likely to bind at a metal site with minimum steric hindrance (*vide infra*) and the chiral induction effected by bulky chiral ligands is thus diminished. However, we have observed

Table 1 Summary of catalytic asymmetric hydrogenation reactions

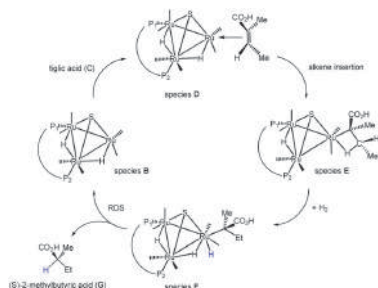
Ligand	Catalyst	Conversion ^a (%)	ee (%)	Configuration ^b
<i>R,R</i> - 1	2	49	23	<i>R</i>
<i>R,R</i> - 1	3	79	56	<i>S</i>
<i>S,S</i> - 1	4	55	24	<i>S</i>
<i>S,S</i> - 1	5	64	52	<i>R</i>

^a The amount of substrate consumed in the catalytic experiments, assessed by ^1H NMR spectroscopy. ^b Favoured enantiomer.

significantly higher enantioselectivities in other cluster-based systems.^{6b} The reversal in enantioselectivity in experiments where **2** and **3** were used as catalysts indicates that it is indeed the clusters that are the active catalysts, or closely related triruthenium species.¹¹ Further, a mechanism involving cluster decomposition during catalysis and regeneration of intact cluster at the end of the catalytic cycle would be accompanied by formation of both diastereomers,¹² even if only one form of the cluster was used initially. However, no trace of the other diastereomer was observed at the end of catalytic cycles employing **2** or **3**.

In previous studies, we have shown that strong chiral induction by chiral phosphines can be achieved in cluster-based hydrogenations^{6b} and, as a consequence, that reversal of enantioselectivity can be effected by reversal of phosphine chirality.¹³ In order to further investigate the reversal in enantioselectivity observed for the sulfide-capped clusters **2** and **3**, the analogous diastereomeric pair based on *S,S*-**1**, viz. **4** (with diphosphine connectivity corresponding to **2**) and **5** (connectivity corresponding to **3**) were prepared, and characterized by comparing spectroscopic data with those of **2** and **3** (cf. ESI†). Again, a reversal of enantioselectivity with reversal in diphosphine connectivity was observed when **4** and **5** were used as hydrogenation catalysts (Table 1). Furthermore, the chiral induction by the diphosphine ligand is confirmed, as the enantioselectivity is reversed with reversal in diphosphine chirality (**2** vs. **4**, and **3** vs. **5**).

From Table 1, it is evident that in these catalytic systems the stereochemistry, as well as the bridging mode of the coordinated chiral ligand, strongly affects the outcome of hydrogenation in terms of both conversion and enantioselectivity. Use of cluster **3** yields an impressive 56% ee for (*S*)-2-methylbutyric acid. The mechanism responsible for the observed catalysis and details concerning the enantioselectivity were computationally investigated by electronic structure calculations.^{14,15} Scheme 2 shows the computed catalytic cycle for the hydrogenation of tiglic acid to (*S*)-2-methylbutyric acid employing cluster **3** (species A), where catalysis is initiated by the site-selective loss of CO from the $\text{Ru}(\text{CO})_3$ center, as shown in Fig. 3.¹⁶



Scheme 2 Catalytic cycle for the hydrogenation of tiglic acid to (S)-2-methylbutyric acid by cluster **3**.

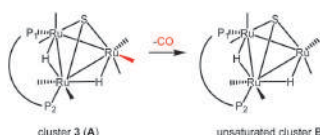


Fig. 3 Site-selective loss of CO from the $\text{Ru}(\text{CO})_3$ center in cluster **3** (see text).

Cluster **B** serves as the entry point into the catalytic cycle, and the free energy profile associated with this reaction is depicted in Fig. 4. *Si*-face coordination of tiglic acid to **B** affords the alkene-substituted cluster **D**. Regiospecific insertion of the alkene into the proximal bridging hydride occurs *via* transition structure **TSDE**, whose energy is $29.6 \text{ kcal mol}^{-1}$ uphill relative to **B** and **C**. The alternative alkene insertion route, which involves hydride transfer to the ester-substituted alkene carbon and the creation of the (*S*) stereogenic center, lies $6.6 \text{ kcal mol}^{-1}$ above **TSDE**. The resulting agostic alkyl cluster **E** reacts with H_2 to furnish the transient trihydride cluster **F**. Reductive elimination in **F** gives (*S*)-2-methylbutyric acid (**G**) and regenerates cluster **B**, completing the catalytic cycle with a net release of $13.2 \text{ kcal mol}^{-1}$. Coordination of the *re* face of the prochiral substrate proceeds through a series of identical steps, all of which lie higher in

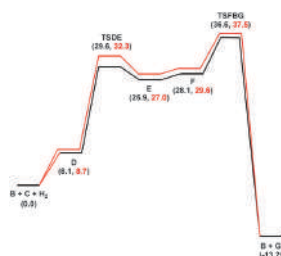


Fig. 4 Free energy profiles for the hydrogenation of tiglic acid catalysed by cluster **3**. Black and red profiles are for the *si*- and *re*-face alkene coordination routes, respectively.

energy than the *si*-face route. The energetics computed for the reaction profiles depicted in Fig. 4 are in concert with the observed preference for the (*S*) enantiomer when cluster **3** is employed as the catalyst precursor. The mechanistic steps computed involve a fixed stereochemistry at the cluster, whose chirality directly influences the asymmetric induction observed in the hydrogenation product. The observed reversal in enantioselectivity with the different cluster diastereomers containing either *R,R*-1 or *S,S*-1 strongly support the involvement of intact Ru_3 clusters as the active hydrogenation catalysts.

In conclusion, we have prepared four diastereomers of the cluster $[(\mu\text{-H})_2\text{Ru}_3(\mu_3\text{-S})(\text{CO})_7(\mu\text{-I})]$, containing chiral cluster frameworks and chiral diphosphine ligands. All diastereomers display different catalytic behaviour in the enantioselective hydrogenation of tiglic acid. The enantioselectivity is not only reversed with reversal in ligand chirality, but also with reversal in cluster chirality. The latter observed reversal in enantioselectivity with the different cluster diastereomers containing either *R,R*-1 or *S,S*-1 strongly supports the involvement of intact Ru_3 clusters as the active hydrogenation catalysts. While the (transient) formation of mononuclear chiral catalysts may be envisaged,¹¹ such reactivity can neither explain the observed enantioselectivities for the diastereomeric pairs 2 and 3, and 4 and 5, nor the isolation of pure cluster diastereomers after catalysis. Application of Occam's razor implicates cluster catalysis.

AFA thanks the EU Erasmus Mundus program for a predoctoral fellowship. AKS thanks the Carl Trygger Foundation for a postdoctoral fellowship. MGR thanks the Robert A. Welch Foundation (grant B-1093) for financial support; NSF support of the computational facilities at the University of North Texas through grant CHE-0741936 is acknowledged. We thank Dr David Hrovat and Prof. Xinzhen Yang for many helpful ONIOM-based discussions.

Notes and references

- (a) P. J. Dyson, *Coord. Chem. Rev.*, 2004, **248**, 2443; (b) R. D. Adams and F. A. Cotton, *Catalysis by Di- and Polynuclear Metal Cluster Complexes*, Wiley-VCH, Weinheim, 1998; (c) R. D. Adams, T. S. Barnard, Z. Li, W. Wu and J. H. Yamamoto, *J. Am. Chem. Soc.*, 1994, **116**, 9103; (d) R. D. Adams and T. S. Barnard, *Organometallics*, 1998, **17**, 2567.
- (a) Y. Lin and R. G. Finke, *Inorg. Chem.*, 1994, **33**, 4891; (b) C. M. Hagen, L. Vieille-Petit, G. Laurenczy, G. Süss-Fink and R. G. Finke, *Organometallics*, 2005, **24**, 1819.
- (a) D. Blazina, S. B. Duckett, P. J. Dyson and J. A. B. Lohman, *Angew. Chem., Int. Ed.*, 2001, **40**, 3874; (b) D. Blazina, S. B. Duckett, P. J. Dyson and J. A. B. Lohman, *Chem. – Eur. J.*, 2003, **9**, 1045.
- J. R. Norton, in *Fundamental Research in Homogeneous Catalysis*, ed. M. Tsutsui, Plenum Press, New York, 1977.
- C. U. Pittman, Jr., M. G. Richmond, M. Absi-Halabi, H. Beurich, F. Richter and H. Vahrenkamp, *Angew. Chem., Int. Ed. Engl.*, 1982, **21**, 786.
- (a) V. Moberg, M. Haukka, I. O. Koshevoy, R. Ortiz and E. Nordlander, *Organometallics*, 2007, **26**, 4090; (b) V. Moberg, R. Duquesne, S. Contaldi, O. Röhrs, J. Nachtigall, L. Damoense, A. T. Hutton, M. Green, M. Monari, D. Santelia, M. Haukka and E. Nordlander, *Chem. – Eur. J.*, 2012, **18**, 12458.
- S. J. Ahmed, M. I. Hyder, S. Kabir, M. A. Miah, A. J. Deeming and E. Nordlander, *J. Organomet. Chem.*, 2006, **691**, 309.
- C. Bergounhou, P. Fompeyrine, G. Commenges and J. J. Bonnet, *J. Mol. Catal.*, 1988, **48**, 285.

- 9 S. P. Tunik, I. O. Koshevoy, A. J. Poe, D. H. Farrar, E. Nordlander, M. Haukka and T. Pakkanen, *J. Chem. Soc., Dalton Trans.*, 2003, 2457.
- 10 E. Tyrell, M. W. H. Tsang, G. A. Skinner and J. Fawcett, *Tetrahedron*, 1996, 52, 9841.
- 11 Formation of a Noyori-type catalyst of the general formula $[\text{Ru}(\mathbf{1})(\text{O}_2\text{CR})_2]$ is in principle possible but cannot explain a reversal of enantioselectivity. Formation of a $[\text{Ru}(\mathbf{1})_2\text{X}_2]$ (X = arbitrary monodentate anion) complex is even less likely, but could in principle form Λ and Δ -isomers; however, a racemic mixture would then expected to be formed, and the reversal of enantioselectivity would not be effected.
- 12 This is especially true with cluster 3, whose DFT-computed ΔG^\ddagger lies 2.0 kcal mol⁻¹ above that of cluster 2. Any fragmentation of 3 during catalysis, followed by cluster reassembly, would thermodynamically afford 2.
- 13 P. Homanen, R. Persson, M. Haukka, T. A. Pakkanen and E. Nordlander, *Organometallics*, 2000, 19, 5568.
- 14 M. J. Frisch *et al.*, *Gaussian 09, revision B.01*, Gaussian, Inc., Wallingford, CT, 2010.
- 15 The DFT calculations were performed using a two-layered ONIOM (B3LYP/genecp:PM6) approach, where the Walphos ligand, except for the phosphorus and iron atoms, was confined to the lower layer. The Ru and Fe atoms were treated using SDD effective core potential (ecp) basis sets, and all of the other high level atoms were described by a 6-31G(d') basis set. Standard-state corrections have been applied to all species to convert concentrations from 1 atm to 1 M.
- 16 The unsaturated cluster **B** and free CO lie 23.0 kcal mol⁻¹ (ΔG) above cluster 3.

Paper II

ARTICLE

Asymmetric hydrogenation of an α -unsaturated carboxylic acid catalyzed by intact chiral transition metal carbonyl clusters – diastereomeric control of enantioselectivity[§]

Cite this:
DOI:
10.1039/x0xx
00000x

www.rsc.org
/

Ahmed F. Abdel-Magied,^[a] Yusuf Theibich,^[a] Amrendra K. Singh,^[a] Isa Doverbratt,^[b] Ahibur Rahaman,^[a] Matti Haukka,^[c] Michael G. Richmond,^[d] and Ebbe Nordlander^{*[a]}

Twenty clusters of the general formula $[(\mu\text{-H})_2\text{Ru}_3(\mu_3\text{-S})(\text{CO})_7(\mu\text{-P-P}^*)]$ (P-P^* = chiral diphosphine of the ferrocene-based Walphos or Josiphos families) have been synthesised and characterised. The clusters have been tested as catalysts for asymmetric hydrogenation of tiglic acid [*trans*-2-methyl-2-butenic acid]. The observed enantioselectivities and conversion rates strongly support catalysis by intact Ru_3 clusters. A catalytic mechanism involving an active Ru_3 catalyst generated by CO loss from $[(\mu\text{-H})_2\text{Ru}_3(\mu_3\text{-S})(\text{CO})_7(\mu\text{-P-P}^*)]$ has been investigated by DFT calculations.

Introduction

Chalcogenide-bridged derivatives of transition metal carbonyl clusters have been widely studied.^{1–7} Examples of such compounds include the triruthenium hydrido clusters $[(\mu\text{-H})_2\text{Ru}_3(\mu_3\text{-E})(\text{CO})_{9-2x}(\text{dppm})_x]$ ($\text{E} = \text{O}, x=2$; $\text{E} = \text{S}, x=1,2$), which have been shown to be efficient catalyst precursors for olefin hydrogenation reactions.^{7,8} In these clusters, the triply bridging chalcogenide ligands may function as “clamps” that maintain an intact cluster framework throughout reactions. It is, however, difficult to clearly identify clusters as active catalysts in homogeneous systems,^{9–11} and there has been considerable debate about whether clusters fragment to form either mononuclear or colloidal species, aggregate to form nanoparticles, or remain as intact clusters during the catalytic cycle. A number of convincing examples of homogeneous cluster catalysis based on indirect evidence have been reported. For example, $[\text{H}_4\text{Pt}_3\text{Ru}_6(\text{CO})_{21}]$ catalyses alkyne hydrosilylation and hydrogenation without appearing to undergo fragmentation.^{12,13} The face-capped trinuclear cluster $[\text{HRu}_3(\text{CO})_9(\mu_3\text{-}\eta^2\text{-NMePy})]$ appears to be the active catalyst in the hydroformylation of diphenylacetylene to α -phenyl- cinnamaldehyde although conversion of $[\text{HRu}_3(\text{CO})_9(\mu_3\text{-}\eta^2\text{-NMePy})]$ to the catalytically inactive dinuclear species $[\text{Ru}_2(\text{CO})_8(\eta^3\text{-NMePyCO})]$ occurs after several cycles.¹⁴ Parahydrogen ($p\text{-H}_2$) NMR methods have been used to identify active catalysts in hydrogenation reactions.^{15,16} By using such techniques, Blazina and co-workers have demonstrated that the clusters $[\text{H}_2\text{Ru}_3(\text{CO})_{10}(\text{L})_2]$ ($\text{L} = \text{PMe}_2\text{Ph}$ or PPh_3) function as homogeneous catalysts for the hydrogenation of

alkynes (diphenylacetylene).¹⁷ The active catalysts that were identified are derived from the dihydride species $[\text{HRu}_3(\mu\text{-H})(\text{CO})_9(\text{L})_2]$.^{18,19} In previous studies, we have investigated asymmetric hydrogenation of α -unsaturated carboxylic acids using catalytic systems based on $[(\mu\text{-H})_2\text{Ru}_4(\text{CO})_{12}]$ clusters derivatised with chiral diphosphines. We have shown that such diphosphine ligands may effect strong chiral induction,^{20,21} and that good conversions and enantioselectivities may be achieved. While catalysis by fragmentation products cannot be excluded, the recovery of unaltered starting clusters after catalytic reactions, recycling of catalysts/catalyst precursors with identical catalytic results, and mercury poisoning tests all implicate the presence of an active cluster catalyst.²¹

Norton²² has identified a criterion which, if fulfilled, provides incontrovertible evidence for a cluster species acting as an active catalyst, viz. the observation of asymmetric induction in a reaction that is catalysed by a cluster that is chiral by virtue of the cluster framework only (i.e. excluding chiral ligands). Based on this concept, the silylation of acetophenone using chiral tetrahedrane clusters has been established, but cluster racemization was found to occur faster than productive catalysis.²³ Here we wish to present the fulfilment of a corollary to Norton's criterion, i.e. proof of diastereomeric control of enantioselectivity when diastereomeric pairs of $[(\mu\text{-H})_2\text{Ru}_3(\mu\text{-S})(\text{CO})_7(\mu\text{-P-P}^*)]$ clusters are used as (asymmetric) hydrogenation catalysts and the chirality of the diphosphine ligand is maintained intact while that of the

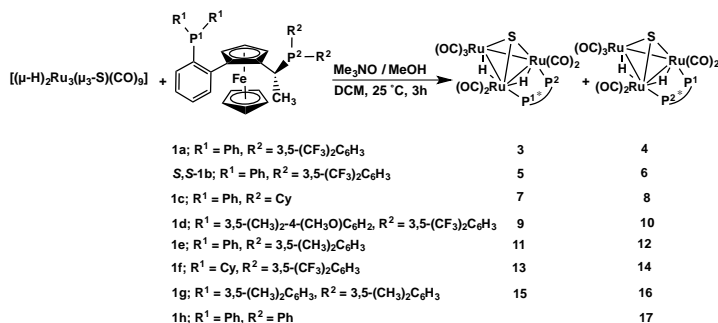
cluster framework changes. Part of these results have been published in an earlier communication.²⁴

Results and Discussion

The syntheses of derivatives of $[(\mu\text{-H})_2\text{Ru}_3(\mu_3\text{-S})(\text{CO})_9]$ containing chiral diphosphine ligands were based on oxidative decarbonylation of the starting cluster (using Me_3NO) in dichloromethane solution at ambient temperature, in the presence of the relevant diphosphine. The clusters were identified via IR, ^1H and ^{31}P NMR spectroscopies, mass spectrometry and, wherever possible, X-ray crystallography.

Synthesis and characterization of sulfide-capped triruthenium hydrido clusters containing Walphos ligands

Using the synthetic methodology described above, clusters **3–17** with the common empirical formula $[(\mu\text{-H})_2\text{Ru}_3(\mu_3\text{-S})(\text{CO})_7(\mu\text{-}1,2\text{-P-P}^*)]$, where the diphosphine P-P^* is one of the chiral Walphos ligands **1a–1h** (Scheme 1), were prepared. Coordination of the heterobidentate ligand to adjacent metals in a bridging mode leads to an intrinsically chiral metallic framework unless there is complete planarity, and the coordination of the enantiomerically pure diphosphine ligand thus yields a mixture of diastereomers due to different connectivities of the heterobidentate ligand (*cf.* Scheme 1).



Scheme 1. Synthesis of clusters **3–17** containing Walphos ligands.

The diastereomers were separated and isolated using thin layer chromatography, and they were identified on the basis of comparison of their IR and $^1\text{H}/^{31}\text{P}$ NMR spectral data with those of $[(\mu\text{-H})_2\text{Ru}_3(\mu_3\text{-S})(\text{CO})_7(\text{dppm})]$.⁷ Clusters **3–17** were completely characterized by spectroscopic methods (*cf.* Experimental section). The empirical formulae of all clusters were confirmed by mass spectrometry and in the cases of clusters **3–6** and **8**, their solid-state structures were determined by X-ray crystallography. The ^1H and ^{31}P NMR data confirmed the difference in the bridging mode of the diphosphine ligands in **3–17**. For **3**, the ^1H NMR in the hydride region shows two signals, a doublet of doublet of doublets at $\delta - 18.13$ ($J_{\text{H-P}} = 12.4$, $J_{\text{H-H}} = 11.2$, $J_{\text{H-H}} = 2.9$ Hz) and an (apparent) doublet of triplets at $\delta - 18.40$ ($J_{\text{H-P}} = 9.8$, $J_{\text{H-H}} = 2.9$

Hz), while for the corresponding diastereomer **4**, the ^1H NMR in the hydride region shows two signals at $\delta - 17.82$ (ddd, $J_{\text{H-P}} = 12.2$, $J_{\text{H-P}} = 8.8$, $J_{\text{H-H}} = 3.5$ Hz) and $\delta - 18.63$ (ddd, $J_{\text{H-P}} = 7.5$, $J_{\text{H-P}} = 3.6$, $J_{\text{H-H}} = 3.5$ Hz). In the ^{31}P NMR spectrum of **3**, the signal for phosphorus P^1 (*cf.* Scheme 1) appears as a triplet, indicating coupling to both hydrides, while the signal for P^2 is a doublet. In contrast, the signal for P^1 in **4** appears as a doublet while that of P^2 is a doublet of doublets. The identities of the two diastereomers were further confirmed by the determination of their crystal structures (Figs 2 and 3). The analogous diastereomeric pair based on S,S-**1b**, viz. **5** (with diphosphine connectivity corresponding to **1**) and **6** (connectivity corresponding to **4**) were prepared, and characterized by comparing their spectroscopic data with those of **3** and **4**. The ^1H NMR spectrum of **5** in the hydride region shows two signals at $\delta - 18.12$ (ddd, $J_{\text{H-P}} = 12.6$, $J_{\text{H-P}} = 11.1$, $J_{\text{H-H}} = 3.0$ Hz) and at $\delta - 18.40$ (d't', $J_{\text{H-P}} = 9.9$, $J_{\text{H-H}} = 3.0$ Hz), while for **6** the corresponding signals are found at $\delta - 17.84$ (ddd, $J_{\text{H-P}} = 12.4$, $J_{\text{H-P}} = 9.1$, $J_{\text{H-H}} = 3.0$ Hz) and $\delta - 18.65$ (ddd, $J_{\text{H-P}} = 7.1$, $J_{\text{H-P}} = 3.2$, $J_{\text{H-H}} = 3.0$ Hz). Similarly, in the ^{31}P NMR spectrum of **5**, the P^1 signal (*cf.* Scheme 1) appears as a doublet of doublets, while the signal for P^2 is a triplet, indicating coupling to both hydrides. In contrast, the signal for P^1 in the corresponding diastereomer **6** appears as a doublet of doublets while that of P^2 is a doublet. Again, the identities of the two diastereomers were further confirmed by the determination of their crystal structures (Figs 2 and 3).

The ^1H NMR of $[(\mu\text{-H})_2\text{Ru}_3(\mu_3\text{-S})(\text{CO})_7(\mu\text{-}1,2\text{-}1\text{g})]$ **16** in the hydride region shows a multiplet signal at $\delta - 18.23$, which indicates fluxionality of the hydrides at ambient temperature. Variable-temperature ^1H NMR spectra in the hydride region for **16** show that the fluxionality may be frozen out at approximately 253 K to give two signals, an apparent triplet of doublets at $\delta - 18.12$ (d't' = ddd, $J_{\text{H-P}} = 10.9$, $J_{\text{H-H}} = 3.0$ Hz) and a doublet of 'triplets' (ddd) at $\delta - 18.19$ ($J_{\text{H-P}} = 9.4$ Hz).

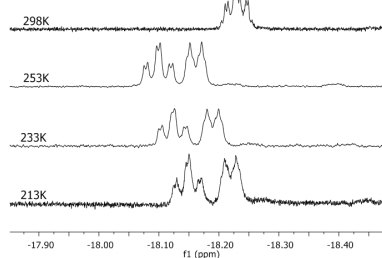


Figure 1. Variable-temperature ^1H NMR spectra (hydride region) of $[(\mu\text{-H})_2\text{Ru}_3(\mu_3\text{-S})(\text{CO})_7(\mu\text{-}1,2\text{-}1\text{g})]$ **16** recorded over the temperature range 298 – 213 K (top to bottom).

Crystal and molecular structures of clusters 3-6, 8 and 17

Molecular structures of $[(\mu\text{-H})_2\text{Ru}_3(\mu_3\text{-S})(\text{CO})_7(\mu\text{-1,2-1a})]$ **3** and **4**²⁴ and $[(\mu\text{-H})_2\text{Ru}_3(\mu_3\text{-S})(\text{CO})_7(\mu\text{-1,2-1b})]$ **5** and **6**

The molecular structures of **3-6** are shown in Figure 2 and selected bond distances and angles are listed in the caption. Details regarding data collection and reduction, and structure refinement are found in the Experimental Section, and relevant crystallographic data are collated in Table 2.

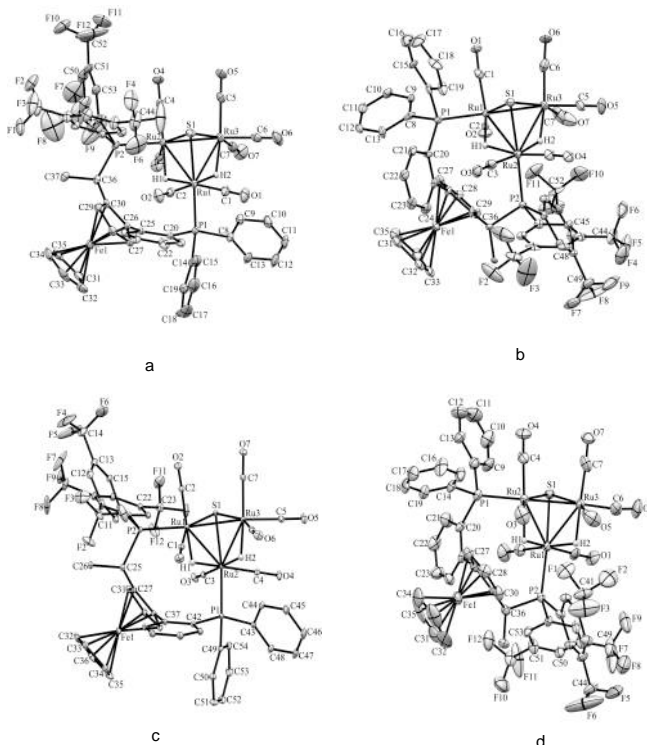


Figure 2. Molecular structures of four diastereomers (two diastereomeric pairs) representing different combinations of cluster framework and ligand chiralities, using pure enantiomeric forms *R,R*-**1a** or *S,S*-**1b** ligands; a) $[(\mu\text{-H})_2\text{Ru}_3(\mu_3\text{-S})(\text{CO})_7(\mu\text{-1,2-1a})]$ **3**, selected bond distances [Å] and angles [°]: Ru1-Ru2 2.8951(7), Ru1-Ru3 2.9023(6), Ru2-Ru3 2.7536(6), Ru1-P1 2.359(2), Ru2-P2 2.333(1), Ru1-S1 2.368(2), Ru2-S1 2.375(2), Ru3-S1 2.346(2), Ru1-H1 1.75(5), Ru1-H2 1.69(5), Ru2-H2 1.76(4), Ru3-H1 1.76(5); b) $[(\mu\text{-H})_2\text{Ru}_3(\mu_3\text{-S})(\text{CO})_7(\mu\text{-1,2-1a})]$ **4**, selected bond distances [Å] and angles [°]: Ru1-Ru2 2.915(2), Ru1-Ru3 2.894(2), Ru2-Ru3 2.746(2), Ru1-P2 2.335(4), Ru2-P1 2.348(5), Ru1-S1 2.361(5), Ru2-S1 2.358(5), Ru3-S1 2.351(5). Ru1-H1 1.53, Ru1-H2 1.57, Ru2-H2 1.90, Ru3-H1 1.67 (riding on Ru atoms); c) $[(\mu\text{-H})_2\text{Ru}_3(\mu_3\text{-S})(\text{CO})_7(\mu\text{-1,2-1b})]$ **5**, selected bond distances [Å] and angles [°]: Ru1-Ru2 2.90542(17), Ru1-Ru3 2.75164(19), Ru2-Ru3 2.8817(2), Ru1-P1 2.3331(5), Ru2-P2 2.3503(5), Ru1-S1 2.3810(4), Ru2-S1 2.3726(4), Ru3-S1 2.3556(4), Ru1-H1 1.70(4), Ru2-H1 1.74(4), Ru2-H2 1.82(3), Ru3-H2 1.68(3), and d) $[(\mu\text{-H})_2\text{Ru}_3(\mu_3\text{-S})(\text{CO})_7(\mu\text{-1,2-1b})]$ **6**, selected bond distances [Å] and angles [°]: Ru1-Ru2 2.9210 (12), Ru1-Ru3 2.893(3), Ru2-Ru3 2.7657(12), Ru1-P2 2.341(2), Ru2-P1 2.361(2), Ru1-S1 2.359(2), Ru2-S1 2.357(2), Ru3-S1 2.355(3), Ru1-H1 1.72(5), Ru1-H2 1.678(17), Ru2-H2 1.57(5), Ru3-H1 1.57(4). Thermal ellipsoids are drawn at the 50% probability level and C-H hydrogen atoms have been omitted for the sake of clarity.

As may be expected, the different diastereomers crystallize in non-centrosymmetric space groups (**3**, **4** and **6**: P2₁2₁2₁; **5**: Cc). The structures of the two diastereomers based on ligand **1a** (**3** and **4**) are discussed in detail below. The molecules consist of triangular ruthenium frameworks involving Ru-Ru bond lengths that are divided into two distinctive classes, the two hydride-bridged Ru-Ru bonds are "long" [**3**: Ru(1)-Ru(2) 2.8951(7), Ru(1)-Ru(3) 2.9023(6) Å; **4**: [Ru(1)-Ru(2) 2.915(2), Ru(1)-Ru(3) 2.894(2) Å] and the non-bridged Ru-Ru bond is "short" [**3**: Ru(2)-Ru(3) 2.7536(6); **4**: Ru(2)-Ru(3) 2.746(2) Å]. The triply bridging sulfur atom caps the ruthenium triangle quite symmetrically [Ru-S 2.375(2)-2.346(2) Å for **3**, and 2.361(5)-2.351(5) Å for **4**]. The hydride ligands were located using XHYDEX. All the carbonyl ligands are coordinated in a terminal monodentate coordination mode. The diphosphine ligands were found to exclusively coordinate in a bridging fashion, giving rise to nine-membered "dimetallacycles". As previously observed for related tetraruthenium tetrahydrido clusters,²¹ the Walphos ligand coordinates in an axial-equatorial mode. In the case of **3**, P1 is coordinated in an axial position to Ru1, the metal that is coordinated to both of the hydrides, while P2 is coordinated in an equatorial position to Ru2, which is coordinated by one hydride. For the diastereomer **4**, P1 is coordinated in an equatorial position to Ru2, which is coordinated to H1, while P2 is coordinated in an axial position to Ru1, which is coordinated to H1 and H2.

In the molecular structures of the analogous diastereomers based on **1b**, **5** and **6**, the same difference in the coordination mode of the diphosphine ligand *S,S*-**1b** is observed - P1 is coordinated in an axial position to Ru2 which is coordinated to both hydrides, in case of **5**, and for **6**, P1 is coordinated in an equatorial position to Ru2 which is bridged only with one hydride H1.

Molecular structures of $[(\mu\text{-H})_2\text{Ru}_3(\mu_3\text{-S})(\text{CO})_7(\mu\text{-1,2-1c})]$ **8** and $[(\mu\text{-H})_2\text{Ru}_3(\mu_3\text{-S})(\text{CO})_7(\mu\text{-1,2-1h})]$ **17**

It was possible to grow crystals suitable for X-ray diffraction also for clusters **8** and **17**, and the identities of these diastereomers were confirmed by single-crystal diffraction studies. The structure

of $[(\mu\text{-H})_2\text{Ru}_3(\mu_3\text{-S})(\text{CO})_7(\mu\text{-1,2-1c})]$ **8** is shown in Figure 3 and that of $[(\mu\text{-H})_2\text{Ru}_3(\mu_3\text{-S})(\text{CO})_7(\mu\text{-1,2-1h})]$ **17** is shown in Figure 4; selected bond lengths and angles are listed in the captions. As expected, the structures of **8** and **17** are directly related to **4**, with identical connectivities for the three clusters.

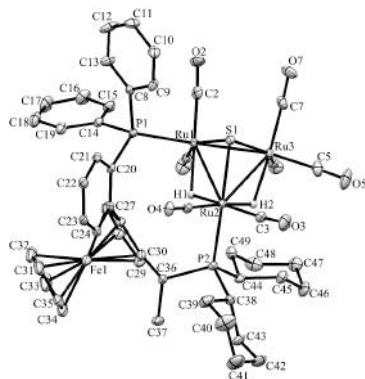


Figure 3. Molecular structure of $[(\mu\text{-H})_2\text{Ru}_3(\mu_3\text{-S})(\text{CO})_7(\mu\text{-1,2-1c})]$ **8** with thermal ellipsoids drawn at the 50% probability level. C-H hydrogen atoms have been omitted for clarity. Selected bond distances [Å] and angles [°]: Ru1-Ru2 2.9276(6), Ru1-Ru3 2.7511(6), Ru2-Ru3 2.9123(6), Ru1-P1 2.3376(13), Ru2-P2 2.3833(13), Ru1-S1 2.3649(14), Ru2-S1 2.3653(13), Ru3-S1 2.3635(13), Ru1-H1 1.90(4), Ru2-H2 1.76(7), Ru2-H1 1.78(4), Ru3-H2 1.94(7).

Again, two different distinctive classes of Ru-Ru bond lengths can be observed, the two hydride-bridged Ru-Ru bonds are "long" [Ru(1)-Ru(2) 2.9276(6), and Ru(2)-Ru(3) 2.9123(6)] and the "shortest" Ru(1)-Ru(3) 2.7511(6)]. A longer P-P bond distance is observed for **8** (5.61 Å) with a torsion angle of 87.70, in comparison to 5.48 Å and torsion angle of 83.98 for **4**. As expected the angles in **8** are a bit different than **4**, where P1-Ru1-Ru2 = 108.84, P2-Ru2-Ru1 = 118.59 and P2-Ru2-P3 = 120.54 in **8**, and for **4** it is 103.95, 120.85 and 123.95, respectively.

In case of **17**, the shortest Ru-Ru distance is the Ru1-Ru3 edge (2.7360(7) Å), which is not bridged by any hydride, while the two Ru-Ru edges that bridged with two hydrides have slightly symmetric longer distances (2.9173(6) Å for Ru1-Ru2 and 2.8922(7) Å for Ru2-Ru3). The two phosphorus atoms of the coordinated ligand are separated by 5.51 Å with a torsion angle of 87.40. The Ru-P bonds are symmetric in lengths (2.3542(16) Å for Ru1-P1 and 2.3562(17) Å for Ru2-P2), and the angles are P1-Ru1-Ru2 = 105.38, P2-Ru2-Ru1 = 116.95 and P2-Ru2-P3 = 121.36.

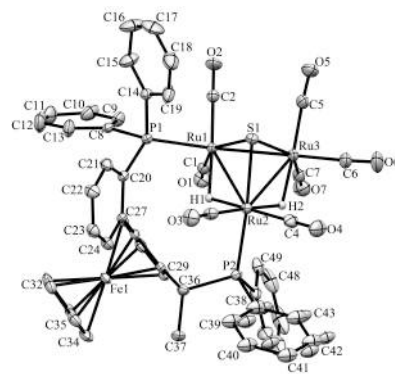
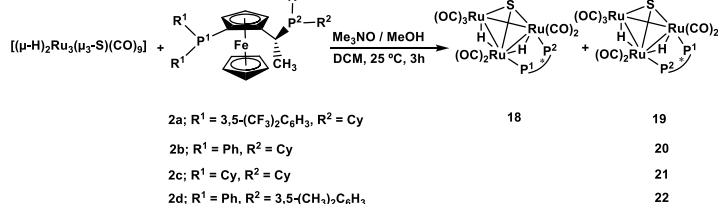


Figure 4. Molecular structure of $[(\mu\text{-H})_2\text{Ru}_3(\mu_3\text{-S})(\text{CO})_7(\mu\text{-1,2-1h})]$ **17** with thermal ellipsoids drawn at the 50% probability level. C-H hydrogen atoms have been omitted for clarity. Selected bond distances [Å] and angles [°]: Ru1-Ru2 2.9173(6), Ru1-Ru3 2.7360(7), Ru2-Ru3 2.8922(7), Ru1-P1 2.3542(16), Ru2-P2 2.3562(17), Ru1-S1 2.3601(19), Ru2-S1 2.3636(18), Ru3-S1 2.3581(19), Ru1-H1 1.7942, Ru2-H2 1.7347, Ru2-H1 1.7328, Ru3-H2 1.7658 (riding on Ru atoms).

Synthesis and characterization of sulfide-capped triruthenium hydrido clusters containing the Josiphos ligands **2a-2e**

The coordination of the Josiphos ligands **2a-2e** to the parent cluster $[(\mu\text{-H})_2\text{Ru}_3(\mu_3\text{-S})(\text{CO})_3]$ was performed by oxidative decarbonylation as discussed above (*cf.* Scheme 2). The bridging coordination mode and the different connectivities of the heterobidentate ligands in the diastereomers **18-22** have been identified by spectroscopic methods and, in the case of **20**, by X-ray crystallography.



Scheme 2. Synthesis of clusters **18-22** by using Josiphos family ligands.

The ¹H and ³¹P NMR data confirmed the difference in the bridging mode of the diphosphine ligand **2a** in clusters **18** and **19**. For **18**, the ¹H NMR in the hydride region shows two signals, a doublet of 'triplets' at δ = 18.29 (dt, *J*_{H-P} = 36.5, *J*_{H-H} = 2.5 Hz) and a doublet of doublet of doublets at δ = 19.46 (ddd, *J*_{H-P} = 13.3, *J*_{H-P} = 7.1, *J*_{H-H} = 2.5 Hz), while the hydride signals for **19** consist of a doublet of doublet of doublets at δ = 17.84 (*J*_{H-P} = 12.7, *J*_{H-P} = 9.0, *J*_{H-H} = 3.6 Hz) and a doublet of doublet of doublets at δ = 18.65 (*J*_{H-P} = 7.5, *J*_{H-P} = 3.6 Hz). In the ³¹P NMR spectrum of **18**, the P1 signal (*cf.*

Scheme 2) appears as a doublet of doublets, indicating coupling to both hydrides, while the signal for P2 is a doublet. In contrast, the signal for P1 in **19** appears as a doublet while that for P2 is a doublet of doublets. The ES+ mass spectrometric data match with the assigned molecular formula $[(\mu\text{-H})_2\text{Ru}_3(\mu_3\text{-S})(\text{CO})_7(\mu\text{-1,2-P-P})]$ ($m/z = 1401 [\text{M}+\text{H}]^+$) for both **18** and **19**. The empirical formulae of clusters **20** – **22** were confirmed by mass spectrometry, and their structures in solution and the solid state were identified by IR and NMR spectroscopy (cf. Experimental section and ESI†).

Due to the high degree of hydride fluxionality exhibited by $[(\mu\text{-H})_2\text{Ru}_3(\mu_3\text{-S})(\text{CO})_7(\mu\text{-1,2-2-d})]$ **22** at ambient temperature, only one sharp multiplet resonance could be detected for the hydride in the ^1H NMR. Variable-temperature (VT) ^1H NMR of cluster **22** shows that the fluxionality may be frozen out at 253 K, to reveal the two hydride signals that were expected for the cluster (Figure 5).

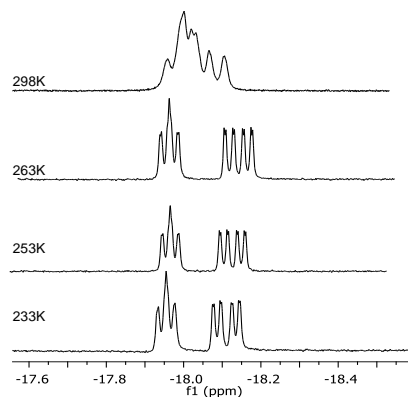


Figure 5. Variable-temperature ^1H NMR spectra in the hydride region of cluster $[(\mu\text{-H})_2\text{Ru}_3(\mu_3\text{-S})(\text{CO})_7(\mu\text{-1,2-2-d})]$ **22** recorded over the temperature range 298 – 233 K (top to bottom).

Crystal and molecular structure of $[(\mu\text{-H})_2\text{Ru}_3(\mu_3\text{-S})(\text{CO})_7(\mu\text{-1,2-2b})]$ **20**

The crystal structure of $[(\mu\text{-H})_2\text{Ru}_3(\mu_3\text{-S})(\text{CO})_7(\mu\text{-1,2-2b})]$ **20** was determined by X-ray diffraction analysis. A view of the molecular structure of **20** is shown in Figure 6 and selected bond distances and angles are listed in the caption. Relevant crystallographic data are listed in Table 2.

The cluster is very similar to **3** - **6**, **8** and **17** (*vide supra*), with one exception: the ligand **2b** bridges Ru1 and Ru2 atoms, but the two phosphine moieties bind in the more common *cis*-eq,eq coordination mode that is expected for diphosphines with a relatively short backbone, rather than the slightly distorted *cis*-eq,ax coordination mode that is observed for the above-mentioned Walphos derivatives. The latter coordination mode is presumably enforced by the relatively long backbone of the Walphos ligands. We have previously observed exactly the same types of coordination modes for Josiphos and Walphos ligands

coordinated to tetraruthenium tetrahydride clusters.²¹ The two metal-metal bonds in **20** that are bridged by hydrides are slightly elongated in comparison to the non-bridged Ru1-Ru3 edge (cf caption, Fig 6). Whereas the average P-P distance in the Walphos complexes **3** – **6**, **8** and **17** is 5.50 Å, it is 4.43 Å in **20** and significant differences are seen for the Ru-P bonds lengths (2.3295(8) Å for Ru1-P1 and 2.3887(7) Å for Ru2-P2).

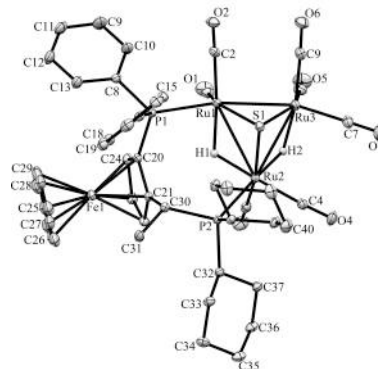


Figure 6. Molecular structure of $[(\mu\text{-H})_2\text{Ru}_3(\mu_3\text{-S})(\text{CO})_7(\mu\text{-1,2-2b})]$ **20** with thermal ellipsoids drawn at the 50% probability level. C-H hydrogen atoms have been omitted for clarity. Selected bond distances [Å] and angles [°]: Ru1-Ru2 2.9272(3), Ru1-Ru3 2.7314(3), Ru2-Ru3 2.8947(3), Ru1-P1 2.3295(8), Ru2-P2 2.3887(7), Ru1-S1 2.3701(8), Ru2-S1 2.3871(8), Ru3-S1 2.3667(7), Ru1-H1 1.82 (4), Ru2-H2 1.79(4), Ru2-H1 1.76(4), Ru3-H2 1.86(4).

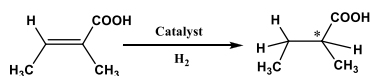
Catalytic activities

In previous studies, we have shown that the chiral diphosphine ligands play an important role in asymmetric hydrogenation^{20,21,25} and that the chiral configurations of the hydrogenated products are dependent on the chiral ligand used.²⁶ The ability of the new clusters **3** - **22** to function as catalysts for asymmetric hydrogenation was investigated. Tiglic acid [*trans*-2-methyl-2-butenic acid] was chosen as a substrate because (i) it has been used as a benchmark substrate in earlier assessments of asymmetric hydrogenation effected by transition metal carbonyl clusters, facilitating comparison with other work,^{20,25,27-30} (ii) there is a well-established and reliable protocol for the evaluation of enantiomeric excess, and (iii) asymmetric hydrogenation of α -unsaturated carboxylic acids and their substituted derivatives, which are essential pharmaceuticals or chiral building blocks for the synthesis of biologically active compounds, is of considerable importance.^{31,32} Instead of the high hydrogen pressure that has been commonly used in previous cluster-based catalysis investigations (130 bar),³³ a hydrogen pressure of 50 bar was used. Lower hydrogen pressure was expected to enhance the chiral induction, as demonstrated by us in a previous investigation.²⁶

The catalysis results for clusters **3-22** are summarized in Table 1. The clusters show moderate catalytic activity in terms of conversion. Furthermore, the enantioselectivities are moderate in

comparison to mononuclear catalysts, but relatively high by the standards of cluster-based systems. The enantioselectivities reflect an inherent weakness in the chiral induction effected by clusters – the substrate is likely to bind at a metal site with minimum steric hindrance (*vide infra*) and the chiral induction effected by bulky chiral ligands is therefore diminished. However, we have observed significantly higher enantioselectivities in other cluster-based systems,^{20,21,27} and it should be borne in mind that ee's exceeding 40% were unprecedented^{29,30,33–35} in cluster-based asymmetric hydrogenation before we began our studies. Unfortunately, the separation of the hydrogenated products from the organic phase after using clusters **13** and **16** as a catalysts (Table 1, entry 11, 14 and 20, respectively) turned out to be unsuccessful in our hands, so we could not determine the enantiomeric excess for these reactions, albeit with full conversion in case of **16**.

Table 1. Asymmetric catalytic hydrogenation of tiglic acid in the presence of clusters **3–22** as catalysts.



Entry	Ligand	Catalyst	Conv. [%] ^a	ee [%]	Config. ^b
1	1a	3	49	23	<i>R</i>
2	1a	4	79	56	<i>S</i>
3	<i>S,S</i> - 1b	5	55	24	<i>S</i>
4	<i>S,S</i> - 1b	6	64	52	<i>R</i>
5	1c	7	83	33	<i>R</i>
6	1c	8	80	21	<i>S</i>
7	1d	9	94	9	<i>R</i>
8	1d	10	77	7	<i>S</i>
9	1e	11	66	17	<i>S</i>
10	1e	12	7	8	<i>R</i>
11	1f	13	14	ND	ND
12	1f	14	23	48	<i>S</i>
13	1g	15	47	21	<i>S</i>
14	1g	16	100	ND	ND
15	1h	17	43	13	<i>R</i>
16	2a	18	88	31	<i>R</i>
17	2a	19	66	13	<i>S</i>
18	2b	20	41	17	<i>S</i>
19	2c	21	68	37	<i>S</i>
20	2d	22	38	25	<i>S</i>
21	1a	3 +Hg	51	26	<i>R</i>

^aThe amount of substrate consumed in the catalytic experiment, assayed by ¹H NMR spectroscopy, p(H₂) = 50 bar, T = 100 °C, solvent = EtOH-toluene 1:1 (5 mL), n(substrate)/n(catalyst) = 100. ^bFavoured enantiomer. ND: not detected.

From Table 1, it is clear that in these catalytic systems the stereochemistry and the bridging mode of the coordinated chiral diphosphine ligands strongly affect the outcome of the hydrogenation reactions, both in terms of conversion and enantioselectivity. In earlier work, we have been able to demonstrate that reversal of enantioselectivity can be effected by reversal of phosphine chirality in cluster-based systems.²⁶ It may be noted that the diastereomeric pairs **3/4**, **5/6**, **7/8**, **9/10**, **11/12**,

and **18/19**, within which the chirality of the diphosphine remains the same, but the chirality of the cluster framework changes, all show a reversal in enantioselectivity when the chirality of the cluster framework changes. Furthermore, the pairs **3/5** and **4/6** are diastereomers where the chirality of the cluster framework remains intact while that of the ligand changes (cf. Fig 2), and for these pairs the enantioselectivity is reversed with reversal in chirality of the ligands. It may thus be concluded that both the cluster framework and the ligand chiralities influence the enantioselectivity for a given cluster. These observations provide compelling evidence for the clusters, or immediate derivatives of the clusters with maintained cluster framework chiralities,³⁶ being the active catalysts. A mechanism involving cluster decomposition during catalysis and regeneration of the intact cluster at the end of the catalytic cycle would be accompanied by formation of both diastereomers,³⁷ even if only one form of the cluster was initially used. However, no trace of such racemization was observed at the end of catalytic cycles employing all clusters. All catalysts were recovered in good yields (~70%) after a complete catalytic experiment, with one exception: only trace amounts (at best) of catalyst **20** could be recovered. For the other catalysts, the recovery may be considered to be quantitative, when the small amount of catalyst used is taken into account. Furthermore, recyclability was proven for cluster **3** - after completion of the reaction (Table 1, entry 1), the cluster was recovered, purified by TLC and reused under identical experimental conditions. Identical conversion rates and enantiomeric excesses for the two catalytic runs were obtained.

Nature of the active catalyst

Hydrogenation in the absence of a catalyst/catalyst precursor

To avoid possibilities of having metallic residues/contaminations that could be responsible for the above-mentioned observations, a blank control catalytic experiment was carried out using standard reaction conditions, where the tiglic acid was dissolved in ethanol/toluene (1:1 v/v) in the absence of any potential catalyst and heated at 100 °C under 50 bar of H₂. No hydrogenated products were detected, which strongly support that the temperature and the hydrogen pressure used in our catalytic experiments are not forcing enough for the hydrogenation of tiglic acid and that no metallic residues or similar contaminations that may cause (catalyze) hydrogenation are present.

Mercury poisoning

It is well known that forcing conditions, such as high temperature and high pressure of hydrogen gas, increase the possibility of formation of colloidal metal particles that may function as catalysts.^{38,39} The ability of Hg(0) to poison metal colloids or heterogeneous catalysts has been used for more than 80 years.⁴⁰ Therefore, a mercury poisoning test⁴¹ was performed in order to investigate the potential formation of (catalytically active) metal colloids in our hydrogenation experiments. Hydrogenation of tiglic acid using **3** was carried out under the typical reaction conditions described above. The reaction was allowed to proceed to ~50% completion, followed by release of H₂ pressure and the addition of a 2000-fold excess of Hg(0) to the reaction mixture. The solution

was stirred for 30 min to enable Hg(0) to react with any colloidal particles present. As we have previously observed for analogous reactions utilizing tetra ruthenium clusters as catalysts/catalyst precursors,²¹ slightly better results were obtained than in the reactions without Hg(0) added. Both the conversion and the enantioselectivity were increased by 2-3 percentage units (Table 1, entries 1 vs 21). The obtained results suggest that the cluster does undergo fragmentation and the formation of colloidal particles occurs during the catalytic reaction; however, the effect of the colloidal particles formed seems very limited for the hydrogenation reaction.

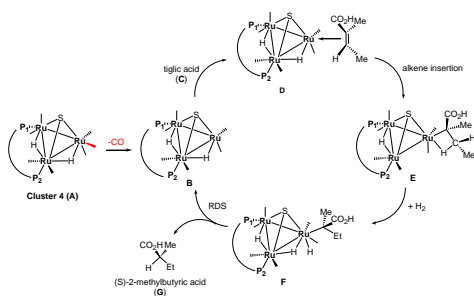
Proposed catalytic cycle

In an earlier study,²⁶ we proposed two plausible mechanisms for the activation of tiglic acid by intact Ru₄ clusters having the composition [H₄Ru₄(CO)₁₀(L)] (where L = chiral diphosphine ligand) - either dissociation of a carbonyl ligand to yield a vacant coordination site or metal-metal bond scission resulting in an open butterfly structure. To help elucidate the catalytic cycle(s) associated with the present Ru₃ clusters, we have modelled the course of the hydrogenation reaction using density functional theory calculations. Cluster **4**, which gives good conversion and enantioselectivity by the standards of these catalysts, was chosen as the model catalyst for comprehensive DFT evaluation. The computed catalytic cycle is depicted in Scheme 3, and the free energy surface for the hydrogenation reaction is shown in Figure 7. The cycle is initiated by a site-selective dissociation of an equatorial CO at the Ru(CO)₃ moiety; of the two equatorial CO groups here, the one that is proximally located to the bridging hydride is preferentially labilized. The formation of the coordinatively unsaturated species **B**, which proceeds without cluster fragmentation, serves as the bifurcation point leading to the 2-methylbutyric acid product.

Si-face coordination of tiglic acid to **B** affords the alkene-substituted cluster **D**. Regiospecific insertion of the alkene into the proximal bridging hydride occurs via transition structure **TSDE**, which lies 29.6 kcal/mol above **B** and **C**. The alternative alkene insertion route that involves the most substituted alkene carbon atom and that would directly yield the (S) stereogenic center, lies 6.6 kcal/mol above **TSDE** (not shown). The resulting agostic alkyl cluster **E** reacts with H₂ to furnish the transient trihydride cluster **F**. Reductive elimination in **F** gives (S)-2-methylbutyric acid (**G**) and regenerates cluster **B**, completing the catalytic cycle with a net release of 13.2 kcal/mol. The geometry-optimized structures for these species are shown in Figure 8.

Re-face alkene coordination at **B** gives the diastereomeric alkene cluster **D_{alt}**, from which the hydrogenation reaction proceeds through a series of identical steps, all of which lie higher in energy than the si-face route. The energetics computed for the reaction profile from **D_{alt}** depicted in Fig. 7 (red energy surface) are in concert with the observed preference for the (S) enantiomer when cluster **4** is employed as the catalyst precursor. The mechanistic steps computed involve a fixed stereochemistry at the cluster, whose chirality directly influences the asymmetric induction observed in the hydrogenation product.

The computed scheme is in agreement with the proposed catalytic cycle for the hydrogenation of ethane by [H₄Ru₄(CO)₁₂]. On the basis of kinetic data, a mechanism, where suppression of catalysis by the addition of CO and the evolution of CO on exposure of a heptane solution of [H₄Ru₄(CO)₁₂] to hydrogen, has been suggested to involve an initial dissociation of CO ligand and formation of [H₄Ru₄(CO)₁₁(alkene)], followed by an alkene insertion reaction to furnish the Ru₄ cluster [H₃Ru₄(CO)₁₁(alkyl)] as an intermediate.⁴²



Scheme 3. Computed catalytic hydrogenation cycle of tiglic acid by cluster **4** to give (S)-2-methylbutyric acid.

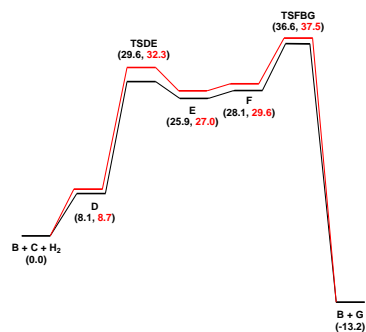


Figure 7. Free energy profiles for the hydrogenation of tiglic acid catalysed by cluster **4** (**A**) starting from the unsaturated cluster **B**. Black and red profiles are for the si- and re-face alkene coordination routes, respectively.

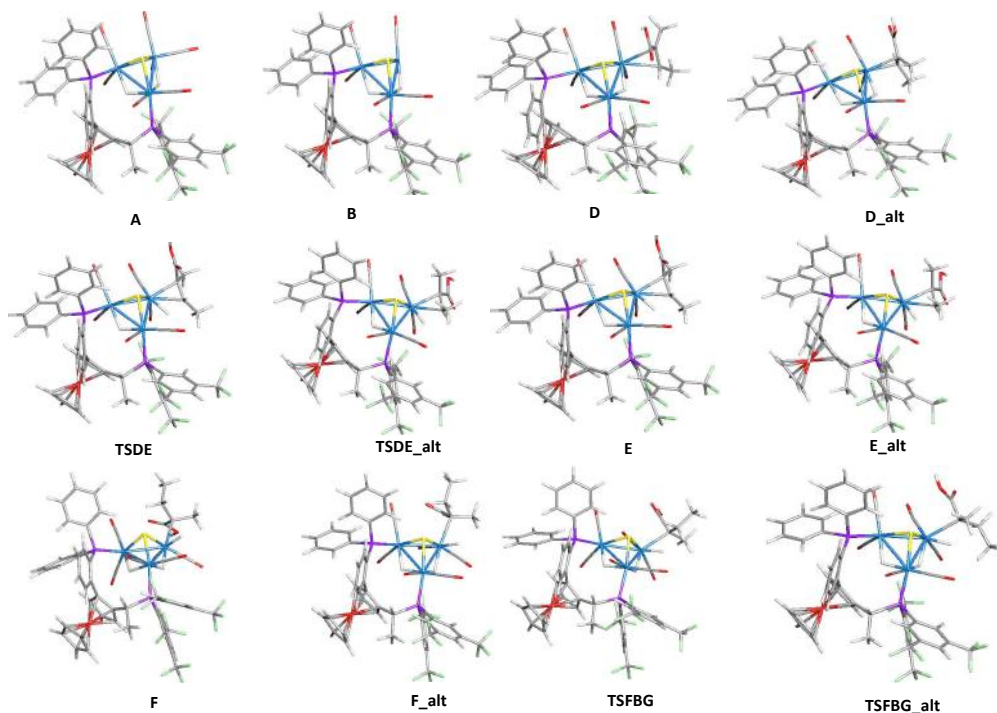


Figure 8. Geometry-optimized structures associated with the hydrogenation of tiglic acid to 2-methylbutyric acid catalyzed by cluster precursor **4**. The optimized structures of CO, H₂, tiglic acid (**C**), and 2-methylbutyric acid (**G**) are not shown.

Conclusions

In summary, twenty clusters of the general formula $[(\mu\text{-H})_2\text{Ru}_3(\mu_3\text{-S})(\text{CO})_7(\mu\text{-}1,2\text{-L})]$ (L = chiral diphosphine ligand), containing chiral clusters frameworks, have been prepared. All cluster diastereomers show different catalytic activities in terms of conversion and enantioselectivity in the asymmetric hydrogenation of tiglic acid under relatively mild conditions. The reversal in enantioselectivity of the hydrogenation reaction when the chirality of the cluster framework is changed, while the chirality of the ligand remains intact, strongly implicates the involvement of intact Ru₃ clusters as the active hydrogenation catalysts. The conversion rates are relatively good but the enantioselectivities are low, albeit good when compared to most other cluster-based catalytic systems for asymmetric reactions.^{29,30,33-35}

Experimental Section

General procedures

All reactions and other manipulations were carried out under a nitrogen atmosphere using standard Schlenk techniques. All solvents were dried and distilled under a nitrogen atmosphere

prior to use. Infra-red spectra were recorded as solutions in 0.5 mm NaCl cells on a Nicolet Avatar 360 FT-IR-spectrometer. ¹H and ³¹P NMR spectra were recorded on a Varian Unity 500 MHz NMR spectrometer; ³¹P NMR shifts were referenced to external H₃PO₄ (85%). The parent cluster $[(\mu\text{-H})_2\text{Ru}_3(\mu_3\text{-S})(\text{CO})_9]$ was prepared according to a literature procedure and its purity was assessed using thin-layer chromatography (TLC) and IR spectroscopy.⁴³ The chiral phosphines, 2-methylbutyric acid, S-methyl mandelate and tiglic acid (*trans*-2-methyl-2-butenic acid) were purchased from Sigma Aldrich. Separations were carried out by preparative thin-layer chromatography on glass plates (20 x 20 cm²) coated with silica gel (Merck, 0.5 mm thick). Catalysis experiments were carried out using a 45-mL Parr autoclave with a PTFE reaction vessel.

General method for the synthesis of sulfide-capped triruthenium hydrido clusters containing chiral Walphos (1a–1h) and Josiphos (2a–2e) ligands

In all preparations, a solution of Me₃NO (13 mg, 173 μmol) in methanol (5 mL) was added dropwise to a stirred solution of $[(\mu\text{-H})_2\text{Ru}_3(\mu_3\text{-S})(\text{CO})_9]$ (42 mg, 71 μmol) and the proper stoichiometric ratio of the ligand (*vide infra*) in dichloromethane (20 mL) under nitrogen atmosphere over a period of 20 minutes.

The reaction mixture was stirred for 3 h and filtered through silica. The solvent was removed *in vacuo* and the resultant residue was subjected to thin layer chromatography using glass plates coated with silica gel F₂₅₄, using a dichloromethane/hexane mixture (3:7 v/v) as eluent (for **11** and **12**, dichloromethane/hexane (3:2) was used as eluent). Clusters **3** and **4** were obtained as two closely spaced yellow bands. Clusters **5** - **6**, **7** - **8**, **9** - **10**, **11** - **12**, **13** - **14**, **15** - **16**, **17** - **18**, **19**, **20** - **21**, **22** and finally **23**, were prepared via identical procedures using **1a**, **S,S-1b**, **1c**, **1d**, **1e**, **1f**, **1g**, **1h**, **2a**, **2b**, **2c**, **2d**, **2e**, respectively. Crystallization of **3** - **6**, **8**, **17** and **20** from CH₂Cl₂-hexane solutions at 4 °C gave red crystals suitable for X-ray diffraction analysis.

[(μ-H)₂Ru₃(μ₃-S)(CO)₇(μ-1,2-1a)], **3 and **4****

A total of 66 mg (71 μmol) of **1a** was reacted with [(μ-H)₂Ru₃(μ₃-S)(CO)₉] to give two diastereomers with the general formula [(μ-H)₂Ru₃(μ₃-S)(CO)₇(μ-1,2-1a)].

[(μ-H)₂Ru₃(μ₃-S)(CO)₇(μ-1,2-1a)] **3**, Yield 32 mg (31 %); (*R*_f = 0.6); IR (ν(CO)/cm⁻¹, Cyclohexane) 2066(s), 2046(vs), 2010(vs), 1994(s), 1979(m), 1951(m); ¹H NMR (500 MHz, CDCl₃, hydride resonance) δ -18.13 (ddd, *J* = 12.4, 11.2, 2.9 Hz, 1H), -18.40 (dt, *J* = 9.8, 2.9 Hz, 1H); ³¹P NMR (202 MHz, CDCl₃) δ 49.75 (d, *J* = 10.6 Hz), 37.74 (t, *J* = 9.1 Hz), ES⁺ MS (*m/z*): 1464 [M]⁺.

[(μ-H)₂Ru₃(μ₃-S)(CO)₇(μ-1,2-1a)] **4**, Yield 39 mg (38%); (*R*_f = 0.4); IR (ν(CO)/cm⁻¹, Cyclohexane) 2066(s), 2048(vs), 2008(vs), 1995(s), 1982(w), 1951(m); ¹H NMR (500 MHz, CDCl₃, hydride resonance) δ -17.82 (ddd, *J* = 12.2, 8.8, 3.5 Hz, 1H), -18.63 (ddd, *J* = 7.5, 3.5 Hz, 1H); ³¹P NMR (202 MHz, CDCl₃) δ 48.52 (dd, *J* = 11.1, 6.6 Hz), 34.41 (d, *J* = 8.2 Hz). ES⁺ MS (*m/z*): 1464 [M]⁺.

[(μ-H)₂Ru₃(μ₃-S)(CO)₇(μ-1,2-1b)], **5 and **6****

A total of 66 mg (71 μmol) of **S,S-1b** was reacted with [(μ-H)₂Ru₃(μ₃-S)(CO)₉] to give two diastereomers with the general formula [(μ-H)₂Ru₃(μ₃-S)(CO)₇(μ-1,2-1b)].

[(μ-H)₂Ru₃(μ₃-S)(CO)₇(μ-1,2-1b)] **5**, Yield 29 mg (28 %); (*R*_f = 0.6); IR (ν(CO)/cm⁻¹, Cyclohexane) 2066(s), 2048(vs), 2008(vs), 1995(s), 1979(m), 1951(m); ¹H NMR (500 MHz, CDCl₃, hydride resonance) δ -18.12 (ddd, *J* = 12.6, 11.1, 3.0 Hz, 1H), -18.40 (dt, *J* = 9.6, 3.1, 3.0 Hz, 1H); ³¹P NMR (202 MHz, CDCl₃) δ 48.68 (dd, *J* = 11.8, 2.0 Hz), 36.60 (t, *J* = 9.8 Hz). ES⁺ MS (*m/z*): 1464 [M]⁺.

[(μ-H)₂Ru₃(μ₃-S)(CO)₇(μ-1,2-1b)] **6**, Yield 40 mg (38%); (*R*_f = 0.5); IR (ν(CO)/cm⁻¹, Cyclohexane) 2066(s), 2046(vs), 2010(vs), 1994(s), 1979(m), 1951(m); ¹H NMR (500 MHz, CDCl₃, hydride resonance) δ -17.84 (ddd, *J* = 12.4, 9.1, 3.0 Hz, 1H), -18.65 (ddd, *J* = 7.1, 3.2, 3.0 Hz, 1H); ³¹P NMR (202 MHz, CDCl₃) δ 48.59 (dd, *J* = 11.3, 5.9 Hz), 35.55 (d, *J* = 8.4 Hz). ES⁺ MS (*m/z*): 1464 [M]⁺.

[(μ-H)₂Ru₃(μ₃-S)(CO)₇(μ-1,2-1c)], **7 and **8****

A total of 48 mg (71 μmol) of **1c** was reacted with [(μ-H)₂Ru₃(μ₃-S)(CO)₉] to give two diastereomers with the general formula [(μ-H)₂Ru₃(μ₃-S)(CO)₇(μ-1,2-1c)].

[(μ-H)₂Ru₃(μ₃-S)(CO)₇(μ-1,2-1c)] **7**, Yield 27 mg (32 %); (*R*_f = 0.5); IR (ν(CO)/cm⁻¹, Cyclohexane) 2057(s), 2038(vs), 1995(vs), 1984(s), 1965(m), 1932(m); ¹H NMR (500 MHz, CDCl₃, hydride resonance) δ -18.51 (ddd, *J* = 11.0, 9.7, 3.0 Hz, 1H), -18.64 (dt, *J* = 11.8, 3.0 Hz, 1H); ³¹P NMR (202 MHz, CDCl₃) δ 56.47 (dd, *J* = 9.6, 5.0 Hz), 37.16 (t, *J* = 9.7 Hz). ES⁺ MS (*m/z*): 1228 [M+Na]⁺.

[(μ-H)₂Ru₃(μ₃-S)(CO)₇(μ-1,2-1c)] **8**, Yield 33 mg (39 %); (*R*_f = 0.4); IR (ν(CO)/cm⁻¹, Cyclohexane) 2057(s), 2034(vs), 1998(vs), 1985(s), 1969(m), 1942(m); ¹H NMR (500 MHz, CDCl₃, hydride resonance) δ -18.08 (ddd, *J* = 10.3, 9.0, 3.0 Hz, 1H), -19.02 ('m', ddd, *J* = not resolved 1H, cf. ES⁺); ³¹P NMR (202 MHz, CDCl₃) δ 59.08 (dd, *J* = 9.6, 6.2 Hz), 35.24 (dd, *J* = 8.6, 2.7 Hz); ES⁺ MS (*m/z*): 1228 [M+Na]⁺.

[(μ-H)₂Ru₃(μ₃-S)(CO)₇(μ-1,2-1d)], **9 and **10****

A total of 74 mg (71 μmol) of **1d** was reacted with [(μ-H)₂Ru₃(μ₃-S)(CO)₉] to give two diastereomers with the general formula [(μ-H)₂Ru₃(μ₃-S)(CO)₇(μ-1,2-1d)].

[(μ-H)₂Ru₃(μ₃-S)(CO)₇(μ-1,2-1d)] **9**, Yield 26 mg (23 %); (*R*_f = 0.5); IR (ν(CO)/cm⁻¹, Cyclohexane) 2063(s), 2044(vs), 2008(vs), 1993(s), 1976(m), 1951(m); ¹H NMR (500 MHz, CDCl₃, hydride resonance) δ -18.09 (dt, *J* = 9.6, 2.8 Hz, 1H), -18.39 (ddd, *J* = 12.8, 10.2, 2.9 Hz); ³¹P NMR (202 MHz, CDCl₃) δ 48.89 (d, *J* = 11.8 Hz), 35.65 (t, *J* = 9.6 Hz). ES⁺ MS (*m/z*): 1580 [M]⁺.

[(μ-H)₂Ru₃(μ₃-S)(CO)₇(μ-1,2-1d)] **10**, Yield 37 mg (33 %); (*R*_f = 0.4); IR (ν(CO)/cm⁻¹, Cyclohexane) 2064(s), 2047(vs), 2006(vs), 1992(s), 1980(m), 1949(m); ¹H NMR (500 MHz, CDCl₃, hydride resonance) δ -17.82 (ddd, *J* = 12.2, 8.8, 3.4 Hz, 1H), -18.63 (ddd, *J* = 7.3, 5., 3.4 Hz 1H); ³¹P NMR (202 MHz, CDCl₃) δ 48.49 (dd, *J* = 11.3, 6.5 Hz), 34.37 (d, *J* = 8.4 Hz). ES⁺ MS (*m/z*): 1603 [M+Na]⁺.

[(μ-H)₂Ru₃(μ₃-S)(CO)₇(μ-1,2-1e)], **11 and **12****

A total of 51 mg (71 μmol) of **1e** was reacted with [(μ-H)₂Ru₃(μ₃-S)(CO)₉] to give two diastereomers with the general formula [(μ-H)₂Ru₃(μ₃-S)(CO)₇(μ-1,2-1e)].

[(μ-H)₂Ru₃(μ₃-S)(CO)₇(μ-1,2-1e)] **11**, Yield 29 mg (33 %); (*R*_f = 0.6); IR (ν(CO)/cm⁻¹, Cyclohexane) 2059(s), 2042(vs), 2000(vs), 1985(m), 1970(w), 1939(w); ¹H NMR (500 MHz, CDCl₃, hydride resonance) δ -17.61 (td, *J* = 9.8, 3.0 Hz, 1H), -18.17 ('m', ddd, *J* = not resolved 1H, cf. ES⁺); ³¹P NMR (202 MHz, CDCl₃) δ 43.88 (dd, *J* = 9.5, 6.2 Hz), 35.63 (dd, *J* = 8.9, 2.4 Hz). ES⁺ MS (*m/z*): 1248 [M]⁺.

[(μ-H)₂Ru₃(μ₃-S)(CO)₇(μ-1,2-1e)] **12**, Yield 38 mg (43 %); (*R*_f = 0.5); IR (ν(CO)/cm⁻¹, Cyclohexane) 2059(s), 2042(vs), 2000(vs),

1985(m), 1970(w), 1939(w); ¹H NMR (500 MHz, CDCl₃, hydride resonance) δ -17.61 (ddd, *J* = 10.0, 3.0 Hz, 1H), -18.16 ('m', ddd, *J* = not resolved 1H, cf. ES†); ³¹P NMR (202 MHz, CDCl₃) δ 49.09 (dd, *J* = 10.2, 1.7 Hz), 36.60 (t, *J* = 9.5 Hz). ES⁺ MS (*m/z*): 1248 [M]⁺.

[(μ-H)₂Ru₃(μ₃-S)(CO)₇(μ-1,2-1f)], 13 and 14

A total of 70 mg (71 μmol) of **1f** was reacted with [(μ-H)₂Ru₃(μ₃-S)(CO)₉] to give two diastereomers with the general formula [(μ-H)₂Ru₃(μ₃-S)(CO)₇(μ-1,2-1f)].

[(μ-H)₂Ru₃(μ₃-S)(CO)₇(μ-1,2-1f)] **13**, Yield 33 mg (31 %); (*R*_f = 0.6); IR (ν(CO)/cm⁻¹, Cyclohexane) 2064(vs), 2047(m), 2038(s), 2003(vs), 1992(s), 1983(m), 1976(w), 1945(m), 1938(w); ¹H NMR (500 MHz, CDCl₃, hydride resonance) δ -18.14 (ddd, *J* = 13.8, 4.5, 2.5 Hz, 1H), -18.31 ('m', ddd, *J* = not resolved 1H, cf. ES†); ³¹P NMR (202 MHz, CDCl₃) δ 52.62 (m), 49.49 (dd, *J* = 11.1, 1.3 Hz). ES⁺ MS (*m/z*): 1502 [M+Na]⁺.

[(μ-H)₂Ru₃(μ₃-S)(CO)₇(μ-1,2-1f)] **14**, Yield 45 mg (43 %); (*R*_f = 0.6); IR (ν(CO)/cm⁻¹, Cyclohexane) 2064(vs), 2047(s), 2037(m), 2003(vs), 1992(m), 1977(w), 1946(w), 1939(w); ¹H NMR (500 MHz, CDCl₃, hydride resonance) δ -18.17 (ddd, *J* = 11.9, 7.0, 3.6 Hz, 1H), -18.83 (ddd, *J* = 4.8, 3.6 Hz, 1H); ³¹P NMR (202 MHz, CDCl₃) δ 48.49 (dd, *J* = 11.3, 6.5 Hz), 34.37 (d, *J* = 8.4 Hz). ES⁺ MS (*m/z*): 1479 [M]⁺.

[(μ-H)₂Ru₃(μ₃-S)(CO)₇(μ-1,2-1g)], 15 and 16

A total of 55 mg (71 μmol) of **1g** was reacted with [(μ-H)₂Ru₃(μ₃-S)(CO)₉] to give two diastereomers with the general formula [(μ-H)₂Ru₃(μ₃-S)(CO)₇(μ-1,2-1g)].

[(μ-H)₂Ru₃(μ₃-S)(CO)₇(μ-1,2-1g)] **15**, Yield 36 mg (39 %); (*R*_f = 0.6); IR (ν(CO)/cm⁻¹, Cyclohexane) 2059(s), 2042(vs), 1999(vs), 1983(s), 1970(m), 1938(m); ¹H NMR (500 MHz, CDCl₃, hydride resonance) δ -17.69 (td, *J* = 9.7, 3.0 Hz, 1H), -18.25 (dt, *J* = 6.4, 3.0 Hz, 1H); ³¹P NMR (202 MHz, CDCl₃) δ 44.05 (dd, *J* = 9.5, 6.4 Hz), 36.51 (dd, *J* = 8.8, 2.6 Hz). ES⁺ MS (*m/z*): 1327 [M+Na]⁺.

[(μ-H)₂Ru₃(μ₃-S)(CO)₇(μ-1,2-1g)] **16**, Yield 48 mg (52 %); (*R*_f = 0.5); IR (ν(CO)/cm⁻¹, Cyclohexane) 2057(s), 2039(s), 2003(s), 2003(vs), 1984(s), 1967(m), 1940(w); ¹H NMR (500 MHz, CDCl₃, hydride resonance) δ -18.16 (m, 2H); (500 MHz, Acetone-*d*₆, 253K) δ -18.12 (dt, *J* = 11.0, 3.0 Hz, 1H), -18.19 ('m', ddd, *J* = not resolved 1H, cf. ES†); ³¹P NMR (202 MHz, CDCl₃) δ 49.32 (dd, *J* = 7.1, 5.1 Hz), 38.10 (t, *J* = 9.6 Hz). ES⁺ MS (*m/z*): 1305 [M+H]⁺.

[(μ-H)₂Ru₃(μ₃-S)(CO)₇(μ-1,2-1h)], 17

A total of 47 mg (71 μmol) of **1h** was reacted with [(μ-H)₂Ru₃(μ₃-S)(CO)₉] to give [(μ-H)₂Ru₃(μ₃-S)(CO)₇(μ-1,2-1h)] **17**.

[(μ-H)₂Ru₃(μ₃-S)(CO)₇(μ-1,2-1h)] **17**, Yield 36 mg (42 %); (*R*_f = 0.5); IR (ν(CO)/cm⁻¹, Cyclohexane) 2060(s), 2043(vs), 2001(vs),

1986(s), 1972(m), 1941(m); ¹H NMR (500 MHz, CDCl₃, hydride resonance) δ -17.75 (ddd, *J* = 10.1, 9.1, 3 Hz, 1H), -18.47 (dt, *J* = 6.1, 3.0 Hz, 1H); ³¹P NMR (202 MHz, CDCl₃) δ 44.95 (dd, *J* = 9.9, 5.7 Hz), 35.39 (dd, *J* = 9.1, 1.8 Hz). ES⁺ MS (*m/z*): 1191 [M]⁺.

[(μ-H)₂Ru₃(μ₃-S)(CO)₇(μ-1,2-2a)], 18 and 19

A total of 62 mg (71 μmol) of **2e** was reacted with [(μ-H)₂Ru₃(μ₃-S)(CO)₉] to give two diastereomers with the general formula [(μ-H)₂Ru₃(μ₃-S)(CO)₇(μ-1,2-2a)].

[(μ-H)₂Ru₃(μ₃-S)(CO)₇(μ-1,2-2a)] **18**, Yield 14 mg (14 %); (*R*_f = 0.6); IR (ν(CO)/cm⁻¹, Cyclohexane) 2066(vs), 2036(s), 2005(vs), 1996(s), 1987(m), 1951(m); ¹H NMR (500 MHz, CDCl₃, hydride resonance) δ -18.29 (dt, *J* = 36.5, 2.5 Hz, 1H), -19.46 (ddd, *J* = 13.3, 7.1, 2.5 Hz, 1H); ³¹P NMR (202 MHz, CDCl₃) δ 56.94 (dd, *J* = 34.7, 5.9 Hz), 25.71 (d, *J* = 11.8 Hz). ES⁺ MS (*m/z*): 1400 [M]⁺.

[(μ-H)₂Ru₃(μ₃-S)(CO)₇(μ-1,2-2a)] **19**, Yield 25 mg (25%); (*R*_f = 0.5); IR (ν(CO)/cm⁻¹, Cyclohexane) 2064(vs), 2039(ms), 2032(w), 2007(vs), 1993(m), 1980(m), 1967(w), 1951(w); ¹H NMR (500 MHz, CDCl₃, hydride resonance) δ -17.84 (ddd, *J* = 12.7, 9.0, 3.6 Hz, 1H), -18.65 (ddd, *J* = 7.5, 3.6 Hz, 1H); ³¹P NMR (202 MHz, CDCl₃) δ 48.59 (dd, *J* = 10.4, 4.7 Hz), 35.54 (d, *J* = 8.4 Hz). ES⁺ MS (*m/z*): 1400 [M]⁺.

[(μ-H)₂Ru₃(μ₃-S)(CO)₇(μ-1,2-2b)], 20

A total of 41 mg (71 μmol) of **2b** was reacted with [(μ-H)₂Ru₃(μ₃-S)(CO)₉] to give [(μ-H)₂Ru₃(μ₃-S)(CO)₇(μ-1,2-2b)] **20**.

[(μ-H)₂Ru₃(μ₃-S)(CO)₇(μ-1,2-2b)] **20**, Yield 33 mg (44 %); (*R*_f = 0.6); IR (ν(CO)/cm⁻¹, Cyclohexane) 2059(vs), 2031(s), 2016(vs), 1998(vs), 1970(w), 1941(m); ¹H NMR (500 MHz, CDCl₃, hydride resonance) δ -18.31 (dd, *J* = 32.6, 2.0 Hz, 1H), -19.13 ('t', ddd, *J* = not resolved 1H, cf. ES†); ³¹P NMR (202 MHz, CDCl₃) δ 57.29 (m), 25.41 (m). ES⁺ MS (*m/z*): 1174 [M]⁺.

[(μ-H)₂Ru₃(μ₃-S)(CO)₇(μ-1,2-2c)], 21

A total of 39 mg (71 μmol) of **2c** was reacted with [(μ-H)₂Ru₃(μ₃-S)(CO)₉] to give [(μ-H)₂Ru₃(μ₃-S)(CO)₇(μ-1,2-2c)] **21**.

[(μ-H)₂Ru₃(μ₃-S)(CO)₇(μ-1,2-2c)] **21**, Yield 44 mg (59 %); (*R*_f = 0.6); IR (ν(CO)/cm⁻¹, Cyclohexane) 2057(vs), 2033(s), 1994(vs), 1980(m), 1969(w), 1926(w); ¹H NMR (500 MHz, CDCl₃, hydride resonance) δ -18.77 (br, 1H), -19.09 (m, 1H); ³¹P NMR (202 MHz, CDCl₃) δ 65.05 (m), 35.49 (m). ES⁺ MS (*m/z*): 1163 [M+Na]⁺.

[(μ-H)₂Ru₃(μ₃-S)(CO)₇(μ-1,2-2d)], 22

A total of 41 mg (71 μmol) of **2d** was reacted with [(μ-H)₂Ru₃(μ₃-S)(CO)₉] to give [(μ-H)₂Ru₃(μ₃-S)(CO)₇(μ-1,2-2d)] **22**.

[(μ-H)₂Ru₃(μ₃-S)(CO)₇(μ-1,2-2d)] **22**, Yield 36 mg (48 %); (*R*_f = 0.6); IR (ν(CO)/cm⁻¹, Cyclohexane) 2059(vs), 2038(s), 2001(vs),

1988(m), 1970(w), 1943(w); ^1H NMR (500 MHz, CDCl_3 , hydride resonance) δ -18.04 (m, 1H); (500 MHz, Acetone- d_6 , 253K) δ -17.93 (ddd, J = 11.8, 2.0 Hz, 1H), -18.10 (ddd, J = 23.4, 10.4, 2.0 Hz); ^{31}P NMR (202 MHz, CDCl_3) δ 41.66 (m), 20.65 (m). ES $^+$ MS (m/z): 1172 [M] $^+$.

Homogeneous Catalytic Experiments

In the catalysis experiments, the catalyst and substrate were loaded into the autoclave under N_2 , and the degassed solvent mixture was added (2.5 mL of EtOH/2.5 mL of toluene). The reaction vessel was closed and purged three times with hydrogen before final pressurizing to 50 bar. The reaction mixture was continuously stirred with a magnetic stirrer (ca. 750 rpm) and heated at 100 $^\circ\text{C}$ for 24 h. After a cooling period of approximately 45 min, the reaction vessel was depressurized and opened. The homogeneous reaction mixture was transferred to a 50-mL flask and concentrated under vacuum. The conversions for the catalysis runs were calculated on the basis of NMR analyses.

Precautions were taken to avoid the possibility of catalytic activity due to contamination of the reaction vessel or the magnetic stir bars: the reaction vessel and the magnetic stir bars were washed with acetone and rinsed with dichloromethane, followed by a careful visual examination. Whenever the magnetic stir bars appeared to be contaminated, they were discarded.

To separate the carboxylic acid from the cluster, the reaction residue was dissolved in 10 mL of diethyl ether and the carboxylic acid was extracted with aqueous sodium hydroxide solution (1M, 3 x 10 mL) and washed with diethyl ether (3 x 5 mL), leaving the cluster in the organic solvent. The carboxylate was protonated with sulfuric acid and extracted with diethyl ether (3 x 10 mL), washed with water (2 x 5 mL) and dried over magnesium sulfate. Filtration, followed by evaporation of the ether under vacuum, yielded the carboxylic acid quantitatively. The original ether phase, from which the carboxylic acid was extracted, was concentrated under vacuum to recover the remaining cluster. In certain cases, where ester formation was obtained during the catalytic experiment, the recovered catalyst was dissolved in a minimum quantity of dichloromethane and the products were separated by preparative TLC, eluting with dichloromethane/petroleum ether (1:2). Usually 60-70% of the cluster was recovered after a catalytic experiment and it was analyzed by IR and NMR spectroscopies. The enantiomeric excess of the product was detected by derivatizing 2-methylbutyric acid with S-methyl mandelate and analyzing the diastereomeric product mixture by NMR, as fully described by Tyrrell *et al.*⁴⁴ It was found that flash chromatography of the final products was not necessary.

Catalyst poisoning test using mercury

The experimental setup followed the procedure described above for catalytic experiments, except that after 4 h the reaction was stopped and the reaction vessel was disconnected and

approximately 2 grams of metallic mercury was added to the reaction mixture before the autoclave was sealed and pressurized and a second hydrogenation reaction was started. After a complete catalytic run, the products were separated and analyzed as described above.

VT ^1H NMR studies

All NMR solvents (Aldrich) were used as received. Approximately 0.5 mL of a saturated acetone- d_6 solution of $[(\mu\text{-H})_2\text{Ru}_3(\mu_3\text{-S})(\text{CO})_7(\mu\text{-1,2-1h})]$ **16** and $[(\mu\text{-H})_2\text{Ru}_3(\mu_3\text{-S})(\text{CO})_7(\mu\text{-1,2-2d})]$ **22** were added to a NMR tube, which was subsequently sealed under N_2 atmosphere. The sample tube was placed into the probe using a ceramic spinner. Dry air (for measurements above RT) or liquid nitrogen was used as the VT control gas. The sample was allowed to equilibrate at each desired temperature for 5 – 10 minutes before the start of shimming and data acquisition. The temperature ranges were 25 to -40 $^\circ\text{C}$ for **16** and 25 to -70 $^\circ\text{C}$ for **22**. For each sample 32 scans were acquired to reach sufficient signal intensity. The residual proton signal of acetone (2.04 ppm rel. to TMS) was used as a chemical shift reference.

X-ray structure determinations

The crystals were immersed in cryo-oil, mounted in a Nylon loop, and measured at a temperature of 100 K for **5**, 170 K for **3**, **4**, **8**, **17** and **20**, and finally 293 K for **6**. The X-ray diffraction data were collected on a Nonius Kappa CCD or on a Bruker AXS Kappa ApexII Duo diffractometer using Mo $\text{K}\alpha$ radiation (λ = 0.71073 Å). The *Denzo-Scalepack*⁴⁵ or *APEX2*⁴⁶ program packages were used for cell refinements and data reductions. The structures were solved by direct methods using the *SHELXS-97* program⁴⁷ with the *WinGX* graphical user interface.⁴⁸ All hydrogens were placed in idealized positions. Positions of hydrides were calculated using the *XHYDEX* program.⁴⁹ Selected crystallographic details are summarized in Table 2.

Computational modelling and DFT calculations

The DFT calculations were carried out with the Gaussian 09 package of programs.⁵⁰ The different species in Scheme 3 were examined computationally using Morokuma's ONIOM method,⁵¹ using a two-layered ONIOM (B3LYP/genecp:PM6) approach. Here the Walphos ligand, except for the phosphorus and iron atoms, was confined to the lower layer. The Ru and Fe atoms were described with the Stuttgart-Dresden effective core potential (ecp) and a SDD basis set, and all of the other high level atoms were described by a 6-31G(d') basis set.

All reported geometries were fully optimized, and the analytical Hessian was evaluated at each stationary point to determine whether the geometry was an energy minimum (no negative eigenvalues) or a transition structure (one negative eigenvalue). Unscaled vibrational frequencies were used to make zero-point and thermal corrections to the electronic energies. The resulting free energies are reported in kcal/mol relative to the specified standard. Standard state corrections were applied to all species to

convert concentrations from 1 atm to 1M according to the treatise of Cramer.⁵² Internal reaction coordinate (IRC) calculations were performed in order to establish the reactant and product species associated with each transition-state structure. The geometry-optimized structures have been drawn with the *JMMP2* molecular visualization and manipulation program.⁵³

Table 2. Crystallographic data for clusters [(μ-H)₂Ru(μ³-S)(CO)(μ-P-P^{nc})] **3**, **6**, **8**, **17** and **20**, where (P-P^{nc})= **1a**, **1b**, **1c**, **1h** and **2b**, respectively).

Formula	3		4		5		6		8		17		20	
	C ₃₃ H ₁₆ F ₁₀ FeO ₄ P ₂ Ru ₂ S	C ₃₃ H ₁₆ F ₁₀ FeO ₄ P ₂ Ru ₂ S	C ₃₃ H ₁₆ F ₁₀ FeO ₄ P ₂ Ru ₂ S	C ₃₃ H ₁₆ F ₁₀ FeO ₄ P ₂ Ru ₂ S	C ₃₃ H ₁₆ F ₁₀ FeO ₄ P ₂ Ru ₂ S	C ₃₃ H ₁₆ F ₁₀ FeO ₄ P ₂ Ru ₂ S	C ₃₃ H ₁₆ F ₁₀ FeO ₄ P ₂ Ru ₂ S	C ₃₃ H ₁₆ F ₁₀ FeO ₄ P ₂ Ru ₂ S	C ₃₃ H ₁₆ F ₁₀ FeO ₄ P ₂ Ru ₂ S	C ₃₃ H ₁₆ F ₁₀ FeO ₄ P ₂ Ru ₂ S	C ₃₃ H ₁₆ F ₁₀ FeO ₄ P ₂ Ru ₂ S	C ₃₃ H ₁₆ F ₁₀ FeO ₄ P ₂ Ru ₂ S	C ₃₃ H ₁₆ F ₁₀ FeO ₄ P ₂ Ru ₂ S	C ₃₃ H ₁₆ F ₁₀ FeO ₄ P ₂ Ru ₂ S
<i>M_r</i>	1463.86	1463.86	1463.86	1463.86	1463.86	1463.86	1463.86	1463.86	1203.95	1191.85	1191.85	1127.86	1127.86	1127.86
<i>T</i> [K]	170 (2)	170 (2)	170 (2)	100 (2)	293 (2)	170 (2)	293 (2)	170 (2)	0.71073	0.71073	0.71073	0.71073	0.71073	0.71073
<i>λ</i> [Å]	0.71073	0.71073	0.71073	0.71073	0.71073	0.71073	0.71073	0.71073	0.71073	0.71073	0.71073	0.71073	0.71073	0.71073
Crystal system	Orthorhombic	Orthorhombic	Monoclinic	Cc	Orthorhombic	Orthorhombic	Orthorhombic	Orthorhombic	Orthorhombic	Orthorhombic	Orthorhombic	Orthorhombic	Orthorhombic	Orthorhombic
Space group	P2 ₁ 2 ₁ 2 ₁	P2 ₁ 2 ₁ 2 ₁	P2 ₁ 2 ₁ 2 ₁	Cc	P2 ₁ 2 ₁ 2 ₁	P2 ₁ 2 ₁ 2 ₁	P2 ₁ 2 ₁ 2 ₁	P2 ₁ 2 ₁ 2 ₁	P2 ₁ 2 ₁ 2 ₁	P2 ₁ 2 ₁ 2 ₁	P2 ₁ 2 ₁ 2 ₁	P2 ₁ 2 ₁ 2 ₁	P2 ₁ 2 ₁ 2 ₁	P2 ₁ 2 ₁ 2 ₁
<i>a</i> [Å]	10.9799(5)	11.9655(4)	14.9044(2)	14.9044(2)	17.9576(9)	10.4751(2)	12.11044(17)	15.06019(16)	10.4751(2)	12.11044(17)	15.06019(16)	18.1823(2)	18.1823(2)	18.1823(2)
<i>b</i> [Å]	14.7027(5)	20.1151(5)	24.9178(4)	24.9178(4)	59.4487(11)	17.5460(4)	20.7626(4)	20.7626(4)	17.5460(4)	20.7626(4)	20.7626(4)	15.73196(19)	15.73196(19)	15.73196(19)
<i>c</i> [Å]	35.1126(9)	49.045(3)	14.7954(2)	14.7954(2)	10.978(5)	30.9412(8)	21.0868(4)	21.0868(4)	30.9412(8)	21.0868(4)	21.0868(4)	15.73196(19)	15.73196(19)	15.73196(19)
<i>α</i> /°	90	90	90	90	90	90	90	90	90	90	90	90	90	90
<i>β</i> /°	90	90	90	90	90	90	90	90	90	90	90	90	90	90
<i>γ</i> /°	90	90	90	90	90	90	90	90	90	90	90	90	90	90
<i>V</i> [Å ³]	5668.4(3)	11804.5(8)	5413.18(13)	5413.18(13)	11720(6)	5686.9(2)	11804.5(8)	4307.87(8)	5686.9(2)	11804.5(8)	4307.87(8)	4307.87(8)	4307.87(8)	4307.87(8)
<i>Z</i>	4	8	4	4	4	4	4	4	4	4	4	4	4	4
<i>ρ</i> _{calc} [g cm ⁻³]	1.715	1.647	1.796	1.796	1.658	1.406	1.493	1.739	1.406	1.493	1.739	1.533	1.533	1.533
<i>μ</i> [mm ⁻¹]	1.216	1.168	1.274	1.274	1.18	1.166	1.251	1.533	1.166	1.251	1.533	1.533	1.533	1.533
<i>F</i> (000)	2880	5760	2880	2880	5760	2416	2368	2256	2416	2368	2256	1872	1872	1872
Crystal size [mm]	0.13 x 0.08 x 0.03	0.173 x 0.081 x 0.036	0.41 x 0.26 x 0.14	0.38 x 0.15 x 0.15	0.196 x 0.103 x 0.043	0.277 x 0.066 x 0.048	0.228 x 0.124 x 0.086	0.228 x 0.124 x 0.086	0.196 x 0.103 x 0.043	0.277 x 0.066 x 0.048	0.228 x 0.124 x 0.086	0.228 x 0.124 x 0.086	0.228 x 0.124 x 0.086	0.228 x 0.124 x 0.086
<i>θ</i> limits/°	3.21 to 27.50	4.298 to 27.499	1.61 to 36.40	3.0 - 27.8	2.053 to 27.500	1.939 to 30.589	1.872 to 34.743	1.872 to 34.743	2.053 to 27.500	1.939 to 30.589	1.872 to 34.743	1.872 to 34.743	1.872 to 34.743	1.872 to 34.743
<i>h</i> range	-14 to 12	-15 to 11	-24 to 16	-23 to 23	-13 to 5	-14 to 16	-23 to 24	-23 to 24	-13 to 5	-14 to 16	-23 to 24	-23 to 24	-23 to 24	-23 to 24
<i>k</i> range	-16 to 19	-10 to 26	-39 to 41	-77 to 78	-22 to 14	-26 to 29	-29 to 25	-29 to 25	-22 to 14	-26 to 29	-29 to 25	-29 to 25	-29 to 25	-29 to 25
<i>l</i> range	-45 to 45	-54 to 63	-24 to 24	-14 to 14	-19 to 39	-30 to 25	-25 to 24	-25 to 24	-19 to 39	-30 to 25	-25 to 24	-25 to 24	-25 to 24	-25 to 24
No. reffns.	31467	42539	50958	249874	26884	12194	14239	17855	50958	249874	26884	12194	14239	17855
Unique reffns.	12988	26879	20611	26884	12194	14239	17855	17855	26884	12194	14239	17855	17855	17855
GOOF (F ²)	1.007	1.073	1.030	1.030	1.94	1.007	1.008	1.077	1.007	1.008	1.077	1.077	1.077	1.077
<i>R</i> _{int}	0.0541	0.0800	0.0227	0.0227	0.050	0.0222	0.0555	0.0583	0.0222	0.0555	0.0583	0.0583	0.0583	0.0583
<i>R</i> ₁ (I ≥ 2σ)	0.0518	0.1029	0.0225	0.0225	0.068	0.0322	0.0466	0.0300	0.0322	0.0466	0.0300	0.0300	0.0300	0.0300
WR2 ^b (I ≥ 2σ)	0.0753	0.1685	0.0529	0.0529	0.192	0.0628	0.0867	0.0608	0.0628	0.0867	0.0608	0.0608	0.0608	0.0608
Largest diff. peak and hole [e.Å ⁻¹]	0.779 and -0.521	1.447 and -1.211	1.154 and -0.791	1.28 and -1.06	0.401 and -0.299	1.086 and -0.785	0.552 and -0.835	0.552 and -0.835	0.401 and -0.299	1.086 and -0.785	0.552 and -0.835	0.552 and -0.835	0.552 and -0.835	0.552 and -0.835
Flack parameter	-0.02(2)	0.04(5)	0.000(8)	0.05(3)	-0.023(14)	-0.025(19)	-0.018(8)	-0.018(8)	-0.023(14)	-0.025(19)	-0.018(8)	-0.018(8)	-0.018(8)	-0.018(8)

ARTICLE

Acknowledgements

AFA thanks the EU Erasmus Mundus program for a predoctoral fellowship. AKS thanks the Carl Trygger Foundation for a postdoctoral fellowship. MGR thanks the Robert A. Welch Foundation (grant B-1093) for financial support and acknowledges computational resources through UNT's High Performance Computing Services and CASCAM. We thank Dr. David Hrovat and Prof. Xinzhen Yang for helpful ONIOM-based discussions.

Notes and references

^a Chemical Physics, Chemical Center, Lund University, Box 124, SE-221 00, Lund, Sweden. Email: Ebbe.Nordlander@chemphys.lu.se

^b Centre for Analysis and Synthesis, Department of Chemistry, Lund University, P.O. Box 124, S-221 00 Lund

^c Department of Chemistry, University of Jyväskylä, Box 35, FI-40014 Jyväskylä, Finland

^d Department of Chemistry, The University of North Texas, Denton, Texas 76203, United States.

† Electronic Supplementary Information (ESI) available: Experimental details, crystallographic details, FT-IR and NMR spectra. Atomic coordinates of all optimized stationary points and transition states. See DOI: 10.1039/b000000

1. A. J. Deeming and M. Underhill, *J. Organomet. Chem.*, 1972, 42, C60-C62.
2. H. Vahrenkamp, *Angew. Chem. Int. Ed. Engl.*, 1975, 14, 322-329.
3. T. A. Cresswell, J. A. K. Howard, F. G. Kennedy, S. A. R. Knox and H. Wade, *J. Chem. Soc., Dalton Trans.*, 1981, DOI: 10.1039/DT9810002220, 2220-2229.
4. K. A. Azam, G. M. Golzar Hossain, S. E. Kabir, K. M. Abdul Malik, M. A. Mottalib, S. Perven and N. C. Sarker, *Polyhedron*, 2002, 21, 381-387.
5. A. J. Deeming, M. M. Hassan, S. E. Kabir, E. Nordlander and D. A. Tocher, *Dalton Trans.*, 2004, DOI: 10.1039/B411833b, 3709-3714.
6. H. Akter, A. J. Deeming, G. M. G. Hossain, S. E. Kabir, D. N. Mondol, E. Nordlander, A. Sharmin and D. A. Tocher, *J. Organomet. Chem.*, 2005, 690, 4628-4639.
7. S. J. Ahmed, M. I. Hyder, S. E. Kabir, M. A. Miah, A. J. Deeming and E. Nordlander, *J. Organomet. Chem.*, 2006, 691, 309-322.
8. C. Bergounhou, P. Pompeyrine, G. Commenges and J. J. Bonnet, *J. Mol. Catal.*, 1988, 48, 285-312.
9. Y. Lin and R. G. Finke, *Inorg. Chem.*, 1994, 33, 4891-4910.
10. C. M. Hagen, L. Vieille-Petit, G. Laurenczy, G. Süß-Fink and R. G. Finke, *Organometallics*, 2005, 24, 1819-1831.
11. L. Vieille-Petit, G. Süß-Fink, B. Therrien, T. R. Ward, H. Stöckli-Evans, G. Labat, L. Karmazin-Brelot, A. Neels, T. Bürgi, R. G. Finke and C. M. Hagen, *Organometallics*, 2005, 24, 6104-6119.
12. R. D. Adams and T. S. Barnard, *Organometallics*, 1998, 17, 2567-2573.
13. R. D. Adams and T. S. Barnard, *Organometallics*, 1998, 17, 2885-2890.
14. P. Nombel, N. Lukan, B. Donnadieu and G. Lavigne, *Organometallics*, 1998, 18, 187-196.
15. S. Aime, R. Gobetto and D. Canet, *J. Am. Chem. Soc.*, 1998, 120, 6770-6773.
16. B. Bergman, E. Rosenberg, R. Gobetto, S. Aime, L. Milone and F. Reineri, *Organometallics*, 2002, 21, 1508-1511.
17. D. Blazina, S. B. Duckett, P. J. Dyson, B. F. G. Johnson, J. A. B. Lohman and C. J. Sleight, *J. Am. Chem. Soc.*, 2001, 123, 9760-9768.
18. D. Blazina, S. B. Duckett, P. J. Dyson and J. A. B. Lohman, *Chem – A Eur. J.*, 2003, 9, 1045-1061.
19. D. Blazina, S. B. Duckett, P. J. Dyson and J. A. B. Lohman, *Angew. Chem. Int. Ed. Engl.*, 2001, 40, 3874-3877.
20. V. Moberg, M. Haukka, I. O. Koshevoy, R. Ortiz and E. Nordlander, *Organometallics*, 2007, 26, 4090-4093.
21. V. Moberg, R. Duquesne, S. Contaldi, O. Röhrs, J. Nachtigall, L. Damoense, A. T. Hutton, M. Green, M. Monari, D. Santelia, M. Haukka and E. Nordlander, *Chem-A Eur. J.*, 2012, 18, 12458-12478.
22. J. Norton, in *Fundamental Research in Homogeneous Catalysis*, eds. M. Tsutsui and R. Ugo, Springer US, 1977, DOI: 10.1007/978-1-4615-7038-7_4, ch. 4, pp. 99-114.
23. C. U. Pittman, M. G. Richmond, M. M. Absi-Halabi, H. Beurich, F. Richter and H. Vahrenkamp, *Angew. Chem.*, 1982, 94, 805-806.
24. A. F. Abdel-Magied, A. K. Singh, M. Haukka, M. G. Richmond and E. Nordlander, *Chem. Commun.*, 2014, 50, 7705-7708.
25. V. Moberg, P. Homanen, S. Selva, R. Persson, M. Haukka, T. A. Pakkanen, M. Monari and E. Nordlander, *Dalton Trans.*, 2006, 279-288.
26. P. Homanen, R. Persson, M. Haukka, T. A. Pakkanen and E. Nordlander, *Organometallics*, 2000, 19, 5568-5574.
27. V. Moberg, R. Duquesne, S. Contaldi, O. Röhrs, J. Nachtigall, L. Damoense, A. T. Hutton, M. Green, M. Monari, D. Santelia, M. Haukka and E. Nordlander, *Chem-A Eur. J.*, 2012, 18, 12458-12478.
28. M. J. Stchedroff, V. Moberg, E. Rodriguez, A. E. Aliev, J. Bottcher, J. W. Steed, E. Nordlander, M. Monari and A. J. Deeming, *Inorg. Chim. Acta*, 2006, 359, 926-937.
29. C. Botteghi, S. Gladiali, M. Bianchi, U. Matteoli, P. Frediani, P. G. Vergamini and E. Benedetti, *J. Organomet. Chem.*, 1977, 140, 221-228.
30. M. Bianchi, U. Matteoli, G. Menchi, P. Frediani, F. Piacenti and C. Botteghi, *J. Organomet. Chem.*, 1980, 195, 337-346.
31. M. Breuer, K. Ditrach, T. Habicher, B. Hauer, M. Keßeler, R. Stürmer and T. Zelinski, *Angew. Chem. Int. Ed. Engl.*, 2004, 43, 788-824.
32. H.-U. Blaser, B. Pugin and F. Spindler, *J. Mol. Catal. A*, 2005, 231, 1-20.
33. U. Matteoli, V. Beghetto and A. Scrivanti, *J. Mol. Catal. A*, 1996, 109, 45-50.
34. U. Matteoli, M. Bianchi, P. Frediani, G. Menchi, C. Botteghi and M. Marchetti, *J. Organomet. Chem.*, 1984, 263, 243-246.
35. U. Matteoli, G. Menchi, P. Frediani, M. Bianchi and F. Piacenti, *J. Organomet. Chem.*, 1985, 285, 281-292.
36. Formation of a Noyori-type catalyst of the general formula [Ru(1)(O2CR)2] is in principle possible but cannot explain a reversal of enantioselectivity. Formation of a [Ru(1)2X2] (X=arbitrary monodentate anion) complex is even less likely, but could in principle form Λ and Δ -isomers; however, a racemic mixture would then expected to be formed, and the reversal of enantioselectivity would not be effected.
37. This is especially true with cluster **4**, whose DFT-computed ΔG° lies 2.0 kcal/mol above that of cluster **3**. Any fragmentation of **4**

- during catalysis, followed by cluster reassembly, would thermodynamically afford **3**, for more information, A. F. Abdel-Magied, A. K. Singh, M. Haukka, M. G. Richmond and E. Nordlander, *Chem Commun*, 2014, 50, 7705-7708.
38. J. G. de Vries, *Dalton Trans.*, 2006, DOI: 10.1039/B506276B, 421-429.
39. L. N. Lewis, *J. Am. Chem. Soc.*, 1986, 108, 743-749.
40. G. M. Whitesides, M. Hackett, R. L. Brainard, J. P. P. M. Lavalleye, A. F. Sowinski, A. N. Izumi, S. S. Moore, D. W. Brown and E. M. Staudt, *Organometallics*, 1985, 4, 1819-1830.
41. J. A. Widegren and R. G. Finke, *J. Mol. Catal. A*, 2003, 198, 317-341.
42. Y. Doi, K. Koshizuka and T. Keii, *Inorg. Chem.*, 1982, 21, 2732-2736.
43. R. D. Adams and D. A. Katahira, *Organometallics*, 1982, 1, 53-59.
44. E. Tyrrell, M. W. H. Tsang, G. A. Skinner and J. Fawcett, *Tetrahedron*, 1996, 52, 9841-9852.
45. Z. Otwinowski and W. Minor, in *International Tables for Crystallography Volume F: Crystallography of biological macromolecules*, eds. M. G. Rossmann and E. Arnold, Springer Netherlands, 2001, vol. F, ch. 24, pp. 226-235.
46. APEX2, in *SAINT-Plus and SADABS*. Bruker AXS Inc., Madison, Wisconsin, USA, , 2008.
47. G. Sheldrick, *Acta Crystallogr. Sect. A*, 2008, 64, 112-122.
48. L. Farrugia, *J. Appl. Crystallogr.*, 1999, 32, 837-838.
49. A. G. Orpen, *J. Chem. Soc., Dalton Trans.*, 1980, DOI: 10.1039/DT9800002509, 2509-2516.
50. Frisch, M. J. *et al.*, Gaussian 09, Revision E.01, Gaussian, Inc., Wallingford, CT, USA, 2009.
51. M. Svensson, S. Humbel, R. D. J. Froese, T. Matsubara, S. Sieber, K. Morokuma, *J. Phys. Chem.* 1996, 100, 19357-19363.
52. Cramer, C.J. *Essentials of Computational Chemistry*, 2nd Ed.; Wiley: Chichester, UK, 2004.
53. (a) JIMP2, version 0.091, a free program for the visualization and manipulation of molecules: Hall, M. B.; Fenske, R. F. *Inorg. Chem.* 1972, 11, 768-775. (b) Manson, J.; Webster, C. E.; Hall, M. B., Texas A&M University, College Station, TX, 2006: <http://www.chem.tamu.edu/jimp2/index.html>.

Paper III

Synthesis, Characterization and Catalytic Activity Studies of Rhenium Carbonyl Complexes Containing Chiral Diphosphines of the Josiphos and Walphos Families

Ahmed F. Abdel-Magied · Manjula S. Patil ·
Amrendra K. Singh · Matti Haukka ·
Magda Monari · Ebbe Nordlander

Received: 2 October 2014
© Springer Science+Business Media New York 2014

Abstract Ten rhenium carbonyl complexes—[Re(H)(CO)₃(**1a**)], [Re₃(μ-H)₃(CO)₁₀(**1a**)], [Re₂(CO)₉(**2a**)], [Re₂(CO)₈(**2a**)], [Re₂(CO)₉(**2b**)], [{Re₂(CO)₉}₂(**2b**)], [Re₂(CO)₈(**2b**)], [Re₂(CO)₈(**1b**)], [Re₂(μ-H)₂(CO)₆(**2b**)] and [Re₃(μ-H)₃(CO)₁₁(**2b**)]—containing different bidentate chiral phosphine ligands of the Josiphos (**1a**, **1b**) and Walphos (**2a**, **2b**) families have been synthesized and fully characterized (**1a**: (*R*)-1-[(*S*_P)-2-[Bis[3,5-bis(trifluoromethyl)phenyl]phosphino]ferrocenyl]ethyldi(3,5-xylyl)phosphine, **1b**: (*R*)-1-[(*S*_P)-2-[Di(2-furyl)phosphino]ferrocenyl]ethyldi-tert-butylphosphine, **2a**: (*R*)-1-[(*R*_P)-2-[2-[Bis(4-methoxy-3,5-dimethylphenyl)phosphino]phenyl]ferrocenyl]ethylbis[3,5-bis(trifluoromethyl)phenyl]phosphine and **2b**: (*R*)-1-[(*R*_P)-2-[2-(Diphenylphosphino)phenyl]ferrocenyl]ethyldicyclohexylphosphine). The phosphine-substituted clusters were tested for hydrogenation of tiglic acid [*trans*-2-methyl-2-butenic acid]. The catalytic reactions gave reasonable conversion rates (15–88 %) under relatively mild conditions but relatively moderate enantiomeric excesses (8–57 %) were observed. The crystal structures of [ReH(CO)₃(**1a**)], [Re₂(CO)₉(**2a**)], [{Re₂(CO)₉}₂(**2b**)] and [Re₂(μ-H)₂(CO)₆(**2b**)] are presented.

Electronic supplementary material The online version of this article (doi:10.1007/s10876-014-0809-y) contains supplementary material, which is available to authorized users.

A. F. Abdel-Magied · M. S. Patil · A. K. Singh · E. Nordlander (✉)
Inorganic Chemistry Research Group, Chemical Physics, Center for Chemistry and Chemical Engineering, Lund University, Box 124, 221 00 Lund, Sweden
e-mail: Ebbe.Nordlander@chemphys.lu.se

M. Haukka
Department of Chemistry, University of Jyväskylä, Box 35, 40014 Jyväskylä, Finland

M. Monari
Dipartimento di Chimica ‘G. Ciamician’, Università degli Studi di Bologna, Via Selmi 2, 40126 Bologna, Italy

Keywords Cluster · Rhenium · Asymmetric hydrogenation · Homogeneous catalysis

Introduction

Many transition metal carbonyl clusters with chiral phosphine ligands function as efficient precursors for the (asymmetric) hydrogenation of unsaturated organic substrates under homogeneous conditions [1–6]. The clusters are often thermally stable, and the presence of more than one metal in the catalyst offers, in principle, regioselectivity in reactions due to differentiated metal binding of a substrate molecule [7]. Most investigations of asymmetric catalytic reactions are based on complexes with chiral bidentate phosphine ligands, since such ligands often offer better control of the coordination number and stereochemistry of the resulting metal complex than corresponding monodentate phosphine ligands [8, 9]. Even though a large number of chiral diphosphines has been synthesized and investigated in homogeneous asymmetric catalysis, only a few of them have been found suitable for industrial processes, e.g. diphosphines based on the BINAP and Josiphos frameworks (Fig. 1) [10].

Examples of homogeneous catalysts containing rhenium are rare, and most of them are mononuclear complexes [11, 12]. Relatively little attention was paid to rhenium carbonyl complexes until their attractive catalytic properties in hydrogenation were revealed by a systematic study by Broadbent and coworkers [13]. Rhenium carbonyl clusters have been shown to be effective catalyst precursors for hydrogenation [14], as well as hydrogen-related reactions, such as hydrosilylation [15], dehydrogenative silylations [16], and dehydrogenative aminoborane coupling reactions [17]. The first successful synthesis of thiacyclopentadienes from a thietane was achieved via the reaction of the trirhenium complex $[\text{Re}_3(\text{CO})_{10}(\mu\text{-SCH}_2\text{CH}_2\text{CH}_2)(\mu\text{-H})_3]$ with thietane to give $[\text{Re}_3(\text{CO})_{10}(\mu\text{-SCH}_2\text{CH}_2\text{CH}_2\text{-12S3})(\mu\text{-H})_3]$; the latter complex was characterized crystallographically to show that it contains a 12S3 thiacyclopentadiene linked to the cluster via a $\text{SCH}_2\text{CH}_2\text{CH}_2$ chain [18–20].

We have previously found that hydride-containing ruthenium carbonyl clusters containing chiral diphosphine ligands are effective catalysts/catalyst precursors for asymmetric hydrogenation of α -unsaturated carboxylic acids, giving excellent conversion rates and, in some cases, high enantiomeric excesses [1, 2, 5, 21]. In some instances, we have also been able to unambiguously demonstrate that the active catalysts are clusters [22]. We were therefore interested in exploring the catalytic properties of chiral derivatives of other hydride-containing metal carbonyl clusters in asymmetric hydrogenation reactions. In the present study, we describe the synthesis and characterization of new rhenium carbonyl complexes containing chiral diphosphines of the Josiphos (**1a–1b**) and Walphos (**2a–2b**) families (Fig. 1), and their performance as catalysts/catalyst precursors for asymmetric hydrogenation of tiglic acid under relatively mild reaction conditions.

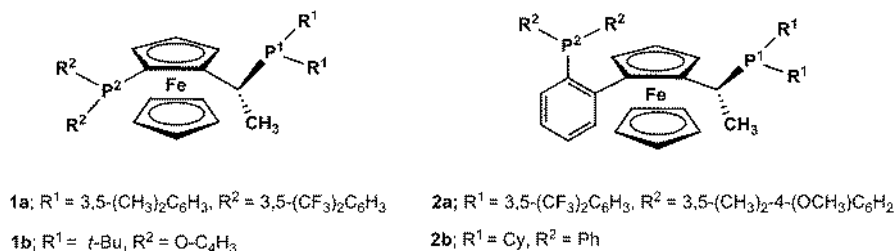


Fig. 1 Structure of phosphine ligands used in this study

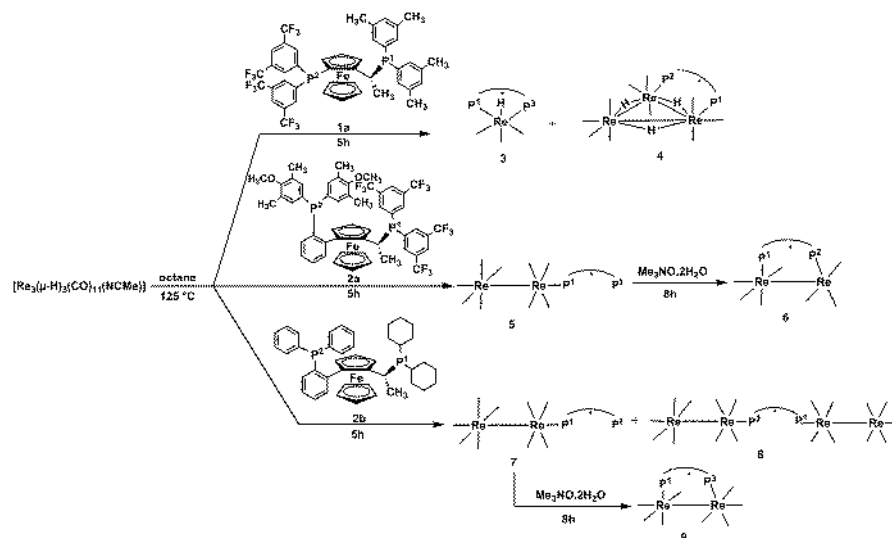
Results and Discussion

The synthesis of the chiral diphosphine derivatives of rhenium carbonyl complexes were based on previously published methods [2, 5], i.e. either (i) thermal substitution in octane in the presence of the diphosphine and $[\text{Re}_3(\mu\text{-H})_3(\text{CO})_{10}(\text{NCMe})]$ (cf. Scheme 1), or (ii) thermal substitution in toluene in the presence of $[\text{Re}_2(\text{CO})_8(\text{NCMe})_2]$ while hydrogen was bubbled through the solution until complete conversion to $[\text{Re}_3(\mu\text{-H})_3(\text{CO})_{10}(\text{NCMe})]$ had occurred (as monitored by IR spectroscopy), followed by the addition of the chiral diphosphine ligand (cf. Scheme 2). The complexes were identified via IR, ^1H and ^{31}P NMR spectroscopies, mass spectrometry and, in the cases of $[\text{ReH}(\text{CO})_3(\mathbf{1a})]$ **3**, $[\text{Re}_2(\text{CO})_9(\mathbf{2a})]$ **5**, $[\{\text{Re}_2(\text{CO})_9\}_2(\mathbf{2b})]$ **8** and $[\text{Re}_2(\mu\text{-H})_2(\text{CO})_6(\mathbf{2b})]$ **11**, X-ray crystallography.

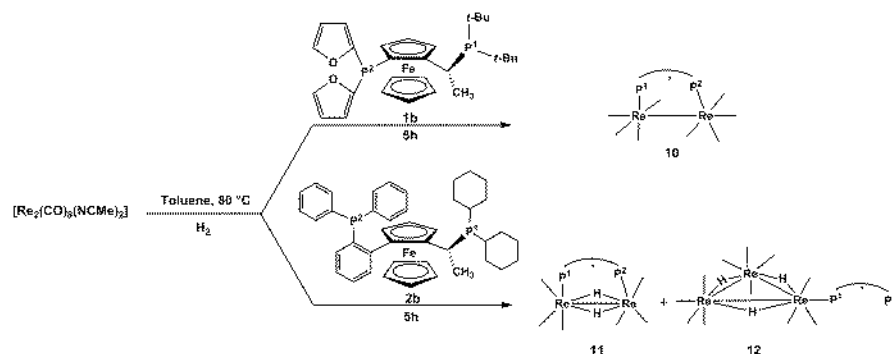
Synthesis of Complexes 3–9

Refluxing of a stoichiometric amount of the chiral diphosphine ligands **1a**, **2a** or **2b** (cf. Fig. 1) with $[\text{Re}_3(\mu\text{-H})_3(\text{CO})_{10}(\text{NCMe})]$ in octane leads to the formation of the complexes **3–5** and **7, 8**, respectively, (cf. Scheme 1). The conversions of the mono-substituted diphosphine clusters **5** and **7** to the diphosphine-bridged clusters **6** and **9**, respectively, were carried out by using $\text{Me}_3\text{NO}\cdot 2\text{H}_2\text{O}$ as an oxidative decarbonylation reagent.

Refluxing of a stoichiometric amount of the Josiphos ligand **1a** (74 mg, 0.074 mmol) (cf. Fig. 1) with the cluster $[\text{Re}_3(\mu\text{-H})_3(\text{CO})_{10}(\text{NCMe})]$ (34 mg, 0.037 mmol) in octane leads to the formation of two orange products, **3** and **4** (cf. Experimental section). The mononuclear nature of product **3** was revealed by its positive mode ESI mass spectrum, which displayed a peak at $m/z = 1181$, in accordance with the molecular formula $[\text{ReH}(\text{CO})_3(\mathbf{1a})]$. Comparison of the $\nu(\text{CO})$ IR stretching frequency pattern of **3** to $[\text{HRe}(\text{CO})_3(\text{dppe})]$ (dppe = 1,2-bis(diphenylphosphino)ethane) [23], indicates that **3** contains the ligand **1a** coordinated to the rhenium metal in a chelating coordination mode. The ^1H NMR spectrum of **3** reveals, in addition to signals for the diphosphine ligand, one triplet hydride signal at $\delta = -4.48$ ppm. The $^{31}\text{P}\{^1\text{H}\}$ NMR spectrum also shows two doublet signals at $\delta = 24.12$ and 10.44. Furthermore, complex **3** was characterized by single-crystal



Scheme 1 Schematic depiction of products formed as a result of reaction of $[\text{Re}_3(\mu\text{-H})_3(\text{CO})_{10}(\text{NCMe})]$ with diphosphine



Scheme 2 Schematic depiction of products formed as a result of reaction of $[\text{Re}_2(\text{CO})_8(\text{NCMe})_2]$ with diphosphine

X-ray diffraction analysis (vide infra). The structure of cluster **4** was confirmed by IR, ^1H and $^{31}\text{P}\{^1\text{H}\}$ NMR spectroscopies, as well as mass spectrometry. The $\nu(\text{CO})$ IR stretching frequency pattern of **4** is similar to that of the known complex $[\text{Re}_3(\mu\text{-H})_3(\text{CO})_{10}(\text{dppm})]$ (dppm = bis(diphenylphosphino)methane) [24]. Its ^1H NMR spectrum shows, in addition to signals for the diphosphine ligand, three hydride signals at $\delta = -14.56$, -15.52 and -17.20 ppm. The $^{31}\text{P}\{^1\text{H}\}$ -NMR spectrum also shows two multiplets at $\delta = 19.26$ and 3.89 ppm. The ESI mass spectrometric data matches with the assigned molecular formula $[\text{Re}_3(\mu\text{-H})_3(\text{CO})_{10}(\mathbf{1a})]$ at $m/z = 1775$ (M^+).

Under the same conditions, *i.e.* refluxing of $[\text{Re}_3(\mu\text{-H})_3(\text{CO})_{11}(\text{NCMe})]$ (80 mg, 0.088 mmol) and **2a** (92 mg, 0.088 mmol) in octane for 4 h gave one orange

product, **5**. Comparison of the $\nu(\text{CO})$ IR stretching frequency pattern of **5** to the known complex $[\text{Re}_2(\text{CO})_9(\text{dppp})]$ [$\text{dppp} = 1,3\text{-bis}(\text{diphenylphosphino})\text{propane}$] [25], indicates that **5** contains the **2a** ligand coordinated in a “dangling” mode, i.e. the diphosphine is coordinated through only one phosphine moiety, and the mass spectrum of **5** reveals a peak at $m/z = 1671$, consistent with the molecular formula $[\text{Re}_2(\text{CO})_9(\text{2a})]$. The ^1H NMR spectrum of **5** reveals the expected signals for the diphosphine ligand. The possibility of coordination isomers thus exists, but the $^{31}\text{P}\{^1\text{H}\}$ NMR spectrum of **4** was found to contain only two doublets at $\delta = 34.94$ and -15.75 ppm. The lower-field signal could be assigned to the (coordinated) $\{[3,5\text{-bis}(\text{trifluoromethyl})\text{phenyl}]\text{phosphine}\}$ moiety [*cf.* Fig. 3, δ (^{31}P) for free **2a** (CDCl_3 , ppm): for $\{\text{P}-[3,5\text{-(CF}_3)_2\text{C}_6\text{H}_3]_2\} = 1.76$; for $\{\text{P}-[3,5\text{-(CH}_3)_2\text{-4-(OCH}_3\text{)C}_6\text{H}_2]_2\} = -17.47$]. The structure of cluster **5** was confirmed by single crystal X-ray diffraction (*vide infra*).

Reaction of $[\text{Re}_2(\text{CO})_9(\text{2a})]$ **5** with $\text{Me}_3\text{NO} \cdot 2\text{H}_2\text{O}$ produces the diphosphine-bridged complex $[\text{Re}_2(\text{CO})_8(\text{2a})]$ **6** in 47 % yield. In principle, the oxidative decarbonylation of the $[\text{Re}_2(\text{CO})_9(\kappa^1\text{-P-P})]$ clusters can yield either the chelate $[(\text{CO})_5\text{Re-Re}(\text{CO})_3(1,1\text{-P-P})]$ or the bridged $[\text{Re}_2(\text{CO})_8(\mu\text{-P-P})]$ clusters. The IR spectra of the two types of possible products can provide strong evidence for the specific diphosphine coordination mode. The IR spectrum of **6** in the carbonyl stretching region confirms the absence of an $[\text{Re}_2(\text{CO})_5]$ unit and is similar to the diphosphine-bridged cluster $[\text{Re}_2(\text{CO})_8(\mu\text{-dppp})]$ [25]. The mass spectrum of **6** reveals a peak at $m/z = 1644$, which is consistent with the molecular formula $[\text{Re}_2(\text{CO})_8(\text{2a})]$. The ^1H NMR spectrum of **5** reveals the signals for the diphosphine ligand, while the $^{31}\text{P}\{^1\text{H}\}$ NMR spectrum shows two multiplets at shifts that are consistent with coordination of both phosphine moieties (*vide supra* and [Experimental](#) section). Complex **6** is most likely formed via Me_3NO -assisted decarbonylation of $[\text{Re}_2(\text{CO})_9(\text{2a})]$ **5**, followed by coordination of the free phosphine moiety of **2a** to rhenium.

Reaction of $[\text{Re}_3(\mu\text{-H})_3(\text{CO})_{11}(\text{NCMe})]$ in refluxing octane with **2b** for 15 h led to the formation of two orange products in good yield, compounds **7** (70 %) and **8** (16 %). Comparison of the $\nu(\text{CO})$ IR stretching frequency pattern of **7** to those of the known complex $[\text{Re}_2(\text{CO})_9(\text{dppe})]$ ($\text{dppe} = 1,2\text{-bis}(\text{diphenylphosphino})\text{ethane}$) [25] and complex **5** (*vide supra*), indicates that **7** contains the **2b** ligand in a “dangling” coordination mode. The $^{31}\text{P}\{^1\text{H}\}$ -NMR spectrum shows two singlet signals at $\delta = 43.38$ and -14.41 ppm, of which the lower-field signal could be assigned to the coordinated $\{\text{P}(\text{-Cy})_2\}$ moiety of the diphosphine ligand [*cf.* δ (^{31}P) for **2b** (CDCl_3 , ppm) for $\{\text{P}(\text{-Cy})_2\} = 13.6$; for $\{\text{P}(\text{-Ph})_2\} = -14.15$] [26]. Again, no evidence for coordination isomers could be detected. The mass spectrum of **7** corroborated the molecular formula $[\text{Re}_2(\text{CO})_9(\text{2b})]$. The characterization of cluster **8** was made on the basis of spectroscopic data and single crystal X-ray diffraction analysis (*vide infra*). The $^{31}\text{P}\{^1\text{H}\}$ NMR spectrum shows two singlet signals at $\delta = 43.83$ and -14.43 ppm. The $\nu(\text{CO})$ IR stretching frequency pattern of **8** is similar to those reported previously for the known dimer $[\{\text{Re}_2(\text{CO})_9\}_2(\text{dppe})]$ [25] and also to $[\text{Re}_2(\text{CO})_9(\text{2a})]$ **5** and $[\text{Re}_2(\text{CO})_9(\text{2b})]$ **7** (*vide supra*), all of which contain $\text{Re}_2(\text{CO})_9(\text{phosphine})$ units with the phosphine coordinated in an axial position w r t the metal–metal bond (*i.e.* *trans* to the metal–metal bond). The mass

spectrum of **8** reveals a peak envelope at $m/z = 1920$, corresponding to the molecular formula $[\{\text{Re}_2(\text{CO})_9(\mathbf{2b})\}]$ **8**. As observed for the conversion of cluster **5** to cluster **6**, reaction of $[\text{Re}_2(\text{CO})_9(\mathbf{2b})]$ **7** with Me_3NO produces the diphosphine-bridged complex $[\text{Re}_2(\text{CO})_8(\mathbf{2b})]$ **9** in 38 % yield, and the IR, $^{31}\text{P}\{^1\text{H}\}$ NMR and mass spectra are in full agreement with the proposed formula and structure for **9** (cf. Experimental section).

Structural Description of Clusters **3**, **5** and **8**

The solid state structures of complexes **3**, **5** and **8** were determined by single crystal X-ray diffraction. For all three complexes, crystals were obtained by slow diffusion of hexane into saturated dichloromethane solutions of the respective cluster at 4 °C. The molecular structures of **3**, **5** and **8** are depicted in Figs. 2, 3 and 4, respectively, and selected bond distances and angles are listed in the captions.

Complex **3** contains a central rhenium atom coordinated by three carbonyl ligands, a hydride and the two phosphine moieties of the ligand **1a** in slightly distorted octahedral coordination geometry. The complex constitutes a *fac* isomer, and no evidence of a *mer* isomer could be detected. The C(3)–Re–P(2) and C(2)–Re–P(1) angles are distorted from the ideal of 180° to 177.7(4)° and 172.5(4)°, respectively, and the P(1)–Re–P(2), C(2)–Re–P(2) and C(3)–Re–P(1) angles are [87.98(8)°, [91.5(3)°] and [90.2(3)°], respectively, due to the relatively narrow bite of the diphosphine ligand in the equatorial position. The Re–P(1) and Re–P(2) distances are very similar—2.449(3) and 2.411(2) Å, respectively; they fall within the expected range of Re–P interactions that are usually found in mononuclear

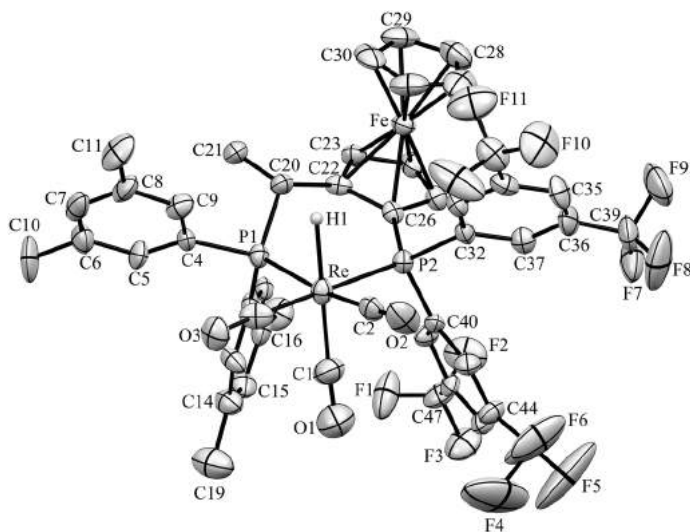


Fig. 2 Molecular structure of $[\text{ReH}(\text{CO})_3(\mathbf{1a})]$ **3** with thermal ellipsoids drawn at the 30 % probability level. C–H hydrogen atoms have been omitted for clarity. Selected bond distances (Å) and angles (°): Re–P(1) 2.449(3), Re–P(2) 2.411(2), P(1)–Re–P(2) 87.98(8), C(1)–Re–P(1) 87.98(8), C(2)–Re–P(1) 172.5(4), C(3)–Re–P(1) 90.2(3), C(1)–Re–P(2) 90.4(4), C(2)–Re–P(2) 91.5(3), C(3)–Re–P(2) 177.7(4)

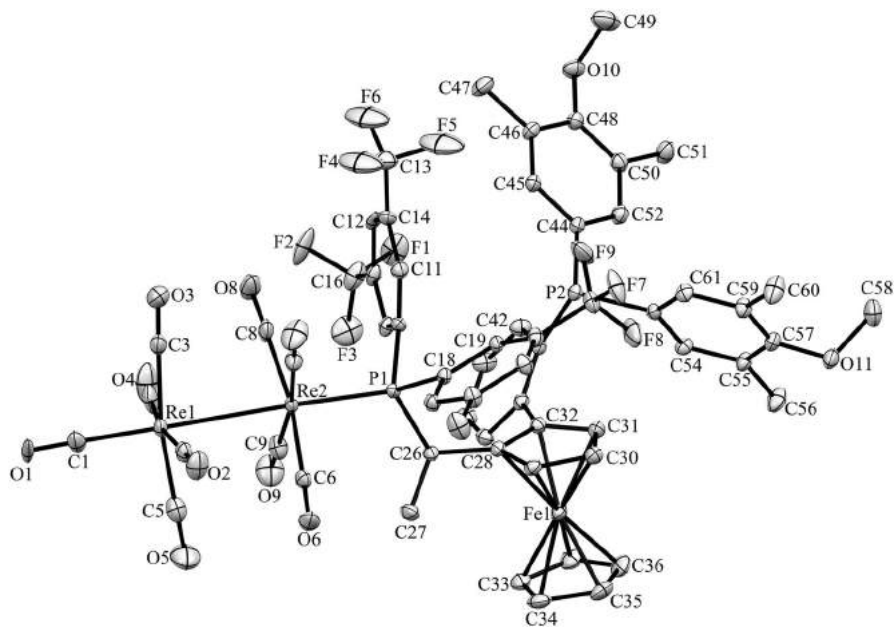


Fig. 3 Molecular structure of $[\text{Re}_2(\text{CO})_9(\mathbf{2a})]$ **5** with thermal ellipsoids drawn at the 50 % probability level. C–H hydrogen atoms have been omitted for clarity. The disordered F atoms in CF_3 groups have been omitted for clarity. Selected bond distances (Å) and angles ($^\circ$): $\text{Re}(1)\text{--Re}(2)$ 3.02637(15), $\text{Re}(2)\text{--P}(1)$ 2.3737(6), $\text{P}(1)\text{--Re}(2)\text{--Re}(1)$ 175.11(18), $\text{C}(1)\text{--Re}(1)\text{--Re}(2)$ 86.27(10), $\text{C}(2)\text{--Re}(1)\text{--Re}(2)$ 172.5(4), $\text{C}(3)\text{--Re}(1)\text{--Re}(2)$ 85.02(11), $\text{C}(6)\text{--Re}(2)\text{--P}(1)$ 95.75(10)

rhenium compounds and are comparable to the Re–P distances observed in, for example, *fac*- $[(\text{CO})_3(\text{OCN})\text{Re}(\text{PPh}_2\text{NHPPH}_2)]$ [27], where Re–P(1) and Re–P(2) are 2.438(3) and 2.447(2) Å, respectively.

The crystal structure of **5** was determined in order to confirm the coordination mode of the diphosphine ligand. The structure of **5** is illustrated in Fig. 3 and selected bond distances and angles are listed in the captions. The two Re octahedra in **5** are approximately staggered, and the presence of the bulky phosphine ligand in the axial position probably precludes an ideal staggered form. Comparison of cluster **5** with the structures of $[\text{Re}_2(\text{CO})_9(\text{dppene})]$ [28] and $[\text{Re}_2(\text{CO})_9(\text{PPh}_2\text{H})]$ [29], in which the phosphines are equatorially coordinated, reveals structural differences. The Re–P bond length of cluster **5** 2.3737(6) Å is shorter than that in $[\text{Re}_2(\text{CO})_9(\text{PPh}_2\text{H})]$ and $[\text{Re}_2(\text{CO})_9(\text{dppene})]$ (2.443(3) Å and 2.4887(9) Å, respectively), and the rhenium–rhenium bond length (3.0264(2) Å) is considerably shorter than those found in the two clusters, ($[\text{Re}_2(\text{CO})_9(\text{PPh}_2\text{H})]$: 3.0526(7); $[\text{Re}_2(\text{CO})_9(\text{dppene})]$: 3.1077(2) Å, respectively; however, it is similar to the Re–Re bond lengths reported for related complexes, e.g. $[\text{Re}_2(\text{CO})_{10}]$ (Re–Re 3.02 Å) [30], and also to $[\{\text{Re}_2(\text{CO})_9\}_2(\mathbf{2b})]$ **8** (Re(1)–Re(2) 3.0347(4) Å and Re(3)–Re(4) 3.0310(4) Å) (vide infra).

The molecular structure of **8** is illustrated in Fig. 4 and selected bond distances and angles are listed in the figure caption. Cluster **8** contains two dinuclear rhenium

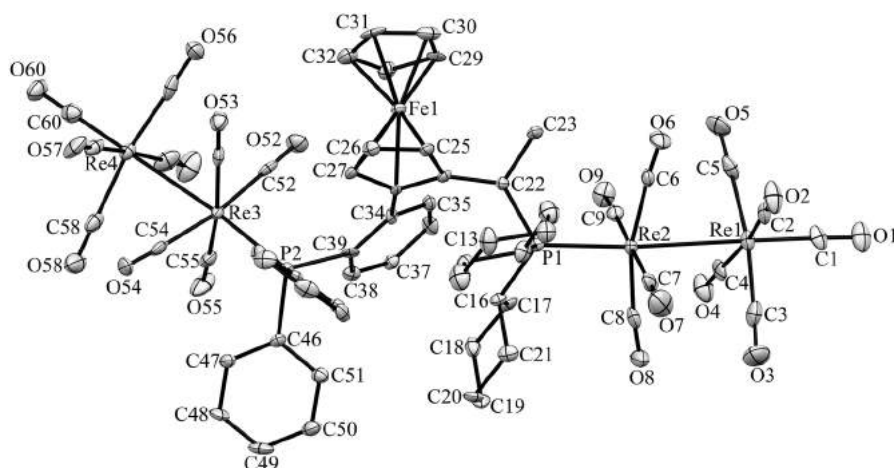


Fig. 4 Molecular structure of $[\{\text{Re}_2(\text{CO})_9\}_2(\mathbf{2b})] \mathbf{8}$ with thermal ellipsoids drawn at the 50 % probability level. C–H hydrogen atoms have been omitted for clarity. Selected bond distances (Å) and angles ($^\circ$): Re(1)–Re(2) 3.0347(4), Re(2)–P(1) 2.4122(16), Re(3)–P(2) 2.3911(17), Re(3)–Re(4) 3.010(4), P(1)–Re(2)–Re(1) 175.12(4), P(2)–Re(3)–Re(4) 172.43(4)

units (Re(1)–Re(2) and Re(3)–Re(4)) that are bridged by the **2b** diphosphine ligand, which coordinates to Re(2) and Re(3). The Re–Re bond distances in cluster **8**, [Re(1)–Re(2) 3.0347(4) Å and Re(3)–Re(4) 3.0310(4) Å], are similar to the Re–Re bond lengths reported for $[\text{Re}_2(\text{CO})_9(\text{PPh}_2\text{H})]$ [3.0526(7) Å] [29], $[\{\text{Re}_2(\text{CO})_9\}_2(\text{dppf})]$ (dppf = 1,1'-bis(diphenylphosphino)ferrocene) [31] and also $[\text{Re}_2(\text{CO})_9(\mathbf{2a})] \mathbf{5}$ (vide supra). The two phosphorus atoms in ligand **2a** are coordinated to Re(2) and Re(3) with bond distances of 2.4122(16) and 2.3911(17) Å, respectively. The Re(1)–Re(2)–P(1) and Re(4)–Re(3)–P(2) angles are distorted to $[175.12(4)^\circ]$ and $[172.43(4)^\circ]$, respectively, which is similar to the corresponding angle in $[\text{Re}_2(\text{CO})_9(\mathbf{2a})] \mathbf{5}$ $[175.11(18)^\circ]$.

Synthesis of Clusters **10–12**

The clusters $[\text{Re}_2(\text{CO})_8(\mathbf{1b})] \mathbf{10}$, $[\text{Re}_2(\mu\text{-H})_2(\text{CO})_6(\mathbf{2b})] \mathbf{11}$ and $[\text{Re}_3(\mu\text{-H})_3(\text{CO})_{11}(\mathbf{2b})] \mathbf{12}$ were prepared by heating $[\text{Re}_2(\text{CO})_8(\text{NCMe})_2]$ at 80 $^\circ\text{C}$ in toluene for 5 h while hydrogen was bubbled through the solution until complete conversion to $[\text{Re}_3(\mu\text{-H})_3(\text{CO})_{10}(\text{NCMe})]$ [32] had occurred (as monitored by IR spectroscopy), followed by the addition of a stoichiometric amount of the chiral diphosphine ligands **1b** or **2b** (cf. Fig. 1). The bubbling of hydrogen was continued until the end of the reaction to produce clusters **10–12**, respectively, (cf. Scheme 2).

The mass spectrum of **10** reveals a peak envelope at $m/z = 1118$, corresponding to the molecular formula $[\text{Re}_2(\text{CO})_8(\mathbf{1b})]$. The $\nu(\text{CO})$ IR stretching frequency pattern of **10** is similar to that of the known complex $[\text{Re}_2(\text{CO})_8(\text{dadpp})]$ (dadpp = 1-(di-*o*-anisylphosphino)-3-(diphenylphosphino) propane) [28], in which the diphosphine ligand bridges the two metal centers, and also to $[\text{Re}_2(\text{CO})_8(\mathbf{2a})] \mathbf{6}$

and $[\text{Re}_2(\text{CO})_8(\mathbf{2b})]$ **9** (vide supra). The ^1H NMR spectrum of **10** reveals the signals for the diphosphine ligand. The $^{31}\text{P}\{^1\text{H}\}$ NMR spectrum shows two signals at $\delta = 55.41$ and -30.61 ppm.

Under reaction conditions similar to those that gave **10** (cf. Scheme 2), *i.e.* initial in situ formation of $[\text{Re}_3(\mu\text{-H})_3(\text{CO})_{10}(\text{NCMe})]$ followed by the addition of a stoichiometric amount of **2b** (49 mg, 0.073 mmol), the formation of two orange products, **11** and **12**, occurred. The ^1H NMR spectrum of **11** contains two hydride signals at $\delta = -6.78$ and -9.28 ppm, in addition to signals for the diphosphine ligand, and the $^{31}\text{P}\{^1\text{H}\}$ NMR spectrum shows two broad signals at $\delta = 43.19$ and 28.08 ppm. Comparison of the $\nu(\text{CO})$ IR stretching frequency pattern of **11** to that of $[\text{Re}_2(\mu\text{-H})_2(\text{CO})_6(\text{dppm})]$ [24] suggests that **11** is isostructural with the dppm derivative, with the diphosphine bridging the two rhenium atoms. The mass spectrum of **11** reveals a peak at $m/z = 1213$, corresponding to the molecular formula $[\text{Re}_2(\mu\text{-H})_2(\text{CO})_6(\mathbf{2b})]$. It was possible to grow crystals of **11** suitable for single-crystal X-ray diffraction analysis, and its crystal structure was determined in order to confirm the proposed molecular structure of the cluster (vide infra).

Comparison of the $\nu(\text{CO})$ IR stretching frequency pattern of **12** to $[\text{Re}_3(\mu\text{-H})_3(\text{CO})_{11}(\text{PPh}_3)]$ [33] suggests an identical formulation for **12**, with the ligand **2b** coordinated in a dangling mode, and the positive mode ESI mass spectrum of the cluster ($M^+ = 1541$) is in agreement with such a molecular formula. The ^1H NMR spectrum of **12** confirms the presence of three hydrides, with one multiplet at $\delta = -16.33$ ppm and two doublets at $\delta = -17.21$ and -17.60 ppm. The $^{31}\text{P}\{^1\text{H}\}$ NMR spectrum also shows two signals at $\delta = 39.16$ and -14.58 ppm. The lower field signal could be assigned to the $\{\text{P}(\text{Cy})_2\}$ moiety, which is coordinated to the $[\text{Re}_3(\mu\text{-H})_3(\text{CO})_{11}]$ framework, and the higher field signal can be assigned to the uncoordinated phosphorus atom [cf. Synthesis of **7** for the ^{31}P resonances of free **2b**]; again, no coordination isomer could be detected. Attempts were made to coordinate the free phosphine moiety in **12** by either (i) dissolving **12** in THF followed by the addition of $\text{Me}_3\text{NO}\cdot 2\text{H}_2\text{O}$ in THF under nitrogen and subsequent reflux of the solution for 8 h or (ii) heating of **12** at 90°C in toluene for 8 h; however, analysis by spot TLC indicated that in both cases, decomposition of **12** was the only result.

Structural Description of $[\text{Re}_2(\mu\text{-H})_2(\text{CO})_6(\mathbf{2b})]$ **11**

The bridging coordination mode and chiral configuration of the diphosphine in **11** have been confirmed by X-ray crystallography; its molecular structure is shown in Fig. 5 and selected bond distances and angles are listed in the captions. The distribution of the carbonyl ligands indicates that the two hydrides bridge the Re–Re edge and lie on opposite sides of the Re_2P_2 plane. The rhenium–rhenium bond length of $2.9009(3)$ Å is considerably shorter than those found in systems containing single Re–Re bonds, *e.g.* $[\text{Re}_2(\text{CO})_{10}]$ (Re–Re 3.02 Å) [30], and also for those with bridging hydrides as in $[\text{Re}_3\text{H}_3(\text{CO})_{12}]^-$ $[\text{Re}(\mu\text{-H})\text{Re}$ 3.177 Å] [34]; however, it is similar to the Re–Re bond lengths reported for related complexes, *e.g.* $[\text{Re}_2\text{H}_2(\text{CO})_8]$ (Re–Re 2.896 Å) [35] and $[\text{Re}_2\text{H}_2(\text{CO})_6(\text{dppm})]$ (Re–Re 2.893 Å) [24]. The two Re–P distances, Re(1)–P(1) and Re(2)–P(2), are very similar ($2.4983(14)$ and

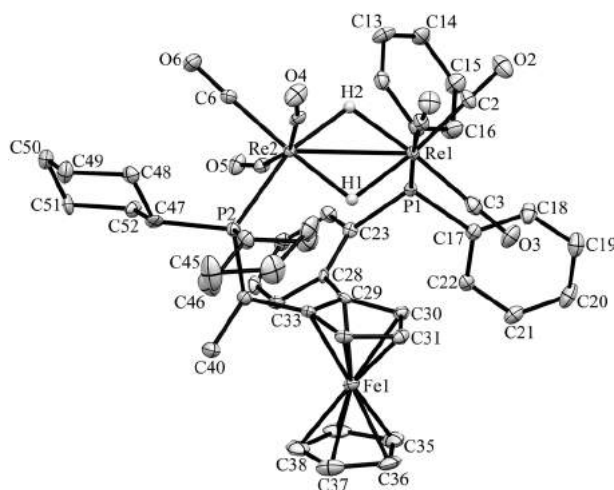


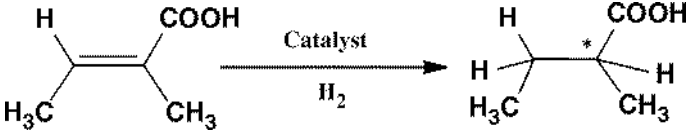
Fig. 5 Molecular structure of $[\text{Re}_2(\mu\text{-H})_2(\text{CO})_6(\mathbf{2b})]$ **11** with thermal ellipsoids drawn at the 50 % probability level. C–H hydrogen atoms have been omitted for clarity. Selected bond distances (Å) and angles (°): Re(1)–Re(2) 2.9009(3), Re(1)–P(1) 2.4983(14), Re(2)–P(2) 2.4135(15), P(1)–Re(1)–Re(2) 96.22(4), P(2)–Re(2)–Re(1) 124.69(3)

2.4135(15) Å, respectively), and also similar to the corresponding Re–P distances reported for $[\text{Re}_2\text{H}_2(\text{CO})_6(\text{dppm})]$ (Re(1)–P(1) and Re(2)–P(2), 2.449(4) and 2.457(4) Å, respectively) [24].

Homogeneous Catalytic Studies

Bearing in mind the excellent catalytic results obtained in asymmetric hydrogenation of tiglic acid by chiral hydride-containing ruthenium clusters [1, 21, 36], we were primarily interested in studying the catalytic properties of the hydride-containing rhenium complexes prepared in this investigation, and the abilities of complexes **3**, **4**, **11** and **12** to act as catalysts were therefore investigated. Tiglic acid was chosen as a substrate since (i) it has been used as a benchmark substrate in earlier assessments of asymmetric hydrogenation effected by transition metal carbonyl clusters, facilitating comparison with other work [1, 2, 21, 36–38] (ii) there is a well-established and reliable protocol for the evaluation of enantiomeric excess, and (iii) the importance of hydrogenation of α -unsaturated carboxylic acids and their substituted derivatives, which are essential pharmaceuticals or chiral building blocks for the synthesis of biologically active compounds [39, 40].

We have previously shown that lower H_2 pressure is expected to enhance the chiral induction in hydrogenation of tiglic acid [5, 21] and the catalysis experiments were carried out at the relatively low H_2 pressure of 50 bar instead of the high pressure (150 bar) used in comparable catalysis tests [41]. In order to obtain reasonable conversions, a temperature of 100 °C and relatively long reaction times [24, 48 or 72 h] were required (the conversion rates were found to decrease appreciably below ca. 80 °C). The results for the catalysis tests for **3**, **4**, **11** and **12** are presented in Table 1. The conversion of tiglic acid was assessed by ^1H NMR

Table 1 Asymmetric catalytic hydrogenation of tiglic acid in the presence of complexes [ReH(CO)₃(**1a**)] **3**, [Re₃(μ-H)₃(CO)₁₀(**1a**)] **4** and [Re₂(μ-H)₂(CO)₆(**2b**)] **11**, [Re₃(μ-H)₃(CO)₁₁(**2b**)] **12** as catalysts


Entry	Catalyst (mg)	Conv. (%) ^a	ee (%)	Configuration ^b
1	3 /10	33	8	<i>R</i>
2 ^c	3 /10	38	8	<i>R</i>
3 ^d	3 /10	52	8	<i>R</i>
4	4 /10	33	—	—
5	11 /10	88	57	<i>R</i>
6	12 /5	15	13	<i>R</i>

Reaction conditions: S/C ratio 1:100, 100 °C, 50 bar of H₂, 24 h

^a The amount of substrate consumed in the catalytic experiment, assed by ¹H NMR spectroscopy, p(H₂) = 50 bar, *T* = 100 °C, solvent = EtOH-toluene 1:1 (5 mL), *n*(substrate)/*n*(catalyst) = 100

^b Favoured enantiomer

^c Reaction time = 48 h

^d Reaction time = 72 h

spectroscopy and the enantioselectivity was investigated according to a published procedure [42]. All compounds yielded low to moderate conversions, even with extended reaction times (72 h); reasonably good conversion rates could be observed for cluster **11**. Only relatively moderate enantiomeric excesses could be observed and in case of **4**, no enantioselectivity could be detected. We have observed significantly higher enantioselectivities in other cluster-based systems [21], but it should be borne in mind that ee's exceeding 40 % were unprecedented [37, 38, 41, 43, 44] in cluster-based asymmetric hydrogenation before we began our studies.

Both the catalytic activity and the chiral induction appear to be dependent on the chemical nature of the phosphine ligand used, although the exact reaction mechanism for the asymmetric catalytic hydrogenation is still uncertain [5, 21]. Clusters **3**, **11** and **12** give (*R*)-2-methylbutyric acid with an enantiomeric excess of 8–57 %. All catalysts show different catalytic activity (*n*_{catalyst}/*n*_{substrate} = 1:100); the catalysts based on Josiphos ligands (**3** and **4**) gave no, or very low, enantioselectivity while the clusters derivatised with Walphos ligands (**11** and **12**) gave relatively good enantioselectivities. This is in agreement with observations for the same catalytic reaction using [Ru₄(μ-H)₄(CO)₁₀(P–P*)] clusters, where Walphos derivatives consistently gave better enantioselectivities relative to Josiphos derivatives [21]. For these ruthenium clusters, the better performance of the Walphos derivatives may be connected with the greater steric bulk of these ligands compared to the Josiphos family, and the (potentially) wider “bite” of the Walphos ligands, which results in a different bridging coordination mode (eq-ax) for these ligands as compared to the Josiphos ligands (eq-eq); presumably these properties result in both better chiral induction by the ligand and different initial orientation of the coordinated substrate to the ruthenium cluster [12]. After catalysis runs, clusters **3**, **4**, **11** and **12** could be recovered unaltered and, despite the 50–70 % recovery of catalysts, no

evidence of fragmentation products were obtained. Considering the small quantities of catalysts/catalyst precursors used in each experiment (5–10 mg), the recovery may be considered to be quantitative. Catalyst recycling was investigated by recovering cluster **11** from the hydrogenation of tiglic acid and reusing it in the exact same experiment (corresponding to entry 5, Table 1). Identical catalytic activity was observed for the two catalytic runs in terms of conversion and enantioselectivities.

Conclusions

In summary, we have synthesized and characterized ten new di-, tri- and tetranuclear rhenium complexes containing the chiral Josiphos and Walphos ligands **1a**, **1b**, **2a** and **2b**. The hydride-containing complexes $[\text{Re}(\text{H})(\text{CO})_3(\mathbf{1a})]$ **3**, $[\text{Re}_3(\mu\text{-H})_3(\text{CO})_{10}(\mathbf{1a})]$ **4**, $[\text{Re}_2(\mu\text{-H})_2(\text{CO})_6(\mathbf{2b})]$ **11** and $[\text{Re}_3(\mu\text{-H})_3(\text{CO})_{11}(\mathbf{2b})]$ **12** have been investigated as catalysts/catalyst precursors for asymmetric hydrogenation of the α -unsaturated carboxylic acid tiglic acid. Catalysis has been achieved under considerably milder reaction conditions than those employed in related systems. The conversion rates are good but the enantioselectivities are relatively low, albeit good when compared to most other cluster-based catalytic systems for asymmetric reactions [37, 38, 41, 43, 44]. The clusters containing diphosphines of the Walphos family gave better enantioselectivities than the related Josiphos-containing clusters, in keeping with observations made for other cluster-based systems [21]; this highlights the importance of the specific chiral diphosphine ligand for the catalytic performance. While it has not been possible to unambiguously determine the nature of the active catalyst(s) in these cluster-based systems, the clusters offer some distinct advantages as catalysts/precatalysts—they are very stable and not air sensitive, separation from products is relatively easy and they permit low catalyst:substrate ratios.

Although the number of potential catalysts that have been studied in this initial investigation is too low to draw distinct conclusions, it may be noted that the dinuclear complex $[\text{Re}_2(\mu\text{-H})_2(\text{CO})_6(\mathbf{2b})]$ **11** exhibited by far the best catalytic properties in the present investigation, both in terms of conversion of substrate and enantioselectivity, and that the enantioselectivity in the hydrogenation reaction is better than for any other published cluster-based catalyst with the exception of the afore-mentioned H_4Ru_4 catalysts. Further investigation of Re_2H_2 complexes with bulky chiral mono- and diphosphine ligands as potential catalysts for asymmetric hydrogenation reactions is therefore warranted.

Experimental

General Procedures

Solvents used in the synthesis and catalysis tests were dried by distillation over appropriate drying agents and deoxygenated by bubbling with nitrogen gas. All reactions were carried out under nitrogen using standard Schlenk techniques and were routinely monitored by IR spectroscopy. The starting material $[\text{Re}_2(\text{CO})_{10}]$ was purchased from Strem Chemicals Inc. and used without further purification, and

$[\text{Re}_2(\text{CO})_8(\text{NCMe})_2]$ and $[\text{Re}_3(\mu\text{-H})_3(\text{CO})_{11}(\text{NCMe})]$ were prepared by literature methods [32]. The chiral phosphines, 2-methylbutyric acid, *S*-methyl mandelate and tiglic acid were purchased from Sigma Aldrich. Separations were carried out by preparative thin-layer chromatography on glass plates ($20 \times 20 \text{ cm}^2$) coated with silica gel (Merck, 0.5 mm thick). Catalysis experiments were carried out using a 45 mL Parr autoclave with a PTFE reaction vessel. Infra-red spectra were recorded as solutions in 0.5 mm NaCl cells on a Nicolet Avatar 360 FT-IR-spectrometer. ^1H and $^{31}\text{P}\{^1\text{H}\}$ NMR spectra were recorded on a Varian Unity 500 MHz NMR spectrometer; ^{31}P NMR shifts were referenced to external H_3PO_4 . Calculations of the percentage yields for the final products are based on the number of moles of Re atoms.

Syntheses

Preparation of $[\text{ReH}(\text{CO})_3(\mathbf{1a})]$ **3** and $[\text{Re}_3(\mu\text{-H})_3(\text{CO})_{10}(\mathbf{1a})]$ **4**

A mixture of $[\text{Re}_3(\mu\text{-H})_3(\text{CO})_{11}(\text{NCMe})]$ (34 mg, 0.037 mmol) and the ligand [(*R*)-1- $\{(\text{S}_\text{P})$ -2-[Bis[3,5-bis(trifluoromethyl)phenyl]phosphino]ferrocenyl}ethylidene(3,5-xylyl) phosphine], **1a**, (74 mg, 0.074 mmol) were refluxed in octane (20 mL) for 40 min under N_2 in a 100 mL flask. During this time the solution gradually darkened from pale yellow to orange. The solvent was removed under vacuum and the resultant residue was dissolved in a minimum quantity of dichloromethane and separated using TLC. Elution with a dichloromethane–petroleum ether mixture (1:1 v/v) gave two orange bands, as well as minor orange and yellow fractions that were obtained in very low yield and were not characterized. The main two products were collected and extracted from silica using dichloromethane, dried under N_2 and identified as (in order of decreasing R_f): orange solid $[\text{ReH}(\text{CO})_3(\mathbf{1a})]$ **3** and $[\text{Re}_3(\mu\text{-H})_3(\text{CO})_{10}(\mathbf{1a})]$ **4**. Single crystals of **3** were grown by slow evaporation from a dichloromethane–hexane solution of the complex cooled to -4°C .

3: Yield 18 mg (41 %); ν_{CO} (cyclohexane)/ cm^{-1} : 2004 (m), 1931 (vs), 1925 (s); ^1H NMR (500 MHz, CDCl_3) δ NMR (500 MHz, CDCl_3) δ 8.64 (d, $J = 10.6$ Hz, 2H, PPh), 7.66 (m, 4H, PPh), 7.62 (m, 2H, PPh), 7.54 (m, 4H, PPh), 4.63 (m, 1H, Cp), 4.43 (s, 5H, Cp'), 4.34 (t, $J = 2.5$ Hz, 3H, Ph- CH_3), 4.04 (t, $J = 8.2$ Hz, 3H, Ph- CH_3), 3.85 (m, 1H, CH_3CH), 3.78 (s, 1H, Cp-H), 3.54 (s, 1H, Cp-H), 2.26 (d, $J = 15.2$ Hz, 3H, Ph- CH_3), 2.08 (d, $J = 28.3$ Hz, 3H, Ph- CH_3), 1.21 (m, 3H, CH_3CH), -4.48 (t, $J = 26.8$ Hz, 1H); $^{31}\text{P}\{^1\text{H}\}$ NMR (202 MHz, CDCl_3) 24.12 (d, $J = 27.2$ Hz), 10.44 (d, $J = 27.4$ Hz); m/z (ESI) 1181 (M^+).

4: Yield 8 mg (12 %); ν_{CO} (Cyclohexane)/ cm^{-1} : 2106 (m), 2083 (s), 1991 (m), 1960 (m), 1858 (sh); ^1H NMR (500 MHz, CDCl_3) δ ^1H NMR (500 MHz, CDCl_3) δ 8.10 (m, 2H, PPh), 7.59 (m, 4H, PPh), 6.87 (m, 6H, PPh), 4.98 (br s, 5H, Cp), 4.56 (br s, 5H, Cp'), 4.08 (m, 1H, Cp), 3.68 (d, $J = 1.3$ Hz, 1H), 2.61 (d, $J = 1.3$ Hz, 3H, Ph- CH_3), 2.16 (d, $J = 1.4$ Hz, 3H, Ph- CH_3), 1.63 (m, 3H), 1.27 (d, $J = 20.8$ Hz, 3H, CH_3CH), -14.55 (d, $J = 18.4$ Hz, 1H), -15.52 (d, $J = 16.5$ Hz, 1H), -17.20 (s, 1H); $^{31}\text{P}\{^1\text{H}\}$ NMR (202 MHz, CDCl_3) 19.26 (m), 3.89 (m); m/z (ESI) 1775 ($\text{M}^+ + \text{Na}$).

Preparation of $[\text{Re}_2(\text{CO})_9(\mathbf{2a})]$ **5**

In a two-necked round flask, $[\text{Re}_3(\mu\text{-H})_3(\text{CO})_{11}(\text{NCMe})]$ (80 mg, 0.088 mmol) and the ligand $[(\text{R})\text{-1-}\{(\text{R}_\text{P})\text{-2-[2-[bis(4-methoxy-3,5-dimethylphenyl)phosphine]phenyl]ferrocenyl}]\text{ethylbis-bis[3,5-bis(trifluoromethyl)phenyl]phosphine}]$, **2a**, (92 mg, 0.088 mmol) were refluxed in octane (20 mL) with stirring for 4 h, while hydrogen was bubbled through the solution. During this time the solution gradually darkened from pale yellow to orange. The solvent was removed under vacuum and the residue dissolved in a minimum quantity of dichloromethane. The product was then separated by TLC on silica using a dichloromethane–hexane mixture (1:3 v/v) as eluent to give one orange band as well as minor orange and colorless fractions that were obtained in very low yield and were not characterized. The product was collected and extracted from silica with dichloromethane, dried under N_2 and identified as solid orange $[\text{Re}_2(\text{CO})_9(\mathbf{2a})]$ **5**. Orange crystals of **5** were obtained by slow evaporation of a dichloromethane–hexane solution.

5: Yield 31 mg (54 %); $\nu_{\text{CO}}(\text{cyclohexane})/\text{cm}^{-1}$: 2103 (m), 2030 (m), 1997 (s), 1967 (m), 1937 (w); ^1H NMR (500 MHz, CDCl_3) δ 8.28 (m, 1H), 8.05 (m, 1H), 7.88 (m, 5H), 7.69 (m, 1H), 7.59 (m, 3H), 7.47 (d, $J = 12.1$ Hz, 1H), 7.29 (m, 2H), 7.07 (m, 4H), 6.89 (m, 5H), 3.69 (d, $J = 26.8$ Hz, 2H), 4.19 (m, 5H, Cp'), 4.17 (d, $J = 2.4$ Hz, 1H), 4.05 (d, $J = 2.5$ Hz, 1H, Cp-H), 3.95 (m, 1H, Cp-H), 3.81 (ddd, $J_1 = 69.1$, $J_2 = 19.3$, $J_3 = 11.3$ Hz, 1H, CH_3CH), 3.58 (s, 3H, OCH_3), 3.49 (s, 3H, OCH_3), 3.21 (br s, 1H, CP-H), 1.41 (m, 3H, CH_3CH); $^{31}\text{P}\{^1\text{H}\}$ NMR 202 MHz, CDCl_3) 34.94 (d, $J = 41.3$ Hz), -15.75 (d, $J = 47.3$ Hz, free-P); m/z (ESI) 1671 (M^+).

Reaction of $[\text{Re}_2(\text{CO})_9(\mathbf{2a})]$ **5** with $\text{Me}_3\text{NO}\cdot 2\text{H}_2\text{O}$

$[\text{Re}_2(\text{CO})_9(\mathbf{2a})]$ **5** (13 mg, 0.007 mmol) was dissolved in 5 mL of freshly distilled and degassed THF. Dropwise addition of $\text{Me}_3\text{NO}\cdot 2\text{H}_2\text{O}$ (1.0 mg, 0.007 mmol) dissolved in 3 mL of THF under nitrogen was carried out. The resultant solution was degassed again and stirred under nitrogen at ambient temperature for 8 h. The solution was then evaporated to dryness and the orange residue was redissolved in a minimum quantity of CH_2Cl_2 and chromatographed on silica TLC plates using a dichloromethane–petroleum ether mixture (1:3 v/v) as eluent, to give one orange band as well as minor orange and colorless fractions that were obtained in very low yield and were not characterized. The product was collected and extracted from silica with dichloromethane, dried under N_2 and identified as solid orange $[\text{Re}_2(\text{CO})_8(\mathbf{2a})]$ **6**.

6: Yield 6 mg (47 %); $\nu_{\text{CO}}(\text{cyclohexane})/\text{cm}^{-1}$: 2069 (w), 2018 (w), 1983 (m), 1967 (s), 1938 (w), 1900 (m); ^1H NMR (500 MHz, CDCl_3) δ 8.24 (m, 1H), 7.99 (m, 1H), 7.83 (m, 5H), 7.64 (dd, $J_1 = 24.0$, $J_2 = 6.6$ Hz, 1H), 7.53 (m, 3H), 7.44 (d, $J = 11.3$ Hz, 1H), 7.22 (m, 2H), 7.01 (m, 4H), 6.78 (m, 5H), 3.63 (d, $J = 25.9$ Hz, 2H), 4.15 (m, 5H, Cp'), 4.12 (d, $J = 2.1$ Hz, 1H), 3.93 (d, $J = 2.1$ Hz, 1H, Cp-H), 3.87 (m, 1H, Cp-H), 3.72 (ddd, $J_1 = 68.8$, $J_2 = 18.3$, $J_3 = 10.4$ Hz, 1H, CH_3CH), 3.53 (s, 3H, OCH_3), 3.44 (s, 3H, OCH_3), 3.16 (br s, 1H, CP-H), 1.36 (m, 3H, CH_3CH); $^{31}\text{P}\{^1\text{H}\}$ NMR 202 MHz, CDCl_3) 19.24 (m), 4.83 (m); m/z (ESI) 1643 (M^+).

Preparation of [Re₂(CO)₉(2b)] 7 and [{Re₂(CO)₉]₂(2b)] 8

The complex [Re₃(μ-H)₃(CO)₁₁(NCMe)] (40 mg, 0.044 mmol) and the ligand [(R)-1-{(R_P)-2-[2-(Diphenylphosphino)phenyl]ferrocenyl}ethylidicyclohexylphosphine], **2b**, (29 mg, 0.043 mmol) were refluxed in octane (20 mL) and stirred for 15 h. During this time the solution gradually darkened from pale yellow to orange. The solvent was removed under vacuum and the residue dissolved in a minimum quantity of dichloromethane. The product was then separated by TLC on silica using a dichloromethane–hexane mixture (1:2 v/v) as eluent to give two orange bands as well as minor orange and colorless fractions that were obtained in very low yield and were not characterized. The products were collected and extracted from silica with dichloromethane, dried under N₂ and identified as (in order of decreasing R_F): solid orange [Re₂(CO)₉(**2b**)] **7** and [{Re₂(CO)₉]₂(**2b**)] **8**. Orange crystals of [{Re₂(CO)₉]₂(**2b**)] **8** were obtained by slow evaporation of a dichloromethane–hexane solution.

7: Yield 16 mg (70 %); ν_{CO}(cyclohexane)/cm⁻¹: 2104 (m), 2022 (w), 1997 (s), 1964 (m), 1927 (m); ¹H NMR(500 MHz, CDCl₃): δ = 8.18 (dd, J₁ = 7.7, J₂ = 4.2 Hz, 1H, Ph-H), 8.10 (m, 6H), 7.52 (m, 5H, P-Ph), 7.38 (d, J₁ = 6.0 Hz, 1H, Ph-H), 7.13 (q, 3H, J₁ = 10.2, J₂ = J₃ = 8.9 Hz, 1H, Ph-H), 6.98 (dd, J₁ = 7.7, J₂ = 3.7 Hz, 1H, Ph-H), 4.13 (m, 1H, CP-H), 3.96 (s, 5H, Cp'), 3.85 (br s, 1H, Cp-H), 3.41 (m, 1H, CH₃CH), 1.90 (dd, J₁ = 17.8, J₂ = 7.4 Hz, 3H, CH₃CH), 1.36 (m, 22H) ppm; ³¹P{¹H} NMR (202 MHz, CDCl₃) 43.38 (s), -14.41 (s, free P); m/z (ESI) 1295 (M⁺).

8: Yield 13 mg (16 %); ν_{CO}(dichloromethane)/cm⁻¹: 2104 (s), 2032 (w), 1995 (vs), 1960 (m), 1928 (w); ¹H NMR (500 MHz, CDCl₃): δ = 8.01 (ddd, J₁ = 7.8, J₂ = 4.5, J₃ = 1.1 Hz, 1H, Ph-H), 7.55 (m, 6H), 7.38 (m, 5H, P-Ph), 7.22 (m, 1H, Ph-H), 6.79 (ddd, J₁ = 7.3, J₂ = 4.7, J₃ = 1.4 Hz, 1H, Ph-H), 4.18 (s, 1H, Cp-H), 4.18 (t, J₁ = J₂ = 2.3 Hz, 1H, CP-H), 3.95 (s, 5H, Cp'), 3.88 (br s, 1H, Cp-H), 3.19 (q, J₁ = 7.4, J₂ = 7.5, J₃ = 6.9 Hz, 1H, CH₃CH), 1.93 (dd, J₁ = 10.1, J₂ = 7.7 Hz, 3H, CH₃CH), 1.32 (m, 22H); ³¹P{¹H} NMR (202 MHz, CDCl₃) 43.83 (s), -14.43 (s); m/z (ESI) 1920 (M⁺+H).

Reaction of [Re₂(CO)₉(2b)] 7 with Me₃NO·2H₂O

[Re₂(CO)₉(**2b**)] **7** (16 mg, 0.0123 mmol) was dissolved in 5 mL of freshly distilled and degassed THF. Dropwise addition of Me₃NO·2H₂O (1.3 mg, 0.0123 mmol) dissolved in 3 mL of THF under nitrogen was carried out. The resultant solution was degassed again and stirred under nitrogen at ambient temperature for 8 h. The solution was then evaporated to dryness and the orange residue was redissolved in a minimum quantity of CH₂Cl₂ and chromatographed on silica TLC plates using a dichloromethane–petroleum ether mixture (1:3 v/v) as eluent, to give one orange band as well as minor orange and colorless fractions that were obtained in very low yield and were not characterized. The product was collected and extracted from silica with dichloromethane, dried under N₂ and identified as solid orange [Re₂(CO)₈(**2b**)] **9**.

9: Yield 5 mg (38 %); $\nu_{\text{CO}}(\text{cyclohexane})/\text{cm}^{-1}$: 2073 (w), 2022 (m), 1981 (w), 1964 (s), 1946 (w), 1920 (m); ^1H NMR (500 MHz, CDCl_3) δ 8.18 (dd, $J_1 = 6.2$, $J_2 = 4.0$ Hz, 1H, Ph-H), 8.09 (m, 6H), 7.47 (m, 5H, P-Ph), 7.28 (d, $J_1 = 3.4$ Hz, 1H, Ph-H), 7.13 (dd, $J_1 = 16.8$, $J_2 = 8.8$ Hz, 1H, Ph-H), 4.22 (s, 1H, Cp-H), 4.13 (dd, $J_1 = 25.6$, $J_2 = 11.4$ Hz, 1H, CP-H), 3.95 (s, 5H, Cp'), 3.85 (br s, 1H, Cp-H), 3.43 (m, 1H, CH_3CH), 1.90 (dd, $J_1 = 17.8$, $J_2 = 7.3$ Hz, 3H, CH_3CH), 1.36 (m, 22H); $^{31}\text{P}\{^1\text{H}\}$ NMR (202 MHz, CDCl_3) 59.01 (s), 31.01 (s); m/z (ESI) 1268 ($\text{M}^+ + \text{H}$).

Preparation of $[\text{Re}_2(\text{CO})_8(\mathbf{1b})]$ **10**

A solution of $[\text{Re}_2(\text{CO})_8(\text{NCMe})_2]$ (50 mg, 0.073 mmol) in toluene (40 mL) was warmed to 80 °C in an oil bath while hydrogen was bubbled through the solution until complete conversion to $[\text{Re}_3(\mu\text{-H})_3(\text{CO})_{11}(\text{NCMe})]$ had occurred (as monitored by IR spectroscopy). Addition of the ligand [*(S)*-1-*(R_P*)-2-[Di(2-furyl)phosphino]ferrocenyl]ethyldi-*tert*-butylphosphine], **1b**, (38 mg, 0.073 mmol) to the reaction mixture led to a darkening of the initial pale yellow solution and a change of the color to deep orange. After 2 h the solvent was evaporated under vacuum and the resultant residue was subjected to TLC, using a dichloromethane–petroleum ether mixture (1:2 v/v) as eluent, to give one orange band as well as minor colorless fractions that were obtained in very low yield and were not characterized. The main product obtained was collected and extracted from silica with dichloromethane, dried under N_2 and identified as orange solid $[\text{Re}_2(\text{CO})_8(\mathbf{1b})]$ **10**.

10: Yield 28 mg (57 %); $\nu_{\text{CO}}(\text{cyclohexane})/\text{cm}^{-1}$: 2065 (w), 2032 (vs), 1990 (w), 1952 (s), 1908 (m); ^1H NMR (500 MHz, CDCl_3) δ 7.90 (d, $J = 3.2$ Hz, 2H, $\text{C}_4\text{H}_3\text{O}$), 7.57 (m, 2H, $\text{C}_4\text{H}_3\text{O}$), 6.53 (m, 2H, $\text{C}_4\text{H}_3\text{O}$), 6.30 (m, 1H, CHCH_3), 5.01 (s, 1H, Cp), 4.48 (s, 1H, Cp), 3.79 (s, 1H, Cp), 3.57 (s, 5H, Cp'), 1.90 (m, 3H, CHCH_3), 1.60 (d, $J = 11.1$ Hz, 9H, $\text{C}(\text{CH}_3)_3$), 0.94 (d, $J = 12.3$ Hz, 9H, $\text{C}(\text{CH}_3)_3$). $^{31}\text{P}\{^1\text{H}\}$ NMR (202 MHz, CDCl_3) 55.41 (d, $J = 26.3$ Hz), -30.61 (d, $J = 26.1$ Hz); m/z (ESI) 1118 (M^+).

Preparation of $[\text{Re}_2(\mu\text{-H})_2(\text{CO})_6(\mathbf{2b})]$ **11** and $[\text{Re}_3(\mu\text{-H})_3(\text{CO})_{11}(\mathbf{2b})]$ **12**

A solution of $[\text{Re}_2(\text{CO})_8(\text{NCMe})_2]$ (50 mg, 0.073 mmol) in toluene (40 mL) was warmed to 80 °C in an oil bath while hydrogen was bubbled through the solution until complete conversion to $[\text{Re}_3(\mu\text{-H})_3(\text{CO})_{11}(\text{NCMe})]$ had occurred (as monitored by IR spectroscopy), followed by the addition of **2b** (49 mg, 0.073 mmol) to the reaction mixture. The initial pale yellow solution darkened upon addition of the diphosphine, and the color changed to deep orange. After 7 h, the solvent was evaporated under vacuum. The resultant residue was subjected to TLC, using a dichloromethane–petroleum ether mixture (1:2 v/v) as eluent, to give two orange bands as well as minor orange and colorless fractions that were obtained in very low yield and were not characterized. The main two products obtained were collected and extracted from silica by using dichloromethane, dried under N_2 and identified as (in order of decreasing R_f): $[\text{Re}_2(\mu\text{-H}_2)(\text{CO})_6(\mathbf{2b})]$ **11** as an orange solid and $[\text{Re}_3(\mu\text{-H})_3$

(CO)₁₁(**2b**)] **12**. Orange crystals of [Re₂(μ-H₂)(CO)₆(**2b**)] **11** were obtained by slow evaporation of dichloromethane–hexane solution.

11: Yield 19 mg (20 %); ν_{CO}(cyclohexane)/cm^{−1}: 2036 (m), 2023 (w), 2011 (m), 1940 (vs), 1918 (s), 1911 (s); ¹H NMR (500 MHz, CDCl₃): δ = 8.03 (ddd, *J*₁ = 7.5, *J*₂ = 4.5, *J*₃ = 1.0 Hz, 1H, Ph-H), 7.42 (m, 6H), 7.32 (m, 5H, P-Ph), 7.12 (m, 1H, Ph-H), 6.74 (ddd, *J*₁ = 7.2, *J*₂ = 4.5, *J*₃ = 1.2 Hz, 1H, Ph-H), 4.19 (s, 1H, Cp-H), 4.15 (t, *J*₁ = *J*₂ = 2.3 Hz, 1H, CP-H), 3.93 (s, 5H, Cp'), 3.84 (br s, 1H, Cp-H), 3.17 (q, *J*₁ = 7.2, *J*₂ = 7.2, *J*₃ = 6.8 Hz, 1H, CH₃CH), 1.90 (dd, *J*₁ = 10.2, *J*₂ = 7.5 Hz, 3H, CH₃CH), 1.31 (m, 22H), −6.78 (t, *J*₁ = *J*₂ = 10.3, 10.3 Hz, 1H), −9.28 (t, *J*₁ = *J*₂ = 8.5 Hz, 1H) ppm; ³¹P{¹H} NMR (202 MHz, CDCl₃): 43.19 (s), 28.08 (s); *m/z* (ESI) 1213 (M⁺).

12: Yield 6 mg (5 %); ν_{CO}(cyclohexane)/cm^{−1}: 2110 (w), 2087 (m), 2034 (w), 2018 (vs), 2005 (w), 1955 (s), 1967 (s), 1951 (w), 1936 (w), 1924 (w); ¹H NMR (500 MHz, CDCl₃): δ = 8.24 (d, *J* = 26.0 Hz, 1H, Ph-H), 7.57 (dd, *J*₁ = 53.6, *J*₂ = 26.7 Hz, 6H), 7.39 (d, *J* = 28.8 Hz, 5H, P-Ph), 7.13 (m, 1H, Ph-H), 5.31 (m, 1H, Ph-H), 4.50 (d, *J* = 26.9 Hz, 1H, Cp-H), 4.12 (t, *J*₁ = *J*₂ = 2.4 Hz, 1H, CP-H), 3.86 (d, *J* = 29.1 Hz, 5H, Cp'), 3.55 (m, 2H), 1.30 (dd, *J*₁ = 84.0, *J*₂ = 28.1 Hz, 3H, CH₃CH), 1.28 (m, 22H), −16.31 (m, 1H), −17.21 (d, *J* = 29.8 Hz, 1H), −17.60 (d, *J* = 29.2 Hz, 1H) ppm; ³¹P{¹H} NMR (202 MHz, CDCl₃): 39.16 (m), 31.30 (d, *J* = 43.1 Hz); *m/z* (ESI) 1541 (M⁺+H).

*Attempted Reaction of [Re₃(μ-H)₃(CO)₁₁(**2b**)] **12** with Me₃NO·2H₂O or Heat (Thermal Substitution)*

[Re₃(μ-H)₃(CO)₁₁(**2b**)] **12** (15 mg, 0.01 mmol) was dissolved in 5 mL of freshly distilled and degassed THF. Addition of Me₃NO·2H₂O (1.1 mg, 0.012 mmol) dissolved in 3 mL of THF under nitrogen was carried out. The resultant solution was degassed again and stirred under nitrogen at ambient temperature for 8 h. Analysis of the reaction by spot TLC (dichloromethane:hexane, 1:3) showed that no reaction had occurred. In another experiment, a total of 15 mg (0.01 mmol) [Re₃(μ-H)₃(CO)₁₁(**2b**)] **12** was dissolved in 8 mL of toluene, and the solution was heated at 90 °C for 8 h under nitrogen. The resultant solution was dried under vacuum, extracted with a small amount of dichloromethane. Analysis of the final product by spot TLC (dichloromethane:hexane, 1:3) showed that decomposition had occurred.

X-Ray Structure Determinations

The diffraction data were collected at 296 K for complex **3** and at 100 K for complexes **5**, **8** and **11**, using a Nonius Kappa CCD or a Bruker AXS ApexII diffractometer with Mo Kα radiation (λ = 0.71073 Å). The Denzo-Scalepack [45] or APEX2 [46] program packages were used for cell refinements and data reductions. The structure solutions were carried out using the SHELXS-97 [47], program with the WinGX [48] graphical user interface. All hydrogens were placed in idealized positions. Positions of hydrides were calculated using the XHYDEX program [49]. The crystallographic details for the reported structures are summarized in Table 2.

Table 2 Crystal data and structure refinement parameters for [ReH(CO)₃(1a)] **3**, [Re₂(CO)₆(2a)] **5**, [[Re₂(CO)₆]₂(2b)] **8** and [Re₂(μ-H)₂(CO)₆(2b)] **11**

Complex	3	5	8	11
Empirical formula	C ₄₇ H ₃₇ F ₁₂ FeO ₃ P ₂ Re	C ₆₁ H ₄₄ F ₁₂ FeO ₁₁ P ₂ Re ₂	C ₆₀ H ₄₄ FeO ₁₈ P ₂ Re ₄	C ₅₀ H ₅₃ FeNO ₆ P ₂ Re ₂
Formula weight	1181.77	3580.23	1919.57	1254.12
Temp (K)	296(2)	100(2)	100(2)	100(2)
λ (Å)	0.71073	0.71073	0.71073	0.71073
Crystal system	Orthorhombic	Monoclinic	Monoclinic	Orthorhombic
Space group	<i>P</i> 2 ₁ -2 ₁	<i>C</i> 2	<i>P</i> 2 ₁	<i>P</i> 2 ₁ -2 ₁
<i>a</i> (Å)	11.9555(11)	25.5435(5)	13.1510(3)	10.5740(3)
<i>b</i> (Å)	19.9407(18)	15.1197(3)	13.0372(4)	13.0328(4)
<i>c</i> (Å)	20.2532(18)	18.2232(3)	17.9002(6)	34.0232(10)
α (°)	90	90	90	90
β (°)	90	106.8210(10)	96.584(2)	90
γ (°)	90	90	90	90
Volume (Å ³)	4828.4(8)	6736.9(2)	3048.79(16)	4688.7(2)
<i>Z</i>	4	2	2	4
ρ _{calc} (Mg/m ³)	1.626	1.765	2.091	1.777
μ(Mo Kα) (mm ⁻¹)	2.957	4.016	8.267	5.574
<i>F</i> (000)	2328	3492	1816	2456
Crystal size (mm)	0.30 × 0.25 × 0.20	0.30 × 0.29 × 0.17	0.15 × 0.08 × 0.05	0.23 × 0.21 × 0.08
θ limits (°)	1.4–25.2	2.44–37.04	1.56–30.02	1.67–28.33
<i>h</i> range	–12 to 14	–43 to 43	–18 to 18	–13 to 14
<i>k</i> range	–23 to 23	–21 to 25	–18 to 17	–17 to 17
<i>l</i> range	–24 to 23	–30 to 30	–25 to 24	–45 to 45
No. refns.	36856	62499	34014	40005
Unique refns.	4818	29925	17233	11601
GOOF (F ²)	1.005	1.037	0.935	1.051

Table 2 continued

Complex Empirical formula	3 $C_{47}H_{37}F_{12}FeO_3P_2Re$	5 $C_{61}H_{44}F_{12}FeO_{11}P_2Re_2$	8 $C_{60}H_{48}FeO_{18}P_2Re_4$	11 $C_{50}H_{53}FeNO_6P_2Re_2$
R_{int}	0.115	0.0240	0.0381	0.0419
$R1^a$ ($I \geq 2\sigma$)	0.0521	0.0299	0.0365	0.0397
$WR2^b$ ($I \geq 2\sigma$)	0.1177	0.0692	0.0541	0.0597
Largest diff. peak and hole ($e \text{ \AA}^{-3}$)	0.81 and -0.56	2.339 and -2.446	1.743 and -1.284	1.656 and -1.355
Absolute structure parameter	-0.028 (10)	-0.012 (3)	-0.014 (5)	0.001 (6)

^a $R1 = \Sigma ||F_o| - |F_c|| / \Sigma |F_o|$
^b $WR2 = [\Sigma [w(F_o^2 - F_c^2)^2] / \Sigma [w(F_o^2)^2]]^{1/2}$

Homogeneous Catalysis Experiments

In the catalysis experiments, the catalyst (5–10 mg) and substrate (100 molar excess) were loaded into the autoclave under N₂ and the degassed solvent mixture was added (2.5 mL of EtOH/2.5 mL of toluene). The reaction vessel was closed and purged three times with hydrogen before final pressurizing to 50 bar. The reaction mixture was continuously stirred with a magnetic stirrer (ca. 750 rpm) and heated at 100 °C for different lengths of time (24, 48 and 72 h). After a cooling period of approximately 45 min, the reaction vessel was depressurized and opened. The homogeneous reaction mixture was transferred to a 50 mL flask and concentrated under vacuum. The conversions for the catalysis runs were calculated on the basis of NMR analysis. To separate the carboxylic acid from the cluster, the reaction residue was dissolved in 10 mL of diethyl ether and the carboxylic acid was extracted with aqueous sodium solution (1 M, 3 × 10 mL) and washed with diethyl ether (3 × 5 mL), leaving the cluster in the organic solvent. The carboxylate was protonated with sulfuric acid and extracted with diethyl ether (3 × 10 mL), washed with water (2 × 5 mL) and dried over magnesium sulfate. Evaporation of the ether under vacuum gave the carboxylic acid quantitatively. The ether phase, from which the carboxylic acid was extracted, was concentrated under vacuum to recover the remaining cluster. In certain cases, where ester formation was obtained during the catalytic experiment, the recovered catalyst was dissolved in a minimum quantity of dichloromethane and the products were separated by preparative TLC, eluting with a dichloromethane/petroleum ether mixture (1:2). Usually 50–70 % of the cluster was recovered after a catalytic experiment and it was analyzed by IR and NMR spectroscopies. The enantiomeric excess of the product was detected by derivatizing 2-methylbutyric acid with *S*-methyl mandelate and analyzing the diastereomeric product mixture by NMR, as fully described by Tyrrell et al. [42]. It was found that flash chromatography of the final products was not necessary. The results of the catalytic experiments and determined enantiomeric excesses are shown in Table 1.

Supporting Information

Additional supporting information may be found in the online version of this article at the publisher's website.

CCDC 1030320-1030323 contain the supplementary crystallographic data for **3**, **5**, **8** and **11**, respectively. These data can be obtained free of charge from the Cambridge Crystallographic Data Centre via www.ccdc.cam.ac.uk/data_request/cif.

Acknowledgments AFA thanks the EU Erasmus Mundus program, FFEEBB1 office, for a scholarship. AKS thanks the Carl Trygger Foundation for a postdoctoral fellowship. MM acknowledges the University of Bologna for financial support.

References

1. V. Moberg, M. Haukka, I. O. Koshevoy, R. Ortiz, and E. Nordlander (2007). *Organometallics* **26**, 4090–4093.

2. M. J. Stchedroff, V. Moberg, E. Rodriguez, A. E. Aliev, J. Bottcher, J. W. Steed, E. Nordlander, M. Monari, and A. J. Deeming (2006). *Inorg. Chim. Acta.* **359**, 926–937.
3. T. Suarez, B. Fontal, M. Reyes, F. Bellandi, R. R. Contreras, A. Bahsas, G. Leon, P. Cancines, and B. Castillo (2004). *React. Kinet. Catal. Lett.* **82**, 317–324.
4. T. Suarez, B. Fontal, M. Reyes, F. Bellandi, R. R. Contreras, J. M. Ortega, G. Leon, P. Cancines, and B. Castillo (2004). *React. Kinet. Catal. L.* **82**, 325–331.
5. P. Homanen, R. Persson, M. Haukka, T. A. Pakkanen, and E. Nordlander (2000). *Organometallics* **19**, 5568–5574.
6. B. Fontal, M. Reyes, T. Suarez, F. Bellandi, and J. C. Diaz (1999). *J. Mol. Catal. A: Chem.* **149**, 75–85.
7. R. D. Adams (2000). *J. Organomet. Chem.* **600**, 1–6.
8. R.-X. Li, K.-C. Tin, N.-B. Wong, T. C. W. Mak, Z.-Y. Zhang, and X.-J. Li (1998). *J. Organomet. Chem.* **557**, 207–212.
9. A. M. Joshi, K. S. MacFarlane, and B. R. James (1995). *J. Organomet. Chem.* **488**, 161–167.
10. R. Noyori *Asymmetric Catalysis in Organic Synthesis* (Wiley, London, 1993).
11. W. A. Herrmann (1990). *J. Organomet. Chem.* **382**, 1–18.
12. T. J. Henly (1989). *Coordin. Chem. Rev.* **93**, 269–295.
13. H. S. Broadbent, L. H. Slaugh, and N. L. Jarvis (1954). *J. Am. Chem. Soc.* **76**, 1519–1523.
14. B. Duddle, K. Rajesh, O. Blacque, and H. Berke (2011). *J. Am. Chem. Soc.* **133**, 8168–8178.
15. L. Liu, S. Bi, M. Sun, X. Yuan, N. Zheng, and P. Li (2009). *J. Organomet. Chem.* **694**, 3343–3348.
16. Y. Jiang, O. Blacque, T. Fox, C. M. Frech, and H. Berke (2009). *Chem. Eur. J.* **15**, 2121–2128.
17. Y. Jiang, O. Blacque, T. Fox, C. M. Frech, and H. Berke (2009). *Organometallics* **28**, 5493–5504.
18. R. D. Adams, J. Cortopassi, and S. Falloon (1993). *J. Organomet. Chem.* **463**, C5–C7.
19. R. D. Adams, The catalytic Synthesis of Thiacrowns from Thietanes and Thiiranes by Metal Carbonyl Complexes, ALDRICH2000.
20. R. D. Adams *In Catalysis by Di- and Polynuclear Metal Cluster Complexes* (Wiley, New York, 1998).
21. V. Moberg, R. Duquesne, S. Contaldi, O. Röhrs, J. Nachtigall, L. Damoense, A. T. Hutton, M. Green, M. Monari, D. Santelia, M. Haukka, and E. Nordlander (2012). *Chem. Eur. J.* **18**, 12458–12478.
22. A. F. Abdel-Magied, A. K. Singh, M. Haukka, M. G. Richmond, and E. Nordlander (2014). *Chem. Commun.* **50**, 7705–7708.
23. N. Flitcroft, J. M. Leach, and F. J. Hopton (1970). *J. Inorg. Nucl. Chem.* **32**, 137–143.
24. D. W. Prest, M. J. Mays, P. R. Raithby, and A. G. Orpen (1982). *J. Chem. Soc., Dalton Trans.* 737–745.
25. W. Fan, R. Zhang, W. K. Leong, and Y. K. Yan (2004). *Inorg. Chim. Acta.* **357**, 2441–2450.
26. Y. Wang, T. Sturm, M. Steurer, V. B. Arion, K. Mereiter, F. Spindler, and W. Weissensteiner (2008). *Organometallics* **27**, 1119–1127.
27. P. Steil, U. Nagel, and W. Beck (1989). *J. Organomet. Chem.* **366**, 313–331.
28. W. Fan, R. Zhang, W. K. Leong, C. K. Chu, and Y. K. Yan (2005). *J. Organomet. Chem.* **690**, 3765–3773.
29. T. S. A. Hor, P. M. N. Low, Y. K. Yan, L.-K. Liu, and Y.-S. Wen (1993). *J. Organomet. Chem.* **448**, 131–137.
30. M. R. Churchill, K. N. Amoh, and H. J. Wasserman (1981). *Inorg. Chem.* **20**, 1609–1611.
31. T. S. A. Hor, H. S. O. Chan, K. L. Tan, L. T. Phang, Y. K. Yan, L. K. Liu, and Y. S. Wen (1991). *Polyhedron* **10**, 2437–2450.
32. M. I. Bruce and P. J. Low (1996). *J. Organomet. Chem.* **519**, 221–222.
33. W. CHiau-Yu, G. Luigi, B. Robert (1981). *J. Organomet. Chem.* **213**, 63.
34. M. R. Churchill, P. H. Bird, H. D. Kaesz, R. Bau, and B. Fontal (1968). *J. Am. Chem. Soc.* **90**, 7135–7136.
35. M. J. Bennett, W. A. G. Graham, J. K. Hoyano, and W. L. Hutcheon (1972). *J. Am. Chem. Soc.* **94**, 6232–6233.
36. V. Moberg, P. Homanen, S. Selva, R. Persson, M. Haukka, T. A. Pakkanen, M. Monari, E. Nordlander (2006). *Dalton Trans.* 279–288.
37. C. Botteghi, S. Gladiali, M. Bianchi, U. Matteoli, P. Frediani, P. G. Vergamini, and E. Benedetti (1977). *J. Organomet. Chem.* **140**, 221–228.
38. M. Bianchi, U. Matteoli, G. Menchi, P. Frediani, F. Piacenti, and C. Botteghi (1980). *J. Organomet. Chem.* **195**, 337–346.
39. M. Breuer, K. Ditrich, T. Habicher, B. Hauer, M. Keßeler, R. Stürmer, and T. Zelinski (2004). *Angew. Chem. Int. Ed.* **43**, 788–824.

40. H.-U. Blaser, B. Pugin, and F. Spindler (2005). *J. Mol. Catal. A* **231**, 1–20.
41. U. Matteoli, V. Beghetto, and A. Scrivanti (1996). *J. Mol. Catal. A* **109**, 45–50.
42. E. Tyrrell, M. W. H. Tsang, G. A. Skinner, and J. Fawcett (1996). *Tetrahedron* **52**, 9841–9852.
43. U. Matteoli, M. Bianchi, P. Frediani, G. Menchi, C. Botteghi, and M. Marchetti (1984). *J. Organomet. Chem.* **263**, 243–246.
44. U. Matteoli, G. Menchi, P. Frediani, M. Bianchi, and F. Piacenti (1985). *J. Organomet. Chem.* **285**, 281–292.
45. W.M. Z. Otwinowski, in: C.W. Carter and J. Sweet (eds.), *Methods in Enzymology, Macromolecular Crystallography*, Part A (Academic Press, New York, **276** 1997) p. 307.
46. APEX2, *Software Suite for Crystallographic Programs* (Bruker AXS, Inc., Madison 2009).
47. G. Sheldrick (2008). *Acta Crystallogr. Sect. A* **64**, 112–122.
48. L. J. Farrugia (1999). *J. Appl. Crystallogr.* **32**, 837–838.
49. A. G. Orpen (1980). *J. Chem. Soc., Dalton Trans.* **19**, 2509–2516.

Paper IV

ARTICLE

Chiral arylphosphido- and phosphinidene-capped tri- and tetraruthenium/osmium hydride clusters

Cite this: DOI: 10.1039/x0xx00000x

Received 00th January 2012,
Accepted 00th January 2012

DOI: 10.1039/x0xx00000x

www.rsc.org/

A. F. Abdel-Magied,^a M. H. Majeed,^a A. Ficks,^b A. K. Singh,^a William Clegg,^b M. Haukka,^c M. Monari,^d M. Jarenmark,^a E. Nordlander^{a*} and L. J. Higham^{b*}

The chiral primary phosphines (S)-[1,1'-binaphthalen]-2-ylphosphine (S)-**1a** and (R)-[2'-methoxy-1,1'-binaphthalen]-2-ylphosphine (R)-**1b** have been reacted with (derivatives of) $[M_3(CO)_{12}]$ (M = Ru, Os) and $[(\mu-H)_4Ru_4(CO)_{12}]$ to afford the phosphinidene-capped, phosphido-bridged and phosphine-substituted clusters $[(\mu-H)_2Ru_3(\mu_3-PAr)(CO)_9]$ (S)-**2a**/(R)-**2b**, $[(\mu-H)Ru_3(\mu_2-PAr)(CO)_8(dppm)]$ (S)-**3a**/(R)-**3b**, $[(\mu-H)_2Ru_3(\mu_3-PAr)(CO)_7(dppm)]$ (S)-**4a**/(R)-**4b**, $[Ru_3(CO)_9(dppm)(PH_2Ar)]$ (S)-**5a**/(R)-**5b**, $[Os_3(CO)_{11}(ArPH_2)]$ (S)-**6a**/(R)-**6b**, $[(\mu-H)Os_3(\mu_2-PAr)(CO)_{10}]$ (S)-**7a**/(R)-**7b**, $[(\mu-H)_2Os_3(\mu_3-PAr)(CO)_8]$ (S)-**8a**/(R)-**8b** and $[(\mu-H)_4Ru_4(CO)_{11}(\mathbf{1a/b})]$ (S)-**9a**/(R)-**9b**. The ability of these clusters to catalyse the (asymmetric) hydrogenation of tiglic acid was studied. While substrate conversion was found to be relatively good for most clusters, the enantioselectivities were poor, with (R)-**9b** giving the best result (conversion: 99%; enantioselectivity: 19%).

Introduction

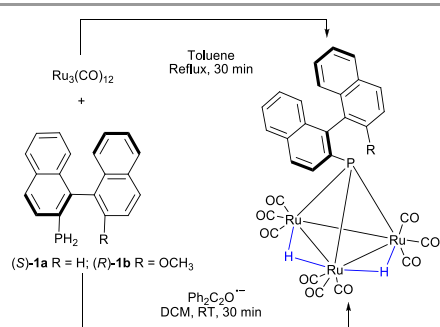
Homogeneous catalytic research has long sought to master the twin objectives of both high selectivity and reactivity.¹ One promising approach is to combine the high turnover frequencies of heterogeneous systems with the stereospecificity engendered by molecular design – in the most challenging of cases this would also afford high enantioselectivity in asymmetric catalysis. In this regard, several investigations into the catalytic properties of metal carbonyl clusters containing chiral phosphine ligands have been studied, under various conditions.^{2, 3} For instance, clusters of the general formulae $[H_4Ru_4(CO)_{10}\{\mu-1,2-(P-P)\}]$ and $[H_4Ru_4(CO)_{10}\{1,1-(P-P)\}]$ (P-P = chiral diphosphine of the Walphos ligand family) have been used successfully in the asymmetric hydrogenation reaction of unsaturated prochiral carboxylic acids under mild conditions.⁴ Aside from tertiary phosphines, phosphido (RHP-M or R_2P-M) and phosphinidene (RP=M) ligands are capable of bridging two or more metal atoms, and achiral phosphido-/phosphinidene-containing clusters have been proven to function as effective hydrogenation catalysts – for example heating the compound $[HRu_3(CO)_9(\mu-H)_2(\mu-PPh_2)]$ in the presence of alkyne substrates yields alkenes.⁵ A well-known route to phosphido and phosphinidene complexes is the thermal reaction of primary phosphines with $[M_3(CO)_{12}]$ (M = Fe, Ru, Os),^{6–11} but to the best of our knowledge, the corresponding work with chiral primary phosphines and their ability to induce

enantioselectivity in asymmetric hydrogenations has not been investigated. Here we describe the reactivity of such ligands with tri- and tetraruthenium and osmium cores, that leads to the formation of phosphido and phosphinidene capped clusters, which were then tested for their ability to act as catalysts in the asymmetric hydrogenation of tiglic acid.

Results and Discussion

Synthesis and characterisation of triruthenium hydride clusters

The cluster $[Ru_3(CO)_{12}]$ and one equivalent of primary phosphine, (S)-**1a** or (R)-**1b**, were refluxed in toluene under nitrogen. After 30 minutes $[(\mu-H)_2Ru_3(\mu_3-PAr)(CO)_9]$ (S)-**2a**/(R)-**2b** was obtained as the major product after chromatographic work-up (Scheme 1). The same product was obtained following the addition of diphenylketyl radical to a solution of $[Ru_3(CO)_{12}]$ and one equivalent of (S)-**1a**/(R)-**1b** in dichloromethane (Scheme 1). The resultant clusters have been characterized by IR, ¹H and ³¹P NMR spectroscopy, and the molecular structure of (S)-**2a** has been determined by single crystal X-ray diffraction (Figure 1).



Scheme 1 Synthesis of the clusters $[(\mu\text{-H})_2\text{Ru}_3(\mu_3\text{-PAr})(\text{CO})_9]$ (*S*)-**2a** and (*R*)-**2b**.

In the solid state, $[(\mu\text{-H})_2\text{Ru}_3(\mu_3\text{-P}(1,1'\text{-binaphthyl}))(\text{CO})_9]$ (*S*)-**2a** consists of a trigonal pyramid formed from three ruthenium atoms capped by an arylphosphinidene moiety. There are four crystallographically independent but structurally similar molecules in the asymmetric unit. The structure of one of these molecules is shown in Fig. 1 and selected bond distances and angles are listed in the caption. Each metal has three terminal carbonyls, and the two metal-metal bonds that are bridged by hydrides are slightly elongated in comparison to the non-bridged Ru-Ru edge (Fig. 1). The Ru-P bond lengths in (*S*)-**2a** are similar to those observed for the phosphinidene cluster $[\text{H}_2\text{Ru}_3(\text{CO})_9(\mu_3\text{-PPh})]$,⁷ and are similarly asymmetric: P(1)-Ru(1) = 2.3432(15), P(1)-Ru(2) = 2.2974(15) and P(1)-Ru(3) = 2.2977(15) Å.

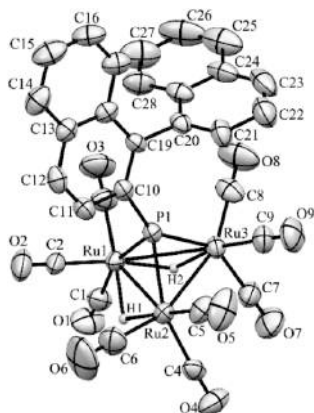


Fig. 1 Molecular structure of $[(\mu\text{-H})_2\text{Ru}_3(\mu_3\text{-P}(1,1'\text{-binaphthyl}))(\text{CO})_9]$ (*S*)-**2a** with thermal ellipsoids drawn at 50% probability level. Aryl hydrogen atoms omitted for clarity. Selected bond lengths (Å) and angles (°): Ru(1)-Ru(2) = 2.9290(7), Ru(1)-Ru(3) = 2.9368(7), Ru(2)-Ru(3) = 2.8276(7), P(1)-Ru(1) = 2.3432(15), P(1)-Ru(2) = 2.2974(15), P(1)-Ru(3) = 2.2977(15), C(10)-P(1) = 1.826(6); Ru(2)-Ru(1)-Ru(3) = 57.640(17), Ru(1)-Ru(2)-Ru(3) = 61.319(18), Ru(1)-Ru(3)-Ru(2) = 61.041(16), Ru(1)-P(1)-Ru(2) = 78.26(5), Ru(1)-P(1)-Ru(3) = 78.51(5), Ru(2)-P(1)-Ru(3) = 75.96(5), Ru(1)-P(1)-C(10) = 121.83(17).

The ^1H NMR spectra of (*S*)-**2a** and (*R*)-**2b** both exhibit a doublet of doublets at δ -19.32 ($^2J_{\text{H-P}} = 14.8$ Hz) and a doublet at -19.30 ($^2J_{\text{H-P}} = 14.7$ Hz) ppm, respectively, which corresponds to the two bridging hydrides and indicates they are equivalent on the NMR timescale. Having demonstrated that both primary phosphines react with $[\text{Ru}_3(\text{CO})_{12}]$ to generate chiral phosphinidene-capped clusters, we wished to investigate whether a related structure could also be synthesised from a cluster containing a pre-bound diphosphine ligand. Thus, a solution of $[\text{Ru}_3(\text{CO})_{10}(\text{dpmm})]$ and one equivalent of (*S*)-**1a** or (*R*)-**1b** in toluene was heated for five hours to obtain the phosphido-capped, singly hydride-bridged clusters $[(\mu\text{-H})\text{Ru}_3(\mu_2\text{-PAr})(\text{CO})_8(\text{dpmm})]$ (*S*)-**3a**/*(R)*-**3b**, and the phosphinidene-capped doubly hydride-bridged clusters $[(\mu\text{-H})_2\text{Ru}_3(\mu_3\text{-PAr})(\text{CO})_7(\text{dpmm})]$ (*S*)-**4a**/*(R)*-**4b** (Scheme 2).

It was observed that (*S*)-**3a**/*(R)*-**3b** was initially formed, whereas further heating at elevated temperature gave (*S*)-**4a**/*(R)*-**4b**, suggesting that the former are slowly converted into the latter compounds. The clusters (*S*)-**3a**/*(R)*-**3b** and (*S*)-**4a**/*(R)*-**4b** have been characterized by IR and NMR spectroscopy as well as mass spectrometry, and the solid state structures of (*R*)-**3b**, (*S*)-**4a** and (*R*)-**4b** have been confirmed by single crystal X-ray diffraction.

Whilst the ^1H NMR spectrum of (*S*)-**3a** shows a doublet of doublet for the hydride at δ -11.61 ppm ($^2J_{\text{H-P}} = 37.3$ Hz); and a peak for the phosphorus-bound proton at 6.88 ppm ($^1J_{\text{H-P}} = 8.6$ Hz), that of (*R*)-**3b** gives an doublet of doublet for the bridging hydride at δ -11.59 ppm ($^2J_{\text{H-P}} = 32.7$ Hz); the peak for the phosphorus-bound proton appears at 6.84 ppm ($^1J_{\text{H-P}} = 8.5$ Hz). The ^{31}P NMR spectra of both (*S*)-**3a** and (*R*)-**3b** indicate three inequivalent, phosphorus-phosphorus coupled environments; the chemical shifts of the phosphorus atoms for the two structures: (*S*)-**3a** 177.54, 22.22, -114.18 ppm; (*R*)-**3b** 187.6, 21.39, -111.28 ppm.

It was possible to gain further insight into the molecular nature of (*R*)-**3b** from its solid state structure. The X-ray crystallographic analysis shows that the monohydride-bridged complex consists of a central triangle of ruthenium atoms, with Ru(2) and Ru(3) binding three terminal carbonyls each while Ru(1) binds only two (Fig. 2). The dpmm ligand bridges Ru(1) and Ru(2), while the Ru(1)-Ru(3) bond is bridged by both the hydride and the phosphide ligands. The Ru(1)-Ru(3) bond distance (2.9340(7) Å) is slightly elongated compared to the Ru(1)-Ru(2) and Ru(2)-Ru(3) bond distances (2.8450(8) and 2.8302(7) Å, respectively). H(2) is attached to P(1), and is oriented over the Ru_3 triangle - the binaphthyl unit points away, minimizing steric interactions with the dpmm ligand. In principle, structural isomers are possible. These would constitute *endo*- and *exo* isomers,¹² with the *exo* derivative being that observed in **3b**, i.e. where the R moiety of a bridging $\mu\text{-PRH}$ unit points away from the cluster core.

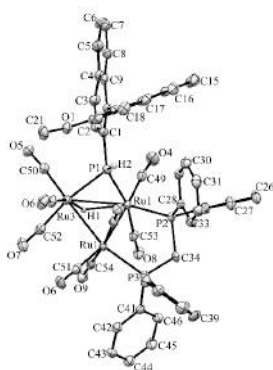


Fig. 2 $[(\mu\text{-H})_2\text{Ru}_3(\mu_3\text{-P}(\text{H}_2\text{-}2'\text{-methoxy-1,1'-binaphthyl}))(\text{CO})_2(\text{dpmp})]$ (**R**)-**3b** molecular structure with thermal ellipsoids drawn at 30% probability. Aryl hydrogens omitted for clarity. Selected bond lengths (Å) and angles (°): Ru(1)–Ru(2) = 2.8450(8), Ru(1)–Ru(3) = 2.9340(7), Ru(2)–Ru(3) = 2.8302(7), Ru(1)–P(1) = 2.367(2), Ru(1)–P(2) = 2.322(2), Ru(2)–P(3) = 2.3265(16), Ru(3)–P(1) = 2.344(2), C(1)–P(1) = 1.814(8); Ru(1)–Ru(2)–Ru(3) = 62.261(18), Ru(1)–Ru(3)–Ru(2) = 59.118(18), Ru(2)–Ru(1)–Ru(3) = 58.621(16), Ru(1)–P(1)–Ru(3) = 77.03(7), Ru(1)–P(1)–C(1) = 119.5(3), Ru(3)–P(1)–C(1) = 115.2(3); P(2)–C(34)–P(3) = 113.0(4).

The crystal structure of the phosphinidene dihydride complex (**S**)-**4a** shows that P(1) is bound to all three metals (Fig. 3). Ru(1) is also bound to three terminal carbonyls, whilst Ru(2) and Ru(3) are bound to two such ligands; P(3) and P(2) of the dpmp ligand bind to Ru(2) and Ru(3), respectively. There are two bridging hydride ligands whose occupancy is spread over the three Ru–Ru edges.

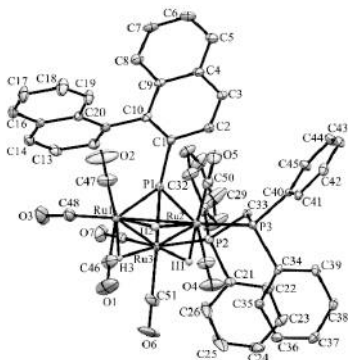


Fig. 3 $[(\mu\text{-H})_2\text{Ru}_3(\mu_3\text{-P}(\text{H}_2\text{-}1,1'\text{-binaphthyl}))(\text{CO})_2(\text{dpmp})]$ (**S**)-**4a** molecular structure with thermal ellipsoids drawn at 30% probability. Aryl hydrogens omitted for clarity. Selected bond lengths (Å) and angles (°): Ru(1)–Ru(2) = 2.8554(4), Ru(1)–Ru(3) = 2.9055(4), Ru(2)–Ru(3) = 2.9112(4), Ru(1)–P(1) = 2.2949(9), Ru(2)–P(1) = 2.3114(9), Ru(3)–P(1) = 2.3275(9), Ru(2)–P(3) = 2.3025(8), Ru(3)–P(2) = 2.3298(9); Ru(2)–Ru(1)–Ru(3) = 60.701(9), Ru(1)–Ru(2)–Ru(3) = 60.501(10), Ru(1)–Ru(3)–Ru(2) = 58.798(9), Ru(1)–P(1)–Ru(2) = 76.61(3), Ru(1)–P(1)–Ru(3) = 77.89(3), Ru(2)–P(1)–Ru(3) = 77.74(3), P(2)–C(33)–P(3) = 115.16(17).

The analogous complex (**R**)-**4b** is depicted in Fig. 4; in this case the two hydrogens could be unambiguously located using XHYDEX, where the two hydride ligands bridged Ru–Ru bonds are “long”; Ru(1)–Ru(3) = 2.9055(4) and Ru(2)–Ru(3) = 2.9112(4).

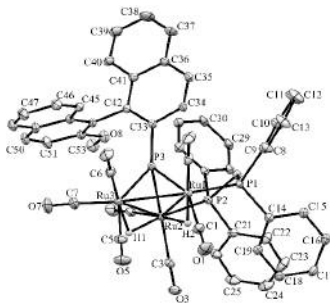


Fig. 4 $[(\mu\text{-H})_2\text{Ru}_3(\mu_3\text{-P}(\text{H}_2\text{-}1,1'\text{-binaphthyl}))(\text{CO})_2(\text{dpmp})]$ (**R**)-**4b** molecular structure with thermal ellipsoids drawn at 30% probability. Aryl hydrogens omitted for clarity. Selected bond lengths (Å) and angles (°): Ru(1)–Ru(2) = 2.9190(3), Ru(1)–Ru(3) = 2.8078(3), Ru(2)–Ru(3) = 2.9725(3), Ru(1)–P(3) = 2.3084(8), Ru(2)–P(3) = 2.3519(8), Ru(3)–P(3) = 2.3059(8), Ru(1)–P(1) = 2.3009(8), Ru(2)–P(2) = 2.3399(8), Ru(2)–Ru(1)–Ru(3) = 62.501(9), Ru(1)–Ru(2)–Ru(3) = 56.917(8), Ru(1)–Ru(3)–Ru(2) = 60.582(8), Ru(1)–P(3)–Ru(2) = 77.56(3), Ru(1)–P(3)–Ru(3) = 74.96(3), Ru(2)–P(3)–Ru(3) = 79.30(3), P(1)–C(20)–P(2) = 117.38(17).

NMR spectral analysis of (**S**)-**4a**/(**R**)-**4b** shows two analogous solution species; the ^1H NMR spectrum of both showing a doublet of triplets for the bridging hydrides, which couple more strongly to the phosphide nucleus and more weakly to the two phosphorus donors of the dpmp ligand ((**S**)-**4a**: $^2J_{\text{H-P}} = 13.7\text{ Hz}$, $^2J_{\text{H-P}} = 5.6\text{ Hz}$; (**R**)-**4b**: $^2J_{\text{H-P}} = 12.8\text{ Hz}$, $^2J_{\text{H-P}} = 5.6\text{ Hz}$) and a broad singlet at -18.57 and -18.46 ppm, respectively, indicating the presence of second fluxional isomer. Variable temperature ^1H NMR for both (**S**)-**4a** and (**R**)-**4b** shows that the fluxionality may be almost completely frozen out at 233 K to reveal the hydride signals of the isomers (Fig. 5). The low temperature spectra (*cf.* Fig. 5) show that in the case of (**S**)-**4a**, a resolved pair of hydride signals at -18.47 and -18.74 ppm belong to one isomer, while a second pair of hydride signal at -18.17 and -18.26 ppm are only partially resolved. The related low temperature spectrum of (**R**)-**4b** shows a similar behavior, but the low field pair of hydride signals are in this case better resolved. The observed behavior may be rationalized by the presence of two structural isomers for each cluster, where the structural difference lies in the location of the hydrides, as indirectly shown in the crystal structure of (**S**)-**4a** (Fig. 3). Location of the two hydrides on the two non-dpmp-bridged Ru–Ru edges provides one isomer. At room temperature, with rapid rotation around the phosphinidene-P-binaphthyl bond, the two hydrides are effectively chemically and magnetically equivalent, giving one multiplet (ddd) for both (**S**)-**4a** and (**R**)-**4b** due to coupling to the three phosphorus atoms. The other isomer is that detected in the crystal structure of (**R**)-**4b**, with two chemically and magnetically inequivalent hydrides. It may

be noted that it is the former isomer that appears to be favoured in solution for **4b**, while the latter is the one that is detected in the crystal structure. The ^{31}P NMR room temperature and low temperature spectra (233 K) for (*S*)-**4a** and (*R*)-**4b** are in agreement with the corresponding ^1H NMR spectra and the proposed isomers. At room temperature, one relatively broad signal is shown for the phosphinidene phosphorus atom with a shift at ~ 260 ppm for both clusters, and relatively complex partially resolved signals with an underlying broad signal are found for the dppm phosphorus resonances at ~ 26 ppm for both clusters. At low temperature, (*S*)-**4a** reveals two relatively broad phosphinidene resonances with shifts of 265 and 260 ppm (the former predominating) and two sets of dppm signals, one relatively sharp and the second consisting of two broad unresolved signals. For (*R*)-**4b**, the low temperature spectrum is similar, but the relative weights of the two phosphinidene signals are reversed, consistent with different isomers being favoured at low temperature for the two clusters. The resolved set of signals for the dppm ligand is complicated, probably because of different possible orientations of the methylene backbone in the frozen out, static structure(s) of the cluster.

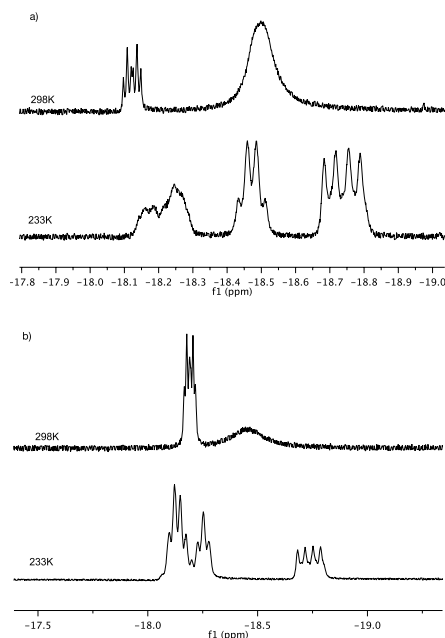


Fig. 5. Variable-temperature ^1H NMR spectra in the hydride region of clusters a) $[(\mu\text{-H})_2\text{Ru}_2(\mu_3\text{-P}(1,1'\text{-binaphthyl}))(\text{CO})_2(\text{dppm})]$ (*S*)-**4a** and b) $[(\mu\text{-H})_2\text{Ru}_2(\mu_3\text{-P}(1,1'\text{-binaphthyl}))(\text{CO})_2(\text{dppm})]$ (*R*)-**4b** recorded in the temperature range 298–233 K (top to bottom).

Considering that the bridging phosphido moieties of (*S*)-**3a**/(*R*)-**3b** could be converted into the corresponding phosphinidene units in (*S*)-**4a**/(*R*)-**4b**, we were curious to know whether an

initial primary phosphine-bound species could also be isolated. It was found that reaction of $[\text{Ru}_3(\text{CO})_{10}(\text{dppm})]$ with trimethylamine *N*-oxide in the presence of (*S*)-**1a** or (*R*)-**1b** did indeed yield the primary phosphine-substituted clusters $[\text{Ru}_3(\text{CO})_9(\text{dppm})(\text{PH}_2\text{Ar})]$ (*S*)-**5a**/(*R*)-**5b**, was indeed produced. Again, the anticipated 2:1 ratio of phosphorus peaks was evident for both compounds in their ^{31}P NMR spectra (*S*)-**5a**: 15.18 ppm (dppm), -78.25 ppm (RPH_2); (*R*)-**5b**: 14.43 ppm (dppm), -78.76 ppm (RPH_2). For both clusters, their ^1H NMR spectra show two broadened diagnostic doublets of doublets at 5.36 ($^1J_{\text{H-P}} = 358.0$ Hz) ppm and 4.94 ($^1J_{\text{H-P}} = 367.7$ Hz) ppm for (*S*)-**5a** and at 5.23 ($^1J_{\text{H-P}} = 360.4$ Hz) ppm and 5.12 ($^1J_{\text{H-P}} = 366.4$ Hz) ppm for (*R*)-**5b**, for the diastereotopic hydrogens, which remain bound to the phosphorus donor atom. When a toluene solution of (*S*)-**5a**/(*R*)-**5b** was heated, (*S*)-**3a**/(*R*)-**3b** and (*S*)-**4a**/(*R*)-**4b** were produced (Scheme 2), and thus we have now successfully characterised the initial bound primary phosphine, the intermediate phosphido-bridged mono-hydride cluster and the final phosphinidene-capped dihydride-bridged product.

Synthesis and characterisation of triosmium hydride clusters

Our next objective was to investigate the effect of changing the group eight metal to osmium. When a dichloromethane solution of the cluster $[\text{Os}_3(\text{CO})_{11}(\text{CH}_3\text{CN})]$ was reacted with (*S*)-**1a** or (*R*)-**1b** (1 eq.) at room temperature, the formation of one product was observed in each case after *ca.* 10 h (Scheme 3). After purification, yellow solids were isolated in good yield, and the products were characterized as the clusters **6a**/**6b**, with the primary phosphine bound to one of the osmium centres – no hydride transfer had occurred at this stage and the ^1H and ^{31}P NMR spectra were similar to those observed for the related clusters $[\text{Os}_3(\text{CO})_{11}(\text{RPH}_2)]$ ($\text{R} = \text{C}_6\text{H}_5$, $p\text{-CH}_3\text{OC}_6\text{H}_4$).¹³

The diastereotopic phosphorus-bound protons in both clusters appear as two doublets of doublets ((*S*)-**6a**: δ 6.01 $^1J_{\text{P-H}} = 383.6$ Hz, δ 5.41 $^1J_{\text{P-H}} = 393.6$ Hz, $^2J_{\text{H-H}} = 3.3$ Hz; (*R*)-**6b**: δ 5.90 $^1J_{\text{P-H}} = 386.2$ Hz, δ 5.80 $^1J_{\text{P-H}} = 391.0$ Hz, $^2J_{\text{H-H}} = 3.6$ Hz). As in the case for ruthenium, the possibility of generating phosphide- and phosphinidene-bridged clusters from **6a/b** was investigated. The phosphide-bridged complexes (*S*)-**7a** and (*R*)-**7b** were generated either by sequential deprotonation-protonation reactions (proceeding via the intermediate formation of $[(\text{Os}_3(\mu_2\text{-RPH})(\text{CO})_{10})^-]$ clusters^{13, 14} or by thermolysis in toluene (Scheme 3). The products were characterized as the edge-bridged phosphido clusters on the basis of their IR, ^1H and ^{31}P NMR and mass spectra, which were similar to those observed for the clusters $[(\mu\text{-H})\text{Os}_3(\mu_2\text{-RPH})(\text{CO})_{10}]$ ($\text{R} = \text{C}_6\text{H}_5$, $p\text{-CH}_3\text{OC}_6\text{H}_4$).¹³ The ^{31}P NMR spectra of our new clusters each showed a downfield resonance ((*S*)-**7a**: $\delta = -51.3$ ppm; (*R*)-**7b**: $\delta = -52.2$ ppm) compared to (*S*)-**6a** and (*R*)-**6b**. The ^1H NMR spectra for these clusters are as expected, indicating that there is only one isomer in solution (either the *endo* or *exo* derivative; *vide supra*). The phosphorus-bound hydrogen resonance in the ^1H NMR spectra appears as a doublet of doublets with $^1J_{\text{H-P}} = 438.4$ Hz and $^3J_{\text{H-H}} = 4.2$ Hz for (*S*)-**7a** and $^1J_{\text{H-P}} = 437.7$ Hz

and $^3J_{\text{H-H}} = 4.2$ Hz for (*R*)-**7b**. The bridging hydride resonance appears as a doublet of doublets ((*S*)-**7a**: $\delta = -19.31$ ppm, $^2J_{\text{P-H}} = 18.4$ Hz, $^3J_{\text{H-H}} = 4.0$ Hz; (*R*)-**7b**: $\delta = -19.32$ ppm, $^2J_{\text{P-H}} = 18.2$ Hz, $^3J_{\text{H-H}} = 4.2$ Hz). The corresponding thermolysis reaction (in refluxing dibutylether) of the primary phosphine-bound osmium clusters **6a/6b** did not give any phosphinidene derivatives, however these could be obtained by reacting the edge-bridged phosphido clusters (*S*)-**7a** and (*R*)-**7b** with 1 eq. of trimethylamine *N*-oxide at room temperature (Scheme 3). The products were characterized as the phosphinidene-capped bridging dihydride clusters (*S*)-**8a** and (*R*)-**8b** on the basis of their IR and NMR spectra, which were similar to those observed for $[(\mu_2\text{-H})_2\text{Os}_3(\mu_3\text{-PPh})(\text{CO})_9]^{13}$. The ^{31}P NMR spectra of these phosphinidene-capped clusters show significant downfield shifts ((*S*)-**8a**: $\delta = 110.1$ ppm; (*R*)-**8b**: $\delta = 111.5$ ppm) compared with the terminally bonded phosphine clusters (*S*)-**6a** and (*R*)-**6b**, and the edge-bridged phosphido derivatives (*S*)-**7a** and (*R*)-**7b** (but not to the extent of the related ruthenium phosphinidenes (*S*)-**2a** and (*R*)-**2b**). The ^1H NMR spectra for the bridging hydrides of **8a/b** appear as two doublets ((*S*)-**8a**: $\delta = -18.29$ ppm, $^2J_{\text{H-P}} = 4.2$, -19.33 ppm, $^2J_{\text{H-P}} = 4.2$; (*R*)-**8b**: $\delta = -18.29$ ppm, $^2J_{\text{H-P}} = 10.6$ Hz, -18.240 ppm, $^2J_{\text{H-P}} = 10.6$ Hz).

Synthesis of tetraruthenium hydride clusters

The reactions of the primary **1a/1b** with $[\text{H}_4\text{Ru}_4(\text{CO})_{12}]$ were made using published methods,⁴ i.e. either thermal substitution under elevated hydrogen pressure (30 bar), or via oxidative decarbonylation using trimethylamine *N*-oxide at room temperature. As for the aforementioned triruthenium clusters - the latter method was found to be superior with respect to both yield and selectivity of the product formation, giving $[(\mu\text{-H})_4\text{Ru}_4(\text{CO})_{11}(\mathbf{1a})]$ (*S*)-**9a**, and $[(\mu\text{-H})_4\text{Ru}_4(\text{CO})_{11}(\mathbf{1b})]$ (*S*)-**9b**, as red-orange solids. Their IR spectra were similar to $[(\mu\text{-H})_4\text{Ru}_4(\text{CO})_{11}(\text{L})]$ (L = PMe_2Ph)¹⁴ and $[(\mu\text{-H})_4\text{Ru}_4(\text{CO})_{11}(\text{NMDPP})]$ (NMDPP = (*S*)-(+)-neomenthylidiphenylphosphine).¹⁵ The ^1H NMR spectra of (*S*)-**9a**/(*R*)-**9b** exhibits doublets at $\delta -17.71$ ($^2J_{\text{H-P}} = 6.0$ Hz) and -17.67 ($^2J_{\text{H-P}} = 4.6$ Hz) ppm, respectively, while the ^{31}P NMR spectra for (*S*)-**9a**/(*R*)-**9b** show shifts at $\delta -79.5$ ppm and -80.8 ppm, respectively. It was found that the tetranuclear parent cluster $[(\mu\text{-H})_4\text{Ru}_4(\text{CO})_{12}]$ could also be used as an alternative starting material for the preparation of $[(\mu\text{-H})_2\text{Ru}_3(\mu_3\text{-PAr})(\text{CO})_9]$, (*S*)-**2a**/(*R*)-**2b** under high pressure. An equimolar amount of the primary phosphines (*S*)-**1a**/(*R*)-**1b** were reacted in an autoclave with the parent cluster $[\text{H}_4\text{Ru}_4(\text{CO})_{12}]$ in 5 mL of benzene, under 30 bar of hydrogen to give the phosphinidene clusters (*S*)-**2a**/(*R*)-**2b**. The products were purified as described earlier, and a sample of (*R*)-**2b** suitable for X-ray crystallographic analysis was obtained by recrystallization from dichloromethane/hexane. The structure of (*R*)-**2b** is shown in Fig. 6 and selected bond distances and angles are listed in the caption.

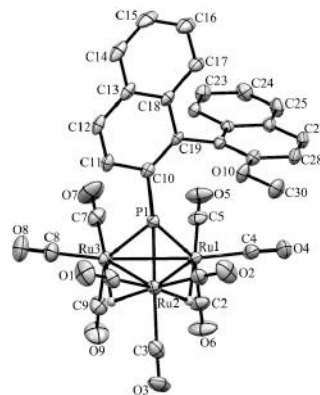
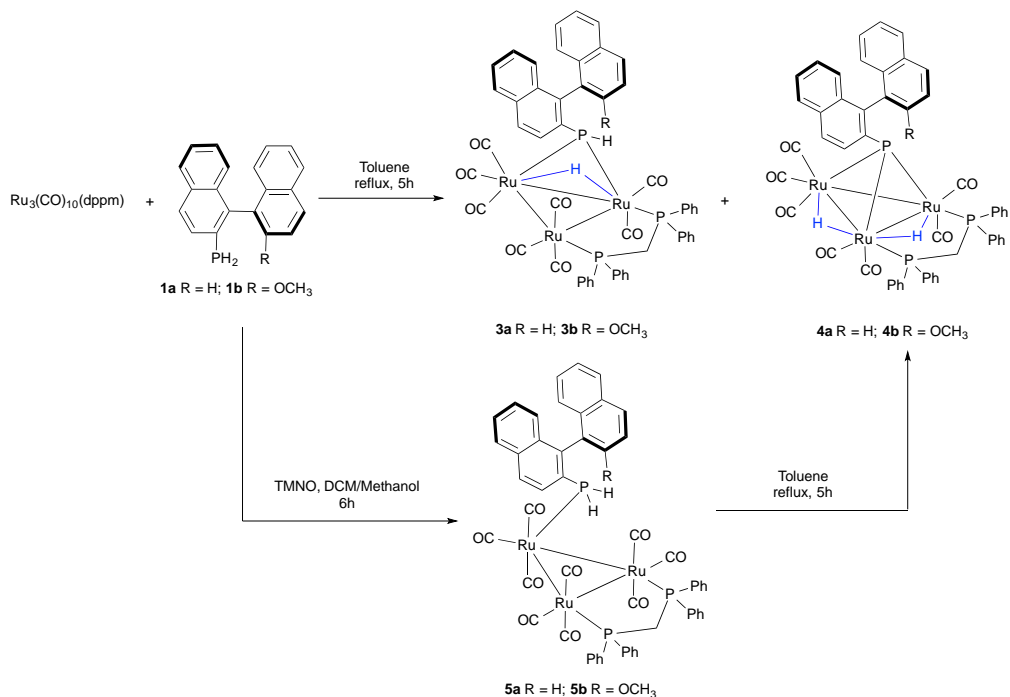


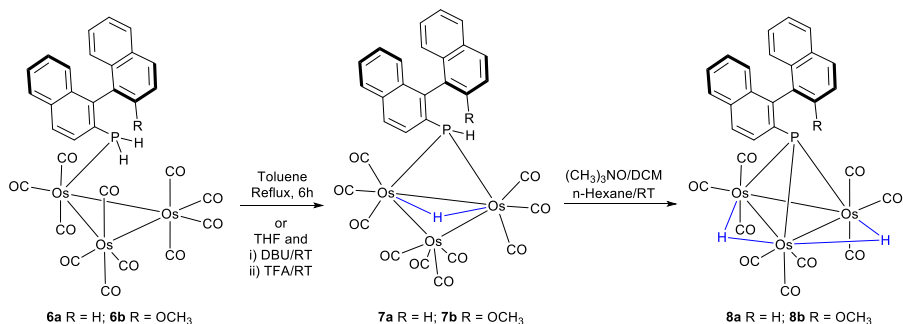
Fig. 6 Molecular structure of $[(\mu\text{-H})_2\text{Ru}_3(\mu_3\text{-P(2'-methoxy-1,1'-binaphthyl))}](\text{CO})_9]$, **2b** with thermal ellipsoids are drawn at 50% probability level. All aryl hydrogen atoms have been omitted for clarity. Selected bond lengths (Å) and angles (°): Ru(1)–Ru(2) = 2.9074(5), Ru(1)–Ru(3) = 2.8195(5), Ru(2)–Ru(3) = 2.9415(5), Ru(1)–P(1) = 2.2923(12), Ru(2)–P(1) = 2.3425(12), Ru(3)–P(1) = 2.2807(13), P(1)–C(10) = 1.807(5); Ru(2)–Ru(1)–Ru(3) = 61.790(13), Ru(1)–Ru(2)–Ru(3) = 57.636(13), Ru(1)–Ru(3)–Ru(2) = 60.574(13), Ru(1)–P(1)–Ru(2) = 77.69(4), Ru(1)–P(1)–Ru(3) = 76.13(4), Ru(2)–P(1)–Ru(3) = 79.01(4), Ru(1)–P(1)–C(10) = 129.20(15).

As for (*S*)-**2a**, the three metal atoms are capped by the phosphorus atom to give a distorted tetrahedral core. The Ru(1)–Ru(2) and Ru(1)–Ru(3) bond lengths of 2.9074 (5) and 2.8195 (5) Å respectively are significantly shorter than the Ru(2)–Ru(3) distance of 2.9415 (5) Å. The hydridic H atoms were not located directly, but in view of the relatively long Ru(1)–Ru(2) and *Ru(2)–Ru(3) bond lengths* and the bent equatorial carbonyls, we assign the hydrides as bridging these edges. The three Ru atoms are each coordinated by three terminal carbonyl groups, and the Ru–P bond lengths in (*R*)-**2b** are also similar to those observed for the phosphinidene cluster $[(\mu\text{-H})_2\text{Ru}_3(\text{PPh})(\text{CO})_9]^{17}$ but are again notably asymmetric,⁷ as for (*S*)-**2a**: Ru(1)–P(1) = 2.2923(12), Ru(2)–P(1) = 2.3425(12) and Ru(3)–P(1) = 2.2807(13) Å.

ARTICLE



Scheme 2 Synthesis of $[(\mu\text{-H})\text{Ru}_3(\mu_2\text{-PAr})(\text{CO})_8(\text{dppm})]$ (*S*)-**3a**/*(R)*-**3b**, $[(\mu\text{-H})_2\text{Ru}_3(\mu_3\text{-PAr})(\text{CO})_7(\text{dppm})]$ (*S*)-**4a**/*(R)*-**4b** and $[\text{Ru}_3(\text{dppm})(\text{CO})_9(\text{PH}_2\text{Ar})]$ (*S*)-**5a**/*(R)*-**5b**.

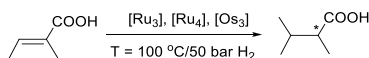


Scheme 3 Synthesis of the clusters $[(\mu\text{-H})\text{Os}_3(\mu_2\text{-PAr})(\text{CO})_{10}]$ (*S*)-**7a**/*(R)*-**7b** and $[(\mu\text{-H})_2\text{Os}_3(\mu_3\text{-PAr})(\text{CO})_9]$ (*S*)-**8a**/*(R)*-**8b** from $[\text{Os}_3(\text{CO})_{10}(\text{ArPH}_2)]$ (*S*)-**6a**/*(R)*-**6b**.

ARTICLE

Asymmetric Catalysis

Having demonstrated hydrogen transfer from the chiral primary phosphine to the metal clusters, we wished to investigate whether our compounds could be used to effect asymmetric hydrogenation of prochiral substrates. In contrast to the high pressures of hydrogen (130 bar) and temperature (100 – 120 °C) which are commonly used in the catalytic reduction of α -unsaturated carboxylic acids,¹⁶ we have shown previously,^{2, 4} that a relatively low temperature (100 °C) and pressure (50 bar) enhances the chiral induction of tiglic acid with high conversion (Scheme 4). In these earlier investigations it was found that at higher temperatures, severe decomposition of the clusters was observed, together with the formation of a considerable amount of organic side-products (cyclohexene and cyclohexene). By contrast, when lower temperatures were used, all reactions remained homogeneous and the aforementioned hydrogenation products of toluene were not detected, although in order to obtain reasonable conversions, a temperature of 100 °C and longer reaction times of 24–72 h were required.



Scheme 4 Catalytic hydrogenation of tiglic acid by Ru_3 , Ru_4 and Os_3 clusters.

Table 1. A summary of the catalytic asymmetric hydrogenation experiments using clusters **2a/b**, **4a/b**, **7a/b**, **8a/b** and **9a/b** as catalysts.^a

Entry	Catalyst/mg	Conversion (%)	ee (%)
1	(S)- 2a /10	7	-
2	(R)- 2b /10	18	1 (R)
3	(S)- 4a /5	78	-
4	(R)- 4b /5	84	-
5	(S)- 7a /5	0	-
6	(R)- 7b /5	0	-
7	(S)- 8a /5	9	-
8	(S)- 8a /5 ^b	92	-
9	(R)- 8b /5	70	-
10	(R)- 8b /5 ^b	90	-
11	(S)- 9a /10	77	7 (R)
12	(S)- 9a /10 ^c	94	7 (R)
12	(S)- 9a /10 ^b	99	7 (R)
13	(R)- 9b /10	99	19 (R)

^a Conditions: $P(\text{H}_2)$ = 50 bar; T = 100 °C; time = 24h; solvent = EtOH-toluene 1:1 (5 mL); conversion based on ^1H NMR spectroscopy. ^b time = 72h; ^c time = 48h.

An examination of Table 1 shows that both the ruthenium and osmium clusters are capable of effecting the hydrogenation. Relatively high to excellent catalytic conversions were observed for the clusters (S)-**4a**/(R)-**4b**, (R)-**8b** and (S)-**9a**/(R)-**9b**, after 24h; cluster (S)-**8a** gave 92% conversion after 72h. The 2'-methoxy derivatives (the 'b' series of clusters described

here) generally effect faster reductions than their 2'-hydrogen counterparts (Table 1). Whilst low (or no) enantioselectivity was generated by the majority of the clusters, (R)-**9b** did afford an ee of 19%, which is, to the best of our knowledge, the first example of an asymmetric hydrogenation induced by a chiral primary phosphine. After the catalysis was complete, we analyzed the mixtures by IR and NMR spectroscopy, in order to establish the fate of the catalyst (catalyst precursor). For (S)-**9a** and (R)-**9b**, we detected (S)-**2a** and (R)-**2b**, respectively, at the end of the catalytic cycles, indicating their conversion to the arylphosphinidene-capped species. These observations do suggest that both clusters (S)-**9a** and (R)-**9b** undergo fragmentation however, during the course of the reaction. The different catalytic behaviour in terms of both conversion and enantioselectivity between (S)-**9a**/(R)-**9b** and (S)-**2a**/(R)-**2b** (see Table 1, entry 1 versus entry 11 and entry 2 versus entry 13) indicates that (S)-**2a** and (R)-**2b** are unlikely to be the active species. In order to assess whether our results are reproducible, fresh samples of (S)-**2a**, (R)-**2b**, (S)-**9a** and (R)-**9b** were used for catalytic hydrogenation under the same conditions in repeat experiments - identical conversion rates and enantioselectivities were obtained for the four catalytic runs (corresponding to entries 1, 2, 11 and 13, Table 1). Our future endeavors will focus on mechanistic studies of the cluster-catalysed asymmetric hydrogenation, in order to probe the possibility of raising the enantioselectivity by ligand design.

Conclusions

We have demonstrated that the chiral primary phosphines (S)-**1a**/(R)-**1b** react with tri- and tetra-ruthenium and triosmium cores to give the characterisable and enantiopure phosphinidene-capped, phosphido and phosphine clusters $[(\mu\text{-H})_2\text{Ru}_3(\mu_3\text{-PAr})(\text{CO})_9]$ **2a/2b**, $[(\mu\text{-H})\text{Ru}_3(\mu_2\text{-PAr})(\text{CO})_8(\text{dpmm})]$ **3a/3b**, $[(\mu\text{-H})_2\text{Ru}_3(\mu_3\text{-PAr})(\text{CO})_7(\text{dpmm})]$ **4a/4b**, $[\text{Ru}_3(\text{CO})_9(\text{dpmm})(\text{PH}_2\text{Ar})]$ **5a/5b**, $[\text{Os}_3(\text{CO})_{11}(\text{ArPH}_2)]$ **6a/6b**, $[(\mu\text{-H})\text{Os}_3(\mu_2\text{-PAr})(\text{CO})_{10}]$ **7a/7b**, $[(\mu\text{-H}_2)_2\text{Os}_3(\mu_3\text{-PAr})(\text{CO})_9]$ **8a/8b** and $[(\mu\text{-H})_4\text{Ru}_4(\text{CO})_{11}(\text{ArPH}_2)]$ **9a/9b**. The ability of these clusters to catalyse the asymmetric hydrogenation of tiglic acid was then examined, where (R)-**9b** capable of achieving a conversion of 99% and an enantioselectivity of 19%.

Experimental

General remarks

All synthetic procedures were performed under dry nitrogen by using standard Schlenk and vacuum-line techniques. The parent

osmium cluster $[\text{Os}_5(\text{CO})_{11}(\text{CH}_3\text{CN})]$ and ruthenium cluster $[\text{Ru}_3(\text{CO})_{10}(\text{dppm})]$ were synthesized according to literature methods.^{17, 18} Solvents were dried by distillation over appropriate drying agents and stored over molecular sieves under nitrogen. Thin layer chromatography was used to separate the products by using commercial 20×20 cm plates coated with Merck Kieselgel 60, 0.25 mm thickness. All chemicals were purchased from Sigma Aldrich and used as received. NMR spectra were recorded on a Varian Inova 500 MHz spectrometer at 25°C. All ^1H NMR spectra were referenced to solvent signals ($\text{CDCl}_3 = 7.25$ ppm) while the ^{31}P NMR spectra were referenced to external 85% H_3PO_4 (0 ppm). IR spectra were recorded on a Nicolet Avatar 360 FT-IR instrument using sealed (0.1 mm) NaCl cells. Mass spectrometric data were obtained by using electrospray ionization (ESI) and high resolution mass spectra (Waters Micromass Q-TOF micro mass spectrometer). Catalytic reactions were carried out using a Berghof BR-25 high pressure laboratory reactor. Abbreviations used are s (singlet), d (doublet), t (triplet), m (multiplet), dd (doublet of doublets), td (triplet of doublets), ddd (doublet of doublet of doublets), br (broad) for ^1H NMR and s (strong), m (medium) and w (weak) for IR.

Synthetic Procedures

Synthesis of triruthenium clusters

Preparation of $[(\mu\text{-H})_2\text{Ru}_3(\mu_3\text{-PAr})(\text{CO})_9]$ **2**, via thermal reaction

A solution of $[\text{Ru}_3(\text{CO})_{12}]$ (100 mg, 0.156 mmol) and one equivalent of **1** ((S)-**1a**: 45 mg, 0.157 mmol; (R)-**1b**: 50 mg, 0.158 mmol) in toluene (20 mL) was heated to reflux in a 2-neck round-bottomed flask fitted with a reflux condenser, under an inert atmosphere. After 30 min, the reaction was stopped, the solvent removed *in vacuo* and the residue subjected to thin layer chromatography using a dichloromethane-hexane (3:7) mixture as eluent. The first yellow band was identified as the known compound $[\text{Ru}_4(\mu\text{-H})_4(\text{CO})_{12}]$, followed by a yellow band for **2** as the major product. (S)-**2a**: 40 mg (30%); IR [$\nu(\text{CO})$, cyclohexane, cm^{-1}]: 2101(w), 2079(m), 2057(s), 2047(vs), 2023(w), 2014(s), 1998(w), 1985(w); ^1H NMR (500 MHz, CDCl_3 , 25 °C): δ 8.11 (dd, $J = 12.6, 8.7$ Hz, 1H), 7.88 (m, 4H), 7.51 (m, 1H), 7.43 (ddd, $J = 8.1, 7.4, 4.1$ Hz, 2H), 7.37 (ddd, $J = 8.2, 4.7, 3.3$ Hz, 1H), 7.17 (m, 2H), 6.9 (d, $J = 8.6$ Hz, 1H), -19.32 (dd, $J = 14.8, 1.0$ Hz, 2H); ^{31}P NMR (202 MHz, CDCl_3 , 25 °C): δ 261.46 (br); HRMS (ESI) $m/z = 838$ ($\text{M}+\text{Na}^+$). (R)-**2b**: 39 mg (29%); IR [$\nu(\text{CO})$, cyclohexane, cm^{-1}]: 2101(w), 2079(s), 2048(vs), 2042(m), 2027(w), 2015(s), 2003(w), 1984(w); ^1H NMR (CDCl_3 , 25 °C): δ 8.07 (dd, $J = 12.4, 8.8$ Hz, 1H), 7.96 (d, $J = 8.9$ Hz, 1H), 7.86 (dd, $J = 17.3, 8.3$ Hz, 2H), 7.77 (d, $J = 8.1$ Hz, 1H), 7.44 (t, $J = 7.4$ Hz, 1H), 7.34 (d, $J = 9.0$ Hz, 1H), 7.16 (d, $J = 7.1$ Hz, 1H), 7.08 (dd 'r', $J = 7.6$ Hz, 1H), 6.92 (dd, $J = 22.4, 8.4$ Hz, 2H), 3.64 (s, 3H), -19.30 (d, $J = 14.7$ Hz, 2H); ^{31}P NMR (202 MHz, CDCl_3 , 25 °C): δ 263.2 (t, $J = 13.6$ Hz); HRMS (ESI) $m/z = 868$ ($\text{M}+\text{Na}^+$). Red crystals of (S)-**2a** were obtained by slow evaporation of a dichloromethane-hexane solution.

$[(\mu\text{-H})_2\text{Ru}_3(\mu_3\text{-PAr})(\text{CO})_9]$ **2**, via diphenylketyl radical ($\text{Ph}_2\text{C}_2\text{O}^\bullet$)

To a solution of $[\text{Ru}_3(\text{CO})_{12}]$ (50 mg, 0.078 mmol) and one equivalent of **1** ((S)-**1a**: 23 mg, 0.08 mmol; (R)-**1b**: 25 mg, 0.08 mmol) in dichloromethane (20 mL), was added dropwise 1.2 equivalents of diphenylketyl radical, $\text{Ph}_2\text{C}_2\text{O}^\bullet$, under an inert atmosphere. After 30 min, the reaction was stopped, the solvent removed *in vacuo* and the residue subjected to thin layer chromatography using a dichloromethane-hexane (3:7) mixture as eluent. The first yellow band was identified as **2** ((S)-**2a**: 24.5 mg, 37%; (R)-**2b**: 23.8 mg, 35%).

Preparation of $[(\mu\text{-H})_2\text{Ru}_3(\mu_3\text{-PAr})(\text{CO})_9]$ **2**, via thermal ligand substitution at high pressure

A mixture of $[(\mu\text{-H})_4\text{Ru}_4(\text{CO})_{12}]$ (30 mg, 0.04 mmol) and one equivalent of **1** (S)-**1a**: 13 mg, 0.045 mmol; (R)-**1b**: 14 mg, 0.045 mmol) were dissolved in 5 mL of benzene and the solution was injected inside a small autoclave (45 mL). The autoclave was sealed and purged three times with 10 bar of H_2 before being pressurized with total of 30 bar H_2 . After 4 h at 125 °C the autoclave was cooled to room temperature. The gases were carefully released and the autoclave was opened. The isolation/purification and identification of the products were identical to that described above. Yields: **2** ((S)-**2a**: 12 mg, 35%; (R)-**2b**: 15 mg, 42%).

$[(\mu\text{-H})\text{Ru}_3(\mu_3\text{-PAr})(\text{CO})_8(\text{dppm})]$ **3** and $[(\mu\text{-H})_2\text{Ru}_3(\mu_3\text{-PAr})(\text{CO})_7(\text{dppm})]$ **4**

A solution of $[\text{Ru}_3(\text{CO})_{10}(\text{dppm})]$ (100 mg, 0.103 mmol) and one equivalent of the phosphine **1** ((S)-**1a**: 30 mg, 0.105 mmol; (R)-**1b**: 33 mg, 0.104 mmol) in toluene (20 mL) was heated to reflux in a 2-neck round-bottomed flask fitted with a reflux condenser, under an inert atmosphere. After 5 h, the reaction was stopped, the solvent was removed *in vacuo* and the residue subjected to thin layer chromatography using a dichloromethane-hexane (3:7) mixture as eluent to give the two major products, **3** and **4**. (S)-**3a**: 14 mg (11%); IR [$\nu(\text{CO})$, cyclohexane, cm^{-1}]: 2081(w), 2061(m), 2011(w), 1996 (vs), 1982 (vs), 1957 (w), 1945 (m); ^1H NMR (500 MHz, CDCl_3 , 25 °C): δ 8.52 (d, $J = 9.6$ Hz, 1H), 7.94 (m, 6H), 7.59 (m, 2H), 7.38 (m, 10H), 7.15 (m, 3H), 6.88 (d, $J_{\text{P-H}} = 8.6$ Hz, 1H), 3.43 (m, 2H), -11.61 (dd, $J = 37.3, 11.3$ Hz, 1H); ^{31}P NMR (202 MHz, CDCl_3 , 25 °C): δ 177.54 (br, s), 22.22 (dd, $J = 229.9, 117.5$ Hz), -114.18 (m); HRMS (ESI) $m/z = 1222$ ($\text{M}+\text{Na}^+$). (R)-**3b**: 33 mg (27%); IR [$\nu(\text{CO})$, cyclohexane, cm^{-1}]: 2081(m), 2057(w), 2022(w), 2011 (vs), 2001(vs), 1982(w), 1959(m), 1940(w); ^1H NMR (CDCl_3 , 25 °C): δ 8.56 (d, $J = 9.2$ Hz, 1H), 8.04 (d, $J = 9.0$ Hz, 1H), 7.87 (m, 7H), 7.39 (m, 12H), 7.13 (m, 2H), 6.92 (dd 'r', $J = 10.0$ Hz, 1H), 6.84 (d, $J_{\text{P-H}} = 8.5$ Hz, 1H), 3.66 (d, $J = 7.7$ Hz, 3H), 3.44 (m, 2H), -11.59 (dd, $J_{\text{P-H}} = 32.7, J_{\text{H-H}} = 10.8$ Hz, 1H); ^{31}P NMR (202 MHz, CDCl_3 , 25 °C): δ 187.6 (br, s), 21.39 (td, $J = 116.9, 115.6, 86.0$ Hz), -111.28 (m); HRMS (ESI) $m/z = 1231$ ($\text{M}+\text{H}^+$). (S)-**4a**: 18 mg (14%); IR [$\nu(\text{CO})$, cyclohexane, cm^{-1}]: 2084(w), 2059(m), 2032(m), 2022(w), 1999(vs), 1991(s), 1950(w), 1935(w); ^1H NMR (500 MHz, CDCl_3 , 25 °C): δ 8.37 (dd, $J = 12.1, 8.7$ Hz, 1H), 7.83 (ddd, $J = 26.7, 17.4, 8.4$ Hz, 53H), 7.70 (dd, $J = 15.7, 7.6$ Hz, 44H), 7.55 (m, 61H), 7.41 (m, 18H), 7.35 (ddd, $J = 12.3, 7.1, 3.9$ Hz, 19H), 7.28 (d, $J = 7.7$ Hz, 19H), 7.05 (m, 222H), 6.74 (m, 71H), 6.58 (d, $J = 6.7$ Hz, 12H), -

18.20 (dt, $J = 13.7$, 5.6 Hz, 2H), -18.57 (br); VT- ^1H NMR (500 MHz, CDCl_3 , 233K, hydride resonance) δ -18.17 (d, $J = 14.2$ Hz, 1H), -18.26 (d, $J = 11.4$ Hz, 1H), -18.47 (q, $J = 13.2$ Hz, 1H), -18.74 (dd, $J = 36.0$, 16.8 Hz, 1H). ^{31}P NMR (202 MHz, CDCl_3 , 25 °C): δ 263.67 (br, s), 26.22 (m); VT- ^{31}P NMR (202 MHz, CDCl_3 , 233K) δ 265.02 (m), 259.89 (m), 26.3 (br), 26.10 (m), 22.98 (br). HRMS (ESI) $m/z = 1174$ (M+2H) $^+$. (R)-**4b**: 32 mg (26%); IR [$\nu(\text{CO})$, cyclohexane, cm^{-1}]; 2084(m), 2057(s), 2031(m), 2022(w), 2012(w), 1998(vs), 1989 (vs), 1951(w), 1935(w); ^1H NMR (CDCl_3 , 25 °C): δ 8.31 (dd, $J = 12.1$, 8.7 Hz, 1H), 7.92 (d, $J = 9.1$ Hz, 1H), 7.79 (m, 9H), 7.50 (dd, $J = 24.3$, 13.6 Hz, 6H), 7.35 (m, 9H), 7.25 (dd, $J = 16.3$, 7.3 Hz, 4H), 7.00 (m, 44H), 3.68 (s, 4H), 3.35 (s, 3H), -18.19 (dt, $J = 12.8$, 5.6 Hz, 2H), -18.46 (br); VT- ^1H NMR (500 MHz, CDCl_3 , hydride resonance) δ -18.14 (q, $J = 13.1$ Hz, 2H), -18.25 (t, $J = 13.3$ Hz, 1H), -18.73 (dd, $J = 35.3$, 17.1 Hz, 1H). ^{31}P NMR (202 MHz, CDCl_3) δ 256.81 (m), 27.11 (m); VT- ^{31}P NMR (202 MHz, CDCl_3 , 233K) δ 297.66 (t, $J = 139.3$ Hz), 256.62 (m), 26.34 (m), 24.40 (d, $J = 56.9$ Hz), 22.21 (br); HRMS (ESI) $m/z = 1225$ (M+Na) $^+$. Red crystals of (R)-**3b**, (S)-**4a** and (R)-**4b** were obtained by slow evaporation of a dichloromethane-hexane solution.

Preparation of $[\text{Ru}_3(\text{CO})_9(\text{dppm})(\text{Ph}_2\text{Ar})]$ 5

A solution of TMNO (9 mg, 0.12 mmol) in 5 mL dichloromethane/methanol (1:1) was added dropwise, to a stirred solution of $[\text{Ru}_3(\text{CO})_{10}(\text{dppm})]$ (100 mg, 0.103 mmol) and one equivalent of the phosphine **1** ((S)-**1a**: 30 mg, 0.105 mmol, (R)-**1b**: 33 mg, 0.104 mmol) in dichloromethane (20 mL) under an inert atmosphere. The reaction mixture was stirred at room temperature for 6 h, filtered through silica, and the solvent removed *in vacuo* to give a red solid. (S)-**5a**: 98 mg (77%); IR [$\nu(\text{CO})$, cyclohexane, cm^{-1}]; 2056(w), 1996(vs), 1981(vs), 1944(w); ^1H NMR (500MHz, CDCl_3 , 25 °C): δ 8.01 (d, $J = 8.3$ Hz, 1H), 7.75 (dd, $J = 12.6$, 8.6 Hz, 1H), 7.67 (dd, $J = 8.3$, 6.9 Hz, 1H), 7.50 (m, 2H), 7.32 (m, 24H), 7.16 (dd 'r', $J = 8.2$ Hz, 3H), 5.36 (dd, $^1J_{\text{P-H}} = 358.0$ Hz, $^2J_{\text{H-H}} = 4.4$ Hz, 1H), 4.94 (dd, $^1J_{\text{P-H}} = 367.7$, $^2J_{\text{H-H}} = 4.3$ Hz, 1H), 4.09 (t, $J = 10.2$ Hz, 2H); ^{31}P NMR (202 MHz, CDCl_3 , 25 °C): δ 15.18 (m), -78.25 (d, $J = 23.6$ Hz); HRMS (ESI) $m/z = 1227$ (M+H) $^+$. (R)-**5b**: 97 mg (75%); IR [$\nu(\text{CO})$, cyclohexane, cm^{-1}]; 2061(w), 1996(vs), 1982(vs), 1945(w); ^1H NMR (CDCl_3 , 25 °C): δ 7.95 (m, 2H), 7.84 (m, 1H), 7.83 (m, 2H), 7.40 (m, 2H), 7.25 (m, 22H), 7.15 (m, 2H), 7.06 (d, $J = 8.5$ Hz, 2H), 6.85 (d, $J = 8.5$ Hz, 1H), 5.23 (dd, $^1J_{\text{P-H}} = 360.4$ Hz, $^2J_{\text{H-H}} = 4.3$ Hz, 1H), 5.12 (dd, $^1J_{\text{P-H}} = 366.4$ Hz, $^2J_{\text{H-H}} = 4.0$ Hz, 1H), 4.08 (t, $J = 10.2$ Hz, 1H), 3.71 (s, 3H). ^{31}P NMR (202 MHz, CDCl_3 , 25 °C): δ 14.43 (m), -78.76 (d, $J = 25.2$ Hz); HRMS (ESI) $m/z = 1258$ (M+H) $^+$.

Thermolysis of $[\text{Ru}_3(\text{Ph}_2\text{Ar})(\text{dppm})(\text{CO})_9]$ 5

A solution of **5** (50 mg, 0.04 mmol) in toluene (10 mL) was heated to reflux for 5 h under an inert atmosphere, then allowed to cool and the solvent removed *in vacuo*. Thin layer chromatography using silica-gel coated glass plates and a mixture of dichloromethane-petroleum ether (1:2) as eluent gave **3** ((S)-**3a**: 11 mg, 22%; (R)-**3b**: 12 mg, 23.5%) and **4** ((S)-**4a**: 24 mg, 46%; (R)-**4b**: 24 mg, 46%).

Synthesis of triosmium clusters

Preparation of $[\text{Os}_3(\text{CO})_{11}(\text{Ph}_2\text{Ar})]$ 6

A solution of $[\text{Os}_3(\text{CO})_{11}(\text{CH}_3\text{CN})]$ in dichloromethane (70 mg, 0.075 mmol) was stirred for 1 h, then one equivalent of **1** ((S)-**1a**: 20 mg, 0.07 mmol; (R)-**1b**: 22 mg, 0.07 mmol) also in dichloromethane was then added dropwise. After 10 h, the stirring was stopped, the solvent removed *in vacuo* and the residue subjected to thin layer chromatography using dichloromethane-petroleum ether (1:4) mixture as eluent, to give **6** as the one major product. (S)-**6a**: 54 mg (61%); IR [$\nu(\text{CO})$, cyclohexane, cm^{-1}]; 2110(m), 2056(vs), 2036(s), 2020(vs), 2002(m), 1990(s), 1978(m); ^1H NMR (500 MHz, CDCl_3 , 25 °C): δ 8.04 (dd, $J = 8.5$, 1.9 Hz, 1H), 7.98 (d, $J = 8.3$ Hz, 1H), 7.92 (d, $J = 8.2$ Hz, 1H), 7.89 (d, $J = 8.2$ Hz, 1H), 7.62 (m, 2H), 7.46 (m, 3H), 7.25 (apt, 2H), 7.12 (m, 1H), 7.21 (dd, $^1J_{\text{P-H}} = 383.6$ Hz, $^2J_{\text{H-H}} = 3.3$ Hz, 1H), 5.41 (dd, $^1J_{\text{P-H}} = 393.6$ Hz, $^2J_{\text{H-H}} = 3.3$ Hz, 1H). $^{31}\text{P}\{^1\text{H}\}$ NMR (202 MHz, CDCl_3 , 25 °C): δ -121.8 (s); HRMS (ESI) $m/z = 1166.9$ (M+H) $^+$. (R)-**6b**: 64 mg (70%); IR [$\nu(\text{CO})$, cyclohexane, cm^{-1}]; 2108(m), 2055(s), 2036(s), 2019(vs), 2001(m), 1990(s), 1977(m); ^1H NMR (500 MHz, CDCl_3 , 25 °C): δ 8.05 (dd, $J = 8.5$, 2.0 Hz, 1H), 8.02 (d, $J = 9.1$ Hz, 1H), 7.90 (d, $J = 8.2$ Hz, 1H), 7.85 (d, $J = 8.2$ Hz, 1H), 7.71 (d, $J = 8.5$ Hz, 1H), 7.47 (m, 1H), 7.41 (d, $J = 9.1$ Hz, 1H), 7.31 (m, 1H), 7.25 (m, 1H), 7.21 (dd, $J = 8.5$, 1.2 Hz, 1H), 7.10 (d, $J = 8.6$ Hz, 1H), 6.85 (d, $J = 8.5$ Hz, 1H), 5.90 (dd, $^1J_{\text{P-H}} = 386.2$ Hz, $^2J_{\text{H-H}} = 3.6$ Hz, 1H), 5.80 (dd, $^1J_{\text{P-H}} = 391.0$ Hz, $^2J_{\text{H-H}} = 3.6$ Hz, 1H), 3.72 (s, 3H). $^{31}\text{P}\{^1\text{H}\}$ NMR (202 MHz, CDCl_3 , 25 °C): δ -122.92 (s); HRMS (ESI) $m/z = 1195.9$ (M) $^+$.

Preparation of $[(\mu\text{-H})\text{Os}_3(\mu\text{-PhAR})(\text{CO})_{10}]$ 7, via DBU base

A solution of $[\text{Os}_3(\text{CO})_{11}(\text{Ph}_2\text{Ar})]$ **6**, in THF ((S)-**6a**: 70 mg, 0.06 mmol, (R)-**6b**: 70 mg, 0.058 mmol) was stirred for 1 h. An excess of DBU (1,8-diazabicyclo[5.4.0]undec-7-ene) ((S)-**6a**: 0.07 mL, 0.46 mmol; (R)-**6b**: 0.06 mL, 0.406 mmol) was added to the stirred solution; the colour of which changed rapidly from yellow to an intense red, followed by a slower decolourisation back to yellow. This solution was then protonated by adding TFA (trifluoroacetic acid) until the solution was acidic. After 6 h, the reaction was stopped, the solvent removed *in vacuo* and the residue purified by thin layer chromatography using dichloromethane-petroleum ether (1:4) mixture as eluent, to give **7** as the major product. (S)-**7a**: 58 mg (84%); IR [$\nu(\text{CO})$, cyclohexane, cm^{-1}]; 2102(m), 2060(vs), 2052(s), 2021(vs), 2010(s), 1992(s), 1981(m); ^1H NMR (500 MHz, CDCl_3 , 25 °C): δ 7.93 (m, 3H), 7.83 (d, $J = 8.1$ Hz, 1H), 7.60 (m, 1H), 7.45 (m, 3H), 7.30 (m, 1H), 7.25 (dd, $J = 5.9$, 1.0 Hz, 2H), 7.14 (dd, $J = 12.9$, 6.4 Hz, 1H), 6.99 (dd, $J = 13.5$, 8.6 Hz, 1H), 6.71 (dd, $^1J_{\text{P-H}} = 438.4$, $^2J_{\text{H-H}} = 4.2$ Hz, 1H), -19.31 (dd, $^1J_{\text{P-H}} = 18.4$, $^2J_{\text{H-H}} = 4.0$ Hz, 1H); ^{31}P NMR (202 MHz, CDCl_3 , 25 °C): δ -52.2 (dd, $J = 17.7$, 8.6 Hz); HRMS (ESI) $m/z = 1142.7$ (M+2H) $^+$. (R)-**7b**: 56 mg (83%); IR [$\nu(\text{CO})$, cyclohexane, cm^{-1}]; 2102(m), 2060(vs), 2052(s), 2020(vs), 2008(s), 1992(s), 1980(m); ^1H NMR (500 MHz, CDCl_3 , 25 °C): 7.98 (d, $J = 9.1$ Hz, 1H), 7.94 (dd, $J = 8.6$, 1.9 Hz, 1H), 7.82 (m, 2H), 7.44 (m, 1H), 7.40 (m, 1H), 7.27 (dd, $J = 10.9$, 4.0 Hz, 1H), 7.22 (m, 3H), 7.02 (dd, $J = 13.4$, 8.6 Hz, 1H), 6.91 (dd, $^1J_{\text{P-H}} = 437.7$, $^2J_{\text{H-H}} = 4.2$ Hz, 1H), 6.83 (d, $J = 8.4$ Hz, 1H), 3.77 (s, 3H), -19.32 (dd, $^1J_{\text{P-H}}$

= 18.2, $^2J_{\text{H-H}} = 4.2$ Hz, 1H); ^{31}P NMR (202 MHz, CDCl_3 , 25 °C): δ -51.3 (dd, $J = 21.3$, 18.0 Hz); HRMS (ESI) $m/z = 1166.8$ (M-H) $^+$.

[(μ -H) $\text{Os}_3(\text{CO})_{10}(\mu_2\text{-PhAr})$] **7**, via thermal reaction

A solution of **6** (30 mg, 0.026 mmol) in toluene (15 mL) was heated to reflux for 6 h under an inert atmosphere, then allowed to cool and the solvent removed *in vacuo*. Thin layer chromatography using silica-gel coated glass plates and a dichloromethane-petroleum ether (1:4) mixture as eluent gave **7** as the one major product ((*S*)-**7a**: 10 mg (33%), (*R*)-**7b**: 12 mg (39%).

Preparation of [(μ -H) $_2\text{Os}_3(\mu_3\text{-PAr})(\text{CO})_9$] **8**

A solution of [(μ -H) $\text{Os}_3(\mu_2\text{-PhAr})(\text{CO})_{10}$] **7**, in hexane ((*S*)-**7a**: 41 mg, 0.044 mmol; (*R*)-**7b**: 25.7 mg, 0.022 mmol) was stirred for 1 h. One equivalent of TMNO ((*S*)-**7a**: 2.7 mg, 0.044 mmol, (*R*)-**7b**: 1.7 mg, 0.022 mmol) in dichloromethane was added dropwise to the stirred solution. After 21 h, the reaction was stopped, the solvents removed *in vacuo* and the residue purified by thin layer chromatography using a dichloromethane-petroleum ether (1:4) mixture as eluent, to give **8** as the major product. (*S*)-**8a**: 13 mg (26%); IR [$\nu(\text{CO})$, cyclohexane, cm^{-1}]: 2075(m), 2038(s), 2025(s), 1996(s), 1985(m), 1972(m), 1964(m), 1955(w); ^1H NMR (500 MHz, CDCl_3 , 25 °C): δ 8.04 (dd, $J = 13.8$, 8.7 Hz, 1H), 7.92 (d, $J = 7.9$ Hz, 1H), 7.84 (dd, $J = 22.2$, 8.1 Hz, 3H), 7.52 (m, 1H), 7.39 (m, 3H), 7.14 (m, 3H), 6.83 (d, $J = 8.8$ Hz, 1H), -19.29 (d, $J = 4.2$ Hz, 1H), -19.33 (d, $J = 4.2$ Hz, 1H); ^{31}P NMR (202 MHz, CDCl_3 , 25 °C): δ 110.1 (t, t, $J = 9.7$ Hz); HRMS (ESI) $m/z = 1144.1$ (M+Na) $^+$. (*R*)-**8b**: 7.2 mg (28%); IR [$\nu(\text{CO})$, cyclohexane, cm^{-1}]: 2074(m), 2038(s), 2024(s), 1994(s), 1984(m), 1973(m), 1964(m), 1955(w); ^1H NMR (500 MHz, CDCl_3 , 25 °C): δ 8.00 (dd, $J = 13.9$, 8.6 Hz, 1H), 7.95 (d, $J = 9.2$ Hz, 1H), 7.79 (m, 3H), 7.36 (m, 2H), 7.10 (m, 2H), 6.91 (d, $J = 8.3$ Hz, 1H), 6.83 (d, $J = 8.6$ Hz, 1H), 3.65 (s, 3H), -18.29 (d, $J = 10.6$ Hz, 1H), -18.40 (d, $J = 10.6$ Hz, 1H); ^{31}P NMR (202 MHz, CDCl_3 , 25 °C): δ 111.5 (t, $J = 10.2$ Hz); HRMS (ESI) $m/z = 1169.9$ (M+Na) $^+$.

Synthesis of tetraruthenium clusters

[(μ -H) $_4\text{Ru}_4(\text{CO})_{11}(\text{PH}_2\text{Ar})$] **9**, via oxidative decarbonylation

A mixture of [(μ -H) $_4\text{Ru}_4(\text{CO})_{12}$] (**5**, 50 mg, 0.067 mmol) and one equivalent of the phosphine **1** ((*S*)-**1a**: 18 mg, 0.162; (*R*)-**1b**: 21 mg, 0.061 mmol) were dissolved in 20 mL of dichloromethane and the solution was stirred for 20 min. Under vigorous stirring, a small excess of Me_3NO (6 mg, 0.08 mmol) dissolved in dichloromethane (5 mL) was added dropwise to the yellowish cluster/ligand solution over 30 min, which instantly started to develop a red colouration. After 6 h the solvent was removed under reduced pressure. The red solid residue was redissolved in a small quantity of dichloromethane and purified by using preparative TLC (dichloromethane-petroleum ether 1:3). Except for traces of starting materials, and one stationary brown band (decomposed material), one band was isolated from the TLC plates, extracted with CH_2Cl_2 and dried under vacuum to afford the red solid **9** as the major product. (*S*)-**9a** (12 mg, 30%); IR [$\nu(\text{CO})$, cyclohexane, cm^{-1}]: 2094(m), 2088(w), 2067(vs), 2057(vs),

2029(vs), 2009(vs), 1992(m), 1971(w); ^1H NMR (500 MHz, CDCl_3 , 25 °C): δ 8.02 (dd, $J = 14.0$, 8.4 Hz, 2H), 7.92 (dd, $J = 19.2$, 8.3 Hz, 2H), 7.64 (m, 2H), 7.48 (m, 2H), 7.42 (d, $J = 6.9$ Hz, 1H), 7.28 (dd, $J = 7.7$ Hz, 2H), 7.14 (dd, $J = 19.6$, 8.6 Hz, 2H), 5.47 (dd, $J_{\text{P-H}} = 359.7$, $^2J_{\text{H-H}} = 3.3$ Hz, 1H), 5.16 (dd, $J_{\text{P-H}} = 367.9$, $^2J_{\text{H-H}} = 4.0$ Hz, 1H), -17.71 (d, $J = 6.0$ Hz, 4H); ^{31}P NMR (202 MHz, CDCl_3): $\delta = -79.5$ (m); HRMS (ESI) $m/z = 1001$ (M) $^+$. (*R*)-**9b** (32 mg, 46%); IR [$\nu(\text{CO})$, cyclohexane, cm^{-1}]: 2094(m), 2088(w), 2065(vs), 2057(vs), 2030(vs), 2007(vs), 1990(m), 1971(w); ^1H NMR (500 MHz, CDCl_3): δ 8.10 (d, $J = 9.2$ Hz, 1H), 7.95 (dd, $J = 19.3$, 8.2 Hz, 1H), 7.76 (dd, $J = 13.1$, 8.5 Hz, 1H), 7.56 (t, $J = 7.3$ Hz, 1H), 7.50 (d, $J = 9.1$ Hz, 1H), 7.39 (t, $J = 7.4$ Hz, 1H), 7.18 (d, $J = 8.3$ Hz, 1H), 6.95 (d, $J = 8.5$ Hz, 1H), 5.80 (d, $J = 3.3$ Hz, 1H), 5.36 (dd, $J_{\text{P-H}} = 364.1$, $^2J_{\text{H-H}} = 3.3$ Hz, 1H), 5.28 (dd, $J_{\text{P-H}} = 370.1$ Hz, $^2J_{\text{H-H}} = 2.8$ Hz, 1H), 3.71 (s, OCH_3), -17.67 (d, $J = 4.6$ Hz, 4H); ^{31}P NMR (202 MHz, CDCl_3): $\delta = -80.8$ (m); HRMS (ESI) $m/z = 1031$ (M) $^+$.

Homogeneous catalytic experiments

In the catalytic experiments, the catalyst and substrate were loaded into the autoclave under N_2 , and the degassed solvent mixture was added (2.5 mL each of EtOH/toluene). The reaction vessel was closed and purged three times with hydrogen, before final pressurization to 50 bar. The reaction mixture was continuously stirred with a magnetic stirrer (*ca.* 750 rpm) and heated at 100 °C for 24 or 72 h. After a cooling period of approximately 45 min, the reaction vessel was depressurized and opened. The homogeneous reaction mixture was transferred to a 50 mL flask and concentrated *in vacuo*. To separate the carboxylic acid from the cluster, the reaction residue was dissolved in 10 mL of diethyl ether and the carboxylic acid was extracted with aqueous sodium hydroxide solution (1M, 3 x 10 mL) and washed with diethyl ether (3 x 5 mL), leaving the cluster in the organic solvent. The carboxylate was protonated with sulfuric acid and extracted with diethyl ether (3 x 10 mL), washed with water (2 x 5 mL), and dried over magnesium sulphate - evaporation of the ether *in vacuo* yielded the carboxylic acid quantitatively. The original ether phase, from which the carboxylic acid was extracted, was concentrated *in vacuo* to retrieve the remaining cluster. The residue was dissolved in a minimum quantity of dichloromethane and the products separated using preparative TLC, eluting with dichloromethane/petroleum ether (1:2). Usually 60-70% of the cluster was recovered after a catalytic experiment and analyzed by IR and NMR spectroscopy. The enantiomeric excess of the product was detected by derivatizing 2-methylbutyric acid with (*S*)-methyl mandelate and analyzing the diastereomeric product mixture by NMR, as fully described by Tyrrell *et al.*¹⁹ It was found that flash chromatography of the final products was not necessary.

X-ray structure determinations

Crystals of (*S*)-**2a**, (*R*)-**2b** and (*R*)-**4b** were immersed in cryo-oil, mounted in a Nylon loop, and measured at a temperature of 293 K for (*S*)-**2a** and 170 K for (*R*)-**2b** and (*R*)-**4b**. The X-ray diffraction data were collected on a Nonius Kappa CCD or on a Bruker AXS Kappa ApexII Duo diffractometer using Mo $\text{K}\alpha$ radiation ($\lambda = 0.71073$ Å).

The *Denzo-Scalepack*²⁰ or *APEX2*²¹ program packages were used for cell refinements and data reductions. The structures were solved by direct methods using the *SHELXS-97* program²² with the *WinGX* graphical user interface.²³ Crystals of (*R*)-**3b** and (*S*)-**4a** were measured at temperature of 150 K and the X-ray diffraction data were collected on Oxford Diffraction Xcalibur (Atlas, Gemini Ultra CCD). All hydrogens were placed in idealized positions. Positions of hydrides were calculated using the XHYDEX program.²⁴ Selected crystallographic parameters are summarized in Table 2.

Table 2. Selected crystallographic parameters for clusters (*S*)-**2a**, (*R*)-**2b**, (*R*)-**3b**, (*S*)-**4a** and (*R*)-**4b**.

	2a	2b	3b	4a	4b
formula	C ₂₉ H ₁₄ O ₉ PRu ₃	C ₃₀ H ₁₇ O ₁₀ PRu ₃	C ₅₆ H ₄₁ Cl ₂ O ₉ P ₃ Ru	C ₅₃ H ₃₇ Cl ₃ O ₇ P ₃ Ru ₃	C ₅₅ H ₃₉ O ₈ P ₃ Ru ₃
<i>M_r</i>	841.58	871.61	1324.91	1288.30	1199.96
<i>T</i> / K	293(2)	170 (2)	150(2)	150(2)	170(2)
λ [Å]	0.71073	0.71073	1.54178	0.71073	0.71073
Crystal system	Monoclinic	Orthorhombic	C2	Orthorhombic	Monoclinic
Space group	P2 ₁	P2 ₁ 2 ₁ 2 ₁	P2 ₁ /c	P2 ₁ 2 ₁ 2 ₁	P2 ₁
<i>a</i> /Å	8.2735(15)	8.4144(10)	24.1296(16)	11.5653(3)	11.61210(8)
<i>b</i> /Å	42.904(8)	16.9342(2)	12.2606(5)	19.4643(5)	16.26694(10)
<i>c</i> /Å	17.206(3)	21.3835(3)	21.8489(14)	22.7362(5)	13.18776(9)
α /°	90	90	90	90	90
β /°	93.506(2)	90	120.444(9)	90	98.0858(6)
γ /°	90	90	90	90	90
<i>V</i> /Å ³	6096.2(19)	3047.8(7)	5572.6(6)	5118.2(2)	2466.31(3)
<i>Z</i>	8	4	4	4	2
ρ_{calc} /g cm ⁻³	1.832	1.900	1.579	1.672	1.616
μ /mm ⁻¹	1.570	1.576	8.643	1.176	1.058
<i>F</i> (000)	3264	1696	2336	2556	1196
θ limits/°	1.28 to 25.0	3.081 to 30.503	2.3 to 62.3	2.88 to 28.71	2.169 to 40.247
<i>h</i> range	-9 to 9	-12 to 11	-27 to 13	-15 to 13	-21 to 21
<i>k</i> range	-51 to 50	-24 to 8	-13 to 12	-25 to 21	-29 to 29
<i>l</i> range	-20 to 20	-30 to 15	-19 to 24	-30 to 23	-23 to 23
No. reflns.	52563	9202	8850	29572	122276
Unique reflns.	19469	8287	5921	10147	31038
GOOF (<i>F</i> ²)	1.052	1.038	1.039	1.031	1.082
<i>R</i> _{int}	0.0305	0.0346	0.0252	0.0324	0.0710
<i>R</i> ¹ (<i>I</i> ≥ 2σ)	0.0335	0.0629	0.0415	0.0297	0.0423
<i>WR</i> 2 ^b (<i>I</i> ≥ 2σ)	0.0623	0.0465	0.1072	0.0585	0.0866
Largest diff. peak and hole [e.Å ⁻³]	0.397 and -0.411	0.600 and -0.617	0.96 and -0.95	0.687 and -0.654	0.870 and -1.468
Flack parameter	0.018(18)	0.02(2)	0.012(12)	-0.03(2)	-0.028(11)

^a $R1 = \Sigma [|F_o| - |F_c|] / \Sigma |F_o|$. ^b $WR2 = [\Sigma (w(F_o^2 - F_c^2)^2) / \Sigma (w(F_o^2)^2)]^{1/2}$.

Acknowledgements

We thank the EPSRC for a Career Acceleration Fellowship (L.J.H.) and a studentship (A.F.), and the Erasmus Mundus program FFEEDB1 office for a scholarship (A.F.A.).

Notes and references

- ^a Chemical Physics, Chemical Center, Lund University, Box 124, SE-221 00, Lund, Sweden.
- ^b School of Chemistry, Bedson Building, Newcastle University, Newcastle upon Tyne, NE1 7RU, UK.
- ^c Department of Chemistry, P.O. Box 35, FI-40014, University of Jyväskylä, Finland.
- ^d Dipartimento di Chimica "G. Ciamician", Università degli Studi di Bologna, Via Selmi 2, I-40126 Bologna, Italy.
1. G. Rothenberg, Wiley-VCH Verlag GmbH & Co. KGaA, Weinheim, 2008, ch. 3, pp. 110-111.
 2. V. Moberg, M. Haukka, I. O. Koshevoy, R. Ortiz and E. Nordlander, *Organometallics*, 2007, 26, 4090-4093.
 3. P. Homanen, R. Persson, M. Haukka, T. A. Pakkanen and E. Nordlander, *Organometallics*, 2000, 19, 5568-5574.
 4. V. Moberg, R. Duquesne, S. Contaldi, O. Rohrs, J. Nachtigall, L. Damoense, A. T. Hutton, M. Green, M. Monari, D. Santelia, M. Haukka and E. Nordlander, *Chem-Eur J*, 2012, 18, 12458-12478.
 5. D. Blazina, S. B. Duckett, P. J. Dyson and J. A. B. Lohman, *Dalton T*, 2004, DOI: 10.1039/B405030D, 2108-2114.
 6. G. Huttner, J. Schneider, G. Mohr and J. Von Seyerl, *J. Organomet. Chem.*, 1980, 191, 161-169.
 7. F. Iwasaki, M. J. Mays, P. R. Raithby, P. L. Taylor and P. J. Wheatley, *J. Organomet. Chem.*, 1981, 213, 185-206.
 8. K. Natarajan, O. Scheidsteger and G. Huttner, *J. Organomet. Chem.*, 1981, 221, 301-308.
 9. H.-G. Ang, C.-H. Koh, L.-L. Koh, W.-L. Kwik, W.-K. Leong and W.-Y. Leong, *J. Chem. Soc., Dalton Trans.*, 1993, DOI: 10.1039/DT9930000847, 847-855.
 10. H. Ghee Ang, S. Gek Ang, S. Du, B. Hwa Sow and X. Wu, *J. Chem. Soc., Dalton Trans.*, 1999, DOI: 10.1039/A902598G, 2799-2805.
 11. T. Kakizawa, H. Hashimoto and H. Tobita, *J. Organomet. Chem.*, 2006, 691, 726-736.
 12. L. Heuer, E. Nordlander, B. F. G. Johnson, J. Lewis and P. R. Raithby, *Phosphorus, Sulfur, and Silicon and the Related Elements*, 1995, 103, 241-252.
 13. S. B. Colbran, P. T. Irele, B. F. G. Johnson, F. J. Lahoz, J. Lewis and P. R. Raithby, *J. Chem. Soc., Dalton Trans.*, 1989, DOI: 10.1039/DT9890002023, 2023-2031.
 14. S. B. Colbran, B. F. G. Johnson, J. Lewis and R. M. Sorrell, *J. Organomet. Chem.*, 1985, 296, c1-c5.
 15. M. J. Stchedroff, V. Moberg, E. Rodriguez, A. E. Aliev, J. Botcher, J. W. Steed, E. Nordlander, M. Monari and A. J. Deeming, *Inorg. Chim. Acta.*, 2006, 359, 926-937.
 16. U. Matteoli, V. Beghetto and A. Scrivanti, *J. Mol. Catal. A*: 1996, 109, 45-50.
 17. J. N. Nicholls, M. D. Vargas, A. J. Deeming and S. E. Kabir, in *Inorganic Syntheses*, John Wiley & Sons, Inc., 2007, DOI: 10.1002/9780470132593.ch58, pp. 232-235.
 18. M. I. Bruce, B. K. Nicholson, M. L. Williams, T. Arligue and G. Lavigne, in *Inorganic Syntheses*, John Wiley & Sons, Inc., 2007, DOI: 10.1002/9780470132593.ch56, pp. 221-230.
 19. E. Tyrrell, M. W. H. Tsang, G. A. Skinner and J. Fawcett, *Tetrahedron*, 1996, 52, 9841-9852.
 20. Z. Otwinowski and W. Minor, in *International Tables for Crystallography Volume F: Crystallography of biological macromolecules*, eds. M. G. Rossmann and E. Arnold, Springer Netherlands, 2001, vol. F, ch. 24, pp. 226-235.
 21. APEX2, in *SAINT-Plus and SADABS*. Bruker AXS Inc., Madison, Wisconsin, USA, 2008.
 22. G. Sheldrick, *Acta Crystallogr. Sec. A*, 2008, 64, 112-122.
 23. L. Farrugia, *J. Appl. Crystallogr.*, 1999, 32, 837-838.
 24. A. G. Orpen, *J. Chem. Soc., Dalton Trans.*, 1980, DOI: 10.1039/DT9800002509, 2509-2516.

Paper V

Synthesis and characterization of chiral phosphirane derivatives of $[(\mu\text{-H})_4\text{Ru}_4(\text{CO})_{12}]$ and their application in hydrogenation of an α -unsaturated carboxylic acid

Ahmed F. Abdel-Magied,^a Maitham H. Majeed,^a Arne Ficks,^b Radwa M. Ashour,^a Ahibur Rahaman,^a William Clegg,^b Matti Haukka,^c Lee J. Higham^{b*} and Ebbe Nordlander^{a*}

^a Chemical Physics, Chemical Center, Lund University, Box 124, SE-221 00, Lund, Sweden.

^b School of Chemistry, Bedson Building, Newcastle University, Newcastle upon Tyne, NE1 7RU, U.K.

^c Department of Chemistry, University of Jyväskylä, P.O. Box 35, FI-40014 Jyväskylä, Finland.

KEYWORDS: *Hydrogenation, Clusters, Ruthenium, Phosphiranes*

ABSTRACT: Eight tetraruthenium clusters containing the chiral binaphthyl-derived mono-phosphiranes [(*S*)-1-([1,1'-binaphthalen]-2-yl)phosphirane] (*S*)-**1a**, [(*R*)-1-(2'-methoxy-1,1'-binaphthyl-2-yl)phosphirane] (*R*)-**1b**, and the diphosphirane [2,2'-di(phosphiran-1-yl)-1,1'-binaphthalene] (*S*)-**1c** have been synthesized and characterized. The clusters are $[(\mu\text{-H})_4\text{Ru}_4(\text{CO})_{11}((\text{S})\text{-1a})]$ **2a**, $[(\mu\text{-H})_4\text{Ru}_4(\text{CO})_{11}((\text{R})\text{-1b})]$ **2b**, $1,1\text{-}[(\mu\text{-H})_4\text{Ru}_4(\text{CO})_{10}((\text{S})\text{-1c})]$ **2c**, $[(\mu\text{-H})_4\text{Ru}_4(\text{CO})_{11}((\text{S})\text{-1a-H}_2)]$ **3a**, $[(\mu\text{-H})_4\text{Ru}_4(\text{CO})_{11}((\text{R})\text{-1b-H}_2)]$ **4a**, $[(\mu\text{-H})_4\text{Ru}_4(\text{CO})_{11}((\text{S})\text{-1b-H}_2)]$ **3b**, $[(\mu\text{-H})_4\text{Ru}_4(\text{CO})_{11}((\text{R})\text{-1b-H}_2)]$ **4b** and the phosphinidene-capped triruthenium cluster $[(\mu\text{-H})_2\text{Ru}_3(\text{CO})_9(\text{PEt})]$ **5**. The phosphirane-substituted clusters were found to be able to catalyze the hydrogenation of *trans*-2-methyl-2-butenic acid, but no enantioselectivity could be detected. The molecular structures of **2c**, **3b** and **5** have been determined and are presented.

Introduction

For more than three decades numerous of researchers in both academia and industry have investigated homogeneous asymmetric hydrogenation extensively, due to its importance for the production of enantiopure, bioactive ingredients on industrial scale [1]. Ruthenium, rhodium and iridium complexes containing chiral diphosphine ligands have shown superior catalytic activity in the asymmetric hydrogenation of olefins, ketones or imines [2, 3]. Greater light has been shed on the using of transition metal carbonyl clusters as catalysts for various chemical reactions of industrial relevance [4-6]. However, relatively few studies have been investigated the potential of clusters to act as catalysts for asymmetric transformations. Indeed, cluster-based catalysts/catalyst precursors have shown interesting catalytic activity for several different chemical reactions, but have not yet proven to be commercially viable. Hydride-containing

trinuclear and tetranuclear ruthenium carbonyl cluster have been used as effective catalysts/catalyst precursors for several asymmetric reactions including isomerization [7], hydroformylation [8], hydrosilylation [9], reductive coupling [10], homogeneous hydrogenation [11-14] of various carboxylic acids as well as the water-gas shift reaction [15]. Salvini *et al.* have reported the application of such clusters to the asymmetric hydrogenation of tiglic acid (*trans*-2-methyl-2-butenic acid) [16]. The hydrogenation was performed under relatively harsh conditions and was found to result in the formation of *S*- and *R*-forms of 2-methylbutyric acid with enantiomeric excesses (ee) that varied between 6 and 39%. The enantiomeric excesses and the catalyst activity were found to be dependent on the chiral phosphines coordinated to the parent cluster. Using relatively bulky chiral diphosphines with ferrocene-based backbones (the Walphos and Josiphos ligand families) and milder hydrogenation conditions, we have been able to show that similar tetraruthenium tetrahydride clusters are effective catalysts/catalyst precursors for asymmetric hydrogenation of α -unsaturated carboxylic acids with enantioselectivities exceeding 90 % in certain cases [17-20].

The use of monodentate binaphthyl based ligands with phosphonite [21], phosphite [22] and phosphoramidite [23] functionalities in asymmetric hydrogenation reactions have received much attention. Phosphiranes are heterocycles consisting of a phosphorus-containing three-membered ring that is highly strained. Incorporation of a phosphorus atom in that three-membered ring is connected with a change in hybridization, which results in poorer σ -donor ability, but significant π -acceptor character for the phosphirane moiety, relative to an analogous phosphine [24]. Up to now, only a few examples where chiral phosphiranes have been synthesized and used in asymmetric synthesis are known. Rhodium precatalysts bearing phosphiranes have been used in asymmetric reactions with different substrates (e.g. α -dehydroamination of acids and itaconates), achieving stereoselectivities up to 76% ee [25]. Higham and coworkers have shown that highly stable enantiopure chiral

phosphiranes can be used as effective ligands in catalytic asymmetric hydrosilylation of styrene with excellent conversion (~100%) and an enantiomeric excess of 80%, as well as in asymmetric allylic alkylation of (*rac*)-(*E*)-1,3-diphenylallyl acetate, giving high conversion (up to 91%) albeit with relatively moderate ee (~17%) [26, 27].

Considering the success of our earlier studies, and the demonstrated effectiveness of binaphthyl-based phosphorus-donor ligands, we have investigated the coordination of chiral phosphiranes to H_4Ru_4 carbonyl clusters and the potential of the resultant chiral ruthenium clusters to catalyze asymmetric reactions. Herein we report the synthesis and characterization of new tetranuclear ruthenium clusters containing the chiral mono- and/or didentate phosphiranes ligands [(*S*)-1-(1,1'-Binaphthalen)-2-yl]phosphirane] (*S*)-**1a**, [(*R*)-1-(2'-Methoxy-1,1'-binaphthyl-2-yl)phosphirane] (*R*)-**1b**, and [2,2'-di(phosphiran-1-yl)-1,1'-binaphthalene] (*S*)-**1c** (Fig. 1), and a study of their performance as catalysts/catalyst precursors for the hydrogenation of tiglic acid.

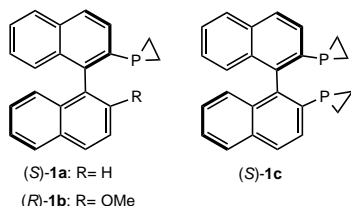


Fig. 1. Structure of phosphiranes ligands used in this investigation.

Results and discussion

Synthesis and characterisation of ruthenium clusters

The synthesis of the chiral MOP-type [(1,1'-binaphthalen)-2-yl]diphenylphosphine derivatives of $[H_4Ru_4(CO)_{12}]$ were based on previously published methods [17, 19, 20]; i.e. *via* thermal substitution in benzene under elevated pressures of hydrogen gas (30–50 bar) or decarbonylation in the presence of the phosphirane ligand in dichloromethane solution at ambient temperature, using Me_3NO as an oxidative decarbonylation reagent (*cf.* Experimental Section). The latter method was found to be superior with respect to both yield and selectivity of product formation, while the thermal, high-pressure route gave rise to phosphirane degradation (*vide infra*). The clusters were identified by IR, 1H and ^{31}P NMR spectroscopy, mass spectrometry and, wherever possible, X-ray crystallography. A summary of the new clusters and the different phosphirane coordination modes found in this study is shown in Table 1.

Table 1. A summary of cluster framework geometries and phosphirane coordination modes detected in this study. Carbonyl and hydride ligands have been omitted for clarity.

$[H_4Ru_4(CO)_{11}((S)\text{-}\mathbf{1a})]$ 2a $[H_4Ru_4(CO)_{11}((R)\text{-}\mathbf{1b})]$ 2b	$1,1\text{-}[H_4Ru_4(CO)_{10}((S)\text{-}\mathbf{1c})]$ 2c
$[H_4Ru_4(CO)_{11}((R)\text{-}\mathbf{1a}\text{-}H_2)]$ 3a $[H_4Ru_4(CO)_{11}((S)\text{-}\mathbf{1a}\text{-}H_2)]$ 4a $[H_4Ru_4(CO)_{11}((S)\text{-}\mathbf{1b}\text{-}H_2)]$ 3b $[H_4Ru_4(CO)_{11}((R)\text{-}\mathbf{1b}\text{-}H_2)]$ 4b	$[H_2Ru_3(CO)_9(P\text{Et})]$ 5

Synthesis and characterization of clusters 2a–2c

Treatment of an equimolar mixture of $[H_4Ru_4(CO)_{12}]$ and (*S*)-**1a** or (*R*)-**1b** or (*S*)-**1c** in dichloromethane at room temperature with 1.2–1.5 eq. of the oxidative decarbonylation reagent Me_3NO led to formation of the monosubstituted clusters $[(\mu\text{-}H)_4Ru_4(CO)_{11}((S)\text{-}\mathbf{1a})]$ **2a**, $[(\mu\text{-}H)_4Ru_4(CO)_{11}((R)\text{-}\mathbf{1b})]$ **2b** and the disubstituted 1,1- $[(\mu\text{-}H)_4Ru_4(CO)_{10}((S)\text{-}\mathbf{1c})]$ **2c**, respectively. Purification by thin-layer chromatography permitted isolation of the clusters as orange-red solids. Their structures were identified on the basis of spectroscopic data. The characterization of clusters **2a** and **2b** were based on their IR spectra, which were similar to those previously reported for the clusters $[(\mu\text{-}H)_4Ru_4(CO)_{11}(L)]$ ($L = PMe_2Ph$) [28] and $[(\mu\text{-}H)_4Ru_4(CO)_{11}(NMDPP)]$ ($NMDPP = (S)\text{-}(+)\text{-neomenthyl}$ diphenylphosphine) [18]. The 1H NMR spectra of **2a** and **2b** reveal, in addition to signals for the chiral phosphirane ligands (*cf.* Experimental section), apparent doublet at $\delta = -17.64$ and an apparent singlet at -17.84 ppm, respectively, which are indicative of complete fluxionality of the hydride ligands (*vide infra*). The ^{31}P NMR spectra of **2a** and **2b** show a broad multiplet ($^2J_{P,H}$ not resolved) at $\delta = -154.22$ ppm and an apparent singlet at $\delta = -155.86$ (J not resolved), respectively, which may be compared with the relatively high field shifts shown by the free ligands [^{31}P NMR: (*S*)-**1a** $\delta = -235.4$ ppm, (*R*)-**1b** $\delta = -235.0$ ppm] [26]. The mass spectra of **2a** and **2b** reveal peak envelopes at $m/z = 1052 [M+Na]^+$ and $1081 [M+Na]^+$, corresponding to the molecular formulae $[(\mu\text{-}H)_4Ru_4(CO)_{11}((S)\text{-}\mathbf{1a})]$ (**2a**) and $[(\mu\text{-}H)_4Ru_4(CO)_{11}((R)\text{-}\mathbf{1b})]$ (**2b**), respectively.

Cluster **2c** exhibits eight absorptions in the CO region of the IR spectrum in cyclohexane. Comparison of the ν_{C-O} IR stretching frequency pattern of **2c** to the known complex

1,1-[(μ -H) $_4$ Ru $_4$ (CO) $_{10}$ (DUPHOS)] [DUPHOS = (2*R*,5*R*)-2,5-dimethyl-1-(2-((2*R*,5*R*)-2,5-dimethylphospholan-1-yl)-phenyl)phospholane] [18], indicates that in **2c** the ligand (*S*)-**1c** chelates one ruthenium apex. The ^1H and ^{31}P NMR spectra of **2c** shows one broad ‘singlet’ at $\delta = -17.20$ ppm in the hydride region of the ^1H NMR spectrum (due to hydride fluxionality) while the ^{31}P NMR spectrum displays two equal intensity doublets at $\delta = -136.61$ ppm and $\delta = -139.18$ ppm, consistent with magnetically inequivalent phosphorus nuclei. The mass spectrum of **2c** reveals a peak at $m/z = 1082$ [$\text{M} + \text{Na}$] $^+$, consistent with the molecular formula [(μ -H) $_4$ Ru $_4$ (CO) $_{10}$ ((*S*)-**1c**)].

It was possible to grow crystals of **2c** suitable for X-ray diffraction, and the crystal structure of the cluster was determined in order to confirm the chelating mode of the diphosphirane ligand. The molecular structure of **2c** is shown in Figure 2. The cluster contains a distorted tetrahedral core of Ru atoms where the ‘basal’ atoms preserve the tricarbonyl units of the parent cluster [$\text{H}_4\text{Ru}_4(\text{CO})_{12}$] [29] while the ‘apical’ atom, Ru1, is coordinated by the diphosphirane which binds in a chelating mode. The Ru-Ru bond lengths provide good indications of the locations of the hydrides and they may be divided into two distinctive classes, the four ‘long’ (hydride-bridged) distances [Ru1-Ru2 2.9795(4), Ru1-Ru3 3.0055(4), Ru1-Ru4 2.9518(4), Ru3-Ru4 2.9229(4) Å] and two ‘short’ distances [Ru2-Ru3 2.7919(4), Ru2-Ru4 2.7945(4) Å]. The arrangement of the four bridging hydrides yields an H_4Ru_4 cluster core with C_s symmetry, rather than D_{2d} as observed for the bis-phosphine-derivatised clusters [$\text{H}_4\text{Ru}_4(\text{CO})_{10}(\text{PPh}_3)_2$] [29]. The C_s symmetry found in the H_4Ru_4 core seems to be a common feature shared by [$\text{H}_4\text{Ru}_4(\text{CO})_{10}(\text{diphosphine})$] clusters and has been reported for both chelating [17] and bridging [17, 18, 20] coordination modes of the diphosphine ligands. The Ru-P distances in cluster **2c** are identical within experimental error [Ru1-P1 2.3017(3), Ru1-P2 2.3019(3) Å]. All CO ligands are bound in a terminal monodentate coordination mode and are staggered with respect to the Ru-Ru vectors. It may be noted that due to the chirality of the binaphthyl backbone, the two phosphorus atoms of the ligand are structurally inequivalent, regardless of hydride fluxionality.

As already mentioned, **2a**, **2b** and **2c** were found to exhibit high degrees of hydride fluxionality at ambient temperature, unlike related (chiral) phosphine derivatives of H_4Ru_4 [19, 20]. Attempts to freeze out the fluxionality in **2a** and **2c** by low temperature ^1H NMR spectroscopy were unsuccessful; the fluxionality remained even at 213 K (cf. ESI †).

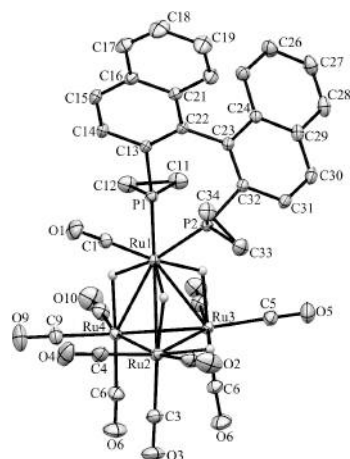
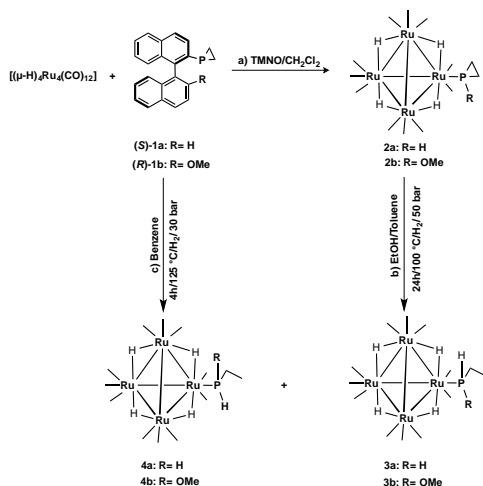


Fig. 2. Molecular structure of 1,1-[(μ -H) $_4$ Ru $_4$ (CO) $_{10}$ ((*S*)-**1c**)] **2c** with thermal ellipsoids drawn at the 50% probability level. All hydrogen atoms except the hydrides have been omitted for the sake of clarity. Selected bond lengths (Å): Ru1-Ru2 2.9795(4), Ru1-Ru3 3.0055(4), Ru1-Ru4 2.9518(4), Ru2-Ru3 2.7919(4), Ru3-Ru4 2.9229(4), Ru2-Ru4 2.7945(4), Ru1-P1 2.3017(3), Ru1-P2 2.3019(3).

Synthesis and characterization of clusters **3a-5**

Reaction of [(μ -H) $_4$ Ru $_4$ (CO) $_{12}$] with equimolar amounts of the monophosphiranes (*S*)-**1a** or (*R*)-**1b** under elevated temperatures and H_2 pressure (30-50 bar, cf. Experimental Section) led to degradation of the phosphirane ligands. Under these reaction conditions, cleavage of a P-C bond in the strained three-membered phosphirane rings occurred and hydrogenation gave resultant chiral PH(Et)(binaphthyl) secondary phosphine moieties, thus introducing a second stereogenic center in each ligand. As a result, the diastereomeric pairs [(μ -H) $_4$ Ru $_4$ (CO) $_{11}$ ((*R*)-**1a**-H $_2$)] **3a** and [(μ -H) $_4$ Ru $_4$ (CO) $_{11}$ ((*S*)-**1a**-H $_2$)] **4a**, [(μ -H) $_4$ Ru $_4$ (CO) $_{11}$ ((*S*)-**1b**-H $_2$)] **3b** and [(μ -H) $_4$ Ru $_4$ (CO) $_{11}$ ((*R*)-**1b**-H $_2$)] **4b** were formed, with different chiralities at the phosphorus atom of each ligand.



Scheme 1. Synthesis of clusters **2a-4b**.

In the above-mentioned reactions, it is unclear whether the ligand transformation occurs before or after coordination to the tetraruthenium clusters, but it was subsequently found that the same diastereomeric pairs could be formed via direct thermolysis of $[(\mu\text{-H})_4\text{Ru}_4(\text{CO})_{11}((S)\text{-1a})]$ **2a** or $[(\mu\text{-H})_4\text{Ru}_4(\text{CO})_{11}((R)\text{-1b})]$ **2b** under high H_2 pressure (cf. Scheme 1 and Experimental Section). When ligand **1a** was heated under identical reaction conditions in the absence of $[(\mu\text{-H})_4\text{Ru}_4(\text{CO})_{12}]$, no hydrogenation or degradation of the ligand was observed, strongly indicating that the hydrogenation of the ligand is mediated by the cluster.

The clusters were isolated as red-orange solids by preparative thin-layer chromatography. Their spectroscopic data were found to be consistent with the proposed structures discussed above and depicted in Scheme 1. The $\nu(\text{C-O})$ IR patterns of **3a/4a** and **3b/4b** are similar to those reported for mono-substituted $[(\mu\text{-H})_4\text{Ru}_4(\text{CO})_{11}(\text{L})]$ clusters (e.g., $\text{L} = \text{PMe}_2\text{Ph}$) [28] or NMDPP ($((S)\text{-}(+)\text{-neomenthylidiphenylphosphine})$) [18]. The ^1H NMR spectra of **3a/4a** and **3b/4b** reveals, in addition to signals for the chiral secondary phosphine ligand, ‘singlets’ at $\delta = -17.64$, -17.81 ppm for **3a** and **4a**, respectively and at $\delta = -17.72$ and -17.87 for **3b** and **4b**, due to complete fluxionality of the hydrides in each cluster at ambient temperature. As observed for **2a** and **2c** (*vide supra*), variable-temperature ^1H NMR of clusters **3a/4a** did not freeze out the fluxionality even at 213 K (cf. ESI†). Furthermore, the ^1H NMR spectra confirm the opening of the three-membered phosphorus-containing rings in the phosphirane ligands, which are highly strained as a result of the small sum bond angles at the phosphorus atom ($\Sigma(\text{P}) < 260^\circ$) [30]. Thus, in all four clusters, ^1H resonances due to new ethyl groups appear as well as signals due to the new hydrogen

coordinated to the phosphorus atom of the ligand that appear at $\delta = 5.23$ (**3a**), 5.28 (**4a**), 5.16 (**3b**) and 5.22 (**4b**) ppm, with $^1J_{\text{H-P}} = 381$, 379, 380 and 378 Hz, respectively. The ^{31}P NMR spectra for clusters **3a/4a** and **3b/4b** also show low field shifts at $\delta = -11.88$, -13.11 , -11.82 and -13.18 ppm, respectively (partial ^1H decoupling, cf. ESI†). The mass spectra reveal peak envelopes at $m/z = 1035$ $[\text{M}+\text{H}]^+$ for **3a/4a**, and 1083 $[\text{M}+\text{Na}]^+$ for **3b/4b**, in agreement with the proposed molecular formulae.

The nature of the transformed phosphirane ligand could be unambiguously confirmed by the determination of the crystal structure of $[(\mu\text{-H})_4\text{Ru}_4(\text{CO})_{11}((R)\text{-1b-H}_2)]$ **3b**. The molecular structure of **3b** is shown in Fig. 3, and relevant bond distances are summarized in the figure caption. Crystallographic data are collated in Table 3. In the solid state, the symmetry of the $\text{Ru}_4(\mu\text{-H})_4$ core of the monosubstituted phosphine derivative **3b** is D_{2d} , as previously found in the crystal structures of other $[\text{H}_4\text{Ru}_4(\text{CO})_{11}(\text{PR}_3)]$ species ($\text{R} = \text{OMe}$ [28], Ph [31], SC_4H_3 [32], C_6F_5 [28], OEt [28]) and the dimeric $[\{\text{H}_4\text{Ru}_4(\text{CO})_{11}\}_2(\mu\text{-Ph}_2\text{P-C}\equiv\text{C-C}\equiv\text{C-PPh}_2)]$ [33] with the exception of $[\text{H}_4\text{Ru}_4(\text{CO})_{11}(\text{NMDPP})]$ (NMDPP = $((S)\text{-}(+)\text{-neomenthylidiphenylphosphine})$) [18], in which the symmetry of the $\text{Ru}_4(\mu\text{-H})_4$ core is C_s instead of D_{2d} . The *trans* P1-Ru4-Ru2 angle (cf. Fig. 3) is close to linear ($170.124(18)^\circ$) and comparable to the value found in $[\text{H}_4\text{Ru}_4(\text{CO})_{11}\text{P}(\text{C}_6\text{F}_5)_3]$ ($172.25(3)^\circ$).

Considering that the four new clusters contain secondary phosphines, it was envisaged that the formation of phosphido clusters via CO dissociation and oxidative addition of a P-H bond at a ruthenium center might be possible. Therefore, attempts were made to further coordinate the phosphine moiety in **3a/4a** and **3b/4b** by either (i) dissolving the cluster species in THF followed by the addition of Me_3NO in THF under nitrogen and subsequently refluxing the solution for 12 hours or (ii) refluxing of **3a/4a** and **3b/4b** in toluene for 5 h; however, analysis by spot TLC indicated that in both cases no reaction had occurred.

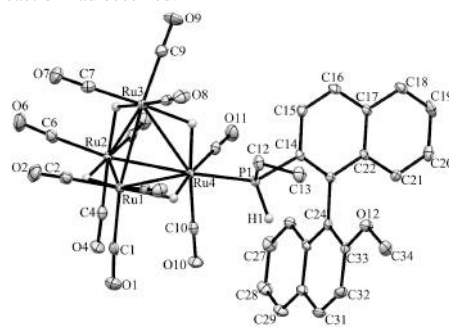


Fig. 3. Molecular structure of $[(\mu\text{-H})_4\text{Ru}_4(\text{CO})_{11}((S)\text{-1b-H}_2)]$ **3b** with thermal ellipsoids drawn at 50% probability level. Hydrogen atoms have been omitted for clarity.

Selected bond lengths (Å): Ru1-Ru2 2.9627(3), Ru1-Ru3 2.7891(3), Ru1-Ru4 2.9615(3), Ru2-Ru3 2.9584(3), Ru3-Ru4 2.3274(6), Ru2-Ru4 2.7863(3), Ru4-P1 2.3274(6).

It was, however, found that thermolysis of $[(\mu\text{-H})_2\text{Ru}_4(\text{CO})_{11}((S)\text{-1a-H}_2)]$ **3a** in benzene under 50 bar of H_2 for 24 h and a temperature of 100 °C led to the formation of a small amount of phosphinidene clusters. One product was identified as $[(\mu\text{-H})_2\text{Ru}_3(\text{CO})_9((S)\text{-1a})]$ on the basis of its ^1H and ^{31}P NMR spectra [34]. The second product was identified as $[(\mu\text{-H})_2\text{Ru}_3(\text{CO})_9(\text{PC}_2\text{H}_5)]$ **5**. These phosphinidene clusters are presumably formed via opening/hydrogenation of the phosphirane moiety, as discussed above, coupled with (subsequent) elimination of either the ethyl (ethane) moiety or the binaphthyl moiety. The characterization of cluster **5** was primarily based on a single crystal X-ray diffraction analysis (*vide infra*). The $\nu(\text{C-O})$ pattern in the IR spectrum of **5** is similar to that of $[(\mu\text{-H})_2\text{Ru}_3(\text{CO})_9(\text{PPh})]$ [35]. The ^1H NMR spectrum of **5** reveals a hydride signal as a doublet at $\delta = -17.69$ ppm, and signals for the new ethyl group appears 0.86 ppm as a multiplet (CH_3) and a singlet at 1.19 ppm (CH_2). ^{31}P NMR spectrum for cluster **5** also shows a singlet at 147.39 ppm. The mass spectrum of **5** reveals a peak envelope at m/z : 617 $[\text{M}]^+$, which is consistent with the proposed molecular formula $[(\mu\text{-H})_2\text{Ru}_3(\text{CO})_9(\text{PEt})]$ **5**.

The molecular structure of **5**, as determined by X-ray crystallography, is shown in Fig. 4 and some selected geometric data are listed in the caption. Relevant crystallographic data are summarized in Table 3. The three metal atoms are capped by the phosphorus atom to give a distorted tetrahedral core. The influence exerted on the Ru1-Ru2 and Ru1-Ru3 bonds by the edge-bridging hydrides is noticeable – these bonds are considerably elongated (2.9392(2) and 2.9413(3) Å, respectively) relative to the Ru2-Ru3 bond (2.8225(2) Å). The Ru-P bond distances in **5** are similar to those observed for the phosphinidene cluster $[\text{H}_2\text{Ru}_3(\text{CO})_9(\text{PPh})]$ [36], but are notably asymmetric, Ru1-P1 = 2.3253(6), Ru2-P1 = 2.2840(6) and Ru3-P1 = 2.2907(8) Å.

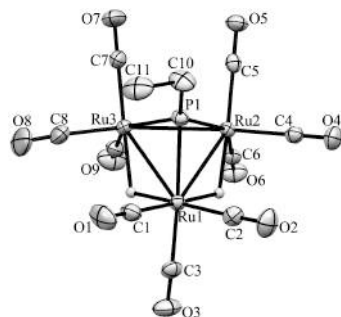


Fig. 4. Molecular structure of $[(\mu\text{-H})_2\text{Ru}_3(\text{CO})_9(\text{PEt})]$ **5** with thermal ellipsoids drawn at 50% probability level. All

hydrogen atoms except the hydrides have been omitted for clarity. Selected bond lengths (Å): Ru1-Ru2 2.9392(2), Ru1-Ru3 2.9413(3), Ru2-Ru3 2.8225(2), Ru1-P1 2.3253(6), Ru2-P1 2.2840(6), Ru3-P1 2.2907(6), Ru1-H1 1.77(3), Ru1-H2 1.72(3), Ru2-H1 1.78(3), Ru3-H2 1.84(3).

Hydrogenation of tiglic acid

We have shown repeatedly that comparatively low temperature (100 °C) and pressure (50 bars of H_2) enhances the chiral induction and maximizes the conversion in the asymmetric hydrogenation of tiglic acid with good enantioselectivity [19, 20]. At high temperature (130-150 °C), severe decomposition of the clusters was observed and it is suspected that the solid particles that were produced were responsible for the catalytic action, which led to the formation of considerable amount of cyclohexene and cyclohexane in addition to the expected 2-methyl butyric acid [18]. When lower temperature was used, all reaction mixtures remained homogeneous and the above-mentioned hydrogenation products of toluene were not detected. In order to obtain reasonable conversions, a temperature of 100 °C and longer reaction times of 48 h were required. The results of the catalysis tests for clusters **2c-5** are presented in Table 2. Clusters **2a** and **2b** were not tested because of the fact that these will yield **3a/4a** and **3b/4b** under the catalytic reaction conditions (*vide supra*, Scheme 1).

Table 2. Asymmetric catalytic hydrogenation of tiglic acid in the presence of clusters **2c-5** as catalysts.

Entry	Catalyst	Conv. ^a %	ee %	Config. ^b
1	2c	51	-	-
2	3a	52	-	-
3	3b	55	-	-
4	4a	49	-	-
5 ^c	4a	78	-	-
6	4b	51	-	-
7 ^c	4b	78	-	-
8	5	15	-	-

^aThe amount of substrate consumed in the catalytic experiment, assessed by ^1H NMR spectroscopy, $p(\text{H}_2) = 50$ bar, $T = 100$ °C, solvent = EtOH-toluene 1:1 (5 mL), $n(\text{substrate})/n(\text{catalyst}) = 100$.

^bFavoured enantiomer. ^cReaction time = 48 h.

All clusters gave moderate to low conversion rates, even when extended reaction times (48 h) were used. Reasonable catalytic conversion rates (relative to the corresponding catalytic reaction using $[\text{H}_2\text{Ru}_4(\text{CO})_{12}]$ under the same reaction conditions [37]) could be observed for clusters **4a** and **4b** when the longer reaction time was used (entries 5 and 7, Table 2). After catalysis runs, clusters **3a/b** and **4a/b** were recovered unaltered in ca. 50-60% yields after work-up, with no evidence of other metal-based products. For

both **2c** and **5**, only unknown decomposed products were obtained at the end of the catalytic cycle.

However, *no* enantioselectivity could be observed for any of the chiral clusters tested as catalysts/catalyst precursors in this study (i.e. all clusters except **5**, which is not chiral). Knowles *et al.* have proposed that in hydrogenation reactions bidentate (phosphine) ligands are generally superior to corresponding monophosphines because the use of bidentate results in rigidity in the catalyst, which leads to higher chiral induction [38]. In clusters **3a/4a** and **3b/4b**, a stereogenic center (phosphorus) is directly coordinated to a ruthenium atom in the cluster, but the effective steric bulk of the ligand is relatively small because there is only one relatively bulky substituent on the phosphorus (*viz* the binaphthyl moiety). The rigidity of the ligand and the cluster framework is low because of the monodentate coordination of the ligand. In cluster **2c**, the diphosphirane is coordinated in a chelating mode, and this coordination mode may be expected to lead to better chiral induction. However, the stereogenic center is relatively remote (skew chirality centered on the binaphthyl moiety) and the expected chiral induction is therefore low, although effective chiral induction by 1,1- $[\text{H}_4\text{Ru}_4(\text{CO})_{10}(\text{P-P}^*)]$ (where P-P^* = chiral primary phosphine ligands of clusters) has been demonstrated previously [17].

The exact reaction mechanism(s) for the cluster-based catalytic hydrogenation reactions is/are still unclear [17]. While the isolation of **3a/4a** and **3b/4b** from the catalytic reactions are consistent with cluster-based catalysis (but does not exclude fragmentation), the decomposition of **2c** and **5** suggests that the clusters fragment. Assuming the presence of intact clusters, it should be borne in mind that the presence of several metal centers is an inherent weakness when it comes to chiral induction in clusters – it is likely that a substrate will coordinate at a ruthenium center that is remote from any (bulky) chiral ligand coordinated to the cluster, for both steric and electronic reasons. The effective chiral induction by a chiral ligand is thus expected to be lower when it is coordinated to a cluster than in a corresponding mononuclear complex.

In previous studies [17, 20, 37], we have noted an (empirical) correlation between hydride fluxionality in $[\text{H}_4\text{Ru}_4(\text{CO})_{10}(\text{P-P}^*)]$ (P-P^* = chiral diphosphine ligand) clusters and the chiral induction by the cluster in catalytic asymmetric hydrogenation of α -unsaturated carboxylic acids – the “greater” the fluxionality, the lower the chiral induction. Clusters with good chiral induction were found to have a very rigid hydride orientation/location, and in one case it was found that one specific hydride remains fixed under the catalytic conditions [17] (temperature and hydrogen pressure) used in the present study [20]. The observed correlation holds true also for the H_4Ru_4 clusters investigated in the present study; they are the most fluxional chiral tetraruthenium clusters that we have thus far studied, and give no chiral induction.

Conclusions

In summary, we have synthesised and characterised a number of new tetranuclear ruthenium clusters, derivatised with chiral primary phosphiranes, diphosphiranes, and secondary phosphines derived from phosphirane precursors, as well as one new phosphidene-capped triruthenium cluster. Several of these clusters are capable of acting as catalysts/catalyst precursors for hydrogenation of tiglic acid, but no chiral induction could be detected in these catalytic reactions. Although it has not been possible to unambiguously determine the nature of the active catalyst in the cluster-based systems, indirect evidence suggests that clusters **3a/4a** and **3b/4b** may be the active catalysts, or direct precursors to an active cluster catalyst.

From the present results, and based on our previous findings using various chiral phosphine derivatives of $[\text{H}_4\text{Ru}_4(\text{CO})_{12}]$ as asymmetric hydrogenation catalysts [19, 37, 39], it is evident that the nature of the chiral ligand is key to the enantioselectivity that is obtained. Based on the arguments above, it is expected that very bulky and polydentate chiral ligands will give the best chiral induction when/if the clusters act as catalysts.

Experimental

All reactions and other manipulations were carried out under a nitrogen atmosphere using standard Schlenk techniques. All solvents were dried and distilled under a nitrogen atmosphere prior to use. Infra-red spectra were recorded as solutions in 0.5 mm NaCl cells on a Nicolet Avatar 360 FT-IR-spectrometer. ^1H and $^{31}\text{P}\{^1\text{H}\}$ NMR spectra were recorded on a Varian Unity 500 MHz NMR spectrometer; $^{31}\text{P}\{^1\text{H}\}$ NMR shifts were referenced to external H_3PO_4 (85%). The parent cluster $[(\mu\text{-H})_4\text{Ru}_4(\text{CO})_{12}]$ was prepared according to the literature procedure [40] and its purity was assessed using thin-layer chromatography (TLC) and IR spectroscopy. The chiral primary phosphiranes ligands [(S)-1-([1,1'-Binaphthalen]-2-yl) phosphirane] (*S*)-**1a**, [(*R*)-1-(2'-Methoxy-1,1'-binaphthyl-2-yl) phosphirane] (*R*)-**1b**, and [2,2'-di(phosphiran-1-yl)-1,1'-binaphthalene] (*S*)-**1c** were prepared as reported [26, 41]. Tiglic acid, and *S*-methyl mandelate were purchased from Sigma-Aldrich. Products were separated with Merck thin-layer chromatography (TLC) plates as supplied; 0.25 mm layer of Kiesel-gel 60 F254. Catalysis experiments were carried out using a 45 mL Parr autoclave with a PTFE reaction vessel.

Synthesis of $[(\mu\text{-H})_4\text{Ru}_4(\text{CO})_{11}((\text{S})\text{-1a})] \text{ 2a}$

A mixture of $[(\mu\text{-H})_4\text{Ru}_4(\text{CO})_{12}]$ (25 mg, 0.033 mmol) and (11 mg, 0.033 mmol) of (*S*)-**1a** [= (*S*)-1-([1,1'-binaphthalen]-2-yl)phosphirane] were dissolved in 20 mL of dichloromethane and the solution was stirred for 20 min. Under vigorous stirring, a small excess of Me_3NO (3 mg, 0.04 mmol) dissolved in dichloromethane (5 mL) was added dropwise to the yellowish cluster/ligand solution for

30 min, which instantly started to change colour towards red. After 6 h the solvents were removed under reduced pressure. The red solid residue was redissolved in a small quantity of dichloromethane and purified by preparative TLC (CH₂Cl₂-petroleum ether 1:3). Except for traces of starting materials and one stationary brown band (decomposed material), one band was isolated from the TLC plates and extracted with CH₂Cl₂ and dried under vacuum to afford a red microcrystalline solid ($R_f = 0.7$) that was identified as [(μ-H)₄Ru₄(CO)₁₁((S)-1a)] **2a** (13 mg, 38 %); ¹H NMR (500 MHz, CDCl₃): δ 8.00 (d, $J = 8.5$ Hz, 1H), 7.93 (m, 2H), 7.85 (d, $J = 8.3$ Hz, 2H), 7.78 (m, 1H), 7.67 (m, 2H), 7.54 (d, $J = 6.9$ Hz, 1H), 7.46 (m, 2H), 7.06 (d, $J = 8.6$ Hz, 1H), 6.95 (d, $J = 8.1$ Hz, 1H), 1.19 (m, 1H), 1.11 (m, 1H), 1.02 (m, 1H), 0.54 (m, 1H), -17.64 ('d', 4H). ³¹P NMR (202 MHz, CDCl₃): δ = -154.22 ('m'br, ² J_{P-H} = not resolved); IR (cyclohexane): 2094 (m), 2088 (w), 2067 (vs), 2057 (vs), 2029 (vs), 2009 (vs), 1990(m), 1969 (w); MS (FAB): m/z : 1052 [M+Na]⁺.

Synthesis of [(μ-H)₄Ru₄(CO)₁₁((R)-1b)] **2b**

A mixture of [(μ-H)₄Ru₄(CO)₁₂] (30 mg, 0.04 mmol) and (14 mg, 0.04 mmol) of (R)-1b [= (R)-1-(2'-Methoxy-1,1'-binaphthyl-2-yl) phosphirane] were dissolved in 20 mL of dichloromethane and the solution was stirred for 20 min. Under vigorous stirring, a small excess of Me₃NO (3.6 mg, 0.048 mmol) dissolved in dichloromethane (5 mL) was added dropwise to the yellowish cluster/ligand solution for 30 min, which instantly started to change colour towards red. After 6 h the solvents were removed under reduced pressure. The red solid residue was redissolved in a small quantity of dichloromethane and purified by using preparative TLC (CH₂Cl₂-petroleum ether 1:3). Except for traces of starting materials and one stationary brown band (decomposed material), one band was isolated from the TLC plates and extracted with CH₂Cl₂ and dried under vacuum to afford a microcrystalline red solid ($R_f = 0.6$), was identified as [(μ-H)₄Ru₄(CO)₁₁((R)-1b)] **2b** (17 mg, 42%); ¹H NMR (500 MHz, CDCl₃): δ 8.02 (d, $J = 9.2$ Hz, 1H), 7.96 (d, $J = 8.2$ Hz, 1H), 7.86 (d, $J = 8.0$ Hz, 2H), 7.77 (m, 1H), 7.46 (m, 2H), 7.32 (m, 1H), 7.22 (m, 1H), 7.03 (d, $J = 8.7$ Hz, 2H), 6.76 (d, $J = 8.8$ Hz, 1H), 3.71 (s, 3H), 1.66 (m, 1H), 1.07 (m, 1H), 0.92 (m, 1H), 0.72 (m, 1H), -17.84 ('s', 4H). ³¹P NMR (202 MHz, CDCl₃): δ = -155.86 (s); IR (cyclohexane): 2092 (m), 2086 (m), 2065 (vs), 2053 (vs), 2030 (vs), 2007 (vs), 1989(m), 1969 (w); MS (FAB): m/z : 1081 [M+Na]⁺.

Synthesis of 1,1-[(μ-H)₄Ru₄(CO)₁₀((S)-1c)] **2c**

A total of 40 mg (0.053 mmol) of [(μ-H)₄Ru₄(CO)₁₂] and 20 mg (0.053 mmol) of (S)-1c [= 2,2'-di(phosphiran-1-yl)-1,1'-binaphthalene] were dissolved in dichloromethane. A small excess of Me₃NO [6 mg, 0.08 mmol] dissolved in 5 mL of dichloromethane contains few drops of acetonitrile was added dropwise over a period of 30 min to the stirred cluster/ligand solution. The initial yellow colored solution

turned into deep red during the addition of Me₃NO. The reaction was monitored continuously by spot TLC (dichloromethane-petroleum ether 1:3) and when no parent cluster could be observed (2h), the solvent was removed under vacuum and the resulting red solid was dissolved in a small quantity of dichloromethane and separated using preparative TLC (CH₂Cl₂-petroleum ether 1:3). Except for traces of starting materials, one red band was isolated from the TLC plates and extracted with CH₂Cl₂ and dried under vacuum. It was identified as 1,1-[(μ-H)₄Ru₄(CO)₁₀((S)-1c)] **2c** (16 mg, 28 %); ($R_f = 0.4$), ¹H NMR (500 MHz, CDCl₃): δ 8.00 (m, 3H), 7.92 (m, 3H), 7.83 (m, 1H), 7.73 (m, 1H), 7.50 (m, 2H), 6.80 (dd, $J = 23.2$, 8.3 Hz, 2H), 1.79 (m, 1H), 1.67 (m, 1H), 1.43 (m, 1H), 1.34 (m, 1H), 0.55 (m, 2H), 0.42 (m, 2H), -17.20 (br, 4H); ³¹P NMR (202 MHz, CDCl₃): δ = -135.61 (d, $J_{P-P} \approx 37$ Hz), -139.18 (d, $J_{P-P} \approx 37$ Hz); IR (cyclohexane): 2076 (s), 2044 (vs), 2024 (vs), 2008 (s), 1993 (w), 1987 (w), 1977 (m), 1953 (br); MS (FAB): m/z : 1082 [M+Na]⁺. Red crystals of **2c** were obtained by slow evaporation of dichloromethane-hexane at 4 °C.

Synthesis of [(μ-H)₄Ru₄(CO)₁₁((S)-1a-H₂)] **3a** and [(μ-H)₄Ru₄(CO)₁₁((R)-1a-H₂)] **4a**

Method A (Thermal ligand substitution at high pressure for **2a**)

In a small laboratory autoclave (45 mL), a total of 45 mg (0.043 mmol) of [(μ-H)₄Ru₄(CO)₁₁((S)-1a)] **2a** was dissolved in 5 mL of EtOH/toluene (1:1). The autoclave was sealed and purged three times with 10 bar of H₂ before being pressurized with a total of 50 bar H₂. After 24 h at 100 °C, the autoclave was cooled to room temperature. The gases were carefully released and the autoclave was opened. The dark brown solution was concentrated and the obtained solid was dissolved in 2 mL of CH₂Cl₂ and subjected to preparative TLC (CH₂Cl₂/petroleum ether 1:3). Except for traces of starting materials and one stationary brown band (decomposed material), two bands were isolated from the TLC plates and extracted with CH₂Cl₂ and dried under vacuum. Two new isomeric products were observed; the first product (red, $R_f = 0.8$), was identified as [(μ-H)₄Ru₄(CO)₁₁((S)-1a-H₂)] **3a** (8 mg, 19 %); ¹H NMR (500 MHz, CDCl₃): ¹H NMR (500 MHz, cdcl₃) δ 8.15 (d, $J = 7.1$ Hz, 1H), 8.09 (d, $J = 9.1$ Hz, 1H), 7.97 (d, $J = 8.2$ Hz, 1H), 7.93 (d, $J = 8.3$ Hz, 1H), 7.67 (dd, $J = 11.2$, 8.7 Hz, 1H), 7.54 (appt, 1H), 7.39 (d, $J = 7.8$ Hz, 1H), 7.32 (m, 2H), 7.26 (appt, 2H), 7.16 (d, $J = 8.5$ Hz, 1H), 6.96 (d, $J = 8.4$ Hz, 1H), 5.23 (dd, ¹ $J_{P-H} = 381$, 10.7 Hz, 1H), 1.26 (s, 2H), 0.86 (dt, $J = 17.8$, 7.5 Hz, 3H), -17.64 (s, 4H); ³¹P NMR (202 MHz, CDCl₃): δ = -11.88 (s); IR (cyclohexane): 2092 (w), 2084 (m), 2064 (m), 2051 (vs), 2030 (vs), 2012 (s), 1984 (m), 1967 (w); MS (FAB): m/z : 1035 [M+H]⁺. The second (red) product ($R_f = 0.7$), was identified as [(μ-H)₄Ru₄(CO)₁₁((R)-1a-H₂)] **4a** (7 mg, 17 %); ¹H NMR (500 MHz, CDCl₃): δ 8.15 (d, $J = 7.0$ Hz, 1H), 8.07 (d, $J = 9.1$ Hz, 1H), 7.97 (d, $J = 8.3$ Hz, 1H), 7.91 (d, $J = 8.1$ Hz, 1H), 7.72 (dd, $J = 11.5$, 8.6 Hz, 1H), 7.56 (appt, 1H), 7.45 (d, J

= 9.1 Hz, 2H), 7.35 (m, 3H), 7.18 (d, J = 8.5 Hz, 1H), 6.90 (d, J = 8.5 Hz, 1H), 5.28 (dd, $^1J_{\text{P-H}}$ = 379, 9.7 Hz, 1H), 1.24 (s, 2H), 1.05 (dt, J = 18.2, 7.5 Hz, 3H), -17.81 (s, 4H); ^{31}P NMR (202 MHz, CDCl_3): δ = -13.11 (s); IR (cyclohexane): 2092 (w), 2086 (m), 2063 (vs), 2057 (vs), 2052(vs), 2030 (vs), 2007 (s), 1987(m), 1966 (w); MS (FAB): m/z : 1035 $[\text{M}+\text{H}]^+$.

Method B (Thermal ligand substitution at high pressure)

A mixture of $[(\mu\text{-H})_4\text{Ru}_4(\text{CO})_{12}]$ (30 mg, 0.04 mmol) and (13 mg, 0.04 mmol) of (*S*)-**1a** ligand [= (*S*)-1-([1,1'-Binaphthalen]-2-yl) phosphirane] were dissolved in 5 mL of benzene and the solution was subjected inside a small autoclave (45 mL). The autoclave was sealed and purged three times with 10 bar of H_2 before being pressurized with total of 30 bar H_2 . After 4 h at 125 °C, the autoclave was cooled to room temperature. The gases were carefully released and the autoclave was opened. The isolation/purification and identification of the products were identical to those described above. Yields: **3a** (9 mg, 20 %) and **4a** (7 mg, 16 %).

Synthesis of $[(\mu\text{-H})_4\text{Ru}_4(\text{CO})_{11}((R)\text{-1b-H}_2)]$ **3b** and $[(\mu\text{-H})_4\text{Ru}_4(\text{CO})_{11}((S)\text{-1a-H}_2)]$ **4b**

Method A (Thermal ligand substitution at high pressure for 2b)

In a small laboratory autoclave (45 mL), a total of 50 mg (0.047 mmol) of $[(\mu\text{-H})_4\text{Ru}_4(\text{CO})_{11}((R)\text{-1b})]$ **2b** was dissolved in 5 mL of EtOH/toluene (1:1). The autoclave was sealed and purged three times with 10 bar of H_2 before being pressurized with a total of 50 bar H_2 . After 24 h at 100 °C, the autoclave was cooled to room temperature. The gases were carefully released and the autoclave was opened. The dark brown solution was concentrated and the obtained solid was dissolved in 2 mL of CH_2Cl_2 and subjected to preparative TLC (CH_2Cl_2 / Petroleum ether 1:3). Except for traces of starting materials and one stationary brown band (decomposed material), two bands were isolated from the TLC plates and extracted with CH_2Cl_2 and dried under vacuum, two new isomer products were observed. The first product (red, R_f = 0.5), was identified as $[(\mu\text{-H})_4\text{Ru}_4(\text{CO})_{11}((R)\text{-1b-H}_2)]$ **3b** (14 mg, 28 %); ^1H NMR (500 MHz, CDCl_3): δ 8.07 (d, J = 8.8 Hz, 1H), 8.02 (d, J = 9.3 Hz, 1H), 7.90 (d, J = 8.1 Hz, 1H), 7.86 (d, J = 8.3 Hz, 1H), 7.59 (m, 1H), 7.49 (appt, 1H), 7.44 (d, J = 9.1 Hz, 1H), 7.28 (m, 2H), 7.09 (d, J = 8.8 Hz, 2H), 6.89 (d, J = 8.0 Hz, 1H), 5.16 (dd, $^1J_{\text{P-H}}$ = 380, 10.3 Hz, 1H), 3.67 (s, 3H), 1.18 (s, 2H), 0.79 (dt, J = 14.6, 7.3 Hz, 3H), -17.72 (s, 4H); ^{31}P NMR (202 MHz, CDCl_3): δ = -11.82 (s); IR (cyclohexane): 2091 (w), 2086 (m), 2061 (vs), 2052 (vs), 2030 (vs), 2012 (sh), 2005 (s), 1988(m), 1967 (w); MS (FAB): m/z : 1083 $[\text{M}+\text{Na}]^+$. The second (red) product (R_f = 0.4), was identified as $[(\mu\text{-H})_4\text{Ru}_4(\text{CO})_{11}((S)\text{-1b-H}_2)]$ **4b** (18 mg, 36 %); ^1H NMR (500 MHz, CDCl_3): δ

8.09 (d, J = 8.3 Hz, 1H), 8.01 (d, J = 9.1 Hz, 1H), 7.92 (d, J = 8.4 Hz, 1H), 7.86 (d, J = 8.1 Hz, 1H), 7.67 (m, 1H), 7.51 (m, 1H), 7.39 (d, J = 9.0 Hz, 2H), 7.30 (m, 2H), 7.13 (d, J = 8.6 Hz, 1H), 6.85 (d, J = 8.5 Hz, 1H), 5.22 (dd, $^1J_{\text{P-H}}$ = 378, 9.0 Hz, 1H), 3.72 (s, 3H), 1.2 (s, 2H), 1.00 (dt, J = 15.2, 7.4 Hz, 3H), -17.87 (s, 4H); ^{31}P NMR (202 MHz, CDCl_3): δ = -13.18 (s); IR (cyclohexane): 2092 (w), 2086 (m), 2062 (vs), 2055 (vs), 2051(vs), 2031 (vs), 2024 (s), 2005 (s), 1988(m), 1966 (w); MS (FAB): m/z : 1083 $[\text{M}+\text{Na}]^+$. Crystallization of **3b** from CH_2Cl_2 -hexane solutions at 4 °C yielded red crystals suitable for X-ray diffraction analysis.

Method B (Thermal ligand substitution at high pressure)

A mixture of $[(\mu\text{-H})_4\text{Ru}_4(\text{CO})_{12}]$ (30 mg, 0.04 mmol) and (14 mg, 0.04 mmol) of (*R*)-**1b** ligand [= (*R*)-1-(2'-methoxy-1,1'-binaphthyl-2-yl) phosphirane] were dissolved in 6 mL of benzene and the solution was transferred to a small autoclave (45 mL). The autoclave was sealed and purged three times with 10 bar of H_2 before being pressurized with total of 30 bar H_2 . After 4 h at 125 °C, the autoclave was cooled to room temperature. The gases were carefully released and the autoclave was opened. The isolation/purification and identification of the products were identical to those described above. Yields: **3b** (7 mg, 16 %) and **4b** (6 mg, 12 %).

Synthesis of $[(\mu\text{-H})_2\text{Ru}_3(\text{CO})_9(\text{PEt})]$ **5**

In a small laboratory autoclave (45 mL), a total of 25 mg (0.024 mmol) of $[(\mu\text{-H})_4\text{Ru}_4(\text{CO})_{11}((S)\text{-1a-H}_2)]$ **3a** was dissolved in 5 mL of benzene. The autoclave was sealed and purged three times with 10 bar of H_2 before being pressurized with a total of 50 bar H_2 . After 24 h at 100 °C, the autoclave was cooled to room temperature. The gases were carefully released and the autoclave was opened. The dark brown solution was concentrated and the obtained solid was dissolved in 2 mL of CH_2Cl_2 and subjected to preparative TLC (CH_2Cl_2 /Petroleum ether 1:3). Except for traces of starting materials and one stationary brown band (decomposed material), one band was isolated from the TLC plates, extracted with CH_2Cl_2 and dried under vacuum to afford a red product (R_f = 0.7) that was identified as $[(\mu\text{-H})_2\text{Ru}_3(\text{CO})_9(\text{PEt})]$ **5** (12 mg, 80 %). ^1H NMR (500 MHz, CDCl_3): δ 1.19 (s, 2H), 0.86 (m, 3H), -17.69 (d, J = 2.4 Hz, 2H); ^{31}P NMR (202 MHz, CDCl_3): δ = 147.39 (s); IR (cyclohexane): 2101 (m), 2084 (m), 2073 (s), 2048 (vs), 2042 (sh), 2030 (vs), 2015 (s), 2002 (w), 1984 (m), 1968 (w); MS (FAB): m/z : 617 $[\text{M}]^+$. Red crystals of **5** were obtained by slow evaporation of acetonitrile-hexane at 4 °C.

Homogeneous catalytic experiments

In the catalysis experiments, the catalyst and substrate were loaded into the autoclave under N_2 , and the degassed solvent mixture was added (2.5 mL of EtOH/2.5 mL of

toluene). The reaction vessel was closed and purged three times with hydrogen before final pressurizing to 50 bar. The reaction mixture was continuously stirred with a magnetic stirrer (ca. 750 rpm) and heated at 100°C for 24 h. After a cooling period of approximately 45 min, the reaction vessel was depressurized and opened. The homogeneous reaction mixture was transferred to a 50 mL flask and concentrated under vacuum. The conversions for the catalysis runs were calculated on the basis of NMR analyses. To separate the carboxylic acid from the cluster, the reaction residue was dissolved in 10 mL of diethyl ether and the carboxylic acid was extracted with aqueous sodium solution (1M, 3 x 10 mL) and washed with diethyl ether (3 x 5 mL), leaving the cluster in the organic solvent. The carboxylate was protonated with sulfuric acid and extracted with diethyl ether (3 x 10 mL), washed with water (2 x 5 mL) and dried over magnesium sulfate. Evaporation of the ether under vacuum, yielded the carboxylic acid quantitatively. The ether phase, from which the carboxylic acid was extracted, was concentrated under vacuum to recover the remaining cluster. In certain cases, where ester formation was obtained during the catalytic experiment, the recovered catalyst was dissolved in a minimum quantity of dichloromethane and the products were separated by using preparative TLC, eluting with dichloromethane/petroleum ether (1:2). The enantiomeric excess of the product was detected by derivatizing 2-methylbutyric acid with *S*-methyl mandelate and analyzing the diastereomeric product mixture by NMR, as fully described by Tyrrell *et al* [42].

Variable temperature ¹H NMR spectroscopy

All NMR solvents (Aldrich) were used as received. Approximately 0.5 mL of a saturated CDCl₃ solution of **2a**, **2c**, **3a** and **4a** were added to a NMR tube, which was subsequently sealed under an N₂ atmosphere. The sample tube was placed into the probe using a ceramic spinner. Dry air (for measurements above room temperature) or liquid nitrogen was used as the temperature control gas. The sample was allowed to equilibrate at each desired temperature for 5 – 10 minutes before the start of shimming and data acquisition. The temperature ranges were 298 to 213 K for all samples. For each sample 128 scans were acquired to reach sufficient signal intensity.

X-Ray data collection and structure solutions

The diffraction data were collected at 100 K for **3b** and 170 K for **2c** and **5**, using a Nonius Kappa CCD or a Bruker AXS Kappa ApexII Duo diffractometer with Mo K α radiation (λ =0.71073 Å). The Denzo-Scalepack [43] or APEX2 [44] program packages were used for cell refinements and data reductions. The structure solutions were carried out using the SHELXS-97 [45] program with the WinGX [46] graphical user interface. All hydrogens were placed in idealized positions. Positions of hydrides were calculated using the XHYDEX program [47]. The

crystallographic details for the reported structures are summarized in Table 3.

Table 3. Crystallographic data for clusters 1,1-[(μ -H)₄Ru₄(CO)₁₀](*S*)-**1c**] **2c**, [(μ -H)₄Ru₄(CO)₁₁](*R*)-**1b**-H₂] **3b** and [(μ -H)₂Ru₃(CO)₉](PEt)] **5**.

	2c	3b	5
formula	C ₃₄ H ₂₀ O ₁₀ P ₂ Ru ₄ CH ₂ Cl ₂	C ₃₃ H ₂₄ O ₁₂ PRu ₄	C ₁₁ H ₄ O ₈ PRu ₃
<i>M</i> _r	1143.68	1059.78	617.35
<i>T</i> [K]	170(2)	100(2)	170(2)
λ [Å]	0.71073	0.71073	0.71073
Crystal system	Triclinic	Monoclinic	Monoclinic
Space group	P $\bar{1}$	C2	P2 ₁ /c
<i>a</i> [Å]	13.0672(2)	26.3595(6)	9.95389(16)
<i>b</i> [Å]	13.4306(2)	8.2898(2)	26.4478(4)
<i>c</i> [Å]	14.0336(2)	17.4298(4)	14.06515(18)
α /°	86.5911(13)	90	90
β /°	63.4062(18)	106.9760(10)	96.7104(13)
γ /°	64.0568(16)	90	90
<i>V</i> [Å ³]	1951.71(7)	3642.72(15)	3677.41(9)
<i>Z</i>	2	4	8
ρ_{calc} [g cm ⁻³]	1.946	1.932	2.230
μ [mm ⁻¹]	1.791	1.731	2.557
<i>F</i> (000)	1112	2060	2336
Crystal size [mm]	0.306 x 0.140 x 0.077	0.24 x 0.09 x 0.05	0.24 x 0.13 x 0.11
θ limits/°	2.078 to 45.650	1.62 to 30.65	2.92 to 28.25
<i>h</i> range	-26 to 26	-37 to 37	-13 to 13
<i>k</i> range	-27 to 27	-8 to 11	-35 to 35
<i>l</i> range	-28 to 28	-22 to 24	-14 to 18
No. reflns.	136726	20745	23874
Unique reflns.	33181	8990	8952
<i>R</i> _{int}	1.024	1.013	1.112
<i>R</i> ₁ ^a (<i>I</i> ≥ 2 σ)	0.0345	0.0189	0.0154
<i>WR</i> ₂ ^b (<i>I</i> ≥ 2 σ)	0.0334	0.0200	0.0186
Largest diff. peak and hole [e.Å ⁻³]	0.0803	0.0373	0.0392
Flack parameter	2.513 and -2.150	0.562 and -0.457	1.870 and -0.527

$$^a R1 = \Sigma ||F_o| - |F_c|| / \Sigma |F_o|, ^b wR2 = [\Sigma (w(F_o^2 - F_c^2)^2) / \Sigma (w(F_o^2)^2)]^{1/2}$$

ACKNOWLEDGMENTS

AFA thanks the EU Erasmus Mundus program, FFEEDB1 office, for a predoctoral fellowship.

References

- [1] H.U. Blaser, F. Spindler, M. Studer, *Appl. Catal. A*: 221 (2001) 119-143.
- [2] E.N. Jacobsen, A. Pfaltz, H. Yamamoto, *Comprehensive Asymmetric Catalysis: Supplement 1*, Springer, 2003.

- [3] E.N. Jacobsen, A. Pfaltz, H. Yamamoto, *Comprehensive Asymmetric Catalysis: Supplement 2*, Springer, 2004.
- [4] A.K. Smith, J.M. Basset, *J. Mol. Catal.*, 2 (1977) 229-241.
- [5] P.J. Dyson, *Coordin. Chem. Rev.*, 248 (2004) 2443-2458.
- [6] G. Hogarth, S.E. Kabir, E. Nordlander, *Dalton Trans.*, 39 (2010) 6153-6174.
- [7] U. Matteoli, M. Bianchi, P. Frediani, G. Menchi, C. Botteghi, M. Marchetti, *J. Organomet. Chem.*, 263 (1984) 243-246.
- [8] M. Bianchi, G. Menchi, P. Frediani, U. Matteoli, F. Piacenti, *J. Organomet. Chem.*, 247 (1983) 89-94.
- [9] R.R. Schmidt, J. Michel, *Angew. Chem. Int. Ed.*, 21 (1982) 72-73.
- [10] G. Süß-Fink, G. Herrmann, *Angew. Chem. Int. Ed.*, 25 (1986) 570-571.
- [11] C. Botteghi, S. Gladiali, M. Bianchi, U. Matteoli, P. Frediani, P.G. Vergamini, E. Benedetti, *J. Organomet. Chem.*, 140 (1977) 221-228.
- [12] U. Matteoli, V. Beghetto, A. Scrivanti, *J. Mol. Catal. A*: 109 (1996) 45-50.
- [13] U. Matteoli, G. Menchi, P. Frediani, M. Bianchi, F. Piacenti, *J. Organomet. Chem.*, 285 (1985) 281-292.
- [14] M. Bianchi, U. Matteoli, G. Menchi, P. Frediani, F. Piacenti, C. Botteghi, *J. Organomet. Chem.*, 195 (1980) 337-346.
- [15] M.W. Payne, D.L. Leussing, S.G. Shore, *J. Am. Chem. Soc.*, 109 (1987) 617-618.
- [16] A. Salvini, P. Frediani, M. Bianchi, F. Piacenti, L. Pistolesi, L. Rosi, *J. Organomet. Chem.*, 582 (1999) 218-228.
- [17] P. Homanen, R. Persson, M. Haukka, T.A. Pakkanen, E. Nordlander, *Organometallics*, 19 (2000) 5568-5574.
- [18] M.J. Stchedroff, V. Moberg, E. Rodriguez, A.E. Aliev, J. Botcher, J.W. Steed, E. Nordlander, M. Monari, A.J. Deeming, *Inorg. Chim. Acta.*, 359 (2006) 926-937.
- [19] V. Moberg, M. Haukka, I.O. Koshevoy, R. Ortiz, E. Nordlander, *Organometallics*, 26 (2007) 4090-4093.
- [20] V. Moberg, R. Duquesne, S. Contaldi, O. Röhrs, J. Nachtigall, L. Damoense, A.T. Hutton, M. Green, M. Monari, D. Santelia, M. Haukka, E. Nordlander, *Chem. - A Eur. J.*, 18 (2012) 12458-12478.
- [21] C. Claver, E. Fernandez, A. Gillon, K. Heslop, D.J. Hyett, A. Martorell, A.G. Orpen, P.G. Pringle, *Chem. Commun.*, (2000) 961-962.
- [22] M.T. Reetz, G. Mehler, *Angew. Chem. Int. Ed.*, 39 (2000) 3889-3890.
- [23] M. van den Berg, A.J. Minnaard, E.P. Schudde, J. van Esch, A.H.M. de Vries, J.G. de Vries, B.L. Feringa, *J. Am. Chem. Soc.*, 122 (2000) 11539-11540.
- [24] E.P.A. Couzijn, A.W. Ehlers, J.C. Slootweg, M. Schakel, S. Krill, M. Lutz, A.L. Spek, K. Lammertsma, *Chem. - A Eur. J.*, 14 (2008) 1499-1507.
- [25] A. Marinetti, F. Mathey, L. Ricard, *Organometallics*, 12 (1993) 1207-1212.
- [26] A. Ficks, I. Martinez-Botella, B. Stewart, R.W. Harrington, W. Clegg, L.J. Higham, *Chem. Commun.*, 47 (2011) 8274-8276.
- [27] A. Ficks, W. Clegg, R.W. Harrington, L.J. Higham, *Organometallics*, 33 (2014) 6319-6329.
- [28] M. Gabriela Ballinas-López, E.V. García-Báez, M.a.J. Rosales-Hoz, *Polyhedron*, 22 (2003) 3403-3411.
- [29] R.D. Wilson, S.M. Wu, R.A. Love, R. Bau, *Inorg. Chem.*, 17 (1978) 1271-1280.
- [30] F. Mathey, *Chemical Reviews*, 90 (1990) 997-1025.
- [31] A.U. Härkönen, M. Ahlgrén, T.A. Pakkanen, J. Pursiainen, *J. Organomet. Chem.*, 530 (1997) 191-197.
- [32] T.M. Räsänen, S. Jäaskeläinen, T.A. Pakkanen, *J. Organomet. Chem.*, 553 (1998) 453-461.
- [33] C.J. Adams, M.I. Bruce, E. Horn, B.W. Skelton, E.R.T. Tiekink, A.H. White, *Journal of the Chemical Society, Dalton Trans.*, (1993) 3299-3312.
- [34] A.F. Abdel-Magied, M.H. Majeed, A. Ficks, A.K. Singh, W. Clegg, M. Haukka, M. Monari, E. Nordlander, L.J. Higham, unpublished results.
- [35] A.J. Deeming, S. Doherty, N.I. Powell, *Inorg. Chim. Acta*, 198-200 (1992) 469-481.
- [36] F. Iwasaki, M.J. Mays, P.R. Raithby, P.L. Taylor, P.J. Wheatley, *J. Organomet. Chem.*, 213 (1981) 185-206.
- [37] V. Moberg, P. Homanen, S. Selva, R. Persson, M. Haukka, T.A. Pakkanen, M. Monari, E. Nordlander, *Dalton Trans.*, (2006) 279-288.
- [38] W.S. Knowles, M.J. Sabacky, B.D. Vineyard, D.J. Weinkauff, *J. Am. Chem. Soc.*, 97 (1975) 2567-2568.
- [39] V. Moberg, R. Duquesne, S. Contaldi, O. Röhrs, J. Nachtigall, L. Damoense, A.T. Hutton, M. Green, M. Monari, D. Santelia, M. Haukka, E. Nordlander, *Chem-Eur J*, 18 (2012) 12458-12478.
- [40] S.A.R. Knox, J.W. Koepke, M.A. Andrews, H.D. Kaesz, *J. Am. Chem. Soc.*, 97 (1975) 3942-3947.
- [41] R.M. Hiney, L.J. Higham, H. Müller-Bunz, D.G. Gilheany, *Angew. Chem. Int. Ed.*, 45 (2006) 7248-7251.
- [42] E. Tyrrell, M.W.H. Tsang, G.A. Skinner, J. Fawcett, *Tetrahedron*, 52 (1996) 9841-9852.
- [43] W.M. Z. Otwinowski, in: C.W. Carter, J. Sweet, Academic Press, New York, 276 (1997) 307.
- [44] APEX2, Software Suite for Crystallographic Programs, Bruker AXS, Inc., Madison, Wisconsin, (2009).
- [45] G. Sheldrick, *Acta Crystallogr. Sec. A*, 64 (2008) 112-122.
- [46] L.J. Farrugia, *J. Appl. Crystallogr.*, 32 (1999) 837-838.
- [47] A.G. Orpen, *J. Chem. Soc. Dalton Transa.*, (1980) 2509-2516.

Paper VI

Cite this: DOI: 10.1039/c0xx00000x

www.rsc.org/xxxxxx

ARTICLE TYPE

Anchored chiral ruthenium clusters in mesoporous silica: one-pot synthesis of a heterogeneous catalyst for asymmetric hydrogenation reactions†

Ahmed F. Abdel-Magied,^a Christoffer Tyrsted,^b Konrad Herbst,^b Reinout Meijboom,^c Reine Wallenberg,^d Michele R. Chierotti,^e Roberto Gobetto,^e and Ebbe Nordlander^{*a}

Received (in XXX, XXX) Xth XXXXXXXXX 200X, Accepted Xth XXXXXXXXX 200X

DOI: 10.1039/b000000x

The chiral cluster $[H_4Ru_4(CO)_{10}(\mu-1,2-W001)]$ ($W001 = (R)-1-[(R_P)-2-[2-(Diphenylphosphino)phenyl]ferrocenyl]ethylbis-[3,5-bis-(trifluoromethyl)phenyl]phosphine$) has been anchored to functionalized MCM-41. The resultant mesoporous solid functions as an enantioselective catalyst for the asymmetric hydrogenation of tiglic acid with up to 80% enantiomeric excess and excellent conversion (>99%).

Homogeneous catalytic systems present the advantages of high selectivities, enantioselectivities and catalytic activities for a variety of asymmetric transformation conducted under mild conditions.¹⁻³ On the other hand, solid heterogeneous catalysts present the advantages of facile separation, recovery and recycling. The combination of these properties by heterogenization of homogeneous single-site catalysts may lead to highly active, yet sturdy and easily recoverable catalysts. One simple protocol for such heterogenization involves immobilization of the active catalytic site on mesoporous inorganic solids having a large surface area. Inorganic solids, particularly those having a structured surface, are more robust than organic polymers and have a considerably larger area; therefore, high catalytic activities should in principle be achievable for catalysts based on such solids. This methodology has been successfully applied to non-asymmetric reactions while heterogeneous asymmetric catalysis remains one of the most challenging areas in catalysis research. Only a few examples have been reported where enantioselective heterogeneous catalysts perform as well as their homogeneous analogues.^{4,5} It has been previously reported that highly active allylic amination,⁶ hydrogenation,⁷⁻⁹ epoxidation¹⁰ and hydroxylation^{11, 12} catalysts may be designed in this manner.

Many heterogenization approaches have been explored, including attaching chiral homogeneous catalysts to different inorganic solids, e.g. polymers, membrane supports, dendrimers and porous silica materials.¹³⁻¹⁶ In "classical" immobilization, the chiral ligands or the catalytically active sites are anchored directly onto the mesoporous inorganic solids. However, with such methodology, it is not unusual to find that the resulting immobilized catalysts display less activity and/or selectivity than their homogeneous counterparts.

Our methodology for heterogenization was to take a well-performing homogeneous catalyst with well-studied catalytic behaviour and, by performing suitable modifications, to tether

this catalyst within a mesopore. In previous studies, we have shown that homogeneous catalytic systems based on $[H_4Ru_4(CO)_{10}(\mu-1,2-L)]$ clusters ($L =$ bulky chiral ferrocene-based diphosphine) are excellent catalysts for asymmetric hydrogenation reactions of α -unsaturated carboxylic acids.^{2, 3} Herein we report that anchoring the chiral cluster $[H_4Ru_4(CO)_{10}(\mu-1,2-W001)]$ **1** (Fig. 1) to functionalized MCM-41 produces a solid catalyst that displays high enantioselectivity for the hydrogenation of tiglic acid, with detected enantiomeric excess (ee) values being identical to those obtained for the unsupported cluster catalyst.¹⁷

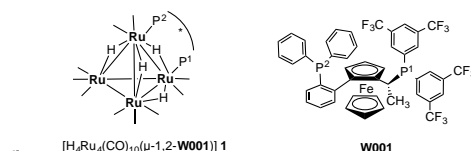
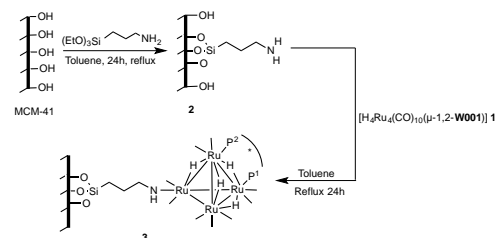


Fig. 1 Structures of the chiral cluster $[H_4Ru_4(CO)_{10}(\mu-1,2-W001)]$ **1** and the chiral diphosphine ligand **W001**.

Our approach to the preparation of the heterogeneous catalytic system is shown in Scheme 1. Cluster **1** was prepared and fully characterized according to a literature method.¹⁷ As a support, mesoporous MCM-41 was used. The mesoporous solid was modified with (3-aminopropyl)triethoxysilane groups¹⁸ to which anchoring is going to occur, yielding activated MCM-41 **2**. Treatment of **2** with an excess of $[H_4Ru_4(CO)_{10}(\mu-1,2-W001)]$ **1** yields the chiral catalytic catalyst **3**.



Scheme 1. The synthetic routes used in the preparation of the mesopore-supported catalyst **3**.

The success of the anchoring process was assessed by analytical methods and spectroscopic analysis of the resultant solid. The presence of cluster **1** in solid **3** was supported by IR spectroscopy. The infrared spectra peaks due to the support dominate the spectra. These include OH vibrations in the range 3700–3300 cm⁻¹ and, as expected, the strong ν(Si-O) stretch from 1000–1280 cm⁻¹. The presence of the cluster species in supported species was indicated by the appearance of carbonyl ν(CO) stretches at 2059 and 1981 cm⁻¹ for **3**.

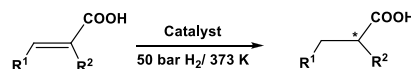
Further characterization of **3** was achieved by methods appropriate to molecular species. The presence of the tethered cluster catalyst **1** was supported by comparison of the ³¹P MAS NMR and ¹H MAS NMR spectra of **3** with that of the untethered homogeneous catalyst **1**. Three ³¹P resonances at δ 36.6, 53.7 and 77.7 were observed, indicating different phosphorus environments (ESI[†]). As controls, the ³¹P MAS NMR spectra were recorded for **1**, a physical mixture of functionalised MCM-41 **2** and **1** (ratio 10:1), and a ground mixture of **2** and **1** (ratio 10:1). All control spectra show three identical ³¹P resonances at δ 35.9, 44.6 and 49.4, indicating that **3** is not a simple mixture of **1** and **2** (cf. ESI[†]). In all cases, the three resonances integrate in the ratio 0.5:0.5:1.0 (low field to high field), indicating that the P^I phosphorus of the diphosphine ligand is found in two different environments (suggesting structural isomers). The low angle X-ray powder diffraction patterns of the catalyst **3** and functionalized MCM-41 **2** match well with the reported pattern of MCM-41.¹⁹ Transmission electron microscopy (TEM) micrographs show retention of the MCM-41 structure and no distinct Ru-clusters can be observed. In fact, well-dispersed Ru-nanoclusters in the pores of MCM-41 should be smaller than 1 nm, i.e. smaller than the fringe width of MCM-41, and should thus not be observable unless an aggregation of metal occurred. The Ru catalyst loading for **3** was determined by ICP-MS to be 0.67 ± 0.02%. The BET surface area of MCM-41, functionalized MCM-41 **2** and the solid catalyst **3** are 766, 266 and 281 m² g⁻¹, respectively (cf. ESI[†]).

In testing our catalysts we decided to choose hydrogenation of benchmark α-unsaturated carboxylic acid substrates, as their hydrogenated products are important chiral building blocks for the synthesis of biologically active compounds.²⁰ Tiglic acid, α-methylcinnamic acid and *trans*-2-methyl-pentenoic acid has been used in earlier assessments of asymmetric hydrogenation affected by cluster-based catalysts systems,^{21, 22} and there is a well-established protocol for the evaluation of enantiomeric excess of these substrates.

Three potential catalysts were examined for the catalytic hydrogenation of tiglic acid²³: the homogeneous catalyst [H₄Ru₄(CO)₁₀(μ-1,2-W001)] **1**, the activated MCM-41 **2**, and the cluster-functionalized mesoporous material **3**. The results achieved are summarized in Table 1. As may be expected, the activated MCM-41 **2** did not show any catalytic activity. The homogeneous catalyst [H₄Ru₄(CO)₁₀(μ-1,2-**1a**)] **1** shows high catalytic conversion (≈100%) with enantiomeric excess approaching 82%. Also in the case of **3**, there is excellent conversion with high enantioselectivity and mass balance (substrate a, Table 1). Importantly, the ee values achieved are as high as those reported in homogeneous catalytic hydrogenation of tiglic acid for the same kind of transition metal catalyst.¹⁷

In order to explore the generality of the catalytic activity in hydrogenation of (prochiral) α-unsaturated acids, and to include catalysts [H₄Ru₄(CO)₁₀(μ-1,2-**1a**)] **1** and solid catalyst **3** in a comparative study of asymmetric hydrogenation, we examined their catalytic capabilities for hydrogenation of α-methylcinnamic acid (substrate b, Table 1) and *trans*-2-methyl-pentenoic acid (substrate c, Table 1). Again, excellent conversion rates (≈100%) with high enantiomeric excess (up to 80% in case of α-methylcinnamic acid and up to 68% for α-methylcinnamic acid) with high mass balance were found when the heterogeneous catalyst **3** was used. As in the case of tiglic acid, the conversion rates and enantioselectivities are maintained for α-methylcinnamic acid and *trans*-2-methyl-pentenoic acid, when the molecular catalyst **1** is heterogenized to form **3**.

Table 1. A summary of the catalytic asymmetric hydrogenation experiments.^[a]



a; R¹ = R² = CH₃
b; R¹ = Ph, R² = CH₃
c; R¹ = CH₂CH₃, R² = CH₃

Substrate	Catalyst	Mass balance (%)	Conv. ^[b] (%)	ee (%)	Config. ^[c]
a	2	> 90	-	-	-
a	1 ^[d]	> 70	100	82	S
a	3	> 90	100	80	S
b	1 ^[d]	> 70	100	75	S
b	3	> 90	100	74	
c	1 ^[d]	> 70	100	68	S
c	3	> 90	100	66	
a	3+Hg(0)	> 90	99	78	S

[a] Reaction conditions: S/C ratio 100:1, 100 °C, 50 bar of H₂, 24h. [b] The amount of substrate consumed in the catalytic experiments, assessed by ¹H NMR spectroscopy. [c] Favoured enantiomer. [d] In homogeneous phase.

The recyclability of **3**, both in terms of conversion and selectivity, was evaluated by carrying out three successive runs in the hydrogenation of tiglic acid under the same catalytic hydrogenation reaction conditions. Identical catalytic performance was observed for all three runs.

In order to confirm the heterogeneous nature of the catalyst and that there is no leaching of ruthenium complexes/clusters from **3** into solution, a series of tests were performed. First, a hot filtration test was carried out.²⁴ In this control experiment, the catalyst **3** was filtered out when 28% conversion of the substrate had been achieved. At this moment stirring was stopped and small parts of the reaction mixture were removed, from which the solid material was filtered off, and the resultant solutions were stirred separately under the same catalytic hydrogenation reaction conditions. It was found that in the original reaction mixture, catalysis in the presence of the anchored catalyst went further to completion, whereas no reaction occurred in the mixtures where the solid material had been removed. This experiment shows that the conversion and enantioselectivity are due to the solid catalyst, i.e. **3**. Second, a mercury poisoning test was performed.²⁴ After 4h of reaction time under normal catalytic conditions, the conversion was determined. Then, a 2000-fold excess of metallic mercury was added to the reaction mixture and the reaction was

continued under the same catalytic conditions till completeness of the catalytic run. The product analysis revealed that upon addition of Hg(0), both the conversion and enantioselectivity decreased by 1-2 percentage units relative to the mercury-free catalytic runs (cf. Table 1, entries 3 vs 4). It is well known that ruthenium clusters/nanoparticles are relatively difficult to poison with Hg(0),²⁵ but our mercury test indicates that the catalytic activity is not due to leached ruthenium forming catalytically active nanoparticles.

In summary, we have shown that the anchoring of chiral ruthenium clusters to the surface of MCM-41 via a long linker is a valid strategy to prepare highly enantioselective heterogeneous catalysts that can be reused without any loss of catalytic activity/enantioselectivity. While immobilization of transition metal carbonyl clusters on solid supports is well established, and there are a number of examples of tethering of chiral mononuclear metal complexes to mesoporous solids,^{6,8,26} this is, to our knowledge, the first example of linkage of a chiral metal cluster to a mesoporous solid, and of enantioselective catalysis effected by such a mesoporous material.

Notes and references

^a Inorganic Chemistry Research Group, Chemical Physics, Center for Chemistry and Chemical Engineering, Lund University, Box 124, Lund SE-221 00, Sweden; E-mail: Ebbe.Nordlander@chemphys.lu.se

^b Haldor Topsøe A/S, Nymøllevej 55, DK-2800 Lyngby, Denmark.

^c Department of Chemistry, University of Johannesburg, P.O. Box 524, Auckland Park 2006, Johannesburg, South Africa

^d Material Chemistry/nCHREM, Lund University, Box 124, SE-221 00 LUND, Sweden.

^e Department of Chemistry, via P. Giuria 7, 10125 Torino, Italy.

† Electronic Supplementary Information (ESI) available: Experimental procedures, synthesis and characterization of catalysts, BET trace, XRPD patterns, SEM and reactivity tests are given. See DOI: 10.1039/b000000x/

1. P. Homanen, R. Persson, M. Haukka, T. A. Pakkanen and E. Nordlander, *Organometallics*, 2000, 19, 5568-5574.
2. V. Moberg, M. Haukka, I. O. Koshevoy, R. Ortiz and E. Nordlander, *Organometallics*, 2007, 26, 4090-4093.
3. V. Moberg, R. Duquesne, S. Contaldi, O. Röhrs, J. Nachtigall, L. Damoense, A. T. Hutton, M. Green, M. Monari, D. Santelia, M. Haukka and E. Nordlander, *Chem. Eur. J.*, 2012, 18, 12458-12478.
4. X.-G. Zhou, X.-Q. Yu, J.-S. Huang, C.-M. Che, S.-G. Li and L.-S. Li, *Chem. Commun.*, 1999, DOI: 10.1039/A905313A, 1789-1790.
5. D. J. Bayston and M. E. C. Polywka, in *Chiral Catalyst Immobilization and Recycling*, Wiley-VCH Verlag GmbH, 2007, DOI: 10.1002/9783527613144.ch09, pp. 211-234.
6. B. F. G. Johnson, S. A. Raynor, D. S. Shephard, T. Mashmeyer, T. Mashmeyer, J. Meurig Thomas, G. Sankar, S. Bromley, R. Oldroyd, L. Gladden and M. D. Mantle, *Chem. Commun.*, 1999, DOI: 10.1039/A902441G, 1167-1168.
7. G. Liu, M. Yao, F. Zhang, Y. Gao and H. Li, *Chem. Commun.*, 2008, DOI: 10.1039/B714575F, 347-349.
8. R. Raja, J. M. Thomas, M. D. Jones, B. F. G. Johnson and D. E. W. Vaughan, *J. Am. Chem. Soc.*, 2003, 125, 14982-14983.
9. S. Jin Bae, S.-W. Kim, T. Hyeon and B. Moon Kim, *Chem. Commun.*, 2000, DOI: 10.1039/A908967E, 31-32.
10. T. Maschmeyer, F. Rey, G. Sankar and J. M. Thomas, *Nature*, 1995, 378, 159-162.
11. C. Nozaki, C. G. Lugmair, A. T. Bell and T. D. Tilley, *J. Am. Chem. Soc.*, 2002, 124, 13194-13203.
12. A. T. Bell, *Science*, 2003, 299, 1688-1691.
13. L. Pu, *Chem. Rev.*, 1998, 98, 2405-2494.
14. L.-X. Dai, *Angew. Chem. Int. Ed.*, 2004, 43, 5726-5729.

15. A. Corma, E. Gutiérrez-Puebla, M. Iglesias, A. Monge, S. Pérez-Ferreras and F. Sánchez, *Adv. Synth. Catal.*, 2006, 348, 1899-1907.
16. N. Madhavan, C. W. Jones and M. Weck, *Acc. Chem. Res.*, 2008, 41, 1153-1165.
17. V. Moberg, R. Duquesne, S. Contaldi, O. Röhrs, J. Nachtigall, L. Damoense, A. T. Hutton, M. Green, M. Monari, D. Santelia, M. Haukka and E. Nordlander, *Chem. Eur. J.*, 2012, 18, 12458-12478.
18. N. H. N. Kamarudin, A. A. Jalil, S. Triwahyono, N. F. M. Salleh, A. H. Karim, R. R. Mukti, B. H. Hameed and A. Ahmad, *Micropor. Mesopor. Mater.*, 2013, 180, 235-241.
19. R. Mokaya, *Chem. Commun.*, 2001, DOI: 10.1039/B101812O, 1092-1093.
20. M. Breuer, K. Ditrich, T. Habicher, B. Hauer, M. Keßeler, R. Stürmer and T. Zelinski, *Angew. Chem. Int. Ed.*, 2004, 43, 788-824.
21. V. Moberg, P. Homanen, S. Selva, R. Persson, M. Haukka, T. A. Pakkanen, M. Monari and E. Nordlander, *Dalton Trans.*, 2006, 279-288.
22. C. Botteghi, S. Gladiali, M. Bianchi, U. Matteoli, P. Frediani, P. G. Vergamini and E. Benedetti, *J. Organomet. Chem.*, 1977, 140, 221-228.
23. E. Tyrrell, M. W. H. Tsang, G. A. Skinner and J. Fawcett, *Tetrahedron*, 1996, 52, 9841-9852.
24. J. A. Widegren and R. G. Finke, *J. Mol. Catal. A*, 2003, 198, 317-341.
25. G. M. Whitesides, M. Hackett, R. L. Brainard, J. P. P. M. Lavallée, A. F. Sowinski, A. N. Izumi, S. S. Moore, D. W. Brown and E. M. Staudt, *Organometallics*, 1985, 4, 1819-1830.
26. S. A. Raynor, J. M. Thomas, R. Raja, B. F. Johnson, R. G. Bell and M. D. Mantle, *Chem. Commun.*, 2000, 1925-1926.

Synthesis and characterization of new transition metal carbonyl clusters has been undertaken, and evaluation of the new clusters to act as catalysts/catalysts precursor in asymmetric reactions has been carried out. The catalytic hydrogenation of tiglic acid under relatively mild conditions, using diastereomeric clusters of the general formula $[(\mu\text{-H})_2\text{Ru}_3(\mu\text{-S})(\text{CO})_7(\mu\text{-1,2-L})]$ (L= chiral diphosphine of the ferrocene-based Walphos and Josiphos families) as catalysts, reveal different catalytic behaviour in terms of conversion and enantioselectivity.



The observed reversal in enantioselectivity when the chirality of the cluster framework is changed strongly supports catalysis by intact Ru_3 clusters. A proposed catalytic cycle generated by CO loss from the parent catalyst has been investigated.

The ability of carbonyl clusters based on rhenium, ruthenium and osmium derivatised with chiral phosphines and phosphiranes to catalyse the asymmetric hydrogenation of tiglic acid shows high to excellent conversion rates with low to moderate enantioselectivity. A high conversion rate (up to 99%) and an enantioselectivity of 19% have been achieved with the cluster $[(\mu\text{-H})_4\text{Ru}_4(\text{CO})_{11}(\text{ArPH}_2)]$ {where $\text{ArP} = (R)\text{-(2'-methoxy-[1,1'-binaphthalen]-2-ylphosphine)}$ } acting as catalyst/catalyst precursor; this is, to the best of our knowledge, the first example of an asymmetric hydrogenation induced by a chiral primary phosphine.

A chiral solid catalyst derived from the immobilization of $[\text{H}_4\text{Ru}_4(\text{CO})_{10}(\mu\text{-1,2-W001})]$ (W001 = chiral diphosphine ligand of the Walphos family) onto functionalized MCM-41 has been shown to exhibit excellent conversion rates (> 99%) and as high enantiomeric excesses ($\approx 80\%$) as that of its homogeneous counterpart. The good catalytic properties are coupled with good recyclability of the mesoporous catalyst.

